University of Houston
Cullen College of Engineering

University of Padova
Department of Civil, Architectural and Environmental Engineering

Master Thesis in Structural Civil Engineering

Effect of the Lode Angle Parameter on the Behavior of Aluminum

Supervisor: Prof. Valentina Salomoni, University of Padova

Co-Supervisor: Prof. Kaspar Willam, University of Houston

Majoring: Elena Bombasaro

Accademic Year 2014-2015

INDICE

Introduction

"As a consequence of the worldwide tendency in reducing CO_2 emissions by producing lighter and more energy-efficient products, the demand for accurate predictions regarding material behavior and material failure has greatly increased in recent years. In particular in the automotive industry, there is also an increasing interest in effectively closing the gap between forming and crash analysis, since the forming operations may highly affect the crashworthiness of the produced parts. In this scenario, a correct depiction of material mechanical degradation and fracture seems indispensable." [On the prediction of material failure in LS-DYNA, F. Andrade, M. Feucht, A. Haufe].

This contribution by Haufe et al. directed my studies along the line of investigating the behavior of metals and whether also the first invariant of the stress tensor and the third deviatoric invariant have some influence on the yield surface of these materials, in addition to the second deviatoric invariant, which has been widely used since now in the metals yield functions.

This thesis concerns the experimental work done in order to investigate the behavior of metals, in particular of aluminum, and inserts in a wider research work, which is now being led by Professor K. Willam and his research group, which aim is that to propone a new asymmetric yield function for metallic materials depending on the first invariant of the stress tensor and the second and third invariant of stress deviator. In this larger research a model will be formulated as a function in the gap between Tresca and von Mises yield criteria and will be based on experimental results, on which I worked on and on which this thesis is about. The tests were performed on aluminum specimen tested

under different load scenarios, which generate different stress tensor invariants. Haigh–Westergaard coordinates were used and the corresponding lode angle for each scenario has been obtained.

In the different loading scenarios, the lode angle parameter is changing from 0 degrees, which corresponds to uniaxial tension condition and goes up to 30 degrees, which is pure shear condition. The results can show how the third invariant of stress deviator affects the behavior of aluminum material.

To look at the compressive behavior, which is not included in this thesis, and capture the possible difference between compressive and tensile behavior, Professor K. Willam and his research group are going to perform further experiments to go beyond 30 degrees up to 60 degrees, which represents the uniaxial compression case. Since the difference between compression and tension cannot be captured by only considering second and third invariants, there will be a need to introduce stress triaxiality measure or the first invariant of stress tensor to capture the difference in behavior of aluminum under tension and compression.

Digital Image Correlation (DIC) was used as a full-field measurement method for displacement field and calculation of the strain distribution of the Aluminum specimen under abovementioned loading scenarios. Using this method, plastic flow rule can be obtained by integration of the plastic strain rate through the physical domain of the specimen and it can be expressed in terms of first invariant of stress tensor and the second and third invariant of stress deviator. The results can be used to investigate the crack growth based on the local and global strain distribution.

In the larger work led by Professor K. Willam and his research group the pressure- sensitivity of Aluminum will be investigated based on the observed localization angle using the captured images by DIC. In case the observed angle of failure for both tension and compression tests is equal to $\pi/2$, one can say that the behavior of Aluminum follows the Tresca yield criterion and it should be considered to behave like a pressure-insensitive material. In case the angle of

friction Φ for Aluminum is not equal to zero, according to the Mohr–Coulomb yield criterion, the observed failure angle will be $\pi/2+\Phi/2$, which shows that Aluminum is behaving like a pressure-sensitive material.
The model, which will be proponed, will be implemented in a finite element code, and the results will be verified with the ones obtained in the experiments.
Analytical and numerical localization analysis will be done using an associated flow rule in 3D to calculate the orientation of failure surface considering von Mises, Tresca, developed two invariant formulations and the three invariant formulations. The localization analysis results will be compared with experimental results.

This thesis is essentially divided in two parts. The first section of the thesis, which includes the parts from Chapter 1 to Chapter 8, summarizes the theoretical background needed to develop the work dealt in the second section, from Chapter 9 to Chapter …, which includes the description of the experiments, the experiments results and the conclusions.

1 Classical Theory and Literature review

1.1 Classical Theory

The engineering design of structures often involves a two-stage process: first the internal force field acting on the structural material must be defined, and second, the response of the material to that force field must be determined. The first stage involves an analysis of the stress acting within the structural elements; the second involves the knowledge of the properties of the structural material. The linear relationship between stress and strain in an idealized material forms the basis of the mathematical theory of elasticity, which has been applied widely in practice to actual materials to estimate stresses and strains in the structural elements under a specific working load condition. These stresses are restricted to be less than the specified working or allowable stress that is chosen as some fraction of the yield strength of the material. An actual structure is a very complex body with an extremely complicated state of stress: many secondary stresses arise due to fabrication and localization. The combination of unknown initial stress, secondary stresses and stress concentration and redistribution due to discontinuities of the structure defy an idealized calculation based on the theory of elasticity. The theory of plasticity represents an extension of the theory of

elasticity and is concerned with the analysis of stresses and strains in the plastic as well as the elastic ranges. It gives more realistic estimates of load carrying capacity and provides a better understanding of the reactions to the forces induced in the material. Theory of elasticity and plasticity are the formalization of experimental observations of the macroscopic behavior of a deformable solid. The first task of plasticity theory is to give relationships between stresses and strains under a complex stress state that can describe adequately the observed plastic deformations. The second task of the plastic theory is to develop numerical techniques for implementing these stress-strain relationships. Because of the nonlinear nature of the plastic deformation rules, solutions of the basic equations of solid mechanics inevitably present considerable difficulties. However in recent years, the development of computers and modern techniques of finite element analysis has provided the engineer with a powerful tool for the solution of nonlinear problems.

Origin of plasticity and of the studies of the behavior of the materials dates back to a series of papers (1864-1872) by Tresca on the extrusion of metals, in which he proposed the first yield condition, which states that a metal yields plastically when the maximum shear stress attains a critical value. The actual formulation of the theory was done in 1870 by St. Venant, who introduced the constitutive relations for rigid, perfectly plastic materials in plane stress. The salient of this formulation was the suggestion of a flow rule stating that the principal axes of the strain increment coincide with the principal axes of stress. Levy in 1870 obtained the general equations in three dimensions. A generalization similar to that of Levy was given by von Mises in 1913 accompanied by his well-known pressure-insensitive yield criterion (J_2 theory). In 1924 Prandtl extended the St. Venant-Levy-von Mises equations for the plane continuum problem to include the elastic component of strain and Reuss in 1930 carried out their extensions to the three dimensions. In 1928 von Mises generalized his previous work for a rigid, perfectly plastic solid to include a general yield function and discussed the

relations between the direction of plastic strain rate and the regular and smooth yield surface, thus introducing the concept of using the yield function as a plastic potential in the incremental stress-strain relation of flow theory. Since greater work was placed on problems involving flow or perfect plasticity in the years before 1940, the development of incremental constitutive relationships foe hardening materials proceeded more slowly. The nearly twenty years after 1940 saw the most intensive period of development of basic concepts and fundamentals ingredients in what is now referred to as theory of metal plasticity.

Independently of the work of Milan in 1938, Prager, in a significant paper published in 1949, arrived at a general framework for the plastic constitutive relations for hardening materials with smooth (regular) yield surfaces. The yield function (also termed the loading function) and the loading-unloading conditions were precisely formulated. Such conditions as the continuity condition (near neutral loading), the consistency condition (for loading from plastic states), the uniqueness condition, and the condition of irreversibility of plastic deformation were formulated and discussed. Also, the interrelationship between the convexity of the (smooth) yield surface and the normality to the yield surface was clearly recognized. In 1958, Prager further extended this general framework to include thermal effects by allowing the yield surface to change its shape with temperature.

A very significant concept of work hardening, was proposed by Drucker in 1951 and amplified in his further papers.

Postulates providing assumptions which play an important role in the development of plasticity relations have been given by Hill in 1948, and extended by Bishop and Hill in 1951 in a study of polycrystalline aggregates.

Further generalization of the plastic stress-strain relations for singular yield surfaces (i.e., in the presence of corners or discontinuities in the direction of the normal vector to the yield surface), is due to Koiter published in 1953.

He introduced the device of using more than one yield (or loading) function in the stress-strain relationships, the plastic strain increment receiving a

contribution from each active yield (loading) surface and falling within the fan of normals to the contributing surfaces.

1.2 Literature Review

This section includes a literature review regarding the research that has been done since now on the influence of the first stress invariant and of the third deviatoric invariant of the stress tensor on the behavior of metals.

Maximum stress, maximum strain and Tresca theories are known from failure criteria that use one parameter to predict failure of structures. The experiments by Bridgman [1] show that the strain at ductile fracture initiation is affected by hydrostatic stress which also is known as stress triaxiality effect and after that several researches have been done that prove the effect of hydrostatic stress on failure of ductile materials. Some of these researches are based on the micromechanical methods by Mc Clintock [2], Rice and Tracey [3], Gurson [4] and Tvergaard and Needleman [5]. Another group is thermodynamics based methods that works by Lemaitre [6] and Chow and Wang [7,8] are some samples. Purely experimental methods, for example works by Atkins [9], Johnson and Cook [10] and Bao [11], is the third group.
Recently, it is understood that besides the effect of stress triaxiality, another parameter which is related to third invariant of deviatoric stress tensor has an effect on the fracture of ductile materials. This parameter which usually is known as Lode angle was studied by Wilkins et al. [12] in the field of ductile fracture. Later Wierzbicki and his colleagues, for example Wierzbicki et al. [13], have started a series of researches on the effect of Lode angle on the fracture initiation. Xue and Xue and Weirzbiki [14] have developed a fracture criterion with the effect of Lode angle and stress triaxiality. Their experiments show that in order to have more accurate results, it is necessary to combine the effects of Lode

angle and triaxiality factor. In this work the failure strain is calculated by multiplying two functions. One of these functions shows the effect of Lode angle and the other shows the effect of triaxiality. In a work by Bai and Weirzbicki [15] a general form of asymmetric metal plasticity considering both the pressure sensitivity (hydrostatic pressure) and the Lode dependence (Lode angle parameter) was presented. 21 experimental tests were performed on aluminum 2024-T351 to validate the new material model. Besides, a new 3D asymmetric fracture locus, in the space of equivalent fracture strain, stress triaxiality and the Lode angle parameter, was determined experimentally from two types of test procedures. One is based on classical round specimens or flat specimens in uniaxial tests, and the other one uses a series of tests on a double curvature butterfly specimen subjected to biaxial loading under different combination of tension/shear and compression/shear. Based on the results, a linear incremental dependence of the damage function D_{ep} on the equivalent plastic strain was shown to work well for monotonic loading. In the case of reverse straining or more complicated loading paths, a nonlinear incremental rule must be considered. Bai and Weirzbicki, according to experiments, suggested a fracture envelope in which fracture strain is an exponential function of triaxiality and a second order polynomial function of Lode angle. According to experiments and analysis done on aluminum 5083 alloy, by Gao et al. [16], failure strain is an exponential function of triaxiality while Lode angle does not have a considerable effect on the failure. In the paper by Gao, Zhang and Roe (2009) a fracture criterion was expressed in terms of the equivalent failure strain as a function of the stress triaxiality and the Lode angle by conducting a series of micromechanics analyses of void-containing unit cells to identify important parameters and show general trends. Besides, experimental studies were performed for a wide range of stress states. 7 different types of specimens were used in this study including smooth and notched round bars, plane strain specimens, plane stress specimens, Lindholm-type torsion specimen, and modified plane stress and plane strain specimens containing holes and/or cut

slots. Numerical modeling was carried out using the finite element software ABAQUS to analyze all the specimens. This failure function was further calibrated for a DH36 steel plate. The results showed that the numerical predictions agreed very well with experimental measurements for a wide range of specimens.

Coppola et al. [17] suggested that based on different values of Lode angle, different branches of failure strain as a function of triaxiality can be considered. In this paper, the dependence of ductile fracture and fracture limit ε_f in metals on the triaxiality level (T) of the stress tensor and the deviatoric parameter (X) of the stress state was studied. Several special fracture tests comprising tensile, torsion, flattening and bending have been devised to define the formability limits for three steel grades under different stress conditions. In addition, numerical simulations have been carried out to provide additional information whenever direct measures could not be feasible. The results stated that fracture limits in the ε_f – T plane can be confined between two boundary curves, characterized by two limits (X = 0 and X = 1) which are due to the application of Tresca criterion for shear failure and are linked together through the material hardening behavior. Furthermore, an asymmetry between tension and compression states could exist as a consequence of the proposed approach. The present results can be directly applicable to monotonic loading paths only, condition which is usually not verified on components of actual applications. For the damage evolution description in complex stress paths (non-proportional and non-monotonic), non-linear damage accumulation mechanisms may be present and, eventually, should be taken into account.

In the research done by Li et al. [18], a comprehensive review and comparison of the ductile failure models are done. In the latest study by Mirone and Corallo [19], it is found that, for the metals they tested, the hydrostatic stress has a significant role in failure, while the Lode angle does not affect the failure strains. The phenomenon of ductile failure was analyzed considering the influence of plastic strain, stress triaxiality and Lode angle parameters. In this study, different

metals (mild steel, stainless steel, pure copper and ASTM steel) and different combinations of load specimen geometry were considered according to three theories (the Tresca criteria and two models by Wierzbicki et al.) and to a procedure previously developed for the stress–strain characterization in the post-necking range. Experimental tests were performed by pulling tensile specimens and notched flat samples up to failure and finite element simulations were performed with the commercial code MSC-MARC to calculate the required failure related variables within the volume of failing specimens. According to the results, failure predictions according to the shear criterion by Tresca were not very accurate, while Wierzbicki models provided good results in predicting failure in terms of both global displacements and local strains. According to the results, within the ranges of triaxiality and Lode angle investigated, θ_N (normalized Lode angle) plays a minor role on the damage process. On the contrary, θ_N shows a considerable influence on the evolution of hardening while the neglected effect of triaxiality on the hardening was inferred to be negligible.

In a work done by Mirone et al. (2014) the failure of APIX-100 steel was experimentally investigated considering the effect of Lode angle along with triaxiality factor on the strain of the material ay failure. The experiments were performed on smooth and notched round bars and flat notched specimens with different notch radius. Simple tension tests up to failure have been performed on the specimens and deformations in different points and different directions were measured. Besides, a series of static, implicit, elastoplastic large deformation (updated Lagrangian) FE analysis were done using nonlinear commercial software MSC Marc to model the above mentioned specimens. The results of the experiments and FE analysis showed that failure strain decreases with TF_{avg}; moreover X_{avg} has no effect on failure strain, where the subscript “avg” implies the plastic strain averaged values of these two parameters.

In a work done by Bardet, 1990, [21] experimental investigations indicate that the third stress invariant; Lode angle α affects significantly the behavior of isotropic pressure-sensitive elastoplastic materials. Seven Lode dependences were reviewed. A new one, referred to as LMN, was proposed to generalize Lade and Duncan, and Matsuoka and Nakai failure surfaces. The performance of the modified model was estimated by comparing experimental and analytical results in the case of true triaxial loadings on normally consolidated clay.

In a paper by M. Alves and N. Jones [22] to investigate the role of the hydrostatic stress on failure, some static and dynamic tensile tests on mild steel axisymmetric notched specimens were performed. Finite Element results and experimental data indicated that the failure site for specimens having a small notch radius occurs in regions of low triaxiality. Comparisons are made between Finite Element and Bridgman analyses and the influence of some material parameters on the triaxiality levels was explored. According to finite element results, large errors are possible when the Bridgman analysis is used to predict stresses and strains at the minimum cross section of the notched specimens. It was observed that the actual value of the triaxiality is a material and geometric dependent parameter. The finite element simulation showed that the triaxiality is highest at the middle (r=0) of the minimum cross section of the notched specimens, regardless of the notch radius. Experimental result on the notched specimens pulled in tension at various speeds revealed that the average strain rate measured by the change in the necking diameter increases significantly, in some cases up to three orders of magnitude during a test. The present results suggest that the stress triaxiality is not the only fundamental parameter for the triggering of failure in the mild steel studied in this paper; the plastic strains appear to be important. It is suggested that a relationship between the stress triaxiality and the plastic strains might determine the actual location where failure commences.

2 Notation and Cartesian tensors

In this chapter it will be presented the set of notations that will be used. It is convenient to use both matrix and tensor notation depending on the particular application.

2.1 Matrix notation

In general, a matrix consists of a collection of certain quantities, which are termed the *components* of the matrix. The components are ordered in rows and columns and if the number of rows or columns is equal to one, the matrix is one-dimensional, otherwise it is two-dimensional. A treatment of matrix algebra can be found in many textbooks. The intention here is not to provide a resume of matrix algebra, but simply to present sufficient information of the notation used. A column matrix is denoted by a bold-face, usually lower-case letter, for instance

$$\mathbf{a} = \begin{bmatrix} a_1 \\ a_2 \\ a_3 \end{bmatrix} \qquad (2.1)$$

where a_1, a_2, a_3 are the components of the matrix **a**. The dimension of a matrix is given by the number of rows and columns, i.e. the column matrix **a** of (2.1) has the dimension 3x1. The transpose $\mathbf{a}^T$ of **a** is given by the row matrix:

$$\mathbf{a}^T = \begin{bmatrix} a_1 & a_2 & a_3 \end{bmatrix} \tag{2.2}$$

The length of **a** or $\mathbf{a}^T$ is denoted by $|\mathbf{a}|$ and we have

$$|\mathbf{a}| = \left(a_1^2 + a_2^2 + a_3^2\right)^{1/2} \tag{2.3}$$

The *scalar product* of two column matrices a and b having the same dimensions is defined according to

$$\mathbf{a}^T\mathbf{b} = \mathbf{a}\,\mathbf{b}^T = \begin{bmatrix} b_1 & b_2 & b_3 \end{bmatrix} \begin{bmatrix} a_1 \\ a_2 \\ a_3 \end{bmatrix} = b_1a_1 + b_2a_2 + b_3a_3 \tag{2.4}$$

where **a** and **b** in the present case are given by (2.1). Therefore, the length $|\mathbf{a}|$ of **a** can be written as

$$|\mathbf{a}| = (\mathbf{a}^T\mathbf{a})^{1/2} \tag{2.5}$$

A two-dimensional matrix is denoted by a bold-face, usually an upper-case letter, for instance

$$\mathbf{B} = \begin{bmatrix} B_{11} & B_{12} & B_{13} \\ B_{21} & B_{22} & B_{23} \\ B_{31} & B_{32} & B_{33} \end{bmatrix} \tag{2.6}$$

where **B** is termed a square matrix since the number of rows and columns is equal. The transpose $\mathbf{B}^T$ of **B** is obtained by interchanging rows and columns in **B**, i.e.

$$\mathbf{B}^T = \begin{bmatrix} B_{11} & B_{21} & B_{31} \\ B_{12} & B_{22} & B_{32} \\ B_{13} & B_{23} & B_{33} \end{bmatrix} \qquad (2.7)$$

and the matrix **B** is symmetric if $\mathbf{B} = \mathbf{B}^T$. The unit matrix **I** is defined

$$\mathbf{I} = \begin{bmatrix} 1 & 0 & 0 \\ 0 & 1 & 0 \\ 0 & 0 & 1 \end{bmatrix} \qquad (2.8)$$

A zero matrix is defined as a matrix where all components are zero. Examples are

$$\mathbf{0} = \begin{bmatrix} 0 & 0 & 0 \\ 0 & 0 & 0 \end{bmatrix}; \qquad \mathbf{0} = \begin{bmatrix} 0 \\ 0 \end{bmatrix} \qquad (2.9)$$

We note that the inverse $\mathbf{B}^{-1}$ of a square matrix **B** is defined by

$$\mathbf{B}^{-1}\mathbf{B} = \mathbf{B}\mathbf{B}^{-1} = \mathbf{I} \qquad (2.10)$$

and that $\mathbf{B}^{-1}$ exists if the determinant det**B** of **B** is different from zero. If det$\mathbf{B} \neq \mathbf{0}$, then **B** is nonsingular, otherwise it is singular. For matrices having the correct dimension the matrix product **AB** exists and we recall that

$$(\mathbf{AB})^T = \mathbf{B}^T\mathbf{A}^T \;; \qquad (\mathbf{AB})^{-1} = \mathbf{B}^{-1}\mathbf{A}^{-1} \qquad (2.11)$$

and for two square matrices we have:

$$\det(\mathbf{AB}) = \det \mathbf{A}\ \det \mathbf{B} \qquad (2.12)$$

For a square matrix **A**, consider the quantity $\mathbf{x^T Ax}$, which is a number; this quantity is called a quadratic form. If

$$\mathbf{x}^T \mathbf{A}\mathbf{x} > 0 \qquad \textit{for all } \mathbf{x} \neq \mathbf{0} \qquad (2.13)$$

then the matrix A is said to be positive definite. It is recalled that

$$\textit{If } \mathbf{A} \textit{ is positive definite then } \det \mathbf{A} \neq \mathbf{0}$$

We also mention that a matrix **A** is called positive semi-definite if

$$\mathbf{x}^T \mathbf{A}\mathbf{x} \geq 0 \qquad \textit{for all } \mathbf{x} \neq \mathbf{0}$$

2.2 Cartesian coordinate system

Whenever a coordinate system is employed in the following, we will for simplicity only make use of the standard orthogonal, rectangular and right-handed coordinate system shown in Fig. 2.1. The word rectangular signifies that the coordinate axes are straight orthogonal lines. For reasons that will be unfolded in a moment we label the coordinate axes by x_1, x_2 and x_3 instead of the usual notation of x, y and z.

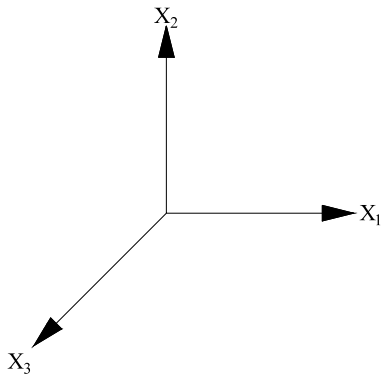

Figure 2.1: Cartesian coordinate system

In order to maintain the standard definition of distance between two points in this coordinate system, the unit length along all the coordinate axes is equal to the unit length scale. Such a coordinate system is termed a Cartesian coordinate system in recognition of the French philosopher and mathematician Descartes (1596-1650), whose Latin name is Cartesius and who introduced the concept of a coordinate system. It is obvious that a certain set of coordinates, i.e. a certain set of x_1, x_2 and x_3-values defines uniquely the position of a point in the coordinate system.

2.3 Index notation

Index notation is often used in tensor algebra and it is therefore often termed as tensor notation. Index notation implies that complicated expressions can be written in a very compact fashion that emphasizes the physical content of these expressions and greatly facilitates mathematical manipulations.

The coordinate axes x_1, x_2 and x_3 in Fig. 2.1 can be written more briefly as x_i, where the index i takes the values i = 1, 2 and 3. The column matrix a given by (2.1) can then be written as $[a_i]$ where the brackets [ ] around a_i emphasize that we in the present case interpret the quantity a_i as a matrix. Therefore

$$\mathbf{a} = [a_i] = \begin{bmatrix} a_1 \\ a_2 \\ a_3 \end{bmatrix} \qquad (2.14)$$

where, again, the index i takes the values 1, 2 and 3. In what follows, Latin indices, unless otherwise specified, assume the values 1, 2 and 3, on the other hand, Greek indices will extend over a range to be specified in each case. If reference is made to a_i we refer to the entire quantity given by a_i, whereas a specific component of a_i like the one given by, for instance, i = 2 is referred to as a_2.

An important convention in index notation is the so-called summation convention, which states that if an index is repeated twice then a summation over this index is implied. As an example, the product $b_i\, a_i$, where the index i is repeated twice, means:

$$b_i a_i = b_1 a_1 + b_2 a_2 + b_3 a_3$$

and a comparison with (2.4) shows that $\mathbf{b}^T\mathbf{a} = b_i a_i$. It is also a convention in index notation that an index cannot be repeated more than twice. If it is repeated twice, it is called a dummy index and if it is not repeated, it is called agree index, i.e

$$index \rightarrow \begin{array}{c} \circ \textit{ free if it appears once} \\ \circ \textit{ dummy if it appears twice} \end{array}$$

An index can only be free or dummy

It is obvious that the specific letter used for a dummy index is immaterial and we have, for instance, $b_i a_i = b_k a_k$. However, for a free index the specific letter used is of extreme importance. It should also be noted that whereas the position of a quantity in a matrix expression is of significance - we have for example $\mathbf{b}^T\mathbf{a} \neq \mathbf{b}\mathbf{a}^T$ - this is not the case in index notation where, for instance, $b_i a_i = a_i b_i = \mathbf{a}^T\mathbf{b} = \mathbf{b}^T\mathbf{a}$.

It is also possible to work with quantities having two indices and it is evident that the matrix **B** given by (2.3) can be written as

$$\mathbf{B} = [B_{ij}] = \begin{bmatrix} B_{11} & B_{12} & B_{13} \\ B_{21} & B_{22} & B_{23} \\ B_{31} & B_{32} & B_{33} \end{bmatrix}$$

where the brackets [ ] around B_{ij} again emphasize that in the present case we interpret the quantity B_{ij} as a matrix.

Using the summation convention, it follows that the inhomogeneous equation system **Bx=a** can be written as $B_{ij}x_j = a_i$ and that

$$B_{ii} = B_{11} + B_{22} + B_{33}$$

From the rules defined, it follows that each term in an expression must possess the same number of free indices, i.e. whereas $B_{ij}x_j=a_i$ is a valid expression, the formulations $B_{ij}x_j=C$ and $B_{ij}x_j=A_{ij}$ are invalid. The operation, where two free indices are made equal to each other, so that a dummy index arises, is called contraction. As an example, contraction of A_{ij} gives A_{ii}.

The Kronecker delta δ_{ij} plays an essential role in index notation and tensor algebra and it is defined as

$$\delta_{ij} = \begin{matrix} 1 \; if \; i = j \\ 0 \; if \; i \neq j \end{matrix} \qquad (2.15)$$

i.e. it is equal to the unit matrix **I** given by (2.8). Using the summation convention it follows that

$$B_{ij}\delta_{jk} = B_{ik} \qquad (2.16)$$

This result follows from the fact that δ_{ij} only contributes with the value of unity provided that j and k takes the same value. Alternatively, the trivial use of the summation convention yields

$$B_{ij}\delta_{jk} = B_{i1}\delta_{1k} + B_{i2}\delta_{2k} + B_{i3}\delta_{3k}$$

and an evaluation of this relation for each i- and k-value results in expression (2.16). Another example of the use of Kronecker's delta arises from the matrix equation **AB = I**. In index notation this is written as

$$A_{ik}B_{kj} = \delta_{ij}$$

which shows that A_{ik} is the inverse of B_{ik}, cf. (2.10). A final important illustration of the use of Kronecker's delta is the expression

$$\frac{\partial a_i}{\partial a_j} = \delta_{ij}$$

This identity follows from the fact that

$$\partial a_i / \partial a_j = \begin{matrix} 0 \ if \ \ i \neq j \\ 1 \ if \ \ i = j \end{matrix}$$

In accordance with the matrix notation, it follows that the quantity M_{ij} is symmetric if

$$M_{ij} = M_{ji}$$

Moreover, a quantity N_{ij} is termed *anti-symmetric* or *skew-symmetric* if

$$N_{ij} = -N_{ji}$$

This implies that all diagonal terms in N_{ij} are equal to zero. Suppose we have an arbitrary quantity P_{ij}. It is always possible to write N_{ij}, according to

$$P_{ij} = P_{ij}^s + P_{ij}^a \qquad (2.17)$$

where the symmetric part $P_{ij}{}^s$ of P_{ij} is defined by

$$P_{ij}^s = \frac{1}{2}(P_{ij} + P_{ij}) \qquad (2.18)$$

and the anti-symmetric part $P_{ij}{}^a$ of P_{ij} is defined by

$$P_{ij}^a = \frac{1}{2}(P_{ij} - P_{ji}) \qquad (2.19)$$

A problem often encountered is the multiplication of a symmetric quantity $A_{ij}{}^s$ with a quantity B_{ij} not necessarily symmetric. It turns out that

$$A_{ij}^s B_{ij} = A_{ij}^s B_{ij}^s$$

A so-called comma convention is also used in index notation. It states that whenever a quantity is differentiated with respect to the coordinates x_i, we use a comma to indicate this differentiation. Examples are

$$\frac{\partial f}{\partial x_i} = f_{,i} \qquad \frac{\partial a_i}{\partial x_j} = a_{i,j}$$

It is finally observed that in matrix notation we are restricted to working with one- and two-dimensional arrays. This is not the case in index notation where, for instance, the quantity e_{ijk} exists and comprises 3x3x3=27 components. Likewise, the quantity D_{ijkl} exists and comprises 3x3x3x3=81 components.

2.4 Cartesian tensors

Now it will be presented a discussion of the concept of tensors and why they appear naturally when formulating physical relations. As we only use Cartesian coordinate systems, no difference exists between so-called covariant and contravariant tensors and therefore, by a tensor we always mean a Cartesian tensor.

As previously mentioned, the essential issue of a tensor is that it behaves in a certain manner when a change of coordinate system is performed. We shall now establish this relation.

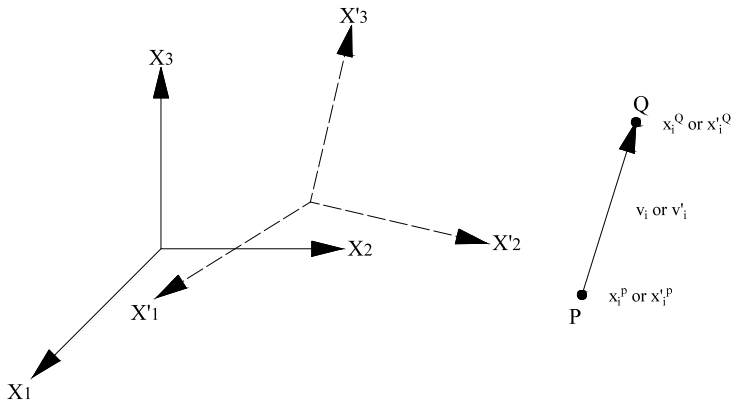

Figure 2.2: vector from P to Q

We define a vector in the usual manner as a quantity having a length and a direction. In Fig. 2.2, the two fixed points *P* and *Q* have the coordinates x_i^P and x_i^Q in the old coordinate system and the coordinates x'^P_i and x'^Q_i in the new x'_i-coordinate system. The components of the vector v_i from *P* to *Q* in the old x_i-system are then given by

$$v_i = x_i^Q - x_i^P \qquad (2.20)$$

where v_1, v_2 and v_3 are the components of the vector in the x_1, x_2 and x_3 direction respectively. Likewise, the components of the vector v'_i from P to Q measured in the new x'_i-system are given by

$$v'_i = x'^{Q}_i - x'^{P}_i \qquad (2.21)$$

where v'_1, v'_2 and v'_3 are the components of the vector in the x'_1, x'_2 and x'_3 direction respectively. We have then

$$x'^{Q}_i = A_{ij}x^{Q}_j - c_i \qquad x'^{P}_i = A_{ij}x^{P}_j - c_i$$

Insertion into (2.21) and recognition of (2.20) result in

$$v'_i = A_{ij}v_j \qquad or \qquad \mathbf{v'=Av} \qquad (2.22)$$

We have now established the important relation that shows how the components of a vector changes if a coordinate transformation is made. Here we have derived (2.22) from the usual definition of a vector, but we will now define a quantity v_i as a vector if it transforms according to (2.22). A vector is also called a first-order tensor, where first order refers to the fact that v_i only possesses one index. Now we have an indication of the statement expressed previously that tensors are quantities, which behave in a certain manner when a coordinate change is performed. It is of extreme importance that whereas any quantity containing three pieces of information can be written in the index form b_i, this does not make b_i, a vector i.e. a first-order tensor as b_i, will not, in general, transform according to (2.22). As an example, assume that **a** is a vector and consider the quantity $b_i = (|\mathbf{a}|, \theta_1, \theta_2)$ where $|\mathbf{a}|$ = the length of **a**, θ_1 = the angle between **a** and the x_1-axis and θ_2 = the angle between **a** and the x_2-axis. In this case, b_i is certainly not a vector, since each of the components of b_i maintains its value irrespectively of the coordinate system, i.e. b_i does not fulfill the transformation

rule (2.22). It is now apparent why we have chosen to use the name column matrix for **a** given by (2.1). Even though a vector a_i can be written in the same manner, the column matrix **a** is not necessary a vector. Multiplication by A_{ik} gives $v_k=A_{ik}v'_I$ i.e.

$$v_i = A_{ji}v'_j \qquad or \qquad \mathbf{v}=\mathbf{A}^T\mathbf{v}' \tag{2.23}$$

As indicated below, it is easy to show formally that velocity and acceleration vectors indeed are vectors. Consider a specific panicle of a body. This particle is described by its coordinates, which are functions of time, i.e. $x_i=x_i(t)$ where t is the time. The velocity components v_i are then defined by

$$v_i = \dot{x}_i \tag{2.24}$$

where a dot denotes the derivative with respect to time and v_1, v_2 and v_3 are the components of v_i in the x_1, x_2 and x_3 direction respectively. Likewise, in a new coordinate system the velocity v'_i is defined by

$$v_i' = \dot{x}'_i \qquad (2.25)$$

Differentiating (2.22) with respect to time and assuming that v_i is the velocity vector it appears that also the acceleration vector is, in fact, a vector.

As a force vector is defined as a quantity having a length and direction it follows in complete analogy with (2.20) and (2.21), which lead to (2.22), that a force vector is, in fact, a vector.

We have already touched upon quantities containing one piece of information and which take the same value irrespectively of the coordinate system. Such a quantity b is called a scalar, an invariant or a zero-order tensor and it transforms according to

$$b' = b$$

i.e. it takes the same value in the old coordinate system x_i and in the new coordinate system x'_i.

We have dwelt on the fact that tensors are quantities, which transform in a particular manner when coordinate changes are made. It is now timely to ask why tensors are of relevance for our present purpose. The reason for this is of extraordinary importance, because it turns out that the relations of physics are conveniently expressed in terms of tensors. To illustrate this important aspect we write Newton's second law for a particle in the old coordinate system x_i according to

$$F_i = ma_i \qquad (2.26)$$

where F_i is the force vector, m is the mass and a_i the acceleration vector. The vectors F_i and a_i are interpreted in the usual way that, for instance, F_2 is the component of F_i in the x_2 direction. When writing (2.26), we did not specify our coordinate system in any manner so in another coordinate system x'_i, we expect that Newton's second law takes the form $F'_i=m'a'_i$ i.e.

$$F'_i = ma'_i \qquad (2.27)$$

where it has been assumed that the mass m is an invariant, i.e. independent of the coordinate system. As F_i and a_i are vectors, they transform according to (2.22) i.e. we have

$$F'_j = A_{ji}F_i \qquad a'_j = A_{ji}a_i$$

Multiply (2.26) by A_{ji} and use the expressions above to obtain

$$F'_j = ma'_j$$

which is precisely the form stipulated in (2.27). It appears that irrespectively of the coordinate system, we write Newton's law in the same form, either (2.26) or (2.27), and this is possible only because F_i and a_i, in fact, are vectors, i.e. first-order tensors and because the mass m is an invariant, i.e. a zero-order tensor. Therefore, the occurrence of vectors and scalars in physical relations is a result of the fact that we expect physical laws to be independent of the particular coordinate system we choose to work with.

Above we illustrated that if a quantity like b_i appears in a physical relation, we expect it to be a vector. Let us pursue the argument above and assume that we have a physical relation, which in the x_i-coordinate system states that

$$b_i = B_{ij} c_j \tag{2.28}$$

where b_i, and c_i are assumed to be vectors and B_{ij} some quantity. When writing (2.28) we did not specify our coordinate system in any manner, so we expect that in another coordinate system x'_i the same physical relation is expressed through

$$b'_i = B'_{ij} c'_j \tag{2.29}$$

Or

$$b'_k = B'_{kl} c'_l \tag{2.30}$$

Multiply (2.29) by A_{ki} and use (2.22) to obtain

$$b'_k = A_{ki} B_{ij} c_j \tag{2.31}$$

Transformation of c_j according to (2.23) yields

$$b'_k = A_{ki} B_{ij} A_{lj} c'_l \tag{2.32}$$

Subtraction of (2.30) and (2.32) provides

$$(B'_{kl} - A_{ki} B_{ij} A_{lj}) c'_l = 0 \tag{2.33}$$

This expression should hold for arbitrary c'_l values and B_{ij} must therefore transform according to

$$B'_{kl} = A_{ki}B_{ij}A_{lj} \qquad \textbf{or} \qquad \mathbf{B'=ABA}^T \tag{2.34}$$

We have found that if it is allowable to write a physical relation as (2.30) in one coordinate system and as (2.31) in another coordinate system, then the quantity B_{ij} must transform according to (2.34). A quantity B_{ij}, which transforms according to (2.34), is defined to be a second-order tensor. It is obvious that whereas any square matrix containing 3x3 components can be written in index notation as B_{ij}, this does not make B_{ij} a second-order tensor. Only those B_{ij} quantities, which transform according to (2.34), are second-order tensors.

We started with (2.30) where b_i and c_i were assumed to be vectors and B_{ij} some quantity. We then concluded that B_{ij} must be a second-order tensor, which transforms according to (2.34). This conclusion is an example of the use of the so-called quotient theorem.

Multiplication of (1.41) by A_{km} gives

$$A_{km}B'_{kl} = B_{mj}A_{il}$$

and multiplication by A_{in} yields

$$B_{mn} = A_{km}B'_{kl}A_{in}$$

which can be written as

$$B_{kl} = A_{lk}B'_{ij}A_{jl} \qquad or \qquad \mathbf{B=A}^T\mathbf{B'A} \tag{2.35}$$

Let us finally consider the following physical relation expressed in the x_i coordinate system by

$$B_{ij} = D_{ijkl}M_{kl}$$

where B_{ij} and M_{kl} are assumed to be second-order tensors. In the x'_i coordinate system we expect the relation

$$B'_{ij} = D'_{ijkl} M'_{kl}$$

If this is true, then by arguments like before, it is easily shown that the quantity D_{ijkl} must transform according to

$$D'_{ijkl} = A_{im} A_{jn} D_{mnpq} A_{kp} A_{iq} \qquad (2.36)$$

Such a quantity is defined as a fourth-order tensor. It follows in a straightforward manner that

$$D_{ijkl} = A_{mi} A_{nj} D'_{mnpq} A_{pk} A_{ql}$$

Matrix formulations are often used instead of tensors, the main reason being that matrices are convenient when it comes to numerical computations. Often, tensors are used to derive the general relations governing the specific problem investigated and hereafter a corresponding matrix formulation is obtained from the tensor formulation. All boldface letters, like **A**, shall be viewed as matrices.

3 Strain Tensor

It is essential to establish a quantity that only describe the deformation of the body, i.e. it should not be influenced by any rigid-body motions. Such a quantity is the strain tensor. It will be presented now a derivation of a number of properties of the strain tensor not only because of the importance of these properties but also because it turns out that many of the properties can be transferred directly to the stress tensor, which is treated in the next chapter.

3.1 Displacement

A body is said to be modeled as a continuum if to any configuration of the body there corresponds a region R in three-dimensional space such that every point of the region is occupied by a particle (maternal point) of the body.
Any configuration may be taken as the reference configuration. Consider a particle that in this configuration occupies the point defined by the vector x_i. When the body is displaced, the same particle will occupy the point x^*_i given by

$$x^*_i = x_i + u_i \tag{3.1}$$

The difference $x^*_i - x_i$ is called the displacement of the particle and will be denoted u_i. The reference position vector **x** will be used to label the given particle, the coordinates x_i, are then called Lagrangian coordinates. Consequently the displacement may be given as a function of **x**, **u**(**x**), and it forms a vector field defined in the region occupied by the body in the reference configuration.
Now consider a neighboring particle labeled by **x**+**Δx**. In the displaced configuration, the position of this point will be

$$\mathbf{x}^* + \Delta\mathbf{x}^* = \mathbf{x} + \Delta\mathbf{x} + \mathbf{u}(\mathbf{x} + \Delta\mathbf{x}) \tag{3.2}$$

so that

$$\Delta\mathbf{x}^* = \Delta\mathbf{x} + \mathbf{u}(\mathbf{x} + \Delta\mathbf{x}) - \mathbf{u}(\mathbf{x}) \tag{3.3}$$

or in indicial notation,

$$\Delta x^*_i = \Delta x_i + u_i(\mathbf{x} + \Delta\mathbf{x}) - u_i(\mathbf{x}) \tag{3.4}$$

But if Δx is sufficiently small, then $u_i(\boldsymbol{x}+\boldsymbol{\Delta x})-u_i(\boldsymbol{x})=u_{i,j}(\boldsymbol{x})\Delta x_j$, the error in the approximation being such that it tends to zero faster than $|\boldsymbol{\Delta x}|$. It is conventional to replace $\boldsymbol{\Delta x}$ by the infinitesimal $d\boldsymbol{x}$, and then to write the approximation as an equality. Defining the displacement-gradient matrix $\boldsymbol{\alpha}$ by $\alpha_{ij} = u_{ij}$, we may write in matrix notation

$$d\mathbf{x}^* = (\mathbf{I} + \boldsymbol{\alpha})d\mathbf{x} \tag{3.5}$$

3.2 Deformation

A body is said to undergo a rigid-body displacement if the distances between all particles remain unchanged; otherwise the body is said to be deformed. Let us limit ourselves, for the moment, to an infinitesimal neighborhood of the particle labeled by ***x***; the deformation of the neighborhood may be measured by the extent to which the length of the infinitesimal vectors ***dx*** emanating from ***x*** change in the course of the displacement. The square of the length of ***dx**** is

$$\left|d\mathbf{x}^*\right|^2 = d\mathbf{x}^* \cdot d\mathbf{x}^* = d\mathbf{x}^T(\boldsymbol{I}+\boldsymbol{\alpha}^T)(\boldsymbol{I}+\boldsymbol{\alpha}^T)d\mathbf{x} = d\mathbf{x}^T(\boldsymbol{I}+2\boldsymbol{E})d\mathbf{x} \qquad (3.6)$$

where

$$\boldsymbol{E} = \frac{1}{2}(\boldsymbol{\alpha}^T + \boldsymbol{\alpha} + \boldsymbol{\alpha}^T\boldsymbol{\alpha}) \qquad (3.7)$$

or, in indicial notation

$$E_{ij} = \frac{1}{2}\left(u_{i,j} + u_{j,i} + u_{k,i}u_{k,j}\right) \qquad (3.8)$$

which defines the symmetric second-rank strain tensor ***E***, known as the Green-St. Venant strain tensor. Clearly ***E(x)*** describes the deformations of the infinitesimal neighborhood of ***x***, and the tensor field ***E*** that of the whole body; ***E(x)=0*** for all ***x*** in R if and only if the displacement is a rigid body one. The deformation of a region R is called homogeneous if ***E*** is constant. It is obvious that a necessary and sufficient conditions for the deformation to be homogeneous is that $u_{i,j}$ are constant, or equivalently, that ***u*** varies linearly within ***x***.

Here we have described the displacement vector u_i as function of its position x_i before any deformations, i.e. $u_i=u_i(x_i, t)$ and such an approach is called a

Lagrangian description. For that reason E_{ij} is often called Lagrange's strain tensor (occasionally, in the literature it is called the Green-Lagrange strain tensor, in fact, it was introduced by Green in 1841 and by St.-Venant in 1844).

The alternative approach is the Eulerian description, often employed in fluid mechanics, where the displacement vector u_i is given as function of the current coordinates x^*_i i.e. $u_i=u_i(x^*_i, t)$.

That E_{ij} is, indeed, a second-order tensor follows from the fact that u_i is a vector and $u_{i,j}$ therefore is a second-order tensor.

3.3 Small strain tensor

In the following, we will only consider situations where the displacement gradients $u_{i,j}$ are small, i.e. each component is small when compared to unity

$$\left|u_{i,j}\right| << 1$$

In that case, the quadratic term in (3.6) can be ignored and the Lagrange strain E_{ij} can be approximated by the small strain tensor ε_{ij} defined by

$$\varepsilon_{ij} = \frac{1}{2}(u_{i,j} + u_{j.i}) \qquad (3.9)$$

which is also symmetric, i.e.

$$\varepsilon_{ij} = \varepsilon_{ji}$$

It is obvious that E_{ij} is a second-order tensor.

3.4 Rigid-body motions

Our aim was to establish a quantity, the strain tensor, that is independent of rigid-body motions. Let us now prove that E_{ij} possesses this property. Any rigid-body motion is characterized by the fact that during motion, the vector PQ of two neighboring material points changes into the vector P^*Q^* in such a way that its

length remains constant. As $ds = |PQ|$ and $ds^* = |P^* Q^*|$, we can then write that during any rigid-body motion, we have

$$ds^{*2} - ds^2 = 0$$

Making use of (3.6) and (3.8) and noting that dx_i is arbitrary, we conclude that

$$2E_{ij} = u_{i,j} + u_{j,i} + u_{k,i}u_{k,j}$$

We observe that Green-Lagranges strain tensor is unaffected by rigid-body motions and within our approximation of small displacement gradients we have $E_{ij} = \varepsilon_{ij}$, i.e. rigid-body motions do not influence the small strain tensor, which proves the desired property of this strain tensor.

3.5 Physical significance of the strain tensor

We shall now evaluate the physical significance of the strain tensor ε_{ij} and its components. Within our assumption of small displacement gradients, we have $E_{ij} = \varepsilon_{ij}$, i.e. (3.6) reads

$$\frac{ds^{*2} - ds^2}{ds^2} = 2\frac{dx_i}{ds}\varepsilon_{ij}\frac{dx_j}{ds}$$

where ds is the length of the vector dx_i between the two neighboring particles P and Q before any deformation takes place and ds^* is the distance between these two particles after the deformation. Therefore

$$n_i = \frac{dx_i}{ds}$$

is a unit vector in the direction of dx_i. From this expression and (3.9) follow that

$$\frac{ds^{*2} - ds^2}{2ds^2} = n_i \varepsilon_{ij} n_j \qquad (3.10)$$

As the displacement gradients are small the components of E_{ij} are also small and this implies that the left-hand side of (3.10) is small. Consequently ds^* is close to ds and we then obtain

$$\frac{ds^{*2} - ds^2}{2ds^2} = \frac{(ds^* + ds)(ds^* - ds)}{2ds^2} \approx \frac{2ds(ds^* - ds)}{2ds^2} = \frac{(ds^* - ds)}{ds}$$

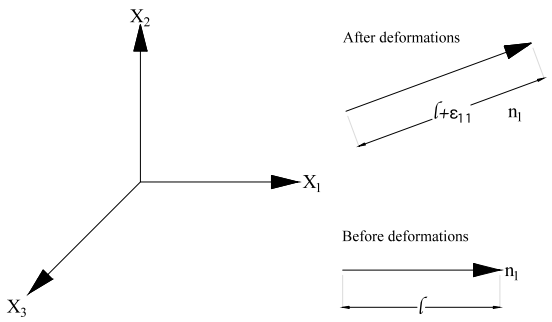

Figure 3.1: strain component ε_{11}

We define the relative elongation or the normal strain ε of the vector PQ deforming into the P^*Q^* vector, by

$$\varepsilon = \frac{(ds^* - ds)}{ds} \tag{3.11}$$

in accordance with the elementary definition of normal strain. A combination of (3.10) and (3.11) yields

$$\varepsilon = n_i \varepsilon_{ij} n_j \qquad \textbf{or} \qquad \boldsymbol{\varepsilon} = \mathbf{n}^T \boldsymbol{\varepsilon} \mathbf{n} \tag{3.12}$$

As an example, choose the direction n_i so that $n_i=(1, 0, 0)$, then we obtain $\varepsilon=\varepsilon_{11}$ as illustrated in Fig. 3.1. Likewise, $n_i=(0, 1, 0)$, we obtain $\varepsilon=\varepsilon_{22}$ whereas $n_i=(0, 1, 0)$, yields $\varepsilon=\varepsilon_{33}$. Therefore, we have achieved a physical interpretation of all the diagonal terms of the strain tensor and it appears from **Errore. L'origine riferimento non è stata trovata.** that the normal strain, i.e. the relative elongation, in an arbitrary direction given by the unit vector n_i, is known once the strain tensor is known.

To obtain a physical interpretation of the off-diagonal terms in the strain tensor, consider two directions $dx_i^{(1)}$ and $dx_i^{(2)}$ in the reference configuration before any deformations take place. These two directions are taken to be orthogonal, i.e.

$$dx_i^{(1)} dx_i^{(2)} = 0 \qquad (3.13)$$

In accordance with Fig. 3.2, the lengths of $dx_i^{(1)}$ and $dx_i^{(2)}$ are given by $ds^{(1)}$

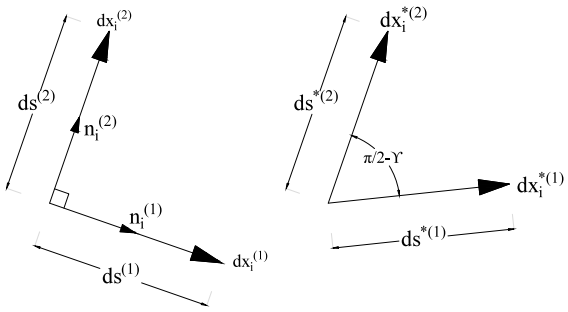

Figure 3.2: change of orthogonal angle in reference configuration due to the deformation

and $ds^{(2)}$ respectively, i.e. we have the following two orthogonal unit vectors

$$n_i^{(1)} = \frac{dx_i^{(1)}}{ds^{(1)}}; \qquad n_i^{(2)} = \frac{dx_i^{(2)}}{ds^{(2)}} \tag{3.14}$$

Due to the deformation, the vector $dx_i{}^{(1)}$ changes to $dx^*{}_i{}^{(1)}$ with length $ds^{*(1)}$ whereas the vector $dx_i{}^{(2)}$ changes to $dx^*{}_i{}^{(2)}$ with length $ds^{*(2)}$, cf. Fig. 3.2. The angle $90°\text{-}\gamma$ between $dx^{*(1)}$ and $dx^{*(2)}$ is then given by

$$\cos(90° - \gamma) = \frac{dx^*{}_i^{(1)}}{ds^{*(1)}} \frac{dx^*{}_i^{(2)}}{ds^{*(2)}} \tag{3.15}$$

From (3.5) we have

$$dx^*{}_i^{(1)} = (\delta_{ij} + u_{i,j})dx_j^{(1)}; \qquad dx^*{}_i^{(2)} = (\delta_{ik} + u_{i,k})dx_k^{(2)}$$

Insertion into (3.15) yields

$$\sin\gamma = (\delta_{ik} + u_{k,j} + u_{j,k} + u_{i,j}u_{i,k}) \frac{dx_j^{(1)}}{ds^{*(1)}} \frac{dx_k^{(2)}}{ds^{*(2)}} \tag{3.16}$$

Due to the small strain approximation, we can ignore the quadratic term and set $ds^{*(1)} \approx ds^{(1)}$ and $ds^{*(2)} \approx ds^{(2)}$ Consequently, (3.16) reduces with (3.9) to

$$\sin\gamma = \frac{dx_k^{(1)}}{ds^{(1)}} \frac{dx_k^{(2)}}{ds^{(2)}} + 2\varepsilon_{jk} \frac{dx_j^{(1)}}{ds^{(1)}} \frac{dx_j^{(2)}}{ds^{(2)}}$$

As we assume small strains we have sinγ ≈ γ. With (3.13) and (3.14) we then obtain

$$\gamma = 2\varepsilon_{jk} n_j^{(1)} n_k^{(2)}$$

To emphasize that the vectors $n_i^{(1)}$ and $n_i^{(2)}$ are orthogonal, we ante $m_i = n_i^{(1)}$ and $n_i = n_i^{(2)}$ and the expression above takes the more convenient form

$$\gamma = 2 m_i \varepsilon_{ij} n_j \qquad (3.17)$$

Hence, due to the deformation the right angle between the unit vectors n_i and m_i in the reference configuration decreases by the amount γ given by (3.17).
As an example, choose $n_i = (1, 0, 0)$ then $\varepsilon_{ij} n_j$ becomes $\varepsilon_{ij} n_j = \varepsilon_{i1}$. If we then choose $m_i = (0, 1, 0)$, we obtain $\gamma = 2\varepsilon_{21}$ and if we choose $m_i = (0, 0, 1)$, we obtain $\gamma = 2\varepsilon_{31}$ I.e. $2\varepsilon_{21}$ is the decrease of the angle between the x_2 and x_1 axes due to deformation, whereas $2\varepsilon_{31}$ is the decrease of the angle between the x_3 and x_1 axes. A similar evaluation holds for $2\varepsilon_{32}$. These off-diagonal terms of the strain tensor are called shear strains as they describe the shearing, i.e. the distortion of the material. With obvious notation we can then write

$$\gamma_{nm} = 2\varepsilon_{nm}$$

where

$$\varepsilon_{nm} = n_i \varepsilon_{ij} m_j = m_i \varepsilon_{ij} n_j \qquad or \qquad \varepsilon_{nm} = \mathbf{n}^T \boldsymbol{\varepsilon} \mathbf{m} = \mathbf{m}^T \boldsymbol{\varepsilon} \mathbf{n} \qquad (3.18)$$

In this expression n_i and m_i are arbitrary unit vectors, which are orthogonal in the reference configuration. The angle decrease γ_{nm} between n_i and m_i caused by the deformation is termed the engineering shear strain to be distinguished from the

tensorial shear strain ε_{nm}. The shearing between two directions parallel with the x_1 and x_2 axes is illustrated in Fig. 3.4.

It appears that the strain tensor contains information by which relative elongation in arbitrary directions and angle changes between arbitrary orthogonal directions can be determined. Consequently, the strain tensor describes the deformation completely and, in addition, we have achieved a direct physical interpretation of all the components of this tensor. These results were already obtained by Cauchy in 1822.

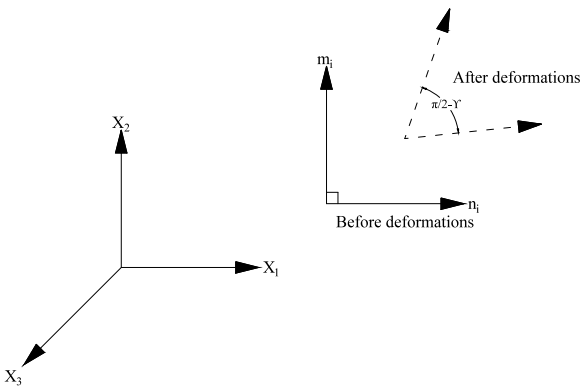

Figure 3.3: illustration of shear component $\varepsilon_{12}=\gamma_{12}/2$

3.6 Change of coordinate system

The implications of coordinate system changes are important in many connections and we have already discussed this aspect in detail in Chapter 1. Let us consider the change from the old xi-coordinate system to the new x-coordinate system. We have

$$x'_i = A_{ij}(x_j - c_i) \qquad or \qquad \mathbf{x}' = \mathbf{A}(\mathbf{x} - \mathbf{c}) \tag{3.19}$$

where A_{ij} is the transformation matrix. Suppose that we know the components of ε_{ij} in the x_i system and suppose that we want to determine the components of ε'_{ij} in the x'_i system. We have already proved that ε_{ij} is a second-order tensor, i.e. it follows directly from (2.34) that

$$\varepsilon'_{ij} = A_{ik}\varepsilon_{kl}A_{jl} \qquad or \qquad \boldsymbol{\varepsilon}' = \mathbf{A}\boldsymbol{\varepsilon}\mathbf{A} \tag{3.20}$$

The inverse relations follow from (2.35), i.e.

$$\varepsilon_{ij} = A_{ik}\varepsilon'_{kl}A_{jl} \qquad or \qquad \boldsymbol{\varepsilon} = \mathbf{A}\boldsymbol{\varepsilon}'\mathbf{A} \tag{3.21}$$

3.7 Principal strains and principal directions – Invariants

We have previously obtained a physical interpretation of the strain tensor components. However, it turns out that for a special choice of coordinate system, the strain tensor takes a particularly simple form. For this purpose, consider a direction in the reference configuration given by the unit vector ***n***. We then define the vector ***q*** by

$$\boldsymbol{q}=\boldsymbol{\varepsilon}\boldsymbol{n} \tag{3.22}$$

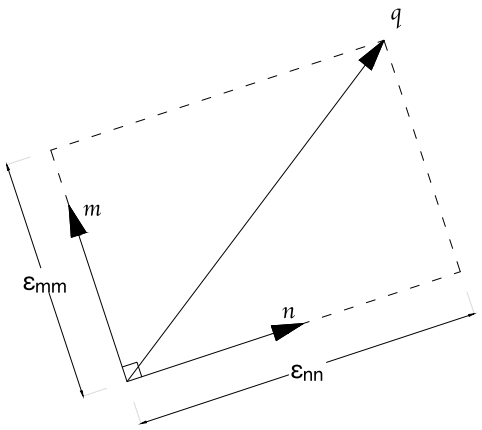

*Figure 3.4: the vector **q**=**εn** and its components after direction **n** and **m***

Referring to Fig. 3.4, the unit vector ***m*** is orthogonal to ***n***. Following Fig. 3.4 and in accordance with **Errore. L'origine riferimento non è stata trovata.** and (3.21) the component of ***q*** in the direction of ***n*** is given by

$$\varepsilon_{nn} = \mathbf{n}^T \mathbf{q} \qquad (3.23)$$

where ε_{nn} is the normal strain in the direction ***n***. Likewise from (3.18) and (3.21) the component of ***q*** in the direction of ***m*** is given by

$$\varepsilon_{nm} = \mathbf{m}^T \mathbf{q}$$

where ε_{nm} is the shear strain between the directions ***n*** and ***m***. We now look for the situation where the direction ***n*** is chosen so that ***q*** is collinear with ***n***, i.e. the shear strain $\varepsilon_{nm} = 0$. To achieve this situation, we must have

$$\mathbf{q} = \lambda \mathbf{n} \qquad (3.24)$$

where λ is an unknown parameter and from (3.23) we conclude that $\varepsilon_{nn}=\lambda$.
Use of (3.21) in (3.24) yields the following requirement

$$(\boldsymbol{\varepsilon}-\boldsymbol{\lambda}\mathbf{I})\mathbf{n}=\mathbf{0} \qquad or \qquad (\varepsilon_{ij}-\lambda\delta_{ij})n_j=0 \tag{3.25}$$

where $\boldsymbol{0}$ is defined as $\boldsymbol{0}^{\mathrm{T}}=[0\ 0\ 0]$.
Expression (3.25) is an example of the well-known eigenvalue problem. It consists of a quadratic set of homogeneous equations and if a nontrivial solution $\boldsymbol{n}$ is to exist, we must require

$$\det(\boldsymbol{\varepsilon}-\boldsymbol{\lambda}\mathbf{I})=\mathbf{0} \tag{3.26}$$

As $\boldsymbol{\varepsilon}$-$\lambda\boldsymbol{I}$ is a 3 x 3 matrix, the expression above provides a cubic equation for the determination of λ - the so-called characteristic equation. That is, (3.26) is fulfilled by three values of λ - the eigenvalues λ_1, λ_2 and λ_3.When λ_1, λ_2 and λ_3 have been determined, then substitution of λ_1 in (3.25) provides the solution $\boldsymbol{n}_1$, substitution of λ_2 provides the solution $\boldsymbol{n}_2$ and substitution of λ_3 provides the solution $\boldsymbol{n}_3$.
The solutions $\boldsymbol{n}_1$, $\boldsymbol{n}_2$ and $\boldsymbol{n}_3$ are the eigenvectors. In accordance with the theory of homogeneous equations the lengths of the eigenvectors will be undetermined whereas the direction will be known. Accordingly, it is always possible to choose a solution so that $\boldsymbol{n}$ becomes a unit vector and this situation will be assumed in the following. In the present context, the λ-values are most frequently called the principal strains, whereas the $\boldsymbol{n}$-vectors are called the principal strain directions.
The importance of the λ-values comes from the fact that they are invariants, i.e. they take the same values irrespective of the coordinate system. From a physical point of view, this is rather obvious as the magnitude of a principal strain λ was found above to be given by the relative elongation ε_{nn} in the fixed direction $\boldsymbol{n}$ and

this relative elongation must be independent of the coordinate system chosen. To prove this formally, assume that we change the coordinate system from the old x_i system to the new x'_i system in accordance with (3.20). Following (3.25), the principal directions and principal strains in the new coordinate system are determined by

$$\boldsymbol{\varepsilon}'\mathbf{n}' = \boldsymbol{\lambda}'\mathbf{n}' \qquad (3.27)$$

where λ' denotes the principal strain in the new coordinate system. Since $\boldsymbol{n}$ is a vector, we have from (2.22) that

$$\mathbf{n}' = \mathbf{A}\mathbf{n}$$

Use of this expression and (3.20) in (3.27) yields

$$\mathbf{A}\boldsymbol{\varepsilon}\mathbf{A}^{\mathbf{T}}\mathbf{A}\mathbf{n} = \boldsymbol{\lambda}'\mathbf{A}\mathbf{n}$$

Premultiplication by $\boldsymbol{A}^{\boldsymbol{T}}$ and using that $\boldsymbol{A}^{\boldsymbol{T}}\boldsymbol{A} = \boldsymbol{I}$, we find

$$\boldsymbol{\varepsilon}\mathbf{n} = \boldsymbol{\lambda}'\mathbf{n}$$

and a comparison with (3.25) proves that $\lambda = \lambda'$ implying that the λ-values are invariants, i.e. independent of the coordinate system. However, since the components of the eigenvector $\boldsymbol{n}'$ are now measured in the new x'_i coordinate system, these components differ from the components of the eigenvector $\boldsymbol{n}$.
Evaluation of the cubic equation (3.26) - the characteristic equation - gives after some algebra

$$-\lambda^3 + \theta_1\lambda^2 - \theta_2\lambda + \theta_3 = 0 \qquad (3.28)$$

where θ_1, θ_2 and θ_3 are defined by

$$\theta_1 = \varepsilon_{11} + \varepsilon_{22} + \varepsilon_{33} = \varepsilon_{ii}$$
$$\theta_2 = \varepsilon_{11}\varepsilon_{22} + \varepsilon_{22}\varepsilon_{33} + \varepsilon_{11}\varepsilon_{33} - \varepsilon_{23}^2 - \varepsilon_{12}^2 - \varepsilon_{13}^2 = \frac{1}{2}\theta_1^2 - \frac{1}{2}\varepsilon_{ij}\varepsilon_{ji} \qquad (3.29)$$
$$\theta_3 = \varepsilon_{11}\varepsilon_{22}\varepsilon_{33} - \varepsilon_{11}\varepsilon_{23}^2 - \varepsilon_{22}\varepsilon_{13}^2 - \varepsilon_{33}\varepsilon_{12}^2 + 2\varepsilon_{12}\varepsilon_{13}\varepsilon_{23} = \det(\varepsilon_{ij})$$

As the λ-values are invariants determined by the values of θ_1, θ_2 and θ_3 is obvious that also the θ_1, θ_2 and θ_3 values are invariants. They are called the Cauchy-strain invariants and any combination of these invariants is also an invariant.

An important issue is that the eigenvectors are orthogonal and that the eigenvalues are real, this is a consequence of the matrix $\boldsymbol{\varepsilon}$ being real and symmetric and it is a well-known result in mathematics. However, we will take the opportunity to prove it here.

To prove that the eigenvectors are orthogonal, assume that we have determined the two eigenvalues $\boldsymbol{\lambda_1}$ and $\boldsymbol{\lambda_2}$ and the corresponding two eigenvectors $\boldsymbol{n_1}$ and $\boldsymbol{n_2}$. We then have

$$\begin{aligned} \boldsymbol{\varepsilon}\mathbf{n}_1 &= \boldsymbol{\lambda}_1\mathbf{n}_1 \\ \boldsymbol{\varepsilon}\mathbf{n}_2 &= \boldsymbol{\lambda}_2\mathbf{n}_2 \end{aligned} \qquad (3.30)$$

Transpose the first equation, utilize that $\boldsymbol{\varepsilon}$ is symmetric and postmultiply it by $\boldsymbol{n_2}$ to obtain

$$\mathbf{n}_1^{\mathrm{T}}\boldsymbol{\varepsilon}\mathbf{n}_2 = \lambda_1\mathbf{n}_1^{\mathrm{T}}\mathbf{n}_2 \qquad (3.31)$$

Premultiply (3.30) by $\boldsymbol{n}_1{}^{\mathrm{T}}$ to obtain

$$\mathbf{n}_1^{\mathrm{T}}\boldsymbol{\varepsilon}\mathbf{n}_2 = \lambda_2\mathbf{n}_1^{\mathrm{T}}\mathbf{n}_2 \qquad (3.32)$$

Subtraction of (3.31) and (3.32) yields

$$(\lambda_1 - \lambda_2)\mathbf{n}_1^{\mathrm{T}}\mathbf{n}_2 = 0$$

If we assume that $\lambda_1 \neq \lambda_2$ then it follows that $\boldsymbol{n_1}$ and $\boldsymbol{n_2}$ must be orthogonal. Similar arguments hold between $\boldsymbol{n_1}$ and $\boldsymbol{n_3}$ and between $\boldsymbol{n_3}$ and $\boldsymbol{n_2}$, i.e. we obtain the following fundamental property

$$\mathbf{n}_1^{\mathrm{T}}\mathbf{n}_2 = \mathbf{n}_1^{\mathrm{T}}\mathbf{n}_3 = \mathbf{n}_2^{\mathrm{T}}\mathbf{n}_3 = 0 \qquad \textit{orthogonality of eigenvectors} \qquad (3.33)$$

When proving this orthogonality, it was assumed that the principal strains were unequal. What happens if some of them are equal? Suppose that in a certain coordinate system, we have the following strain tensor

$$\boldsymbol{\varepsilon} = \begin{bmatrix} a & 0 & 0 \\ 0 & a & 0 \\ 0 & 0 & a \end{bmatrix} = a\mathbf{I}$$

It is obvious that in this coordinate system the principal strains are all equal and given by the quantity *a*. Suppose now that the coordinate system is changed from the present $\mathbf{x_i}$ system to the new $\mathbf{x'_i}$ system in accordance with (3.19). In this new $\mathbf{x'_i}$ system, the strain tensor transforms into the one given by (3.20), i.e.

$$\boldsymbol{\varepsilon}' = \mathbf{A}\boldsymbol{\varepsilon}\mathbf{A}^T = a\mathbf{A}\mathbf{I}\mathbf{A}^T = a\mathbf{A}\mathbf{A}^T = a\mathbf{I} = \boldsymbol{\varepsilon}$$

Consequently, we have proved that if all three principal strains are equal, then any coordinate system corresponds to the principal directions.

Suppose now that in a certain coordinate system, we have the following strain tensor

$$\boldsymbol{\varepsilon} = \begin{bmatrix} a & 0 & 0 \\ 0 & b & 0 \\ 0 & 0 & b \end{bmatrix} = b\mathbf{I} + \begin{bmatrix} a-b & 0 & 0 \\ 0 & 0 & 0 \\ 0 & 0 & 0 \end{bmatrix}$$

i.e. two of the principal strains are equal. Suppose furthermore that we rotate the coordinate system according to (3.19). However, we will make the special choice that this rotation consists of a rotation about the $\mathbf{x_1}$ axis. This implies that $e'^T_1=[1;\ 0;\ 0]$, cf. Fig. 2.3. According to (3.20), the strain tensor in the new $\mathbf{x'_i}$ system becomes

$$\boldsymbol{\varepsilon}' = b\mathbf{A}\mathbf{I}\mathbf{A}^T + \mathbf{A}\begin{bmatrix} a-b & 0 & 0 \\ 0 & 0 & 0 \\ 0 & 0 & 0 \end{bmatrix}\mathbf{A}^T$$

$$= b\mathbf{I} + \begin{bmatrix} e_1'^T \\ e_2'^T \\ e_3'^T \end{bmatrix}\begin{bmatrix} a-b & 0 & 0 \\ 0 & 0 & 0 \\ 0 & 0 & 0 \end{bmatrix}\begin{bmatrix} e_1' & e_2' & e_3' \end{bmatrix}$$

As we only consider a rotation about the x_1 axis, i.e. $e'^T_1=[1;\ 0;\ 0]$, we obtain

$$\varepsilon' = b\mathbf{I} + \begin{bmatrix} a-b & 0 & 0 \\ 0 & 0 & 0 \\ 0 & 0 & 0 \end{bmatrix}\begin{bmatrix} e_1' & e_2' & e_3' \end{bmatrix}$$

i.e.

$$\varepsilon' = b\mathbf{I} + \begin{bmatrix} a-b & 0 & 0 \\ 0 & 0 & 0 \\ 0 & 0 & 0 \end{bmatrix} = \varepsilon$$

Consequently, we have proved that if two of the principal strains are equal, then any coordinate system obtained by rotation about that axis, which corresponds to the principal strain different from the other principal strains, corresponds to the principal directions.

In conclusion, we find that it is always allowable to take the principal directions as orthogonal directions in accordance with (3.33).

Remembering the physical interpretation of λ, cf. the discussion of (3.24), it is evident that the λ-values must be real. However, a formal proof is readily achieved. For the eigenvalue λ and the corresponding eigenvector $\boldsymbol{n}$, $\boldsymbol{\varepsilon n}=\boldsymbol{\lambda n}$ holds. Take the complex conjugate of this equation to obtain

$$\boldsymbol{\varepsilon}\mathbf{n}^* = \boldsymbol{\lambda}^* \mathbf{n}^* \qquad (3.34)$$

where an asterisk * for the time being denotes the complex conjugate and where it has been used that ε is real and that $(\lambda\boldsymbol{n})^* = \lambda^*\boldsymbol{n}^*$. Premultiplying $\boldsymbol{\varepsilon n}=\lambda\boldsymbol{n}$ by $\boldsymbol{n}^{*T}$ gives

$$\mathbf{n}^{*\mathrm{T}}\boldsymbol{\varepsilon}\mathbf{n} = \lambda\mathbf{n}^{*\mathrm{T}}\mathbf{n} \qquad (3.35)$$

whereas transposing (3.34), utilizing the symmetry of $\boldsymbol{\varepsilon}$ and postmultiplying by $\boldsymbol{n}$ provides

$$\mathbf{n}^{*\mathrm{T}}\boldsymbol{\varepsilon}\mathbf{n} = \lambda^*\mathbf{n}^{*\mathrm{T}}\mathbf{n} \qquad (3.36)$$

Then, finally, subtraction of (3.35) and (3.36) yields

$$(\lambda - \lambda^*)\mathbf{n}^{*\mathrm{T}}\mathbf{n} = 0$$

However, $\boldsymbol{n^{*T}n}$ is certainly different from zero implying that $\lambda=\lambda^*$ and it has then been proved that the eigenvalues are real. It follows immediately that also the eigenvectors are real, i.e.

The eigenvalues and the eigenvectors are real

We are now in a position to illustrate a significant feature related to the eigenvalues and eigenvectors. As $\boldsymbol{n_1}$, $\boldsymbol{n_2}$ and $\boldsymbol{n_3}$ are orthogonal, we can change our coordinate system from the x_i system to a x'_i system collinear with the $\boldsymbol{n_1}$, $\boldsymbol{n_2}$ and $\boldsymbol{n_3}$ directions. Following (3.19), we then have

$$\mathbf{x}' = \mathbf{A}\mathbf{x} - \mathbf{c} \qquad \textit{where} \qquad \mathbf{A}^T = \begin{bmatrix} n_1 & n_2 & n_3 \end{bmatrix}$$

In this new x'_i system the strain tensor becomes, cf. (3.20)

$$\varepsilon' = \begin{bmatrix} n_1^T \\ n_2^T \\ n_3^T \end{bmatrix} \varepsilon \begin{bmatrix} n_1 & n_2 & n_3 \end{bmatrix} = \begin{bmatrix} n_1^T \\ n_2^T \\ n_3^T \end{bmatrix} \begin{bmatrix} \varepsilon n_1 & \varepsilon n_2 & \varepsilon n_3 \end{bmatrix}$$

Using that $\boldsymbol{\varepsilon n_1 = \lambda_1 n_1}$ and the similar relations, cf. (3.25), we obtain

$$\boldsymbol{\varepsilon}' = \begin{bmatrix} n_1^T \\ n_2^T \\ n_3^T \end{bmatrix} \begin{bmatrix} \lambda_1 n_1 & \lambda_2 n_2 & \lambda_3 n_3 \end{bmatrix} = \begin{bmatrix} \lambda_1 n_1^T n_1 & \lambda_2 n_1^T n_2 & \lambda_3 n_1^T n_3 \\ \lambda_1 n_2^T n_1 & \lambda_2 n_2^T n_2 & \lambda_3 n_2^T n_3 \\ \lambda_1 n_3^T n_1 & \lambda_2 n_3^T n_2 & \lambda_3 n_3^T n_3 \end{bmatrix}$$

However, as the ***n***-vectors are unit vectors orthogonal to each other we finally obtain

$$\boldsymbol{\varepsilon}' = \begin{bmatrix} \lambda_1 & 0 & 0 \\ 0 & \lambda_2 & 0 \\ 0 & 0 & \lambda_3 \end{bmatrix} \qquad (3.37)$$

Accordingly, we have obtained the important result that if the coordinate system is chosen collinearly with the principal directions $\boldsymbol{n_1}$, $\boldsymbol{n_2}$ and $\boldsymbol{n_3}$, then the strain tensor becomes diagonal and the normal strains become equal to $\boldsymbol{\lambda_1}$, $\boldsymbol{\lambda_2}$ and $\boldsymbol{\lambda_3}$. This result is in accordance with the physical conditions, which were specified in the beginning when the eigenvalue problem was formulated. This important result also illustrates why the eigenvalues are called the principal strains and the eigenvectors the principal directions. The principal strains are often denoted by $\boldsymbol{\varepsilon_1}$, $\boldsymbol{\varepsilon_2}$ and $\boldsymbol{\varepsilon_3}$, i.e. $\boldsymbol{\varepsilon_1} = \boldsymbol{\lambda_1}$, $\boldsymbol{\varepsilon_2} = \boldsymbol{\lambda_2}$, and $\boldsymbol{\varepsilon_3} = \boldsymbol{\lambda_3}$. The above result can be summarized by stating that if the coordinate system is collinear with the principal directions we have in accordance with (3.20) and (3.37) that

$$\boldsymbol{\varepsilon}' = \mathbf{A}\boldsymbol{\varepsilon}\mathbf{A}^{\mathbf{T}} = \begin{bmatrix} \varepsilon_1 & 0 & 0 \\ 0 & \varepsilon_2 & 0 \\ 0 & 0 & \varepsilon_3 \end{bmatrix} \quad for \quad \mathbf{A}^T = \begin{bmatrix} n_1 & n_2 & n_3 \end{bmatrix} \qquad (3.38)$$

3.8 Extremum values of the normal strain

The normal strain $\boldsymbol{\varepsilon}$ in any direction n_i is determined by **Errore. L'origine riferimento non è stata trovata.**, i.e.

$$\boldsymbol{\varepsilon} = n_i \varepsilon_{ij} n_j$$

For different directions of n_i, different $\boldsymbol{\varepsilon}$ -values are achieved. It will now be proved that the normal strain $\boldsymbol{\varepsilon}$ takes stationary values, i.e. maximum or minimum values, when the direction n_i is in the direction of one of the principal axes.

To find the stationary values of $\boldsymbol{\varepsilon}$, the n_i -vector is varied. However, the n_i components cannot be varied arbitrarily, as we have the constraint

$$n_i n_i - 1 = 0$$

Accordingly, we employ the method of Lagrange and find stationary values of the function

$$\psi = n_i \varepsilon_{ij} n_j - \alpha(n_i n_i - 1) \qquad (3.39)$$

where now the n_i-components and α are independent quantities, α being a Lagrangian multiplier. From (3.39), where $\psi = \psi(n_i, \alpha)$ we obtain

$$\frac{\partial \psi}{\partial n_k} = \varepsilon_{kj} n_j + \varepsilon_{ki} n_i - \alpha(n_k + n_k) = 0 \qquad (3.40)$$

and

$$\frac{\partial \psi}{\partial \alpha} = n_i n_i - 1 = 0 \qquad (3.41)$$

Equation *(3.40)* can be written as

$$\varepsilon_{kj} n_j - \alpha n_k = 0 \qquad \textbf{or} \qquad (\varepsilon_{ij} - \alpha \delta_{ij}) n_j = 0 \qquad (3.42)$$

Therefore, stationary values for the normal strain $\boldsymbol{\varepsilon}$ are obtained by solution of the homogeneous equation system (3.42) subject to the condition (3.41). We immediately observe that this is exactly the same eigenvalue problem as stated by (3.25) proving that stationary values, i.e. maximum and minimum values, of the normal strain $\boldsymbol{\varepsilon}$ occur in the principal directions.

3.9 Cayley-Hamilton's theorem

We will now prove an interesting relation for the strain tensor (occasionally also called the strain matrix).
Considering the eigenvalue problem (3.25), we premultiply this equation by $\boldsymbol{\varepsilon}$, i.e.

$$\boldsymbol{\varepsilon}^2 \mathbf{n} = \lambda \boldsymbol{\varepsilon} \mathbf{n} = \lambda^2 \mathbf{n}$$

where the notation

$$\boldsymbol{\varepsilon}^2 = \boldsymbol{\varepsilon}\boldsymbol{\varepsilon} \qquad (3.43)$$

has been used. Proceeding, we obtain the general result

$$\varepsilon^{\alpha}\mathbf{n} = \lambda^{\alpha}\mathbf{n}; \qquad \alpha = 0, \pm 1, \pm 2.... \tag{3.44}$$

where α is any integer (positive, negative or zero). If α is negative, say α=-*2* then, in accordance with (3.43), we define

$$\varepsilon^{-2} = \varepsilon^{-1}\varepsilon^{-1}$$

Hence, (3.44) holds even for negative values of the integer α provided that $\boldsymbol{\varepsilon}^{-1}$ exists i.e. provided that $det\boldsymbol{\varepsilon} \neq 0$. Moreover, in accordance with the usual definition that $\boldsymbol{x}^{0}=1$ we make the following definition

$$\varepsilon^{0} = \mathbf{I}$$

From this definition follows that (3.43) holds even when $\alpha=0$.

Equation (3.43) shows that if $\boldsymbol{\varepsilon}$ has the eigenvalue λ and eigenvector $\boldsymbol{n}$, then $\boldsymbol{\varepsilon}^{\alpha}$ will have the same eigenvector and the eigenvalue $\boldsymbol{\lambda}^{\alpha}$. Now, multiply the characteristic equation for λ, as given by (3.28), by $\boldsymbol{n}$ to obtain

$$-\lambda^{3}\mathbf{n} + \theta_1\lambda^{2}\mathbf{n} - \theta_2\lambda\mathbf{n} + \theta_3\mathbf{n} = \mathbf{0} \tag{3.45}$$

where $\boldsymbol{0}$ is given by $\boldsymbol{0}^{\boldsymbol{T}}$ = *[0 0 0]*. Use of (3.44) in (3.45) gives

$$(-\varepsilon^{3} + \theta_1\varepsilon^{2} - \theta_2\varepsilon + \theta_3\mathbf{I})\mathbf{n} = \mathbf{0}$$

We know that this equation is fulfilled for $\boldsymbol{n}$ given by any of the three eigenvectors, i.e. these three matrix equations can be combined into the following format

$$(-\varepsilon^3 + \theta_1\varepsilon^2 - \theta_2\varepsilon + \theta_3\mathbf{I})\begin{bmatrix} n_1 & n_2 & n_3 \end{bmatrix} = \mathbf{0} \qquad (3.46)$$

where $\boldsymbol{0}$ now denotes the 3 x 3 null matrix. As the unit vectors $\boldsymbol{n_1}$, $\boldsymbol{n_2}$ and $\boldsymbol{n_3}$ are orthogonal, we have that

$$\begin{bmatrix} n_1 & n_2 & n_3 \end{bmatrix} = \mathbf{A}^T$$

where A is some transformation matrix. Expression (3.46) therefore takes the form

$$(-\varepsilon^3 + \theta_1\varepsilon^2 - \theta_2\varepsilon + \theta_3\mathbf{I})\mathbf{A}^T = \mathbf{0}$$

Postrnultiplication by $\boldsymbol{A}$ and noting that $\boldsymbol{A^TA = I}$ give

$$-\varepsilon^3 + \theta_1\varepsilon^2 - \theta_2\varepsilon + \theta_3\mathbf{I} = \mathbf{0} \qquad (3.47)$$

This equation is similar to the characteristic equation for λ, cf. (3.28) and the result is thus often stated by saying that

The strain matrix satisfies its own characteristic equation

This important result is the Cayley-Hamilton theorem. Note that (3.47) is a matrix equation.

A significant implication of (3.47) is that an expression involving the term $\boldsymbol{\varepsilon^3}$ can always be simplified so that it only involves teams of $\boldsymbol{\varepsilon^2}$, and $\boldsymbol{I}$. More generally, if we multiply (3.47) by $\boldsymbol{\varepsilon^\alpha}$, where α is any integer (positive, negative or zero), we obtain

$$\varepsilon^{3+\alpha} = \theta_1 \varepsilon^{2+\alpha} - \theta_2 \varepsilon^{1+\alpha} + \theta_3 \varepsilon^{\alpha}$$

If $\alpha \geq 0$ this means that any $\boldsymbol{\varepsilon^{3+\alpha}}$ term can be replaced by lower order powers of $\boldsymbol{\varepsilon}$. If $\alpha \leq 0$ (which presumes that $\boldsymbol{\varepsilon^{-1}}$ exists), then any $\boldsymbol{\varepsilon^\alpha}$ term can be replaced by higher order powers of $\boldsymbol{\varepsilon}$.

3.10 Deviatoric strains

Instead of the full strain tensor, it is often convenient to operate with the so called deviatoric strain tensor e_{ij} defined by

$$e_{ij} = \varepsilon_{ij} - \frac{1}{3}\varepsilon_{kk}\delta_{ij} \qquad (3.48)$$

where $1/3\varepsilon_{kk}\delta_{ij}$ is the volumetric or spherical strain tensor, which only involves diagonal terms. As both ε_{ij} and δ_{ij} are second-order tensors, it follows directly that so is e_{ij}. Therefore, by analogy with (3.20) and (3.21) we have

$$e'_{ij} = A_{ik} e_{kl} A_{jl} \qquad or \qquad \mathbf{e'} = \mathbf{A e A}^T$$

and

$$e_{ij} = A_{ik} e'_{kl} A_{jl} \qquad or \qquad \mathbf{e} = \mathbf{A e' A}^T$$

Moreover, we observe from definition (3.48) that

$$e_{ii} = 0 \tag{3.49}$$

In a principal coordinate system the principal strains become ε_1, ε_2 and ε_3.
Referring to (3.11), this means that the relative volume change due to the deformation becomes

$$\frac{dV^* - dV}{dV} = \frac{(1+\varepsilon_1)dx_1(1+\varepsilon_2)dx_2(1+\varepsilon_3)dx_3 - dx_1dx_2dx_3}{dx_1dx_2dx_3}$$

where dV is the infinitesimal volume before deformation, which owing to the deformation changes to dV^*. In accordance with our assumption of small strains, we ignore higher order strain terms and the expression above becomes

$$\frac{dV^* - dV}{dV} = \varepsilon_1 + \varepsilon_2 + \varepsilon_3 = \varepsilon_{kk} \qquad (3.50)$$

We conclude that ε_{kk} is equal to the relative volume change, i.e. an incompressible material is characterized by $\varepsilon_{kk} = 0$. Moreover, it may be recalled that ε_{kk} is an invariant.
Referring to (3.48), it appears that the off-diagonal terms of e_{ij} and ε_{ij} are identical. Consequently, it can be concluded that the volumetric strain tensor only influences the volumetric changes whereas the deviatoric strain tensor only influences the shearing (distortion) of the material.
Retuning to the eigenvalue problem (3.25), we may eliminate ε_{ij} by means of (3.48) to obtain

$$\left[e - \left(\lambda - \frac{\varepsilon_{kk}}{3} \right) \mathbf{I} \right] \mathbf{n} = \mathbf{0}$$

It is concluded that the eigenvalues e_{ij} are given by $\lambda - \varepsilon_{kk}/3$ whereas the eigenvectors, i.e. the principal directions, are identical for the deviatoric strain tensor and the strain tensor. The fact that the principal directions of e_{ij} and ε_{ij} are

identical follows also directly from the observation that they have identical off-diagonal terms, i.e. when ε_{ij} is diagonal, so is e_{ij}.

3.11 Important strain invariants

We have seen quite a number of different invariants and it might be convenient to summarize these invariants and make use of the opportunity to introduce additional invariants which later turn out to be of importance. The Cauchy invariants are given by (3.29)

$$\theta_1 = \varepsilon_{ii}; \qquad \theta_2 = \frac{1}{2}\theta_1^2 - \frac{1}{2}\varepsilon_{ij}\varepsilon_{ji}; \qquad \theta_3 = \det(\varepsilon_{ij}) = \varepsilon_1\varepsilon_2\varepsilon_3 \tag{3.51}$$

In general, to prove that a quantity is an invariant, we must demonstrate that it takes the same value in all coordinate systems. As a prototype of such an evaluation we consider

$$\varepsilon'_{ij}\,\varepsilon'_{ij} = A_{ik}\varepsilon_{kl}A_{jl}A_{is}\varepsilon_{st}A_{jt} = \delta_{ks}\varepsilon_{kl}\varepsilon_{st}\delta_{lt} = \varepsilon_{sl}\varepsilon_{sl}$$

where advantage is taken of the transformation rule (3.20). This demonstrates that the quantity $\varepsilon_{ij}\varepsilon_{ij}$ is an invariant. Likewise, it is easily shown that ε_{ii} and $\varepsilon_{ij}\varepsilon_{jk}\varepsilon_{ki}$ are invariants. We can therefore list the following so-called generic invariants, where the term generic reflects the systematic manner of their definition

Occasionally, it is convenient to express these invariants in matrix notation and for that purpose, we define the trace of a 3 x 3 square matrix ***B*** by

$$tr\mathbf{B} = B_{ii}$$

i.e.

$$\tilde{\mathbf{I}}_1 = tr\varepsilon$$

Define the quantity B_{ij} by

$$B_{ij} = \varepsilon_{ik}\varepsilon_{kj} \qquad or \qquad \mathbf{B} = \boldsymbol{\varepsilon\varepsilon} = \boldsymbol{\varepsilon}^2$$

i.e. $tr\boldsymbol{B}=B_{ii}=\varepsilon_{ik}\varepsilon_{kj}$ and we therefore obtain

$$\tilde{I}_2 = \frac{1}{2}tr(\varepsilon^2) \qquad and\ likewise \qquad \tilde{I}_3 = \frac{1}{3}tr(\varepsilon^3)$$

It turns out that it is possible to obtain a unique relation between the Cauchy-invariants θ_1, θ_2 and θ_3 and the generic invariants $\tilde{I}_1$, $\tilde{I}_2$ and $\tilde{I}_3$. We have

$$\tilde{I}_1 = \theta_1; \qquad \tilde{I}_2 = \frac{1}{2}\theta_1^2 - \theta_2; \qquad \tilde{I}_3 = \frac{1}{3}\theta_1^3 - \theta_1\theta_2 + \theta_3; \qquad (3.53)$$

The inverse relations of (3.53) provide the following expressions

$$\begin{aligned}
\tilde{\mathbf{I}}_1 &= \varepsilon_{ii} = \varepsilon_1 + \varepsilon_2 + \varepsilon_3 \\
\tilde{\mathbf{I}}_2 &= \frac{1}{2}\varepsilon_{ij}\varepsilon_{ji} = \frac{1}{2}(\varepsilon_1^2 + \varepsilon_2^2 + \varepsilon_3^2) \\
\tilde{\mathbf{I}}_3 &= \frac{1}{3}\varepsilon_{ij}\varepsilon_{jk}\varepsilon_{ki} = \frac{1}{3}(\varepsilon_1^3 + \varepsilon_2^3 + \varepsilon_3^3)
\end{aligned} \qquad (3.52)$$

$$\theta_1 = \tilde{I}_1; \qquad \theta_2 = \frac{1}{2}\tilde{I}_1^2 - \tilde{I}_2; \qquad \theta_3 = \tilde{I}_3 + \frac{1}{6}\tilde{I}_1^3 - \tilde{I}_1\tilde{I}_2;$$

It appears that a unique relation exists between θ_1, θ_2, θ_3 and $\widetilde{I_1}$, $\widetilde{I_2}$, $\widetilde{I_3}$.
Now, let us turn to the generic invariants of the deviatoric strain tensor defined by analogy with (3.52). We have

$$\begin{aligned}
\tilde{J}_1 &= e_{ii} = tr(e) = e_1 + e_2 + e_3 \\
\tilde{J}_2 &= \frac{1}{2}e_{ij}e_{ji} = \frac{1}{2}tr(e^2) = \frac{1}{2}(e_1^2 + e_2^2 + e_3^2) \\
\tilde{J}_3 &= \frac{1}{3}e_{ij}e_{jk}e_{ki} = \frac{1}{3}tr(e^3) = \frac{1}{3}(e_1^3 + e_2^3 + e_3^3) = e_1e_2e_3
\end{aligned} \qquad (3.54)$$

To prove the last relation that $\widetilde{J_3} = e_1e_2e_3$, we first observe that

$$(e_2 + e_3)^3 = e_2^3 + e_3^3 + 3e_2e_3(e_2 + e_3)$$

and since $e_2 + e_3 = -e_1$, we obtain

$$-e_1^3 = e_2^3 + e_3^3 - 3e_1e_2e_3$$

From the definition of $\widetilde{J_3} = \frac{1}{3}(e_1^3 + e_2^3 + e_3^3)$, it then follows that

$$\tilde{J}_3 = e_1e_2e_3$$

which was to be proved. Moreover, using the definition of the deviatoric strain tensor as given by (3.48) in (3.54), we obtain

$$\tilde{J}_2 = \tilde{I}_2 - \frac{1}{6}\tilde{I}_1^2; \qquad \tilde{J}_3 = \tilde{I}_3 - \frac{2}{3}\tilde{I}_1\tilde{I}_2 + \frac{2}{27}\tilde{I}_1^3 \qquad (3.55)$$

and the inverse relations become

$$\tilde{I}_2 = \tilde{J}_2 + \frac{1}{6}\tilde{I}_1^2; \qquad \tilde{I}_3 = \tilde{J}_3 + \frac{2}{3}\tilde{I}_1\tilde{J}_2 + \frac{2}{27}\tilde{I}_1^3 \tag{3.56}$$

Therefore, instead of using the set of invariants $\widetilde{I_1}, \widetilde{I_2}, \widetilde{I_3}$ we may equally well use the set and $\widetilde{I_1}, \widetilde{J_2}, \widetilde{J_3}$.

An octahedral plane is defined as a plane where the normal to that plane makes equal angles to the three principal strain directions. Eight such planes exist and one example is shown in Fig. 3.5 where the axes 1,2 and 3 refer to the principal strain directors.

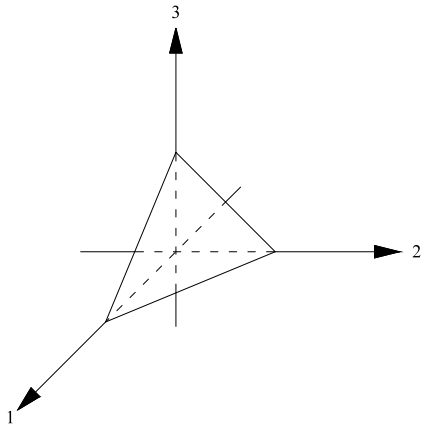

Figure 3.5: octahedral plane

For the normal to the octahedral plane shown in Fig. 3.5, we have

$$\mathbf{n} = \frac{1}{\sqrt{3}}\begin{bmatrix} 1 \\ 1 \\ 1 \end{bmatrix}$$

In the coordinate system collinear with the principal strain directions, the strain tensor takes the form

$$\boldsymbol{\varepsilon} = \begin{bmatrix} \varepsilon_1 & 0 & 0 \\ 0 & \varepsilon_2 & 0 \\ 0 & 0 & \varepsilon_3 \end{bmatrix}$$

The vector $\boldsymbol{q}$ is defined by $\boldsymbol{q}=\boldsymbol{\varepsilon n}$ cf. (3.22). It then follows from Fig. 3.4 that the normal strain ε_0 and tensorial shear strain $\gamma_0/2$ on the octahedral plane are given by

$$\varepsilon_0 = \mathbf{n}^{\mathrm{T}}\mathbf{q}; \qquad \frac{\gamma_0}{2} = \sqrt{q^T q - \varepsilon_0^2}$$

where ε_0 is called the octahedral normal strain and γ_0 is called the octahedral shear strain. It follows that

$$\varepsilon_0 = \frac{1}{3}\tilde{I}_1; \qquad \frac{\gamma_0}{2} = \sqrt{\frac{1}{3}(\varepsilon_1^2 + \varepsilon_2^2 + \varepsilon_3^2) - \frac{1}{9}\tilde{I}_1^2}$$

According to (3.48), we have

$$\varepsilon_1 = e_1 + \frac{1}{3}\tilde{I}_1; \qquad \varepsilon_2 = e_2 + \frac{1}{3}\tilde{I}_1; \qquad \varepsilon_3 = e_3 + \frac{1}{3}\tilde{I}_1;$$

i.e.

$$\frac{\gamma_0}{2} = \sqrt{\frac{1}{3}[e_1^2 + e_2^2 + e_3^2 + \frac{1}{3}\tilde{I}_1^2 + \frac{2}{3}(e_1 + e_2 + e_3)\tilde{I}_1] - \frac{1}{9}\tilde{I}_1^2}$$

Due to (3.49) and (3.54), we conclude that

$$\varepsilon_0 = \frac{1}{3}\tilde{I}_1; \qquad \gamma_0 = 2\sqrt{\frac{2}{3}\tilde{J}_2} \qquad (3.57)$$

It is easily shown that these relations hold not only for the octahedral plane shown in Fig. 3.5, but also for all the other octahedral planes. Finally, it is emphasized that γ_0 is the engineering shear strain as already suggested by the notation.

3.12 Special states of strain

Several special states of strain, which are often encountered in practice, will now be discussed.

A state of uniform dilatation occurs, if the strain tensor is given by

$$\varepsilon_{ij} = b\delta_{ij}$$

where b is an arbitrary scalar. It appears from (3.48) that the deviatoric strain tensor e_{ij} becomes $e_{ij} = 0$ and according to the discussion of (3.50), the strain state corresponds to a uniform dilatation, i.e. a volume change, where the extension - or contraction - in any direction is the same and equal to the parameter b.

Uniaxial strain occurs if the displacement vector u_i is given by

$$[u_i] = \begin{bmatrix} u_1(x_1,t) \\ 0 \\ 0 \end{bmatrix}$$

which implies that $\varepsilon_{11} = \partial u_1 / \partial x_1$ and all other strain components being zero, cf. Fig.3.6.

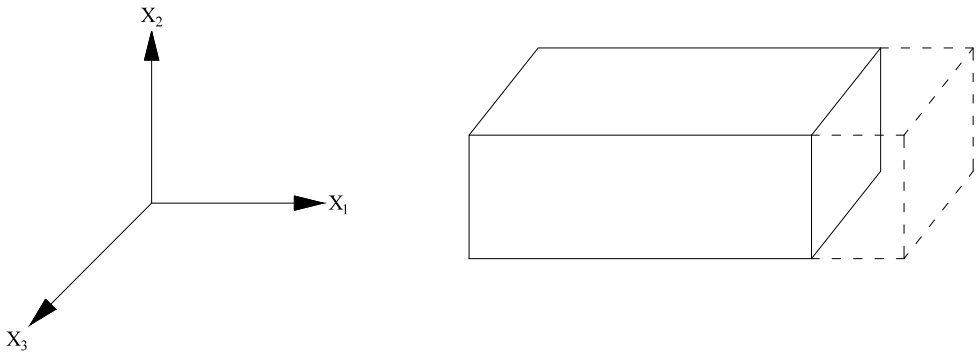

Figure 3.6: uniaxial strain

Plane strain or plane deformation occurs if the displacement vector u_i is given by

$$[u_i] = \begin{bmatrix} u_1(x_1, x_2, t) \\ u_2(x_1, x_2, t) \\ 0 \end{bmatrix}$$

which implies

$$\varepsilon_{ij} = \begin{bmatrix} \varepsilon_{11} & \varepsilon_{12} & 0 \\ \varepsilon_{21} & \varepsilon_{22} & 0 \\ 0 & 0 & 0 \end{bmatrix} \qquad (3.58)$$

This strain state occurs often in practice when a long prismatic or cylindrical body is loaded by forces which are perpendicular to the longitudinal elements and which do not vary along the length. In this case, it can be assumed that all cross sections are in the same state and if, moreover, the body is restricted from moving in the length direction, a state of plane strain exists. An example is an internally pressurized tube with end sections confined between smooth and rigid walls, Fig. 3.7.

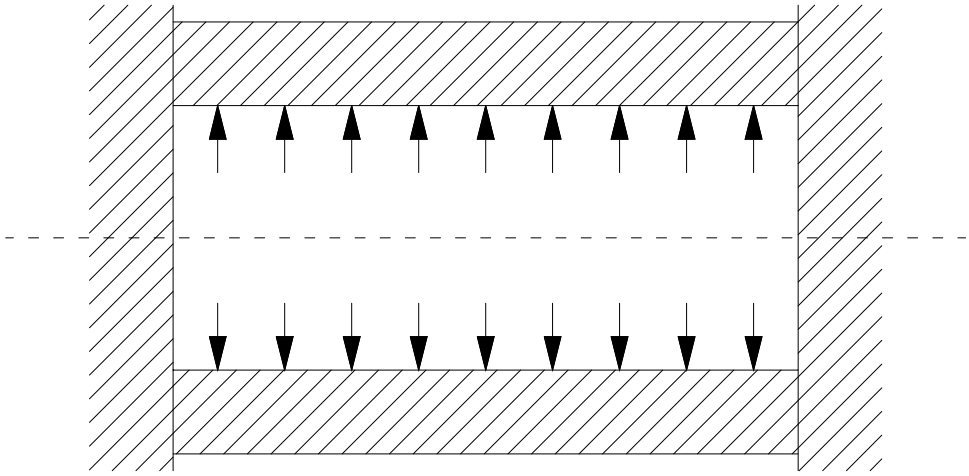

Figure 3.7: example of plane strain. Pressurizes tube with end sections confined between smooth and rigid walls.

So-called generalized plane strain or generalized plane deformation occurs if

$$[u_i] = \begin{bmatrix} u_1(x_1, x_2, t) \\ u_2(x_1, x_2, t) \\ u_3(x_1, x_2, t) \end{bmatrix}$$

which leads to

$$\varepsilon_{ij} = \begin{bmatrix} \varepsilon_{11} & \varepsilon_{12} & \varepsilon_{13} \\ \varepsilon_{21} & \varepsilon_{22} & \varepsilon_{23} \\ \varepsilon_{31} & \varepsilon_{32} & 0 \end{bmatrix}$$

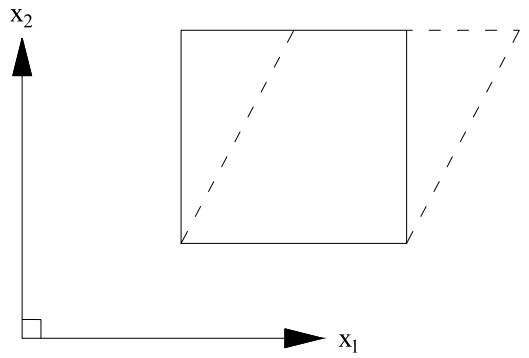

Figure 3.8: simple shear

Finally, a state of simple shear exists if

$$\varepsilon_{ij} = \begin{bmatrix} 0 & \varepsilon_{12} & 0 \\ \varepsilon_{21} & 0 & 0 \\ 0 & 0 & 0 \end{bmatrix}$$

corresponding to $u_1 = u_1(x_2, t)$ and $u_2 = u_3 = 0$, as illustrated in Fig. 3.8. It appears that for simple shear, we have $\varepsilon_{ii} = 0$, i.e. no volume change and it is easily shown that the principal strains become $\varepsilon_1 = \varepsilon_{12}$, $\varepsilon_2 = -\varepsilon_{12}$ and $\varepsilon_3 = 0$.

4 Stress Tensor

Before we proceed discussing the characteristics of the uniaxial behavior of a material and subsequently generalizing these concepts to a combined state of stress, an analysis of the state of combined stresses is introduced to provide the necessary background for the subsequent study.

4.1 Stress at a Point and the Stress Tensor

Stress is defined as the intensity of internal forces acting between particles of a body across imaginary internal surfaces. Consider a body, which is supposed to be continuous and two kinds of forces are assumed: body forces (i.e. force per unit volume) and surface forces (i.e. force per unit area).

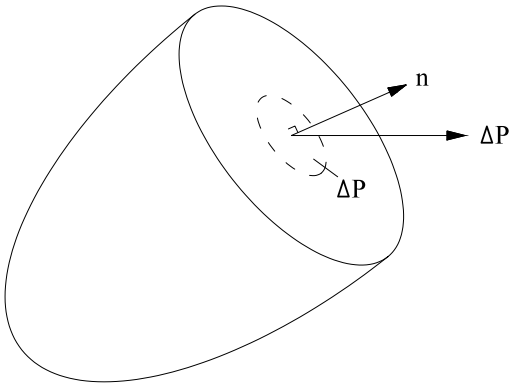

Figure 4.1: force ΔP on area ΔA with outer unit normal vector

Consider a surface of the body as shown in Fig. 4.1. This surface can be an external surface or an internal surface obtained by a section of the body. The vector ***n*** is a unit vector normal to the surface and directed out of the body. The incremental force vector *ΔP* acts on the incremental surface area *ΔA*. When *ΔA* approaches zero, it is assumed that the ratio *ΔP/ΔA* approaches a value **t**,
i.e.

$$\lim_{\Delta A \to 0} \frac{\Delta P}{\Delta A} = \mathbf{t} \qquad \mathbf{t} = \begin{bmatrix} t_1 \\ t_2 \\ t_3 \end{bmatrix}$$

The vector ***t***, with components t_1, t_2 and t_3 in the x_1, x_2 and x_3 directions respectively, is termed the traction vector and has the unit [N/m^2].
The traction vector ***t*** defined above is related to a surface with the outer unit normal vector ***n***. It is obvious that the traction vector will, in general, be different when other sections through the same point are considered. What we are looking for is a quantity - the stress tensor - which for a particular point, contains all the information necessary to determine the traction vector for arbitrary sections through that point.

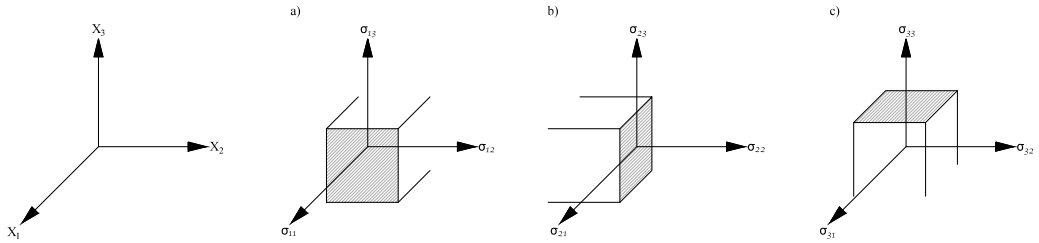

Figure 4.2: stress components

Let us first consider some special traction vectors, namely those obtained when sections perpendicular to the coordinate axes are considered. Assume that the outer normal vector ***n*** (see Fig. 4.1) is taken in the direction of the x_1 axis. The corresponding traction vector is denoted by t_1 and we can resolve this vector into its components along the coordinate axes, i.e.

$$t_1^T = \begin{bmatrix} \sigma_{11} & \sigma_{12} & \sigma_{13} \end{bmatrix} \qquad (4.1)$$

where σ_{11}, σ_{12} and σ_{13} denote the components of t_1 in the x_1, x_2 and x_3 directions respectively. These components are illustrated in Fig. 4.2a.

Likewise, if the outer normal unit vector ***n*** is taken in the direction of the x_2 axis, we denote the corresponding traction vector by t_2, i.e.

$$t_2^T = \begin{bmatrix} \sigma_{21} & \sigma_{22} & \sigma_{23} \end{bmatrix} \qquad (4.2)$$

where σ_{21}, σ_{22} and σ_{23} denote the components of t_2 in the x_1, x_2 and x_3 directions respectively, cf. Fig. 4.2b. Finally, if the outer normal unit vector ***n*** is taken in the direction of the x_3-axis, we denote the corresponding traction vector by t_3, i.e.

$$t_3^T = \begin{bmatrix} \sigma_{31} & \sigma_{32} & \sigma_{33} \end{bmatrix} \tag{4.3}$$

where σ_{31}, σ_{32} and σ_{33} denote the components of t_3 in the x_1, x_2 and x_3 directions respectively, cf. Fig. 4.2c.

The components given by (4.1)-(4.3) are termed the stress components and σ_{11}, σ_{22} and σ_{13} are called normal stresses, whereas σ_{12}, σ_{13}, σ_{21}, σ_{23}, σ_{31} and σ_{32} are referred to as shear stresses. We observe the consistent notation of the stress components where, for instance, σ_{23} is the x_3 component of the traction vector for a surface with the outer unit vector in the x_2 direction. Likewise, σ_1 is the x_2 component of the traction vector for a surface with the outer unit vector in the x_l direction.

Using the special traction vectors considered above, we define the quantity σ_{ij} by

$$\left[\sigma_{ij}\right] = \begin{bmatrix} t_1^T \\ t_2^T \\ t_3^T \end{bmatrix} = \begin{bmatrix} \sigma_{11} & \sigma_{12} & \sigma_{13} \\ \sigma_{21} & \sigma_{22} & \sigma_{23} \\ \sigma_{13} & \sigma_{23} & \sigma_{33} \end{bmatrix} \tag{4.4}$$

We shall later prove that σ_{ij} is a second-order tensor and σ_{ij} is therefore called the stress tensor.

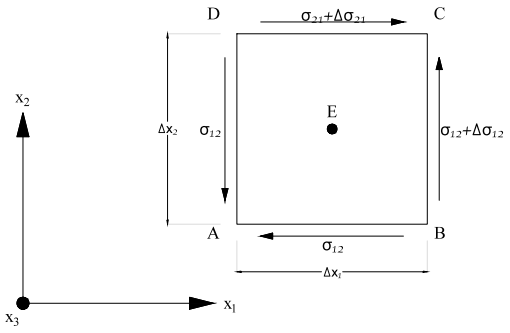

Figure 4.3: moment about an axis through the center E and parallel to the x_3 axis

Let us first prove that σ_{ij} is symmetric. From the body we cut a small parallelepiped with planes parallel to the coordinate planes. We then consider the moment equilibrium about an axis through the center *E* of this parallelepiped and parallel to the x_3 axis, cf. Fig. 4.3. It appears that body forces do not provide a moment about this axis. It is also obvious that only forces acting on planes parallel to the moment axis can contribute to the moment equilibrium.

On these planes, only shear stresses normal to the moment axis can give rise to the moments, see Fig. 4.3.

Referring to this figure, the positive direction of the shear stresses along *BC* and *DC* is in accordance with the previous interpretation of the stress components, cf. Fig. 3.2. The positive direction of the shear stresses along *AB* and *AD* follows from the law of action and reaction. Taking moments as positive in the counter-clockwise direction, moment equilibrium about point *E* yields

$$(\sigma_{12}+\Delta\sigma_{12})\Delta x_2\Delta x_3\frac{1}{2}\Delta x_1-(\sigma_{21}+\Delta\sigma_{21})\Delta x_1\Delta x_3\frac{1}{2}\Delta x_2$$
$$+\sigma_{12}\Delta x_2\Delta x_3\frac{1}{2}\Delta x_1-\sigma_{21}\Delta x_1\Delta x_3\frac{1}{2}\Delta x_2=0$$

i.e.

$$2\sigma_{12}-2\sigma_{21}+\Delta\sigma_{12}-\Delta\sigma_{21}=0$$

Letting Δx_1, Δx_2 and Δx_3 approach zero, both $\Delta\sigma_{12}$ and $\Delta\sigma_{21}$ also approach zero; that is, moment equilibrium requires that $\sigma_{12}=\sigma_{21}$. Likewise, considering moment equilibrium about axes parallel to the x_1 and x_2 axes implies that $\sigma_{23}=\sigma_{32}$ and $\sigma_{13}=\sigma_{31}$ respectively. In conclusion, we have proved that σ_{ij} is symmetric, i.e.

$$\sigma_{ij}=\sigma_{ji} \qquad \textbf{or} \qquad \boldsymbol{\sigma}=\boldsymbol{\sigma}^{\mathrm{T}}$$

Our aim was to establish a quantity which contains all the information necessary to determine the traction vector **t** for arbitrary sections through the point in question. We shall now prove that the stress tensor σ_{ij} contains this information. Consider the small tetrahedron shown in Fig. 4.4a). At the surface *ABC* with the

outer unit normal vector ***n***, we have the traction vector ***t***. On the planes parallel to the coordinate planes, the traction vectors are t_1, t_2 and t_3, cf. (4.1)-(4.3) (minus signs appear because of the law of action and reaction and because the outer normal vectors are in the negative direction of the coordinate axes). The area *ABC* is denoted by ΔA, the area *AOC* by ΔA_1, the area *AOB* by ΔA_2 and the area *BOC* by ΔA_3. In Fig. 4.4b) the line *CP* is orthogonal to the line *AB*. As ***n*** is perpendicular to the surface *ABC*, it is also perpendicular to the lines *CP* and *AB*. The vector ***n*** is therefore located in the plane *OCP*. The components of the unit vector n_i are given by $n_i = (n_1, n_2, n_3)$ and by definition we have $n_2 = \cos\theta$ where θ is the angle shown in Fig. 4.4b). From Fig. 4.4b) follows that

$$\Delta A_2 = \frac{1}{2}|OP| \cdot |AB|; \qquad |OP| = |CP|\cos\vartheta = |CP| n_2$$

i.e.

$$\Delta A_2 = \frac{1}{2}|CP| \cdot |AB| n_2 = n_2 \Delta A$$

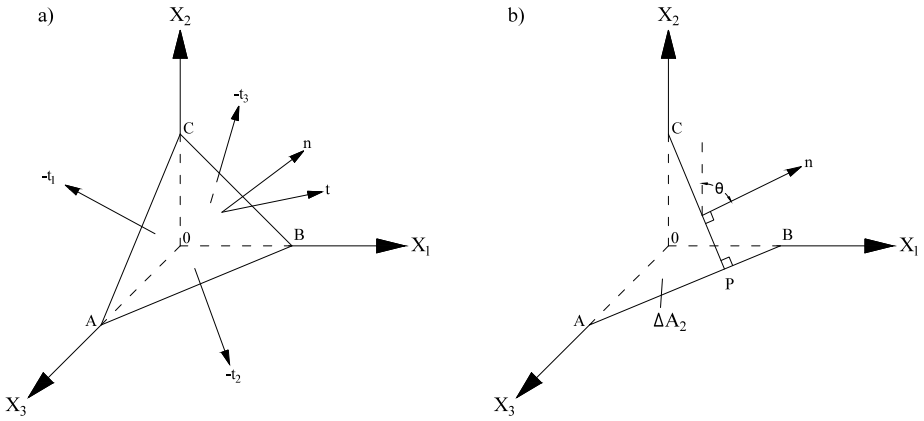

Figure 4.4: a) traction vectors on a tetrahedron: ***t*** *acts on ABC,* $-\mathbf{t}_1$ *on AOC,* $-\mathbf{t}_2$ *on AOB and* $-\mathbf{t}_3$ *on BOC ; b) determination of* ΔA *by geometrical arguments. Vector* ***n*** *is located in the plane OCP*

By analogous arguments we find that

$$\Delta A_1 = n_1 \Delta A; \qquad \Delta A_2 = n_2 \Delta A; \qquad \Delta A_3 = n_3 \Delta A; \tag{4.5}$$

The condition of force equilibrium of the tetrahedron of Fig. 4.4a) requires that

$$t\Delta A - t_1 \Delta A_1 - t_2 \Delta A_2 - t_3 \Delta A_3 + \mathbf{b}\Delta V = 0 \tag{4.6}$$

where ***b*** is the body force per unit volume and ΔV is the volume of the small tetrahedron. The body force ***b*** has the components

$$\mathbf{b}^T = \begin{bmatrix} b_1 & b_2 & b_3 \end{bmatrix}$$

Use of (4.5) in (4.6) gives

$$t - t_1 n_1 - t_2 n_2 - t_3 n_3 + \mathbf{b}\frac{\Delta V}{\Delta A} = 0$$

Letting the size of the tetrahedron shrink towards zero, we have $\Delta V/\Delta A \rightarrow 0$ (volume has the unit m^3 and area has the unit m^2) and we then obtain

$$\mathbf{t} = t_1 n_1 + t_2 n_2 + t_3 n_3$$

which may be written as

$$\mathbf{t} = \begin{bmatrix} t_1 & t_2 & t_3 \end{bmatrix} \begin{bmatrix} n_1 \\ n_2 \\ n_3 \end{bmatrix} = \boldsymbol{\sigma}^T \mathbf{n}$$

where (4.4) was used. Due to the symmetry of $\boldsymbol{\sigma}$ we arrive at

$$t_i = \sigma_{ij} n_{ij} \qquad or \qquad \mathbf{t} = \boldsymbol{\sigma}\mathbf{n} \tag{4.7}$$

This expression proves that knowledge of the stress tensor ***a*** provides sufficient information for the traction vector ***t*** to be derived for any direction ***n***. It should be observed that on the exterior surface of the body, (4.7) represents a boundary condition expressing a relation between the forces acting on the external surface and the stress tensor. Equation (4.7) was derived by Cauchy in 1822 and it is therefore occasionally referred to as Cauchy's formula, the stress tensor is called the Cauchy stress tensor. When considering large deformations, it turns out that a number of different stress tensors exist, but for small strains and rotations they all reduce to the Cauchy stress tensor.

Moreover, since t_i and n_i are first-order tensors (vectors), it follows from the quotient theorem that σ_{ij} is a second-order tensor.

4.2 Change of coordinate system

If we instead of the x_i-coordinate system change to a x'_i-coordinate system, we have as usual that

$$x'_i = A_{ij}(x_j - c_j) \qquad or \qquad \mathbf{x'=A(x-c)}$$

where A_{ij} is the transformation matrix and where $\mathbf{A^T A = I}$.

Since σ_{ij} is known to be a second-order tensor, we can directly write the following relations between the components σ_{ij} in the x_i-system and the components σ'_{ij} in the x'_i-system.

$$\sigma'_{ij} = A_{ik}\sigma_{kl}A_{jl} \qquad or \qquad \boldsymbol{\sigma'=A\sigma A}^T \tag{4.8}$$

and

$$\sigma_{ij} = A_{ki}\sigma'_{kl}A_{jl} \qquad or \qquad \boldsymbol{\sigma=A\sigma' A}^T \tag{4.9}$$

4.3 Principal stresses and principal directions - Invariants

The traction vector ***t*** on a surface with the outer normal unit vector ***n*** is given by (4.7). The traction vector ***t*** can be resolved into a component parallel to ***n*** and a component perpendicular to ***n***. The component parallel to ***n*** is called the normal stress in direction ***n*** and denoted by σ_n. From (4.7) we obtain

$$\sigma_n = n_i t_i = n_i \sigma_{ij} n_j \qquad \textbf{or} \qquad \sigma_n = \mathbf{n^T t = n^T \sigma n} \tag{4.10}$$

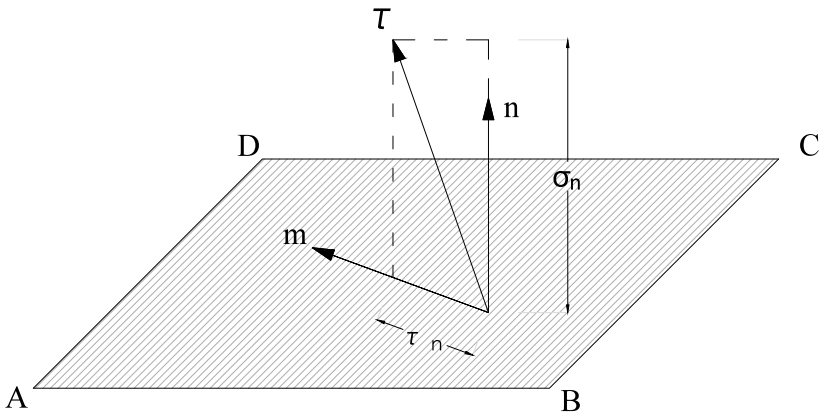

Figure 4.5: illustration of normal stress σ_n and shear stress τ_n

The component of ***t*** perpendicular to ***n*** is called the shear stress and is denoted by τ_n. Both σ_n and τ_n are illustrated in Fig. 4.5, where the unit vector ***m*** is perpendicular to ***n*** and located in the plane *ABCD*. It readily appears that

$$\tau_n = m_i t_i = m_i \sigma_{ij} n_j \qquad \textbf{or} \qquad \tau_n = \mathbf{m}^{\mathrm{T}}\mathbf{t} = \mathbf{m}^T \boldsymbol{\sigma} \mathbf{n} \qquad (4.11)$$

Alternatively we may write

$$\tau_n^2 = t_i t_i - \sigma_n^2$$

With these preliminary results, we may obtain a physical interpretation of the important eigenvalue problem of the stress tensor and with the solution of the eigenvalue problem, we arrive at the stress invariants. Moreover, it turns out that for a special choice of coordinate system, the stress tensor takes a particularly simple form.

Returning to Fig. 4.5, we look for a situation where the traction vector ***t*** is collinear with the unit vector **n**. From Fig. 4.5, the direction ***n*** should be chosen so that

$$t_i = \lambda n_i \qquad (4.12)$$

where λ is some factor and (4.10) implies that $\lambda=\sigma_n$. Since n_i and m_i are orthogonal, (4.11) gives in the present situation that the shear stress $\tau_n=0$. Insertion of (4.7) into (4.12) yields

$$(\sigma_{ij} - \lambda \delta_{ij}) n_j = 0 \qquad or \qquad (\boldsymbol{\sigma} - \lambda \mathbf{I})\mathbf{n} = \mathbf{0} \qquad (4.13)$$

This constitutes an eigenvalue problem and a comparison with (3.25) shows a complete analogy. Therefore all the conclusions that were delved for the strain tensor apply also for the stress tensor. That is, the characteristic equation

$$\det\left(\boldsymbol{\sigma}\text{-}\lambda\mathbf{I}\right)=\mathbf{0}$$

determines the three principal stresses $\sigma_1=\lambda_1$, $\sigma_2=\lambda_2$ and $\sigma_3=\lambda_3$ and for each λ-value (4.13) provides the corresponding principal direction $\boldsymbol{n}$. The principal stresses and directions are real, the principal stresses are invariants and the principal directions may always be taken to be orthogonal. If the coordinate system is taken collinear with the principal directions $\boldsymbol{n_1}$, $\boldsymbol{n_2}$ and $\boldsymbol{n_3}$, the stress tensor takes the following simple form

$$\boldsymbol{\sigma}'=\mathbf{A}\boldsymbol{\sigma}\mathbf{A}^T=\begin{bmatrix}\sigma_1 & 0 & 0\\ 0 & \sigma_2 & 0\\ 0 & 0 & \sigma_3\end{bmatrix}\quad \textit{where}\quad \mathbf{A}^T=\begin{bmatrix}\mathbf{n_1} & \mathbf{n_2} & \mathbf{n_3}\end{bmatrix}$$

Also the stress tensor satisfies the Cayley-Hamilton theorem. Moreover, the coefficients in the characteristic equation are the Cauchy-stress invariants, but of more importance are the following generic stress invariants

$$\mathbf{I}_1=\sigma_{ii}\qquad \mathbf{I}_2=\frac{1}{2}\sigma_{ij}\sigma_{ji}\qquad \mathbf{I}_3=\frac{1}{3}\sigma_{ij}\sigma_{jk}\sigma_{ki}\qquad (4.14)$$

where the term ‘generic’ refers to the systematic definition of these invariants (we may refer to (3.52) for a comparison with the corresponding strain invariants).

4.4 Stress deviator tensor

Similarly to the exposition of the strain tensor, we define the stress deviator tensor by

$$s_{ij} = \sigma_{ij} - \frac{1}{3}\sigma_{kk}\delta_{ij} \qquad (4.15)$$

where $\sigma_{kk}/3$ is called the hydrostatic stress. The σ_{ij} and s_{ij} tensors have identical off-diagonal elements and thus they have identical principal directions.
The generic invariants of the stress deviator tensor are given by

$$\mathbf{J}_1 = s_{ii} = 0; \qquad \mathbf{J}_2 = \frac{1}{2}s_{ij}s_{ji}; \qquad \mathbf{J}_3 = \frac{1}{3}s_{ij}s_{jk}s_{ki}; \qquad (4.16)$$

Similar to (3.54) we have

$$\mathbf{J}_3 = s_1 s_2 s_3 \qquad (4.17)$$

Moreover, similar to (3.55) and (3.56) we find the following relations

$$\mathbf{J}_2 = \mathbf{I}_2 - \frac{1}{6}\mathbf{I}_1^2; \qquad \mathbf{J}_3 = \mathbf{I}_3 - \frac{2}{3}\mathbf{I}_1\mathbf{I}_2 + \frac{2}{27}\mathbf{I}_1^3 \tag{4.18}$$

and

$$\mathbf{I}_2 = \mathbf{J}_2 + \frac{1}{6}\mathbf{I}_1^2; \qquad \mathbf{I}_3 = \mathbf{J}_3 + \frac{2}{3}\mathbf{I}_1\mathbf{I}_2 - \frac{2}{27}\mathbf{I}_1^3 \tag{4.19}$$

Therefore, instead of using the set of invariants $\boldsymbol{I_1}$, $\boldsymbol{I_2}$ and $\boldsymbol{I_3}$ we may equally well use the set $\boldsymbol{I_1}$, $\boldsymbol{J_2}$ and $\boldsymbol{J_3}$.

Finally, and in analogy with (3.57), we have the octahedral normal stress σ_0 and octahedral shear stress τ_0 defined by

$$\sigma_0 = \frac{1}{3}\mathbf{I_1}; \qquad \tau_0 = \sqrt{\frac{2}{3}\mathbf{J_2}} \tag{4.20}$$

where σ_0 and τ_0 are the normal stress shear and stress respectively, that act on an octahedral plane. Here, the normal to an octahedral plane makes equal angles to the principal stress directions, when comparing (4.20) with (3.57) note the difference between engineering shear strain and tensorial shear strain.

4.5 Special states of stress

Several special states of stress, which are often encountered in practice, will now be discussed.

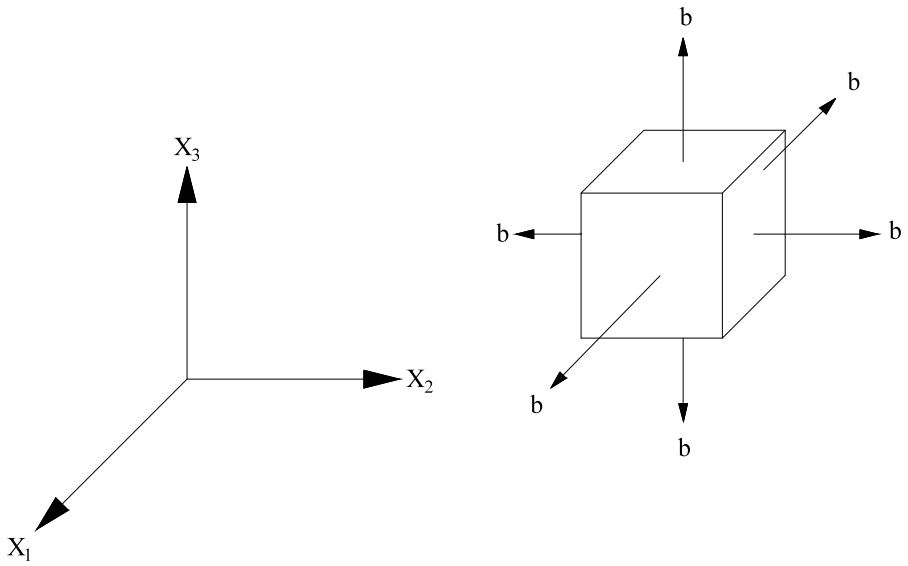

Figure 4.6: hydrostatic state of stress

A state of hydrostatic stress exists, if the stress tensor is given by

$$\sigma_{ij} = b\delta_{ij}$$

where *b* is an arbitrary scalar. It appears that the deviatoric stress tensor s_{ij} is zero and that the loading consists of equal normal stresses having the amount b, cf. Fig. 4.6.

Uniaxial stress occurs if the stress tensor is given by

$$\sigma_{ij} = \begin{bmatrix} \sigma_{11} & 0 & 0 \\ 0 & 0 & 0 \\ 0 & 0 & 0 \end{bmatrix}$$

Plane stress exists if the stress tensor is given by

$$\sigma_{ij} = \begin{bmatrix} \sigma_{11} & \sigma_{12} & 0 \\ \sigma_{21} & \sigma_{22} & 0 \\ 0 & 0 & 0 \end{bmatrix}$$

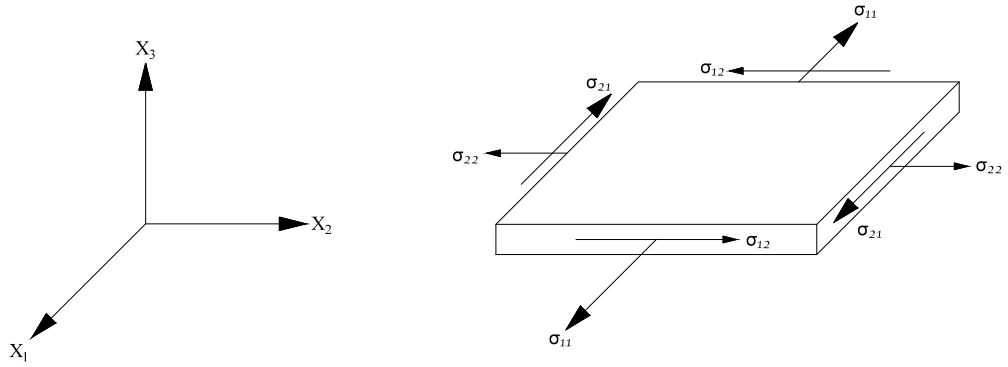

Figure 4.7: plane stress

and a disc loaded by in-plane stresses comprises an illustration of this type of loading, cf. Fig. 4.7.

Finally, a state of pure shear exists, if

$$\sigma_{ij} = \begin{bmatrix} 0 & \sigma_{12} & 0 \\ \sigma_{21} & 0 & 0 \\ 0 & 0 & 0 \end{bmatrix}$$

which holds for pure torsion of a cylindrical specimen. It is easily shown that the principal stresses become $\sigma_1 = \sigma_{12}$, $\sigma_2 = -\sigma_{12}$ and $\sigma_3 = 0$.

4.6 Heigh-Westergaard coordinate system - Geometrical interpretation of stress invariants

It is evident that the yield surface may be interpreted as a surface in the Cartesian coordinate system with axes σ_1, σ_2 and σ_3 - the so-called Heigh-Westergaard coordinate system. Moreover, with this interpretation it will turn out that it is

possible to identify certain geometrical quantities related to the stress invariants I_1, J_2 and $cos3\theta$.

For this purpose, consider an arbitrary point P with coordinates (σ_1, σ_2, σ_3) in the Haigh-Westergaard coordinate system, cf. Fig.4.8a). In this stress space, we may identify the unit vector n_i along the space diagonal. This vector is given by

$$n_1 = \frac{1}{\sqrt{3}}(1,\ 1,\ 1) \qquad (4.21)$$

If the stress point is located along the space diagonal, all principal stresses are equal and the space diagonal is therefore called the hydrostatic axis.

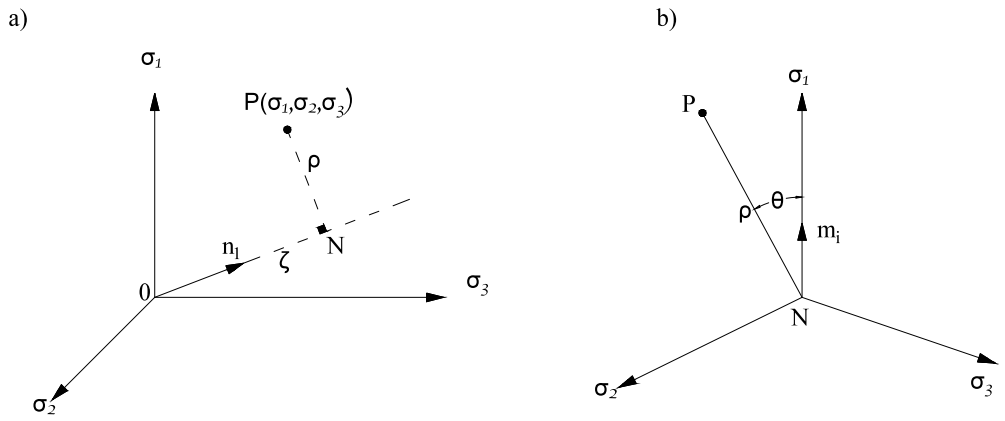

Figure 4.8: a) Haigh-Westergaard coordinate system; b) deviatoric plane perpendicular to the hydrostatic axis and containing line NP

For any stress point P we may locate a plane which is perpendicular to the hydrostatic axis and which contains the point P. This plane is called the deviatoric plane and it contains the line PN in Fig. 4.8a). When viewed in the direction of the hydrostatic axis, the projections of the σ_1, σ_2 and σ_3 axes on the deviatoric plane are shown in Fig. 4.8b). The particular deviatoric plane that contains the origin O of the stress space is occasionally called the *π-plane*.

The position of the arbitrary stress point P is given by the Cartesian coordinates (σ_1, σ_2, σ_3). However, instead of these coordinates, we may equally well use the coordinates (ξ, ρ, θ) illustrated in Fig. 4.8. The coordinate ξ is then the distance from the origin O to the point N and ξ is a positive or negative quantity, if the vector ON has the same or opposite direction as the unit vector n_i respectively. The coordinate ρ denotes the distance $|NP|$ in the deviatoric plane of the point P to the hydrostatic axis. Finally, θ is the angle in the deviatoric plane between the projection of the σ_1-axis on the deviatoric plane and the line NP. It appears that ρ and θ are the polar coordinates of point P in the deviatoric plane.

With this qualitative description, we will now derive explicit expressions for the coordinates (ξ, ρ, θ). From Fig. 4.8a) and (4.21), the coordinate ξ is given by

$$\xi = n^T \bar{O}\bar{P} = \frac{1}{\sqrt{3}} \begin{bmatrix} 1 & 1 & 1 \end{bmatrix} \begin{bmatrix} \sigma_1 \\ \sigma_2 \\ \sigma_3 \end{bmatrix}$$

i.e.

$$\xi = \frac{I_1}{\sqrt{3}} \tag{4.22}$$

It follows that the vector $ON = \xi \boldsymbol{n}$ is given by

$$\bar{O}\bar{N} = \frac{I_1}{3} \begin{bmatrix} 1 \\ 1 \\ 1 \end{bmatrix}$$

The vector NP in the deviatoric plane then becomes

$$\overline{NP} = \overline{OP} - \overline{ON} = \begin{bmatrix} \sigma_1 \\ \sigma_2 \\ \sigma_3 \end{bmatrix} - \frac{I_1}{3}\begin{bmatrix} 1 \\ 1 \\ 1 \end{bmatrix} = \begin{bmatrix} s_1 \\ s_2 \\ s_3 \end{bmatrix} \qquad (4.23)$$

where s_1, s_2 and s_3 are the principal deviatoric stresses. We recall that NP is located in the deviatoric plane and since NP is given entirely in terms of the deviatoric stresses, this suggests the notation of the deviatoric plane. The length $\rho=|NP|$ of the vector $\overline{NP}$ is given by $\rho^2 = \overline{NP^T}\overline{NP} = s_1^2 + s_2^2 + s_3^2$ i.e.

$$\rho = \sqrt{2J_2} \qquad (4.24)$$

It should be observed that, by definition, both ρ and J_2 are non-negative quantities. With (4.22) and (4.24), we have seen that the coordinates ξ and ρ can be expressed in terms of stress invariants. To obtain an expression for the angle θ, cf. Fig. 3.8b), some further manipulations are necessary.

Referring to Fig. 4.8b), the unit vector mi located in the deviatoric plane and directed along the projection of the σ_1-axis on the deviatoric plane must have the form

$$m_i = (a, -b, -b)$$

where $a > 0$ and $b > 0$. Since m_i is orthogonal to the hydrostatic axis we have $m_i n_i = 0$, cf. Fig. 4.8, and this leads to $b = a/2$. Moreover, as m_i is a unit vector, we conclude that

$$m_i = \frac{1}{\sqrt{6}}(2, -1, -1) \qquad (4.25)$$

The angle θ is measured from the m_i -vector in the counter-clockwise direction towards the vector *NP*, i.e. we obtain with (4.23) and (4.25)

$$\rho\cos\theta = \mathbf{m}^T\bar{N}\bar{P} = \frac{1}{\sqrt{6}}\begin{bmatrix} 2 & -1 & -1 \end{bmatrix}\begin{bmatrix} s_1 \\ s_2 \\ s_3 \end{bmatrix} = \frac{2s_1 - s_2 - s_3}{\sqrt{6}}$$

With ρ given by the above equation and since $s_2+s_3=-s_1$ we obtain

$$\cos\theta = \frac{\sqrt{3}}{2}\frac{s_1}{J_2} \qquad (4.26)$$

Use of the trigonometric identity $cos3\theta = 4cos^3\theta-3cos\theta$ then results in

$$\cos 3\theta = \frac{3\sqrt{3}}{2J_2^{3/2}}s_1(s_1^2 - J_2) \qquad (4.27)$$

To obtain a more convenient expression for $cos3\theta$, we shall perform some algebraic manipulations. From the definition of J_2, and since $s_2+s_3=-s_1$ we find

$$s_1^2 - J_2 = \frac{1}{2}\left(s_1^2 - s_2^2 - s_3^2\right) = \frac{1}{2}\left[\left(s_2^2 + s_3^2\right) - s_2^2 - s_3^2\right] = s_2 s_3 \qquad (4.28)$$

We next note that the invariant J_3 also can be written as

$$J_3 = s_1 s_2 s_3$$

Finally use of this expression and (4.28) in (4.27) provides the result

$$\cos 3\theta = \frac{3\sqrt{3}}{2}\frac{J_3}{J_2^{3/2}} \qquad (4.29)$$

i.e. we have established the relation and we have expressed the angle θ in terms of stress invariants. The angle θ is often called the Lode angle after Lode (1926). Clearly, the angle θ is also given by (4.26), but the advantage of (4.29) is that here θ is expressed in terms of the stress invariants and not the principal stresses. This implies that the eigenvalue problem does not have to be solved as the stress invariants are obtained directly from the stress tensor.

Let us return to the formulation

$$F(I_1, J_2, \cos 3\theta) \qquad (4.30)$$

It appears that we have established a very convenient formulation where all the stress invariants can be interpreted geometrically. Moreover, formulation (4.29) separates the influence of the hydrostatic stress I_1 from the influence of the deviatoric stresses as expressed by J_2 and $cos3\theta$. Whereas the invariant J_2 tells us about the influence of the magnitude of the deviatoric stresses, cf. (4.24), the invariant $cos3\theta$ informs us about the influence of the direction of the deviatoric stresses. In addition, the presence of the term $cos3\theta$ enables us to derive a number of symmetry properties of the failure or initial yield criterion.

A state of stress $(\sigma_1, \sigma_2, \sigma_3)$ can be expressed by (ξ, ρ, θ) where the relation between the two coordinate systems can be established in the following manner. From (4.26), we know

$$s_1 = \frac{2}{\sqrt{3}}\sqrt{J_2}\cos\theta \qquad (4.31)$$

In a similar manner the deviatoric stress components s_2 and s_3 can also be obtained in terms of the angle θ. These components are given by

$$s_2 = \frac{2}{\sqrt{3}}\sqrt{J_2}\cos\left(\frac{2\pi}{3} - \theta\right) \tag{4.32}$$

and

$$s_2 = \frac{2}{\sqrt{3}}\sqrt{J_2}\cos\left(\frac{2\pi}{3} + \theta\right) \tag{4.33}$$

These relations are satisfied only if the angle lies in the range

$$0 \le \theta \le \frac{\pi}{3} \tag{4.34}$$

The three principal stresses of σ_{ij} are therefore given by

$$\begin{aligned}\begin{Bmatrix}\sigma_1\\ \sigma_2\\ \sigma_3\end{Bmatrix} &= \begin{Bmatrix}p\\ p\\ p\end{Bmatrix} + \frac{2}{\sqrt{3}}\sqrt{J_2}\begin{Bmatrix}\cos\theta\\ \cos(\theta - 2\pi/3)\\ \cos(\theta + 2\pi/3)\end{Bmatrix}\\ &= \frac{1}{\sqrt{3}}\begin{Bmatrix}\xi\\ \xi\\ \xi\end{Bmatrix} + \sqrt{\frac{2}{3}}\rho\begin{Bmatrix}\cos\theta\\ \cos(\theta - 2\pi/3)\\ \cos(\theta + 2\pi/3)\end{Bmatrix}\end{aligned} \tag{4.35}$$

5 Linear Elasticity

In the previous chapter the concepts of strain and stress were established, with no reference to the material and within the assumption of small strains and small rotations, it was said that the results hold for any material. It is obvious however that stresses and strains must be related in some way and this specific relation is controlled by the specific material in question. The expression between stresses and strains is the constitutive relation and a variety of such relations has been established Examples are: elasticity, plasticity, viscoelasticity and viscoplasticity. In this chapter it will be considered the simplest constitutive model: the linear elasticity.

5.1 Elasticity

In the absence of thermal, electromagnetic and chemical effects experimental evidence indicates that, within a certain allowable limit of deformation, most materials encountered in our daily life exhibit the following properties:

1. If it is not under the influence of any external disturbance, a body of material is free of any internal stress and can remain in this "unstressed" or "natural" state indefinitely.

2. When subject to external loads, the state of stress at each point in the body depends only on the state of strain at the same point and conversely.
3. The body returns to the unstressed state once the external loads are removed.

We call such a body an elastic body and the properties l.-3. elasticity.
For many materials at the working load level, the elastic range also includes a region throughout which stress and strain have a linear relationship.
To indicate other possible modes of behavior, we note for instance that the stress state at a point of a body may depend on the time history of the strain state at that same point (viscoelasticity) or on the strain state of all points in some neighborhood of the given point (nonlocal theory). We are interested only in elastic bodies in this chapter

5.2 Introduction to linear elasticity

The simplest mechanical test consists of placing a standardized specimen with its ends in the grips of a tensile testing machine and then applying load under controlled conditions. Uniaxial loading conditions are thus approximately obtained. A force balance on a small element of the specimen yields the longitudinal (true) stress as

$$\sigma = \frac{\mathbf{F}}{A} \qquad (5.1)$$

where $\boldsymbol{F}$ is the applied force and A is the (instantaneous) cross sectional area of the specimen. Alternatively if the initial cross sectional area A_0 is used one obtain the engineering stress:

$$\boldsymbol{\sigma}_e = \frac{\mathbf{F}}{A_0} \tag{5.2}$$

For loading in the elastic regime, for most engineering materials $\boldsymbol{\sigma_e \approx \sigma}$.
Likewise, the true strain is defined as

$$\boldsymbol{\varepsilon} = \int_{l_0}^{l} \frac{dl}{l} = \ln\left(\frac{l}{l_0}\right) \tag{5.3}$$

while the engineering strain is given by

$$\boldsymbol{\varepsilon} = \int_{l_0}^{l} \frac{dl}{l_0} = \frac{l - l_0}{l_0} \tag{5.4}$$

Again, for loading in the elastic regime, for most engineering materials $\boldsymbol{\varepsilon_e \approx \varepsilon}$.
Linear elastic behavior in the tension test is well described by Hooke's law, namely

$$\boldsymbol{\sigma} = \mathbf{E}\boldsymbol{\varepsilon} \tag{5.5}$$

where $\boldsymbol{E}$ is the modulus of elasticity or Young's modulus. For most materials, this is a large number of the order of 10^{11} Pa.

5.3 Generalized Hooke' s Law

For sufficiently "small" external loads, experimental results indicate that strain components of an elastic medium will be small compared to unity and that the elastic stress strain relations are effectively linear. We will be interested in these notes only in this particular range of elasticity. In this range, the stress strain relations are essentially a generalization of Hooke's original observation and are often referred to as generalized Hooke's law, and the body is said to be linearly elastic. The most general form of the linear stress strain relations may then be written as

$$\boldsymbol{\sigma} = \mathbf{E} : \boldsymbol{\varepsilon} \qquad or \qquad \sigma_{ij} = E_{ijkl}\varepsilon_{kl} \tag{5.6}$$

where σ_{ij} and ε_{kl} are respectively the stress and strain tensor components and both are second order tensors. The quantity E_{ijkl} is the fourth order tensor of elastic constants and it characterizes the elastic properties of the material. Since the stress and strain tensors are symmetric, the elastic constants tensor consists of 36 components. This may be further reduced to 21 elastic constants if we invoke major symmetry of the elasticity tensor i.e.

$$\mathbf{E} = \mathbf{E}^{\mathrm{T}} \qquad or \qquad E_{ijkl} = E_{klij} \quad with \quad E_{ijkl} = E_{ijlk} \quad and \quad E_{ijkl} = E_{jilk} \tag{5.7}$$

This number of constant is further reduced in special cases. For instance for isotropic materials (elastic properties the same in all directions) the number of elastic constants is 2. For orthotropic materials (characterized by three mutually perpendicular planes of symmetry) the number of constants is 9. If the material

exhibits symmetry with respect to only one plane, the number of constants is 13. An elastic body is homogeneous if the elastic moduli E_{ijkl} are constants throughout the body. It is inhomogeneous otherwise.

5.4 Isotropic linear elastic stress-strain relations

For an isotropic material, the elastic constants in eq. (5.7) must be the same in all directions. Thus tensor E_{ijkl} must be an isotropic fourth order tensor. It can be shown that the most general form for the isotropic tensor E_{ijkl} is given by

$$\mathbf{E} = a_0 \mathbf{1}\otimes\mathbf{1} + a_1 \mathbf{1}\overline{\otimes}\mathbf{1} + a_2 \mathbf{1}\underline{\otimes}\mathbf{1} \qquad or \qquad E_{ijkl} = a_0\delta_{ij}\delta_{kl} + a_1\delta_{ik}\delta_{jl} + a_2\delta_{il}\delta_{jk} \qquad (5.8)$$

where $\boldsymbol{1}=[\delta_{ij}]$ stands for the second order unit tensor. The three parameters expression may be recast in terms of symmetric and skew symmetric fourth order tensors components as

$$\mathbf{E} = a_0 \mathbf{1}\otimes\mathbf{1} + b_1 \mathbf{I} + b_2 \mathbf{I}^{skew} \qquad (5.9)$$

where the symmetric fourth order unit tensor reads

$$\mathbf{I} = \frac{1}{2}\left[\mathbf{1}\otimes\mathbf{1} + \mathbf{1}\underline{\otimes}\mathbf{1}\right] \qquad or \qquad I_{ijkl} = \frac{1}{2}\left[\delta_{ik}\delta_{jl} + \delta_{il}\delta_{jk}\right] \qquad (5.10)$$

and the skewed symmetric one

$$\mathbf{I}^{skew} = \frac{1}{2}\left[\mathbf{1}\overline{\otimes}\mathbf{1} - \mathbf{1}\underline{\otimes}\mathbf{1}\right] \qquad or \qquad I^{skew}_{ijkl} = \frac{1}{2}\left[\delta_{ik}\delta_{jl} - \delta_{il}\delta_{jk}\right] \qquad (5.11)$$

Because of the symmetry of stress and strain the skewed symmetric contribution is not present, $b_2=0$, thus isotropic linear elasticity the material behavior is fully described by two independent elastic constants. The fourth order material stiffness tensor reduces to

$$\mathbf{E} = \Lambda \mathbf{1}\otimes\mathbf{1} + 2G\mathbf{I} \qquad or \qquad E_{ijkl} = \Lambda\delta_{ij}\delta_{kl} + G[\delta_{ik}\delta_{jl} + \delta_{il}\delta_{jk}] \qquad (5.12)$$

where the two elastic constants Λ, G are the Lamè constants

$$\Lambda = \frac{E\nu}{[1+\nu][1-2\nu]} \tag{5.13}$$

is the cross modulus, and

$$G = \frac{E}{2[1+\nu]} \tag{5.14}$$

denotes the shear modulus, which has a one to one relationship with the modulus of elasticity and Poisson's ratio, E, ν.
In absence of initial stresses and strains due to environmental effects, the linear elastic relation reduces to

$$\boldsymbol{\sigma} = \Lambda[tr\boldsymbol{\varepsilon}]\mathbf{1} + 2G\boldsymbol{\varepsilon} \qquad or \qquad \sigma_{ij} = \Lambda\varepsilon_{kk}\delta_{ij} + 2G\varepsilon_{ij} \tag{5.15}$$

where the trace operator is the sum of the diagonal entities of the second order tensor corresponding to double contraction with the identity tensor $tr\boldsymbol{\varepsilon}=\varepsilon_{kk}=\boldsymbol{1:\varepsilon}$.

5.5 Matrix form of elastic stiffness σ=Eε

Isotropic linear elastic behavior may be described also in a matrix format using the engineering definition of shear strain $\gamma_{ij} = 2\varepsilon_{ij}$. The elastic stiffness matrix may be written for isotropic behavior as

$$\mathbf{E} = \begin{bmatrix} \Lambda+2G & \Lambda & \Lambda & & & \\ \Lambda & \Lambda+2G & \Lambda & & 0 & \\ \Lambda & \Lambda & \Lambda+2G & & & \\ & & & G & & \\ & 0 & & & G & \\ & & & & & G \end{bmatrix} \tag{5.16}$$

5.6 Matrix for of elastic compliance ε=Cσ

In the isotropic case the normal stress σ_{11} gives rise to three normal strain contributions, the direct strain $\varepsilon_{11} = 1/E\ \sigma_{11}$ and the normal strains $\varepsilon_{22} = -\nu/E\ \sigma_{11}$ and $\varepsilon_{33} = \nu/E\ \sigma_{11}$ because of the cross Poisson's effect. The additional strain contributions due to σ_{22} and σ_{33} enter the compliance relation for isotropic elasticity in the matrix format

$$\begin{bmatrix} \varepsilon_{11} \\ \varepsilon_{22} \\ \varepsilon_{33} \end{bmatrix} = \frac{1}{E} \begin{bmatrix} 1 & -\nu & -\nu \\ -\nu & 1 & -\nu \\ -\nu & -\nu & 1 \end{bmatrix} \begin{bmatrix} \sigma_{11} \\ \sigma_{22} \\ \sigma_{33} \end{bmatrix} \tag{5.17}$$

In the isotropic case the shear response is entirely decoupled from the direct response of the normal components. Thus the compliance matrix expands into the partitioned form

$$\mathbf{C} = \frac{1}{E}\begin{bmatrix} 1 & -\nu & -\nu & & & \\ -\nu & 1 & -\nu & & 0 & \\ -\nu & -\nu & 1 & & & \\ & & & 2[1-\nu] & & \\ & 0 & & & 2[1-\nu] & \\ & & & & & 2[1-\nu] \end{bmatrix} \qquad (5.18)$$

where isotropy entirely decouples the shear response from the normal stress - strain response. This cross effect of Poisson is illustrated in Figure 5.1, which shows the interaction of lateral and axial deformations under axial compression.

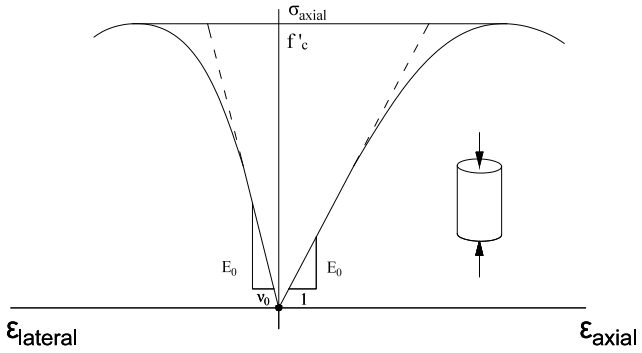

Figure 5.1: Poisson effect in axial compression

The elastic compliance relation reads in direct and indicial notations

$$\mathbf{C} = -\frac{\nu}{E}\mathbf{1}\otimes\mathbf{1} + \frac{1}{2G}\mathbf{I} \qquad or \qquad C_{ijkl} = -\frac{\nu}{E}\delta_{ij}\delta_{kl} + \frac{1+\nu}{2E}\left[\delta_{ik}\delta_{jl} + \delta_{il}\delta_{jk}\right] \qquad (5.19)$$

Using the index notation, we can write the stress-strain relation in a concise form

$$\varepsilon_{ij} = \frac{1+\nu}{E}\sigma_{ij} - \frac{\nu}{E}\sigma_{kk}\delta_{ij} \qquad (5.20)$$

5.7 Canonical Format of isotropic Elasticity

Decomposing the stress and strain tensors into spherical and deviatoric components

$$\begin{aligned} \mathbf{s} &= \boldsymbol{\sigma} - \sigma_{vol}\mathbf{1} \qquad where \qquad \sigma_{vol} = \frac{1}{3}[tr\boldsymbol{\sigma}] \\ \mathbf{e} &= \boldsymbol{\varepsilon} - \varepsilon_{vol}\mathbf{1} \qquad where \qquad \varepsilon_{vol} = \frac{1}{3}[tr\boldsymbol{\varepsilon}] \end{aligned} \qquad (5.21)$$

leads to the stress deviator

$$\mathbf{s}(\mathbf{x},t) = \begin{bmatrix} \frac{1}{3}[2\sigma_{11} - \sigma_{22} - \sigma_{33}] & \sigma_{12} & \sigma_{12} \\ \sigma_{21} & \frac{1}{3}[2\sigma_{22} - \sigma_{11} - \sigma_{33}] & \sigma_{23} \\ \sigma_{31} & \sigma_{32} & \frac{1}{3}[2\sigma_{33} - \sigma_{22} - \sigma_{11}] \end{bmatrix} \qquad (5.22)$$

and the strain deviator

$$\mathbf{e}(\mathbf{x},t)=\begin{bmatrix} \frac{1}{3}\left[2\varepsilon_{11}-\varepsilon_{22}-\varepsilon_{33}\right] & \varepsilon_{12} & \varepsilon_{12} \\ \varepsilon_{21} & \frac{1}{3}\left[2\varepsilon_{22}-\varepsilon_{11}-\varepsilon_{33}\right] & \varepsilon_{23} \\ \varepsilon_{31} & \varepsilon_{32} & \frac{1}{3}\left[2\varepsilon_{33}-\varepsilon_{22}-\varepsilon_{11}\right] \end{bmatrix} \qquad (5.23)$$

which have the property $tr\mathbf{s} = 0$ and $tr\mathbf{e} = 0$. The decomposition decouples the volumetric from the distortional response, because of the underlying orthogonality of the spherical and deviatoric partitions, $\mathbf{s}:[\sigma_{vol}\,\mathbf{1}]=0$ and $\mathbf{e}:[\varepsilon_{vol}\,\mathbf{1}]=0$. The decoupled response reduces the elasticity tensor to the scalar form,

$$\sigma_{vol}=3K\varepsilon_{vol} \qquad \textit{and} \qquad \mathbf{s}=2G\mathbf{e} \qquad (5.24)$$

in which the bulk and the shear moduli,

$$K=\frac{E}{3\left[1-2\nu\right]}=\Lambda+\frac{2}{3}G \qquad \textit{and} \qquad G=\frac{E}{2[1+\nu]}=\frac{3}{2}\left[K-\Lambda\right] \qquad (5.25)$$

define the volumetric and the deviatoric material stiffness.
Consequently, the internal strain energy density expands into the canonical form of two decoupled contributions

$$2W=\boldsymbol{\sigma}:\boldsymbol{\varepsilon}=\left[\sigma_{vol}\mathbf{1}\right]:\left[\varepsilon_{vol}\mathbf{1}\right]+\mathbf{s}:\mathbf{e}=9K\varepsilon_{vol}^{2}+2G\mathbf{e}:\mathbf{e} \qquad (5.26)$$

such that the positive strain energy argument delimits the range of possible values of Poisson's ratio $-1 \leq \nu \leq 0.5$

5.8 Isotropic Elasticity under Initial Volumetric Strain

In the case of isotropic material behavior, with no directional properties, the size of a representative volume element may change due to thermal effects or shrinkage and swelling, but it will not distort.
Consequently, the expansion is purely volumetric, i.e. identical in all directions. Using direct and indicial notation, the additive decomposition of strain into elastic and initial volumetric components, $\boldsymbol{\varepsilon}=\boldsymbol{\varepsilon}_e + \boldsymbol{\varepsilon}_0$ leads to the following extension of the elastic compliance relation:

$$\boldsymbol{\varepsilon} = -\frac{\nu}{E}\left[tr\boldsymbol{\sigma}\right]\mathbf{1} + \frac{1}{2G}\boldsymbol{\sigma} + \varepsilon_0\mathbf{1} \qquad or \qquad \varepsilon_{ij} = -\frac{\nu}{E}\sigma_{kk}\delta_{ij} + \frac{1}{2G}\sigma_{ij} + \varepsilon_0\delta_{ij} \qquad (5.27)$$

where $\boldsymbol{\varepsilon_0} = \varepsilon_0 \boldsymbol{1}$ denotes the initial volumetric strain e.g. due to thermal expansion. The inverse relation reads

$$\boldsymbol{\sigma} = -\Lambda\left[tr\boldsymbol{\varepsilon}\right]\mathbf{1} + 2G\boldsymbol{\varepsilon} - \mathbf{3}\varepsilon_0 K\mathbf{1} \qquad or \qquad \sigma_{ij} = \Lambda\varepsilon_{kk}\delta_{ij} + 2G\varepsilon_{ij} - 3\varepsilon_0 K\delta_{ij} \qquad (5.28)$$

Rewriting this equation in matrix notation we have

$$\begin{bmatrix} \sigma_{11} \\ \sigma_{22} \\ \sigma_{33} \end{bmatrix} = \begin{bmatrix} K+\frac{4}{3}G & K-\frac{2}{3}G & K-\frac{2}{3}G \\ K-\frac{2}{3}G & K+\frac{4}{3}G & K-\frac{2}{3}G \\ K-\frac{2}{3}G & K-\frac{2}{3}G & K+\frac{4}{3}G \end{bmatrix} \begin{bmatrix} \varepsilon_{11} \\ \varepsilon_{22} \\ \varepsilon_{33} \end{bmatrix} - 3K\varepsilon_0 \begin{bmatrix} 1 \\ 1 \\ 1 \end{bmatrix} \qquad (5.29)$$

Considering the special case of plane stress, $\sigma_{33}=0$, the stress strain relation reduces in the presence of initial volumetric strain to

$$\begin{bmatrix} \sigma_{11} \\ \sigma_{22} \end{bmatrix} = \frac{E}{1-\nu^2} \begin{bmatrix} 1 & \nu \\ \nu & 1 \end{bmatrix} \begin{bmatrix} \varepsilon_{11} \\ \varepsilon_{22} \end{bmatrix} \frac{E}{1-\nu} \varepsilon_0 \begin{bmatrix} 1 \\ 1 \end{bmatrix} \qquad (5.30)$$

where the shear components are not affected by the temperature change in the case of isotropy.

5.9 Free thermal expansion

Under stress free conditions the thermal expansion $\boldsymbol{\varepsilon_0}=\alpha[T-T_0]\boldsymbol{1}$ leads to $\boldsymbol{\varepsilon}=\boldsymbol{\varepsilon_0}$ i.e.

$$\begin{aligned} \varepsilon_{11} &= \alpha\left[T-T_0\right] \\ \varepsilon_{22} &= \alpha\left[T-T_0\right] \\ \varepsilon_{33} &= \alpha\left[T-T_0\right] \end{aligned} \qquad (5.31)$$

Thus the change of temperature results in free thermal expansion, while the mechanical stress remains zero under zero confinement, $\boldsymbol{\sigma}=\boldsymbol{E}:\boldsymbol{\varepsilon_e}=\boldsymbol{0}$.

5.10 Thermal stress under full confinement

In contrast with the unconfined situation above, the thermal expansion is equal and opposite to the elastic strain $\boldsymbol{\varepsilon_e}=-\boldsymbol{\varepsilon_0}$ under full confinement, when $\boldsymbol{\varepsilon}=\boldsymbol{0}$. In the case of plane stress, the temperature change $\Delta T=T-T_0$ leads to the thermal stresses

$$\begin{aligned}\sigma_{11} &= -\frac{E}{1-\nu}\alpha\left[T-T_0\right] \\ \sigma_{22} &= -\frac{E}{1-\nu}\alpha\left[T-T_0\right]\end{aligned} \qquad (5.32)$$

6 Nonlinear Elasticity

As mentioned in the previous chapter the elastic response is independent of the load history, or, in other words, the elastic material response is path independent and it follows that the response for loading and unloading follows the same path as illustrated in Fig. 6.1. After removal of the loading, the material returns therefor to its original configuration. It should be emphasized that elastic response, in general, is nonlinear, as also illustrated in Fig. 6.1.

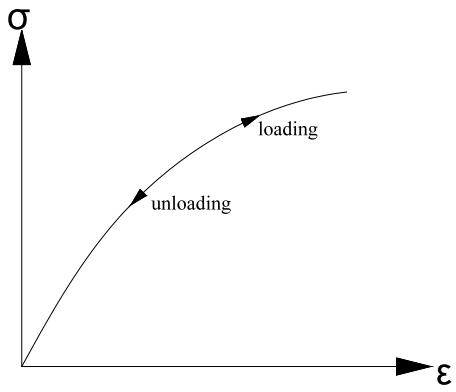

Figure 6.1: nonlinear elasticity for uniaxial loading

The linear elastic stress-strain relations discussed in the previous chapter are isotropic and reversible. A simple extension of these relations with the elastic moduli replaced by scalar functions associated with either stress and/or strain invariants have the properties of isotropy and reversibility also. For instance,

scalar function associated with the state of stress may include the values of the principal stresses σ_1, σ_2 and σ_3, or equally the three independent invariants I_1, J_2 and J_3. Therefore different scalar functions such as $F(I_1,J_2,J_3)$ may be employed to describe various nonlinear elastic constitutive models. The nonlinear stress-strain relations for each of these models reduce to the linear forms when the scalar functions are taken to be constants.

6.1 Hyper Elasticity – Green Elasticity

The hyperelastic format of elasticity dates back to the original work of George Green. This is an integral description of elasticity and starts from the postulate of a strain energy function from which the stresses are derived by differentiation. Let us first introduce the concept of strain energy W per unit volume of the body, i.e. W has the unit [Nm/m^3]. For a uniaxial stress state, the incremental strain energy is defined by

$$dW = \sigma d\varepsilon \qquad i.e. \qquad W = \int_0^{\varepsilon} \sigma(\varepsilon^*) d\varepsilon^* \tag{6.1}$$

where ε^* is an integration variable whereas ε denotes the current strain. Equation (6.1) is illustrated in Fig. 6.2.

Adopting this approach to the general situation we obtain

$$dW = \sigma_{ij} d\varepsilon_{ij} \qquad i.e. \qquad W = \int_0^{\varepsilon_{ij}} \sigma_{ij}(\varepsilon^*_{kl}) d\varepsilon^*_{ij} \tag{6.2}$$

where ε_{ij} denote the current strains whereas ε^*_{ij} denotes the integration variables. Even though the current stresses σ_{ij} only depend on the current strains ε_{ij}, we will in general have that the strain energy W as determined by (6.2) depends both on the current strains ε_{ij} as well as on the manner in which these strains were achieved, i.e.

$$W = W(\varepsilon_{ij},\ load\ history) \tag{6.3}$$

This is just to say that W as determined by (6.2) depends not only on the current strains, but also on the integration path, where the integration path represents the load history.
We will now make the assumption that W is independent on the integration path and (6.3) then reduces to

$$W = W(\varepsilon_{ij}) \tag{6.4}$$

From this expression follows that

$$dW = \frac{\partial W}{\partial \varepsilon_{ij}} d\varepsilon_{ij} \tag{6.5}$$

Subtraction of (6.5) from (6.2) gives

$$\left(\sigma_{ij} - \frac{\partial W}{\partial \varepsilon_{ij}} \right) d\varepsilon_{ij} = 0 \tag{6.6}$$

In general, the incremental strains $d\varepsilon_{ij}$ can be chosen arbitrarily and independently of each other and we therefore conclude from (6.6) that

$$\sigma_{ij} = \frac{\partial W}{\partial \varepsilon_{ij}} \qquad (6.7)$$

There is one exception where the incremental strains $d\varepsilon_{ij}$ cannot be chosen arbitrarily, namely the case of incompressible response. Since σ_{ij} is obtained from W by a differentiation, one uses the phrase that W serves as a potential function for the stresses.

We observe that (6.4) and (6.7) imply $\sigma_{ij} = \sigma_{ij}(\varepsilon_{ij})$ and a material that obeys the constitutive relation (6.4) and thereby (6.7) is called a hyper-elastic material, hyper meaning to a higher degree.

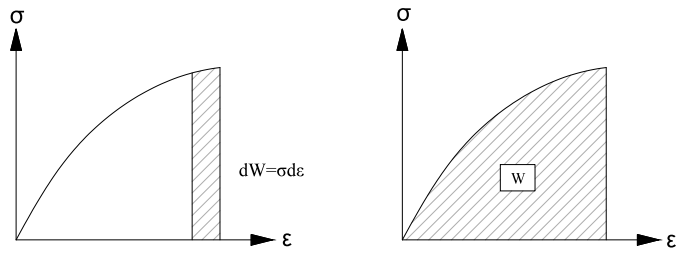

Figure 6.2: incremental strain energy dW and strain energy W for uniaxial loading

Occasionally, the term Green-elasticity is used since this formulation was adopted by Green in 1839 and even today most work on elasticity is based on this format.

Another feature often related to elasticity is reversibility also from a thermo-dynamical point of view. Therefore, hyper-elasticity implies reversibility not

only between stresses and strains, but also reversibility in the thermo-dynamical sense.

Let us return to (6.2) and (6.7) and the issue of the strain energy W being independent of the integration path i.e. independent of the load history. As an illustration consider the quantity *Q* given by

$$Q = \int_A^B (L\,dx + M\,dy)$$

which means that *Q* is obtained as an integration along some curve in the *xy* plane from point A to point B; moreover, $L = L(x, y)$ and M = $M(x, y)$. From standard mathematics, it is well known that *Q* only depends on the end points *A* and *B* and not on the path between *A* and *B* if *Ldx+Mdy* is a perfect deferential. The necessary and sufficient condition for *Ldx+Mdy* being a perfect differential is

$$\frac{\partial L}{\partial y} = \frac{\partial M}{\partial x}$$

$$\frac{\partial \sigma ij}{\partial y} = \frac{\partial M}{\partial x}$$

Generalizing these concepts to (6.2), we see that *W* is independent on the integration path if

$$\frac{\partial \sigma_{ij}}{\partial \varepsilon_{kl}} = \frac{\partial \sigma_{kl}}{\partial \varepsilon_{ij}} \qquad (6.8)$$

and use of (6.7) demonstrates this condition to be fulfilled - as expected.

Using the transformation rule for the second-order tensors σ_{ij} and $d\varepsilon_{ij}$ it is readily shown that $\sigma_{ij} d\varepsilon_{ij}$ is an invariant. It therefore follows from (6.2) that *dW* is an invariant, i.e. we have that

$$\textit{Strain energy } W \textit{ is an invariant} \tag{6.9}$$

The path independence of the line integral defines the internal strain energy

$$W(\boldsymbol{\varepsilon}) = \int_{\varepsilon} \boldsymbol{\sigma}\, d\boldsymbol{\varepsilon} = \int_{\varepsilon} \frac{\partial W}{\partial \boldsymbol{\varepsilon}} d\boldsymbol{\varepsilon} = \int_{\varepsilon} dW \tag{6.10}$$

in terms of the total differential *dW*. The traditional notion of elasticity, such as reversibility and lack of energy dissipation under closed cycles of strain, are a direct consequence of path independence, i.e.

$$W(\boldsymbol{\varepsilon}) = \oint_{\varepsilon} dW = 0 \tag{6.11}$$

In other terms, the hyperelastic material description is non-dissipative and preserves energy under arbitrary strain histories.
The corresponding hyperelastic stiffness tensor is a measure of the curvature of the strain energy function involving the second derivatives of $W = W(\boldsymbol{\varepsilon})$,

$$\dot{\boldsymbol{\sigma}} = \mathbf{E}_t \dot{\boldsymbol{\varepsilon}} \qquad \textit{where} \qquad \mathbf{E}_t = \frac{\partial^2 W}{\partial \boldsymbol{\varepsilon} \otimes \partial \boldsymbol{\varepsilon}} \tag{6.12}$$

Consequently, the elasticity tensor is symmetric, $\boldsymbol{E_t} = \boldsymbol{E^T_t}$, if $W(\boldsymbol{\varepsilon})$ is sufficiently smooth. This reduces the 36 elastic constants to 21 in the general case of anisotropic elasticity, and to two in case of isotropy. The positive definiteness of the hyperelastic tangent operator, $\det \boldsymbol{E_t} > 0$, is directly connected to the convexity of the strain energy functional and the uniqueness argument of boundary value problems in elasticity.

Having established the strain energy W and the fundamental relation (6.7), we will now perform an interesting reformulation. Define the function C - the complementary energy per unit volume – by

$$C = \sigma_{ij}\varepsilon_{ij} - W(\varepsilon_{ij}) \tag{6.13}$$

It is obvious that C only depends on the current state and not on the manner in which this state was established. By differentiation we obtain

$$dC = d\sigma_{ij}\varepsilon_{ij} + \sigma_{ij}d\varepsilon_{ij} - \frac{\partial W}{\partial \varepsilon_{ij}}d\varepsilon_{ij} \tag{6.14}$$

which together with (6.7) gives

$$dC = \varepsilon_{ij}d\sigma_{ij} \tag{6.15}$$

We assume that the inverse relation of $\sigma_{ij} = \sigma_{ij}(\varepsilon_{ij})$ exists i.e.

$$\varepsilon_{ij} = \varepsilon_{ij}(\sigma_{kl}) \tag{6.16}$$

and we obtain

$$C(\sigma_{ij}) = \int_0^{\sigma_{ij}} \varepsilon_{kl}(\sigma^*_{mn})d\sigma^*_{kl} \tag{6.17}$$

where σ_{ij} is the current stress state whereas σ^*_{kl}, denotes the integration variable.

We mentioned that the complementary energy C only depends on the current state and not on the history. Moreover, we found that $C=C(\sigma_{ij})$.
We assume that $C=C(\sigma_{ij},\varepsilon_{ij})$ and obtain

$$dC = \frac{\partial C}{\partial \sigma_{ij}} d\sigma_{ij} + \frac{\partial C}{\partial \varepsilon_{ij}} d\varepsilon_{ij} \qquad (6.18)$$

and a comparison with (6.15) indicates that $\partial C/\partial \varepsilon_{ij}=0$ i.e. $C=C(\sigma_{ij})$. We therefore have

$$dC = \frac{\partial C}{\partial \sigma_{ij}} d\sigma_{ij} \qquad (6.19)$$

It appears that by the format (6.13) we have shifted the old variable ε_{ij} in $W=W(\varepsilon_{ij})$ into a new variable σ_{ij}, in $C=C(\sigma_{ij})$ without knowing the explicit relation between ε_{ij} and σ_{ij}. Subtraction of (6.19) from (6.15) yields

$$(\varepsilon_{ij} - \frac{\partial C}{\partial \sigma_{ij}}) d\sigma_{ij} = 0$$

Since this relations holds for arbitrary stress states, it follows that

$$\varepsilon_{ij} = \frac{\partial C}{\partial \sigma_{ij}}; \qquad C = C(\sigma_{ij}) \qquad (6.20)$$

i.e. the complementary energy C serves as a potential function for ε_{ij}. In the uniaxial case, an illustration of C given by (6.17) is shown in Fig. 6.3.

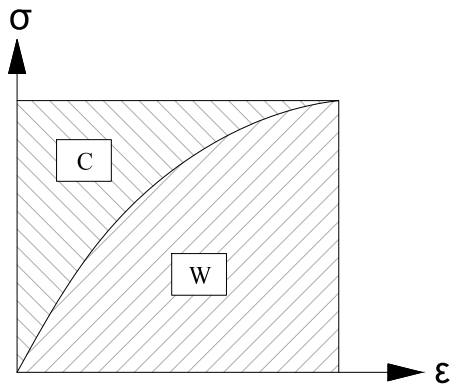

Figure 6.3: complementary energy C and strain energy W for uniaxial loading

By arguments similar to those adopted when we evaluated the strain energy W, it follows that

$$Complementary\ energy\ C\ is\ invariant \tag{6.21}$$

Moreover, from (6.20) appears that

$$\frac{\partial \varepsilon_{ij}}{\partial \sigma_{kl}} = \frac{\partial \varepsilon_{kl}}{\partial \sigma_{ij}} \tag{6.22}$$

6.2 Isotropic hyperelastic models

The strain energy depends on the current strains ε_{ij} through $W=W(\varepsilon_{ij})$ and according to (6.9), the strain energy is an invariant. The strain tensor ε_{ij} can be expressed by the principal strains ε_1, ε_2 and ε_3 and the corresponding principal strain directions. Isotropy means that the material has no directional properties and this implies that we may write the strain energy as $W=W(\varepsilon_1,\varepsilon_2,\varepsilon_3)$. As the principal strains are given uniquely by the strain invariants, we may equally well write the strain energy W as

$$W = W(\tilde{I}_1, \tilde{I}_2, \tilde{I}_3) \tag{6.23}$$

Formulation (6.23) is evidently in accordance with (6.9), stating that W is an invariant. The choice of the set of invariants is particularly convenient, since we have the following neat relations

$$\frac{\partial \tilde{I}_1}{\partial \varepsilon_{ij}} = \delta_{ij}; \qquad \frac{\partial \tilde{I}_2}{\partial \varepsilon_{ij}} = \varepsilon_{ij}; \qquad \frac{\partial \tilde{I}_3}{\partial \varepsilon_{ij}} = \varepsilon_{ik}\varepsilon_{kj} \tag{6.24}$$

We are now in a position to derive the most general constitutive law for isotropic hyper-elastic materials. From (6.7) and (6.23) we obtain

$$\sigma_{ij} = \frac{\partial W}{\partial \tilde{I}_1}\frac{\partial \tilde{I}_1}{\partial \varepsilon_{ij}} + \frac{\partial W}{\partial \tilde{I}_2}\frac{\partial \tilde{I}_2}{\partial \varepsilon_{ij}} + \frac{\partial W}{\partial \tilde{I}_3}\frac{\partial \tilde{I}_3}{\partial \varepsilon_{ij}} \tag{6.25}$$

With the notation

$$\phi_1 = \frac{\partial W}{\partial \tilde{I}_1}; \qquad \phi_2 = \frac{\partial W}{\partial \tilde{I}_2}; \qquad \phi_3 = \frac{\partial W}{\partial \tilde{I}_3} \tag{6.26}$$

(6.25) reduces with (6.24) to

$$\sigma_{ij} = \phi_1 \delta_{ij} + \phi_2 \varepsilon_{ij} + \phi_3 \varepsilon_{ik} \varepsilon_{kj} \tag{6.27}$$

Instead of the index notation, we may write $\sigma_{ij}=\boldsymbol{\sigma}$ and $\varepsilon_{ij}=\boldsymbol{\varepsilon}$, i.e. (6.27) can be written as

$$\boldsymbol{\sigma} = \phi_1 \mathbf{I} + \phi_2 \boldsymbol{\varepsilon} + \phi_3 \boldsymbol{\varepsilon}^2 \tag{6.28}$$

From the definition of the parameters ϕ_1, ϕ_2 and ϕ_3 it follows directly that they may depend on the strain invariants. However, these parameters are not independent, since (6.26) results in the following constraints

$$\frac{\partial \phi_1}{\partial \tilde{I}_2} = \frac{\partial \phi_2}{\partial \tilde{I}_1}; \qquad \frac{\partial \phi_1}{\partial \tilde{I}_3} = \frac{\partial \phi_3}{\partial \tilde{I}_1}; \qquad \frac{\partial \phi_2}{\partial \tilde{I}_3} = \frac{\partial \phi_3}{\partial \tilde{I}_2} \tag{6.29}$$

On the issue of volumetric-deviatoric coupling we observe that the trace operation leads to

$$tr\boldsymbol{\sigma} = 3\phi_1 + \phi_2 tr\boldsymbol{\varepsilon} + \phi_3 tr\boldsymbol{\varepsilon}^2 \tag{6.30}$$

Considering a simple shear deformation, with $\varepsilon_{12}=1/2\gamma$, ϕ_3 and thus the dependence of $\phi=\phi(I_1, I_2, I_3)$ on the third invariant is responsible for volumetric-deviatoric interaction. On another note, the quadratic expansion of the strain energy density function leads exactly to the two Lamé constants of linear isotropic elasticity since $\phi_3=0$.

Strain energy density function can be decomposed into two independent functions, one defining the volumetric and the other the deviatoric behavior.

$$\phi(\boldsymbol{\varepsilon}) = \phi_{vol}(tr\boldsymbol{\varepsilon}) + \phi_{dev}(tr\boldsymbol{\varepsilon}^2) \tag{6.31}$$

This infers, however, that the influence of the third invariant I_3 remains negligible, since it is this term, which is responsible for coupling the volumetric and deviatoric response behavior.

The decomposition of the strain energy function leads to the concept of nonlinear *K-G* models, because of their inherent simplicity, which retain the two-modular form of linear elasticity. Figures 6.4a and 6.4b illustrate the secant stiffness relations, which may be expressed best in the form of the octahedral components of stress σ_0, τ_0 and strain ε_0, γ_0

$$\begin{bmatrix} \sigma_0 \\ \tau_0 \end{bmatrix} = \begin{bmatrix} 3K_s & 0 \\ 0 & 2G_s \end{bmatrix} \begin{bmatrix} \varepsilon_0 \\ \gamma_0 \end{bmatrix} \tag{6.32}$$

where $K_S=K(tr\boldsymbol{\varepsilon})$ and $G_S=G(tr\boldsymbol{\varepsilon}^2)$. The so-called *K-G* models shown in Figures 6.4a and 6.4b play a prominent role for modeling nonlinear material behavior.

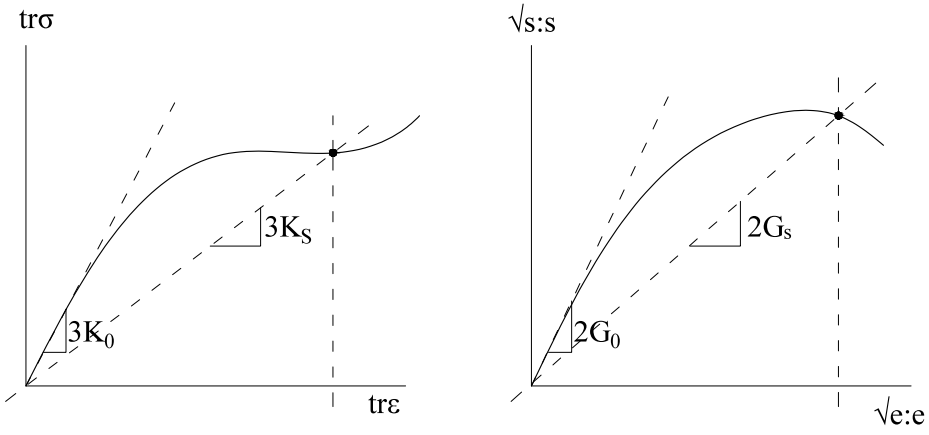

Figure 6.4: a) nonlinear volumetric response behavior; b) nonlinear deviatoric response behavior

Combining the volumetric and deviatoric scalar relations leads to the secant stiffness relation

$$\boldsymbol{\sigma} = \mathbf{E}_s \boldsymbol{\varepsilon} \qquad \textit{where} \qquad \mathbf{E}_s = \left[K_s - \frac{2}{3} G_s \right] \mathbf{1} \otimes \mathbf{1} + 2 G_s \mathbf{I} \tag{6.33}$$

where the elastic material constants have been simply replaced by their secant values.

6.3 Hyperelastic model in principal coordinates

In this case the strain energy function is expressed in terms of the principal strain values,

$$W = W(\varepsilon_1, \varepsilon_2, \varepsilon_3) = W(\varepsilon_2, \varepsilon_3, \varepsilon_1) = W(\varepsilon_3, \varepsilon_2, \varepsilon_1) \tag{6.34}$$

whereby the underlying isotropy infers cyclic permutation of indices. Because of the underlying coaxiality of the principal axes of stress and strain, the stress-strain relation involves only their principal values, i.e.

$$\sigma_i = \frac{\partial W(\varepsilon_1, \varepsilon_2, \varepsilon_3)}{\partial \varepsilon_i} \tag{6.35}$$

The tangential stress-strain relation leads to the following matrix representation of the principal coordinates:

$$\begin{bmatrix} \dot{\sigma}_1 \\ \dot{\sigma}_2 \\ \dot{\sigma}_3 \end{bmatrix} = \begin{bmatrix} \frac{\partial^2 W}{\partial \varepsilon_1 \partial \varepsilon_1} & \frac{\partial^2 W}{\partial \varepsilon_1 \partial \varepsilon_2} & \frac{\partial^2 W}{\partial \varepsilon_1 \partial \varepsilon_3} \\ \frac{\partial^2 W}{\partial \varepsilon_2 \partial \varepsilon_1} & \frac{\partial^2 W}{\partial \varepsilon_2 \partial \varepsilon_2} & \frac{\partial^2 W}{\partial \varepsilon_2 \partial \varepsilon_3} \\ \frac{\partial^2 W}{\partial \varepsilon_3 \partial \varepsilon_1} & \frac{\partial^2 W}{\partial \varepsilon_3 \partial \varepsilon_2} & \frac{\partial^2 W}{\partial \varepsilon_3 \partial \varepsilon_3} \end{bmatrix} \begin{bmatrix} \dot{\varepsilon}_1 \\ \dot{\varepsilon}_2 \\ \dot{\varepsilon}_3 \end{bmatrix} \tag{6.36}$$

This illustrates the symmetry of the tangential stiffness properties if the strain energy function is sufficiently smooth. Moreover, the tangential stiffness properties are positive definite if the strain energy function remains convex. Although the tangential relation appears to be anisotropic in principal coordinates, the nonlinear stress-strain rate relation maintains coaxiality between $\boldsymbol{\sigma}$-$\boldsymbol{\varepsilon}$ as long as the tangential shear terms satisfy the condition

$$\begin{bmatrix} \dot{\tau}_{12} \\ \dot{\tau}_{23} \\ \dot{\tau}_{31} \end{bmatrix} = \begin{bmatrix} \frac{\sigma_2 - \sigma_1}{\varepsilon_2 - \varepsilon_1} & 0 & 0 \\ 0 & \frac{\sigma_3 - \sigma_2}{\varepsilon_3 - \varepsilon_3} & 0 \\ 0 & 0 & \frac{\sigma_1 - \sigma_3}{\varepsilon_1 - \varepsilon_3} \end{bmatrix} \begin{bmatrix} \dot{\gamma}_{12} \\ \dot{\gamma}_{23} \\ \dot{\gamma}_{31} \end{bmatrix} \qquad (6.37)$$

6.4 Cauchy Elasticity $\sigma = f(\varepsilon)$

We will now deal with a type of elasticity, which is more general than the hyperelasticity. The stress-strain relation expresses stress in terms of a nonlinear function of strain. In this case, the triaxial state of stress is a nonlinear tensor function of the strain tensor and has an algebraic format, i.e. in indicial notation $\sigma_{ij}=f_{ij}(\varepsilon_{kl})$. Using the representation theorems of second order symmetric tensor functions the possibilities are restricted to a small set of possible choices when isotropy is invoked. In this case, the most general format of Cauchy elasticity may have one of the two representations,

$$\boldsymbol{\sigma} = \phi_1 \mathbf{1} + \phi_2 \boldsymbol{\varepsilon} + \phi_3 \boldsymbol{\varepsilon}^2 \qquad or \qquad \boldsymbol{\sigma} = \psi_1 \mathbf{1} + \psi_2 \boldsymbol{\varepsilon} + \psi_3 \boldsymbol{\varepsilon}^{-1} \qquad (6.38)$$

because of the Cayley-Hamilton theorem. Thereby, the three response functions Φ_i, and Ψ_i, are scalar functions of the three invariants of either stress or strain. It is important to keep in mind that Cauchy elasticity is based on a second order symmetric tensor function of a second order symmetric tensor.

6.5 Secant or Pseudo-Elasticity $\sigma=E_s:\varepsilon$

In the pseudo-elastic format of elasticity, the nonlinearity is incorporated into the fourth order secant stiffness tensor. This format is an algebraic format, that has been used early on in different engineering disciplines to develop nonlinear extensions of simple classes of linear elasticity. The so-called variable stiffness models retain the format of linear elasticity and simply replace the two elastic constants of linear elasticity by nonlinear functions: we have in fact to consider the modification of the linear relations of equation (5.24). The elastic bulk and shear moduli are taken as scalar functions of the stress and/or strain tensor invariants. Thus eq. (5.24) may now be written as

$$\boldsymbol{\sigma}_{vol} = 3K_s\boldsymbol{\varepsilon}_{vol} \qquad \textit{and} \qquad \mathbf{s} = 2G_s\mathbf{e} \tag{6.39}$$

where K_s and G_s are now the secant bulk modulus and the secant shear modulus, respectively. The scalar functional forms of K_s and G_s in terms of the stress and strain invariants are developed mainly from experimental data. For any given state of stress, σ_{ij} the value of $F(I_1,J_2,J_3)$ and consequently the strain components ε_{ij} are uniquely determined without regard to the loading path. However this does not imply that the strain energy W and the complementary energy C, calculated from such stress-strain relations, are path independent. Certain restrictions must be imposed on the chosen scalar functions in order to ensure the path independent character of W and C. This assures that energy is not generated during any loading-unloading cycle. We will see later on that the nonlinear K-G models are theoretically sound if the nonlinear response decouples the volumetric from the deviatoric response, i.e. $K = K(\varepsilon_{vol})$ and $G = G(tr\mathbf{e}^2)$ where $tr\mathbf{e}^2 = e:e$.
It is not very surprising that elastic damage models did start from this secant format of nonlinear elasticity using arguments of effective stiffness properties,

which are in some sense equivalent to distributed micro-mechanical defects. In fact, the original proposal of scalar damage was nothing but a nonlinear pseudo-elastic model in which the secant stiffness is in matrix notation

$$\boldsymbol{\sigma} = \mathbf{E}_s \boldsymbol{\varepsilon} \qquad \textit{where} \qquad \mathbf{E}_s = [1-d]\mathbf{E}_0 \qquad \textit{and} \qquad d = 1 - \frac{\mathbf{E_s}}{\mathbf{E_0}} \qquad (6.40)$$

In its basic format the secant matrix of elastic damage retains the structure of the initial elastic stiffness except for the factor *[1 - d]*

$$\mathbf{E}_s = \frac{[1-d]E_0}{[1+v_0][1-2v_0]} \begin{bmatrix} 1-v_0 & v_0 & v_0 & & & \\ v_0 & 1-v_0 & v_0 & & 0 & \\ v_0 & v_0 & 1-v_0 & & & \\ & & & \frac{1-2v_0}{2} & & \\ & 0 & & & \frac{1-2v_0}{2} & \\ & & & & & \frac{1-2v_0}{2} \end{bmatrix} \qquad (6.41)$$

which measures the remaining integrity of the material when the damage variable increases from zero to one, $0 \leq d \rightarrow 1$. Restricting damage to the format of isotropic linear elasticity, it is natural to decompose degradation into volumetric and deviatoric damage components such that

$$K_s = [1-d_{vol}]K_0 \qquad \textit{and} \qquad G_s = [1-d_{dev}]G_0 \qquad (6.42)$$

From this expression we observe that the secant format of isotropic elastic damage is very simple because of the underlying decoupling of volumetric from deviatoric degradation. As long as we are only interested in a given state of

damage, this isotropic pseudo-elastic formulation suffices to describe the response behavior using effective material properties based on the principle of stress or strain equivalence.

6.6 Truesdell Elasticity or hypoelasticity

The hypoelasticity is a differential format with this formulation: $\dot{\boldsymbol{\sigma}} = \boldsymbol{g}(\boldsymbol{\sigma}, \dot{\boldsymbol{\varepsilon}})$. In the differential format of elasticity the stress rate is expanded into a symmetric tensor function of two second order tensors. In the case of a stress-based formulation, the two independent arguments of the tensor function are the stress and the rate of strain tensors. The irreducible set of base tensors encompasses the following terms:

$$1,\ \sigma,\ \sigma^2,\ \dot{\varepsilon},\ \dot{\varepsilon}^2,\ (\sigma\cdot\dot{\varepsilon}+\dot{\varepsilon}\cdot\sigma),\ (\sigma\cdot\dot{\varepsilon}^2+\dot{\varepsilon}^2\cdot\sigma),\ (\sigma^2\cdot\dot{\varepsilon}+\dot{\varepsilon}\cdot\sigma^2),\ (\sigma^2\cdot\dot{\varepsilon}^2+\dot{\varepsilon}^2\cdot\sigma^2) \qquad (6.43)$$

Consequently, an isotropic tensor function of two symmetric tensors involves in the most general case nine response functions, $\phi_1,..\phi_9$, which depend in turn on the six moment invariants of the stress and strain rate tensors below,

$$\bar{I}_1^{\sigma} = tr\boldsymbol{\sigma},\quad \bar{I}_2^{\sigma} = tr\boldsymbol{\sigma}^2,\quad \bar{I}_3^{\sigma} = tr\boldsymbol{\sigma}^3,\quad \bar{I}_1^{\dot{\varepsilon}} = tr\dot{\boldsymbol{\varepsilon}},\quad \bar{I}_2^{\dot{\varepsilon}} = tr\dot{\boldsymbol{\varepsilon}}^2,\quad \bar{I}_3^{\dot{\varepsilon}} = tr\dot{\boldsymbol{\varepsilon}}^3 \qquad (6.44)$$

The general format results in the general stress-strain rate relation,

$$\begin{aligned}\dot{\boldsymbol{\sigma}} = {} & \phi_1\mathbf{1} + \phi_2\boldsymbol{\sigma} + \phi_3\boldsymbol{\sigma}^2 + \phi_4\dot{\boldsymbol{\varepsilon}} + \phi_5\dot{\boldsymbol{\varepsilon}}^2 + \phi_6(\boldsymbol{\sigma}\cdot\dot{\boldsymbol{\varepsilon}} + \dot{\boldsymbol{\varepsilon}}\cdot\boldsymbol{\sigma}) + \\ & + \phi_7(\boldsymbol{\sigma}\cdot\dot{\boldsymbol{\varepsilon}}^2 + \dot{\boldsymbol{\varepsilon}}^2\cdot\boldsymbol{\sigma}) + \phi_8(\boldsymbol{\sigma}^2\cdot\dot{\boldsymbol{\varepsilon}} + \dot{\boldsymbol{\varepsilon}}\cdot\boldsymbol{\sigma}^2) + \phi_9(\boldsymbol{\sigma}^2\cdot\dot{\boldsymbol{\varepsilon}}^2 + \dot{\boldsymbol{\varepsilon}}^2\cdot\boldsymbol{\sigma}^2)\end{aligned} \qquad (6.45)$$

For rate independence, the expansion must be homogeneous of order one, thus the rate terms of the tensor function must be restricted to the first order. In other terms, the hypo-elastic material law is rate independent, if and only if,

$$\mathbf{g}(\boldsymbol{\sigma}, \alpha\dot{\boldsymbol{\varepsilon}}) = \alpha\mathbf{g}(\boldsymbol{\sigma}, \dot{\boldsymbol{\varepsilon}}) \qquad (6.46)$$

Among the numerous possibilities, two classes of hypoelastic constitutive models may be distinguished.

a) Incrementally Linear Hypoelastic Models:

The linear restriction of the hypoelastic stress-strain relations leads to the classical tangential stiffness format

$$\dot{\boldsymbol{\sigma}} = \mathbf{E}_t : \dot{\boldsymbol{\varepsilon}} \qquad \textit{where} \qquad \mathbf{E}_t = \mathbf{E}(\boldsymbol{\sigma}) \qquad (6.47)$$

This stress-based format is reversible in the small, but not in the large. In other terms, the classical hypoelastic formulation leads to path-dependence

$$\boldsymbol{\sigma} = \int_{\varepsilon} \mathbf{E}_t(\boldsymbol{\sigma}) : \frac{d\boldsymbol{\varepsilon}}{dt} dt \qquad (6.48)$$

This infers energy dissipation and irreversible behavior for arbitrary load histories as opposed to hyperelasticity. In fact, the hyperelastic property of path-independence is recovered only if appropriate integrability conditions are satisfied, which assure that the stress is the gradient of a single potential function, i.e. $\sigma = \frac{\partial W}{\partial \varepsilon}$.

The most general format of the hypoelastic tangent operator involves 12 hypoelastic response functions which depend in general on all ten stress

invariants, $C_i=C_i(I_j,J_k)$. The tensorial structure involves twelve fourth order tensor products between the second order unit tensor and stress tensors up to the fourth power.

$$\mathbf{E}_t = \begin{bmatrix} C_1\mathbf{1}\otimes\mathbf{1} & +C_2\boldsymbol{\sigma}\otimes\mathbf{1} & +C_3\boldsymbol{\sigma}^2\otimes\mathbf{1} \\ +C_4\boldsymbol{\sigma}\otimes\mathbf{1} & +C_5\boldsymbol{\sigma}\otimes\boldsymbol{\sigma} & +C_6\boldsymbol{\sigma}^2\otimes\boldsymbol{\sigma} \\ +C_7\mathbf{1}\otimes\boldsymbol{\sigma}^2 & +C_8\boldsymbol{\sigma}\otimes\boldsymbol{\sigma}^2 & +C_9\boldsymbol{\sigma}^2\otimes\boldsymbol{\sigma}^2 \\ C_{10}[\mathbf{1}\bar{\otimes}\mathbf{1}+\mathbf{1}\otimes\mathbf{1}] & C_{11}[\boldsymbol{\sigma}\bar{\otimes}\mathbf{1}+\mathbf{1}\otimes\boldsymbol{\sigma}] & C_{12}[\boldsymbol{\sigma}^2\bar{\otimes}\mathbf{1}+\mathbf{1}\otimes\boldsymbol{\sigma}^2] \end{bmatrix} \qquad (6.49)$$

Under the name of variable moduli models, a good number of simplified hypoelastic material models have proposed and are still used in structural and geotechnical engineering.

b) Incrementally Nonlinear Hypoelastic Models:

Another rate independent restriction leads to a class of incrementally nonlinear models, which have been proposed under the name of hypoplastic models. Because of the incremental nonlinearity they are capable to distinguish between different loading and unloading stiffness properties in analogy to the endochronic time model introduced by K. Valanis [1975]. In the absence of a loading function, it is understood that the irreversible contribution leads to continuous energy dissipation under repeated load cycles in contrast to unload-reload cycles in elastoplasticity.

7 Yield and Failure Criteria

As a beginning to the plasticity theory, in this chapter it will be dealt with the criteria, which tell us whether plastic deformations - i.e. yielding of the material – or failure occurs. This chapter deals with the limits of elasticity and the limits of strength under all possible combinations of stresses.

7.1 Uniaxial behavior

The simplest type of loading is represented by the uniaxial stress condition, e.g. the simple tension test, for which $\sigma_1>0$, $\sigma_2=\sigma_3=0$, or the simple compression test, for which $\sigma_3<0$, $\sigma_2=\sigma_1=0$. The uniaxial stress-strain diagram, in which the axial principal stress σ_1 (or σ_3) is plotted against the axial strain ε_1 (or ε_3), affords a useful representation of the plastic as well as the elastic behavior.

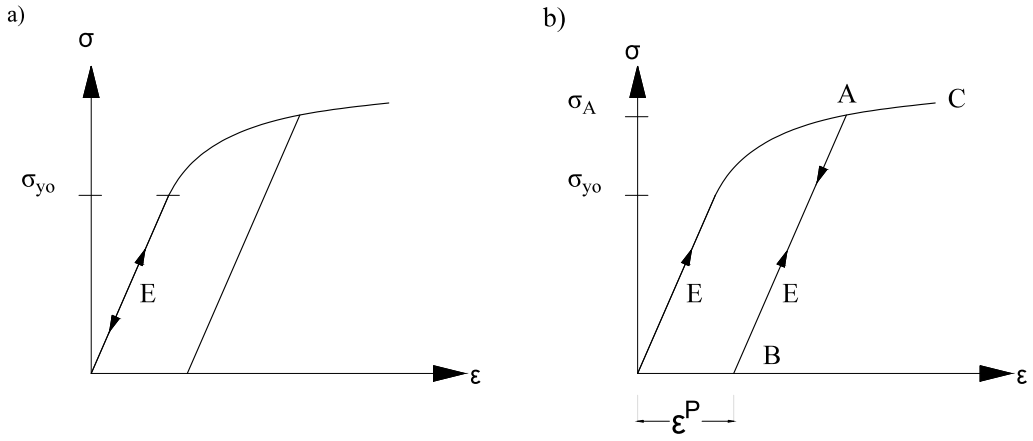

Figure 7.1: a) loading below the initial yield stress σ_{y0}; b) loading above the initial yield stress

Consider then the uniaxial stress-strain curve shown in Fig. 7.1. If the stress is below the initial yield stress σ_{yo} the material is assumed to behave linear elastic with a stiffness given by Young's modulus *E*, cf. Fig. 7.la). If the material is loaded to the stress σ_A, cf. Fig. 7.1b), yielding occurs and at unloading to point *B* we are left with the plastic strain ε_p.

The unloading from *A* to *B* is assumed to occur elastically with the stiffness E.

Reloading from point *B* first follows the linear path *BA* and at point *A*, yielding is again activated and the path *AC* is then traced as if the unloading at point *A* had never occurred. It appears that for unloading from point A and subsequent reloading, the stress *GA* that is needed to activate further plastic deformations has increased when compared with the initial yield stress σ_{yo}. We therefore have a hardening effect.

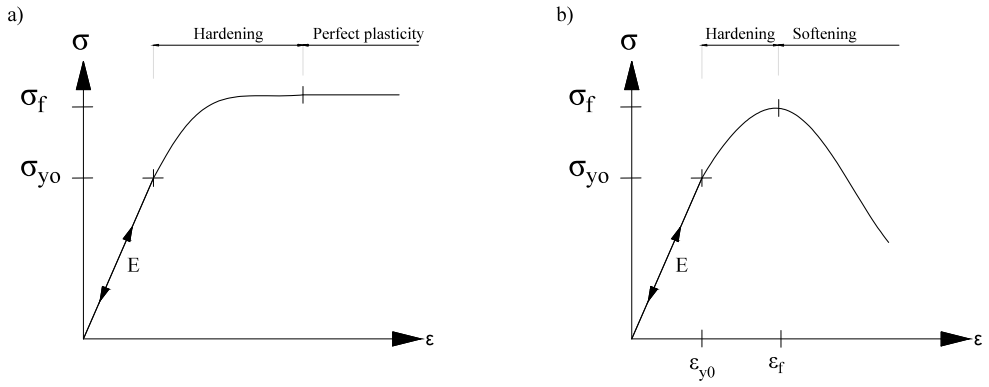

Figure 7.2: a) hardening and perfect plasticity; b) hardening and softening plasticity

If the strain is increased sufficiently, we may reach the situations illustrated in Fig. 7.2. After a hardening phase, we reach in Fig. 7.2a) a maximum stress σ_f - the failure stress - and with continued straining, the stress remains at the value σ_f, that is we have now reached a situation of perfect or ideal plasticity.

In Fig. 7.2b), on the other hand, after having obtained the failure stress σ_f, the stress decreases with continued deformation. This so-called softening behavior is typical for materials like concrete, soil and rocks and other cementitious materials when loaded in compression.

In this chapter, we will be conceded with the identification of the initial yield stress σ_{yo} and the failure stress σ_f. Later on, in the plasticity theory, we will establish rules for how the material behaves when loaded beyond the initial yield stress.

It is obvious that the initial yield stress and the failure stress are important engineering quantities. Whereas their identification is trivial for uniaxial stress states, this is not the case for general stress states. In general, the stress state is defined by the stress tensor, which comprises six independent stress components, the task is therefore to determine critical combinations of these components that result in initial yielding or failure of the material. We will see that for isotropic materials, it is possible to obtain a large amount of information on the general form of such criteria without knowing the specific material.

As apparent from Fig. 7.2, the term failure stress is slightly misleading since the material does not necessarily lose its load-carrying capacity when the failure stress σ_f is reached. Rather, the stress σ_f refers to that peak stress a homogeneously loaded specimen can carry and therefore the term ultimate stress seems more appropriate. However, by tradition we will use the word failure stress. While the identification of the failure stress is unambiguous, this is not the case for the initial yield stress σ_{yo}. The reason is that most materials exhibit a smooth transition from the elastic region to the elastic-plastic region with no distinct point where yielding is initiated, examples are shown in Fig. 7.2. The identification of the initial yield stress σ_{yo}, therefore becomes a matter of convention. In handbooks, the initial yield stress σ_{yo} for metals and steel is most often identified as the so-called $\sigma_{0.2}$-*stress*, i.e. the stress at which the remaining plastic strain after unloading equals 0.2%.

7.2 General stress states

For general stress states, the conditions for failure or initial yielding are called failure or initial yield criteria respectively. We will see that stress invariants play an extremely important role in failure and yield criteria.

In general, the material is anisotropic, i.e. for a given loading the orientation of the material influences its response. We seek a criterion, i.e. a function, which takes the value of zero when the conditions for initial yielding or failure are fulfilled.

Consider a specimen of a homogeneous material loaded by a homogeneous stress state. Considering proportional loading, we will assume that the yield or failure criterion is independent of the loading rate. Under these conditions, the initial yield or failure criterion can only depend on the stress tensor σ_{ij}, i.e.

$$F(\sigma_{ij}) = 0 \tag{7.1}$$

When this condition is fulfilled, initial yielding and failure occur in the material.
By convention the function F is normalized in such a manner that if the stress state is below the yield or failure limit then $F(\sigma_{ij})<0$. This implies that if the stress state is above the yield or failure limit then $F(\sigma_{ij})>0$. The conditions that $F(\sigma_{ij})<0$, $F(\sigma_{ij})=0$ and $F(\sigma_{ij})>0$ hold when the stress state is below, equal to and above the yield or failure limit respectively, were established in an arbitrary x_i-coordinate system. To make sense they must therefore also hold when we adopt another x'_i-coordinate system. This implies that the value of F is an invariant.
The stress tensor σ_{ij} can also be expressed by the principal stresses σ_1, σ_2 and σ_3 and the corresponding principal stress directions. As an isotropic material has no directional properties, it is expected that we can write $F=F(\sigma_1, \sigma_2, \sigma_3)$. As the principal stresses are given uniquely in terms of the three stress invariants, we may equally well write F as

$$F(I_1, I_2, I_3) = 0 \tag{7.2}$$

We will now show this result in a more formal manner.
In the x_i -coordinate system, we have $F(\sigma_{ij})$ and if we instead adopt the x'_i -coordinate system, we have $F^*(\sigma'_{ij})$. Since the criterion is an invariant, we conclude that

$$F(\sigma_{ij}) = F^*(\sigma'_{ij}) \tag{7.3}$$

This condition is just a result of F being an invariant, i.e. a zero-order tensor.
The function F is a response function and in accordance with the discussion following, the response function is denoted F in the x_i -coordinate system and F^* in the x'_i -coordinate system.
Isotropy means that the response function is the same in all coordinate systems. This implies

$$F(\sigma'_{ij}) = F^*(\sigma'_{ij}) \qquad isotropy \tag{7.4}$$

Insertion of (7.4) in (7.3) and noting that $\sigma'_{ij} = A_{ik}\sigma_{kl}A_{jl}$, we obtain

$$F(\sigma_{ij}) = F(A_{ik}\sigma_{kl}A_{jl}) \qquad cordinate\ in\,\mathrm{var}iance\ +\ isotropy \tag{7.5}$$

and this result shows that F is an isotropic scalar tensor function.
Instead of (7.2) we may write alternatively

$$F(\sigma_1, \sigma_2, \sigma_3) = 0 \tag{7.6}$$

where σ_1, σ_2, σ_3 are the principal stresses. The principal stresses are invariants, but it is observed that σ_1 is the principal stress in the first principal direction, σ_2 is the principal stress in the second principal direction and σ_3 is the principal stress in the third principal direction. However, since the yield or failure criterion (7.6) only depends on invariants having no directional preferences, the ordering of σ_1, σ_2 and σ_3 (7.6) is indifferent. That is, (7.6) should be interpreted as a function of principal stresses without any reference to specific principal axes. To emphasize this, we may write (7.6) as

$$F(\sigma_1,\sigma_2,\sigma_3) = F(\sigma_2,\sigma_1,\sigma_3) = F(\sigma_1,\sigma_3,\sigma_2)$$
$$= F(\sigma_3,\sigma_1,\sigma_2) = F(\sigma_3,\sigma_2,\sigma_2) = F(\sigma_2,\sigma_3,\sigma_1) = 0 \qquad (7.7)$$

Determination of the principal stresses requires the solution of an eigenvalue problem and this obstacle is avoided by expressing the criterion in terms of the stress invariants. However, instead of the invariants used in the format (7.2), it turns out to be more convenient to use another set of invariants and write the yield or failure criterion as $F(I_1, J_2, J_3) = 0$ or, even more advantageously, as

$$F(I_1, J_2, \cos 3\theta) \qquad (7.8)$$

where

$$J_2 = \frac{1}{2} s_{ij} s_{ji}; \qquad \cos 3\theta = \frac{3\sqrt{3}}{2} \frac{J_3}{J_2^{3/2}}; \qquad J_3 = \frac{1}{3} s_{ij} s_{jk} s_{ki} \qquad (7.9)$$

where s_{ij} is the deviatoric stress tensor.

One advantage of the format (7.8) is that it separates the influence of the hydrostatic stress I_1 from the influence of the deviatoric stresses expressed by J_2 and $\cos 3\theta$. Moreover, the invariants I_1, J_2 and $\cos 3\theta$ may be given an illuminating geometrical interpretation as shown in a moment.

Identification of failure and initial yield criteria is one of the classical topics in constitutive mechanics and the literature on this subject is therefore very extensive. The intention of this chapter is not to provide an overview of all the different criteria proposed, but rather to present some main contributions. In addition to being of practical interest, each of the criteria presented therefore involves features not considered by the other criteria dealt with. Thus, the

exposition in this chapter aims at a presentation of the mainstream within failure and initial criteria.

7.3 Symmetry properties of the failure or initial yield curve in the deviatoric plane

It is evident that the failure or initial yield surface intersects the deviatoric plane in a certain curve, cf. Fig. 4.8. It turns out that due to the presence of the term $cos3\theta$ in criterion (4.30), we are able to derive a number of general symmetry properties.

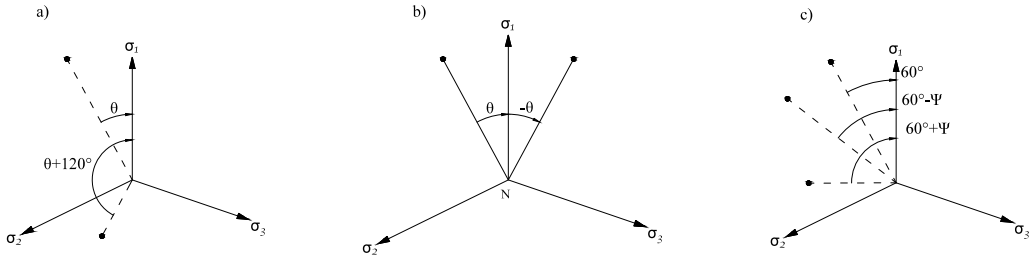

Figure 7.3: general symmetry properties of the failure or initial yield curve in the deviatoric plane; a) 120° period; b) symmetry about θ=0°; c) symmetry about θ=60°

Referring to the general criterion (4.30), the trace of this surface with an arbitrary deviatoric plane is obtained for I_1 = constant. As the cos-function is periodic with a period of 360°, we conclude that the failure or yield curve in the deviatoric plane is periodic with a period of 120°. That is, the distance ρ, cf. Fig. 4.8.b), is the same for θ and for $\theta+120°$ as well as for $\theta+240°$, this symmetry property is illustrated in Fig. 7.3a). Moreover, as $cos3\theta= cos(-3\theta)$ we find that the curve in the deviatoric plane is symmetric about $\theta=0°$; this symmetry property is illustrated in Fig. 7.3b). Due to the periodicity of 120°, the curve is also symmetric about $\theta = 120°$ and $\theta = 240°$. Finally, setting $\theta = 60° + \psi$, i.e. $\psi= 0°$ corresponds to $\theta = 60°$, we obtain $cos3\theta= -cos3\psi$ and setting $\theta = 60°- \psi$ yields

cos3θ= -cos3ψ. Accordingly, we have the same distance ρ for θ=60° + ψ and *θ=60°- ψ*, it is concluded that the curve in the deviatoric plane is symmetric about *θ=60°* and thereby also symmetric about *θ=180°* and *θ=300°*. This symmetry property is illustrated in Fig. 7.3c). In conclusion, the symmetry properties shown in Fig. 7.3 imply that the curve in the deviatoric plane is completely characterized by its form for *0°≤θ≤60°* and that this shape is repeated in the remaining sectors of the deviatoric plane. We observe that this far-reaching conclusion is a consequence of the material being isotropic.

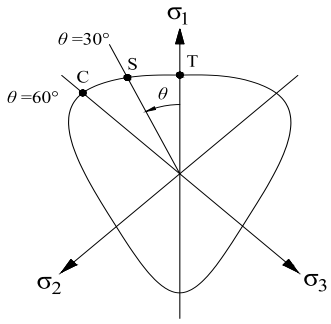

Figure 7.4: possible shape of failure or initial yield curve in the deviatoric plane. T=tensile meridian, C=compressive meridian, S=shear meridian

A possible shape of the failure or initial yield curve in the deviatoric plane fulfilling the above-mentioned 60°-symmetry property is illustrated in Fig. 7.3
Here, the curve is shown as a convex curve, a property that does not follow from the mathematical analysis above, but which is strongly confirmed by experimental evidence, irrespective of the material in question.
We found above that the shape of the curve in the deviatoric plane is characterized by its form for *0°≤θ≤60°* and it may be of interest to identify the corresponding stress range. For this purpose, let us arrange the principal stresses according to

$$\sigma_1 \geq \sigma_2 \geq \sigma_3 \qquad (7.10)$$

where tension is considered as a positive quantity. This allows us to write

$$\sigma_2 = (1-\alpha)\sigma_1 - \alpha\sigma_3; \qquad 0 \le a \le 1$$

i.e.

$$s_1 = \frac{1}{3}(1+\alpha)(\sigma_1 - \sigma_3); \qquad s_2 = \frac{1}{3}(1+2\alpha)(\sigma_1 - \sigma_3);$$
$$s_3 = -\frac{1}{3}(2+\alpha)(\sigma_1 - \sigma_3)$$

With these expressions, (4.26) takes the form

$$\cos\theta = \frac{1+\alpha}{2\sqrt{\alpha^2 - \alpha + 1}} \qquad (7.11)$$

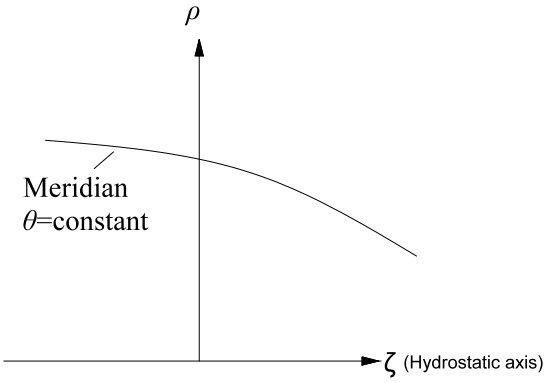

Figure 7.5: meridian plane obtained by the intersection of the failure or initial yield surface with a plane containing the hydrostatic axis

For α in the range $0 \le \alpha \le 1$, it follows that $0 \le \theta \le 60°$, i.e. with the ordering of the principal stresses given by (7.10), all stress states are covered by the range $0 \le \theta \le 60°$. The meridians of the failure or initial yield surface are the curves

where θ = constant applies, i.e. they are obtained by the intersection of the failure or initial yield surface with a plane containing the hydrostatic axis. Meridians may conveniently be depicted in a ξ, ρ-coordinate system or in a I_1, $\sqrt{J_2}$-coordinate system, the so-called meridian plane, cf. Fig. 7.5. Three meridians are of particular interest.

If $\sigma_1 > \sigma_2 = \sigma_3$ applies then $\alpha = 1$ and it follows from (7.11) that $\theta = 0$. This meridian is termed the tensile meridian, as the stress state $\sigma_1 > \sigma_2 = \sigma_3$ corresponds to a hydrostatic stress state superposed by a tensile stress in the σ_1-direction. We have

$$\sigma_1 > \sigma_2 = \sigma_3 \qquad i.e. \qquad \theta = 0 \qquad \Rightarrow \qquad \textit{tensile meridian}$$

Uniaxial tensile stress states are located on the tensile meridian, cf. Fig. 6.6a), and so are biaxial compressive stress states when the two compressive principal stresses are equal.

If $\sigma_1 = \sigma_2 > \sigma_3$ holds then $\alpha = 0$ and (7.11) shows that $\theta = 60°$. This meridian is termed the compressive meridian, as the stress state $\sigma_1 = \sigma_2 > \sigma_3$ corresponds to a hydrostatic stress state superposed by a compressive stress in the σ_3-direction. Consequently

$$\sigma_1 = \sigma_2 > \sigma_3 \qquad i.e. \qquad \theta = 60° \qquad \Rightarrow \qquad \textit{compressive meridian}$$

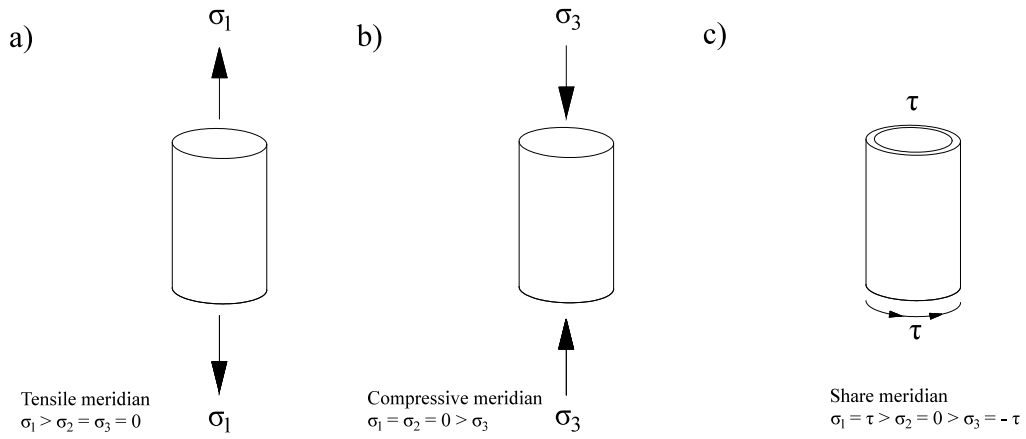

Figure 7.6: simple examples of stress states located on different meridians; a) uniaxial tension; b)uniaxial compression; c) pure shear

Uniaxial compressive stress conditions are therefore located on the compressive meridian, cf. Fig. 7.6b).

Finally, if $\sigma_1>\sigma_2=(\sigma_1+\sigma_3)/2>\sigma_3$ then $\alpha=1/2$ and it follows from (7.11) that $\theta=30°$. This meridian is termed the shear meridian, as the stress state $\sigma_1>\sigma_2=(\sigma_1+\sigma_3)/2>\sigma_3$ corresponds to a hydrostatic stress state superposed by a positive stress, τ, in the σ_1-direction and a negative stress, $-\tau$, in the σ_3-direction. That is

$$\sigma_1 = \sigma_2 = \frac{\sigma_1 + \sigma_3}{2} > \sigma_3 \qquad i.e. \qquad \theta = 30° \qquad \Rightarrow \qquad \textit{shear meridian}$$

A stress state corresponding to pure shear is therefore located on the shear meridian, cf. Fig. 7.6c).

The points where the tensile, compressive and shear meridians intersect the deviatoric plane are illustrated in Fig. 7.4. (Points *T*, *C* and *S*).

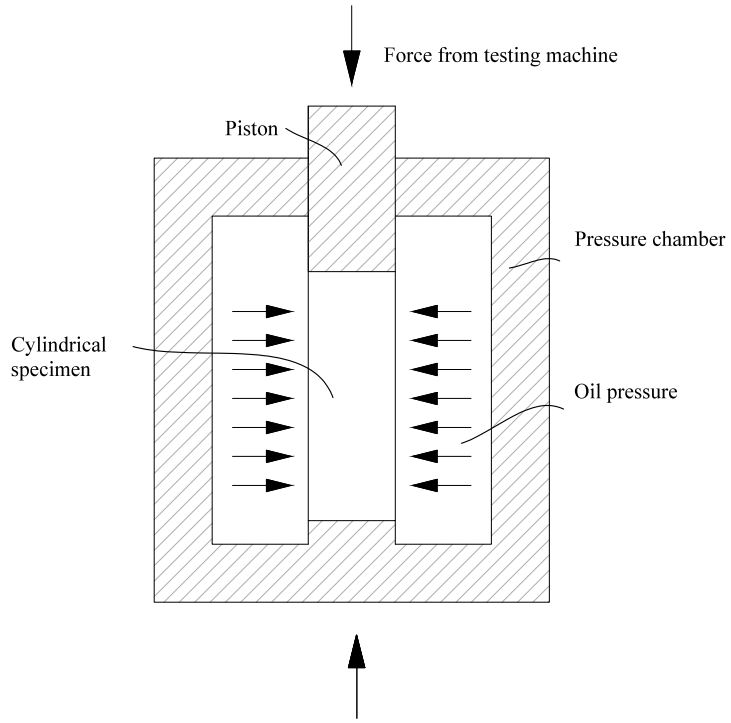

Figure 7.7: sketch of von Karman pressure cell allowing to test cylindrical specimens under multiaxial stress states

To identify points on certain meridians for multiaxial stress states, the von Karman pressure cell is often used, especially for soil and cementitious materials like concrete and rocks. This type of pressure cell is named after von Karman in recognition of his triaxial tests on marble and sandstone using this kind of equipment, cf. von Karman (1911). A cylindrical specimen is inserted into a pressure chamber, cf. Fig. 7.7. The oil inside the pressure chamber is pressurized providing stresses on the lateral surface of the specimen and, via a piston, an ordinary testing machine supplies a pressure to the end surfaces of the specimen.
It is evident that the von Karman pressure cell enables one to test materials along two meridians only: the tensile meridian for which $\sigma_1 > \sigma_2 = \sigma_3$ and the compressive meridian where $\sigma_1 = \sigma_2 > \sigma_3$, cf. Fig. 7.8 (recall that tension is considered as a positive quantity).

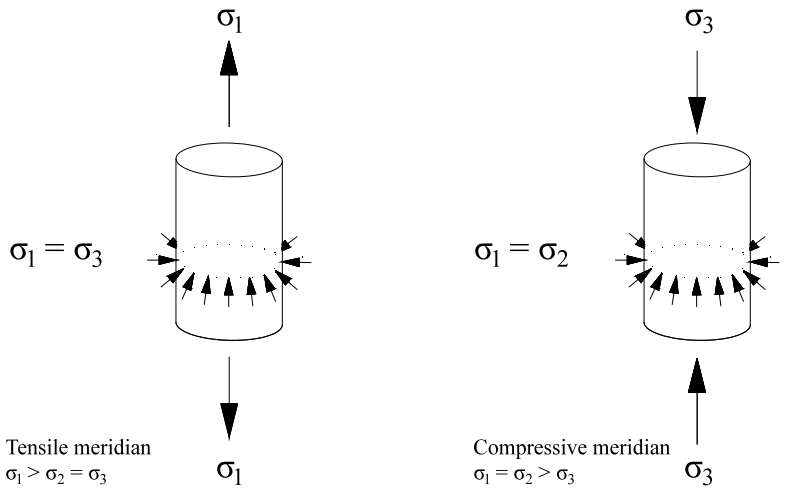

Figure 7.8: stress states that can be obtained in a von Karman pressure cell

Previously, we deduced the general symmetry properties of the curve in the deviatoric plane, cf. Figs.7.3 and 7.4, and we will now establish some additional symmetry properties, which hold under some specialized conditions.

Let us assume that the occurrence of failure or initial yield is independent of the hydrostatic stress I_1, i.e. (4.30) reduces to

$$F(J_2, \cos 3\theta) = 0 \tag{7.12}$$

This implies that the corresponding surface in the principal stress space consists of a cylindrical surface with the meridians parallel with the hydrostatic axis.

Consequently irrespective of the deviatoric plane considered the same trace of the failure or initial yield surface is obtained. For metals and steel, yielding turns out to be independent of the hydrostatic stress, i.e. (7.12) is a valid assumption.

Let us further assume that criterion (7.12) is fulfilled both for the stress state σ_{ij} and the stress state $-\sigma_{ij}$. As an example, for metals and steel the initial yield stress is the same for uniaxial tension and uniaxial compression. Let us now investigate the consequences of the two assumptions mentioned above. For the stress state σ_{ij}, we may determine J_2, J_3 and thereby $\cos 3\theta$, cf. (4.29).

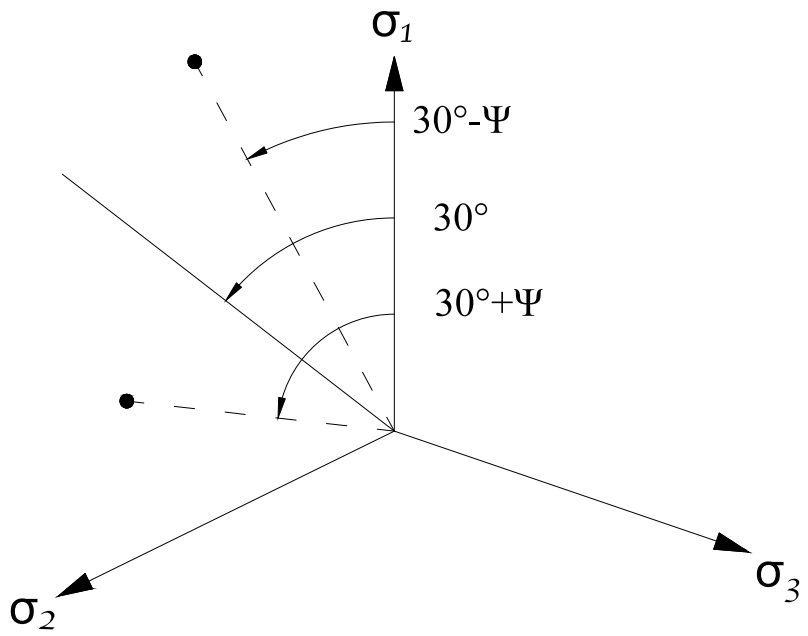

Figure 7.9: Symmetry about $\theta=30°$ when (6.12) holds and when σ_{ij} and $-\sigma_{ij}$ both fulfill the criterion

Likewise, for the stress state $\sigma^*_{ij}=-\sigma_{ij}$, we obtain $J_2 = J^*_2$, $J_3 = -J^*_3$ i.e. $\cos 3\theta^* = -\cos 3\theta$. This means that for the same J_2-value, criterion (7.12) is fulfilled both for $\cos 3\theta$ and for $-\cos 3\theta$, i.e. both θ as well as $\theta \pm 180°$ fulfill the criterion. Consider now $\theta=30°+\psi$, i.e. $\psi=0°$ corresponds to $\psi=30°$, cf. Fig. 7.9. We found above that both θ and $\theta-180°$ fulfill the criterion, therefore, when $\theta=30°+\psi$ fulfills the criterion, so does $\theta=30°+\psi-180°=-150°+\psi$.

The latter value leads to $\cos 3\theta=\cos(-450°+3\psi) = \cos(-90°+3\psi) = \cos(90°-3\psi)$, which may be interpreted as $\theta=30°-\psi$. It is concluded that both $\theta=30°+\psi$ and $\theta=30°-\psi$ fulfill the criterion and in addition to the general symmetry properties shown in Fig. 7.3, we also have symmetry about $\theta=30°$. This symmetry property is illustrated in Fig. 7.9 and it implies that the tensile and compressive meridians have the same distance to the hydrostatic axis.

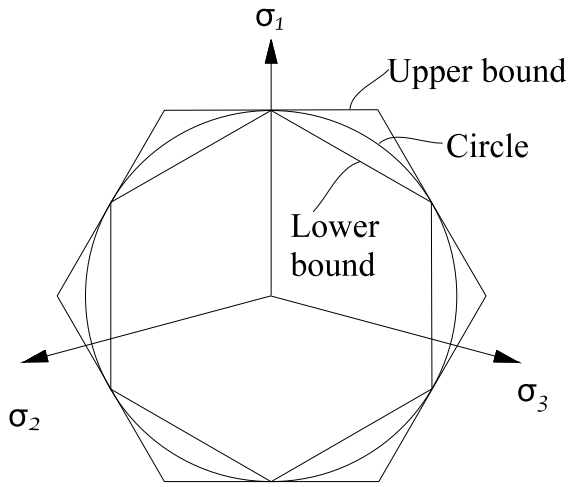

Figure 7.10: upper and lower bounds for curve in the deviatoric plane when (6.12) holds and when σ_{ij} and-σ_{ij} both fulfill the criterion

The general symmetry properties imply that the curve in the sector $0° \leq \theta \leq 60°$ is repeated in the remaining sectors of the deviatoric plane, cf. Fig. 7.4. With the assumptions described above, we also have a symmetry line about $\theta = 30°$.

If we, in addition, assume that the trace in the deviatoric plane is convex - an assumption that is strongly supposed by experimental evidence for all materials - we are led to the upper and lower bounds for the trace in the deviatoric plane as shown in Fig. 7.10.

Let us recall the assumptions that led to these upper and lower bounds. As discussed, these assumptions are in close agreement with the initial yield properties for metals and steel and it is therefore convenient to make the following summation

Initial yields of metals and steel is characterized in that:
·*the idrostatic stress has no* inf*luence*
·*if* σ_{ij} *results in the yielding, so does* $-\sigma_{ij}$
·*the trace in the deviatoric plane is convex* *(7.13)*

Recalling that (7.12) implies that the surface in the stress space is a cylindrical surface with the meridians parallel with the hydrostatic axes and observing the upper and lower bounds in the deviatoric plane illustrated in Fig. 7.10, we conclude that there are very narrow bounds within which a valid initial yield criterion for metals and steel can be chosen. Indeed, we shall later see that the circle of Fig. 7.10 corresponds to the von Mises yield criterion whereas the lower bound of Fig. 7.10 corresponds to the Tresca yield criterion.

Having discussed issues that are of relevance for metals and steel, it may be of interest to evaluate the general experimental evidence for another large group of materials, namely concrete, soil and rocks. These materials are characterized by smooth stress-strain curves exhibiting no well defined initial yield stress. Moreover, the analysis of constructions involving these materials is often focused on the determination of the ultimate load capacity and whereas the ratio $\varepsilon_f/\varepsilon_{yo}$, cf. Fig. 7.2b, is large for metals and steel, it is much smaller for concrete, soil and rocks. For these reasons, the failure criterion is of primary importance for concrete, soil and rocks. Quite generally, the experimental evidence for these materials may be summarized as follows

$$\begin{aligned} &\textit{Failure of concrete soil and rocks is characterized that}: \\ &\cdot\textit{the hydrostatic stress has a strong } \inf\textit{luence} \\ &\cdot\textit{inclusion of the terms } \cos 3\theta \textit{ s of impor}\tan\textit{ce} \\ &\cdot\textit{the failure surface is convex} \end{aligned} \qquad (7.14)$$

It follows that we expect the failure curve in the deviatoric plane to take the form sketched in Fig. 7.4. We finally observe that experimental observations for cast iron fall somewhere between the characteristics defined by (7.13) and (7.14).

Since elasticity, per definition, only occurs within the initial yield surface, this surface is independent of the previous load history. On the other hand, to reach the failure surface significant inelastic strains are developed and, in principle, the failure surface is therefore expected to depend on the load history. However,

experimental evidence shows for concrete (cf. China and Zimmerman (1965), Schickert and Winkler (1977)), soil (cf. Scott (1963)) and rocks (cf. Swanson and Brown (1971)) that whether the loading is proportional or non-proportional only influences the failure surface to a very modest degree.

7.4 Failure criteria for pressure dependent materials

Failure of a material is usually defined in terms of its load-carrying capacity. However, for perfectly plastic materials, yielding itself implies failure, so the yield stress is also the limit of strength. As in the case of the yield criteria, a general form of the failure criteria can be given by

$$f = (\sigma_{ij}, k_1, k_2, ...) = 0 \tag{7.15}$$

for anisotropic materials and by

$$f = (\sigma_1, \sigma_2, \sigma_3, k_1, k_2, ...) = 0 \tag{7.16}$$

through

$$f(\xi, \rho, \theta, k_1, k_2, ...) = 0 \tag{7.17}$$

for isotropic ones.

As we already know, yielding of most ductile metals is hydrostatic pressure independent. However, the behavior of many nonmetallic materials, such as

soils, rocks and concrete is characterized by its hydrostatic pressure dependence. Therefore, the stress invariant I_1 or ξ should not be omitted from eqation

$$f = (I_1, I_2, I_3, k_1, k_2, ...) = 0 \qquad (7.18)$$

and equation (7.17) respectively. The general shape of a failure surface, $f(I_1, I_2, I_3)=0$ or $f(\xi,\rho,\theta)=0$, in a three-dimensional stress space can be described by its cross-sectional shapes in the deviatoric plane, which is perpendicular to the hydrostatic curves between this surface and a plane (the meridian plane) containing the hydrostatic axis with $\theta=const$.

For an isotropic material, the labels 1, 2, 3 attached to the coordinate axes are arbitrary; it follows that the cross sectional shape of the failure surface must have a threefold symmetry of the type shown in fig. 7.11b). Therefore, when performing experiments, it's necessary to explore only the sector $\theta=0°$ to $60°$, the other sectors being known by symmetry.

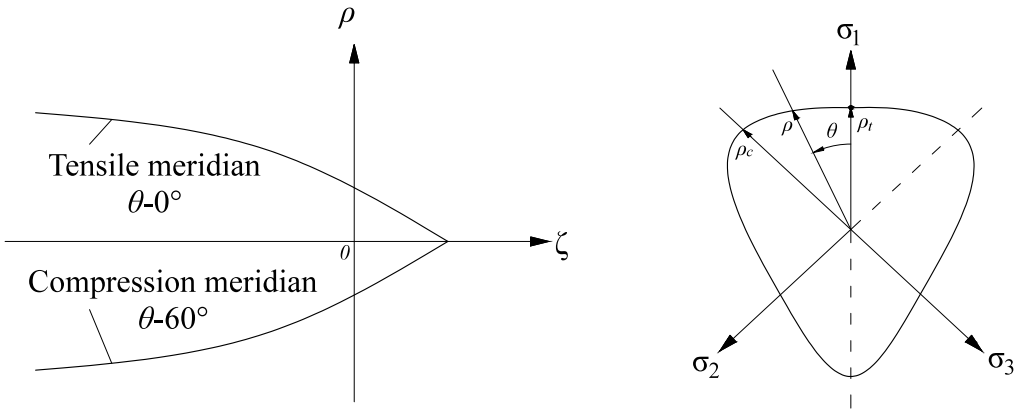

Figure 7.11: general shape of failure surface for an isotropic material: a)meridians; b) deviatoric section

The typical sector shown in fig. 7.11b) by a heavy line corresponds to the regular ordering of the principal stresses, $\sigma_1 \geq \sigma_2 \geq \sigma_3$. Within this ordering, there are two extreme cases:

$$\sigma_1 = \sigma_2 > \sigma_3 \tag{7.19}$$

and

$$\sigma_1 > \sigma_2 = \sigma_3 \tag{7.20}$$

corresponding to $\theta_1=60°$ and $\theta_2=0°$, respectively. To show this, we substitute equations (7.19) and (7.20) into equation (4.26) and get

$$\cos\theta_1 = \frac{\sqrt{3}}{2}\frac{s_1}{\sqrt{J_2}} = \frac{2\sigma_1 - \sigma_1 - \sigma_3}{2\sqrt{3}\sqrt{\frac{2}{6}(\sigma_1 - \sigma_3)^2}} = \frac{1}{2}$$

and

$$\cos\theta_2 = \frac{2\sigma_1 - \sigma_3 - \sigma_3}{2\sqrt{3}\sqrt{\frac{2}{6}(\sigma_1 - \sigma_3)^2}} = 1$$

respectively. The meridian corresponding to $\theta_1=60°$ is the compression meridian in that equation (7.19) represent a stress state corresponding to a hydrostatic stress state with a compressive stress superimposed in one direction. The meridian determined by $\theta=0°$, corresponding to equation (7.20), represent a hydrostatic stress state with a tensile stress superimposed in one direction and is therefore called the tensile meridian. The meridian determined by $\theta=30°$ is the shear meridian. Based on the above considerations, a general shape of the failure surface for an isotropic material may be illustrated in the Haigh-Westergaard stress space as shown in fig.7.11a).

7.4.1 Drucker-Prager criterion

The general failure properties for such materials are summarized in (7.14) and we note that the hydrostatic stress I_1 is of paramount importance. All terms in the general criterion (4.30) must therefore be considered. Even though the term $cos3\theta$ is of great importance, this term complicates the criterion considerably, thus we may, as an approximation, simply ignore its influence. We are thereby left with

$$F(I_1, J_2) = 0 \tag{7.21}$$

The Drucker-Prager criterion, formulated in 1952, is a simple modification of the von Mises criterion, where the influence of a hydrostatic stress component on failure is introduced, by inclusion of an additional term in the von Mises formulation. This formulation is often referred to as an octahedral criterion since the octahedral normal stress so and the octahedral shear stress τ_0 are related to I_1 and J_2 via (4.20), i.e.

$$\sigma_0 = \frac{1}{3} I_1; \qquad \tau_0 = \sqrt{\frac{2}{3} J_2} \tag{7.22}$$

The simplest possible explicit form of (7.21) is a linear relation between I_1 and$\sqrt{J_2}$, i.e.

$$\sqrt{3J_2} + \alpha I_1 - \beta = 0 \tag{7.23}$$

where α and β are material parameters. Moreover, α is dimensionless whereas β has the dimension of stress. The reason for the factor 3 in front of J_2 is that for $\alpha=0$, (7.23) then reduces exactly to the von Mises criterion.

Both the octahedral normal stress σ_0 and the octahedral shear stress τ_0 act on the octahedral plane. Thus, a physical interpretation of the Drucker-Prager criterion is to claim that failure (or yielding) occurs when the octahedral shear stress τ_0 exceeds a certain value that depends on the octahedral normal stress.

Using variables ξ and ρ equation (7.23) leads to

$$\sqrt{3}\alpha\xi + \rho - \beta = 0 \qquad (7.24)$$

The failure surface in equation (7.24) in principal stress space is clearly a right circular cone as shown in Fig. 7.13.

The deviatoric plane is defined by I_1 = *constant*, i.e. (7.23) implies that $\sqrt{3J_2}$ or ρ is constant in the deviatoric plane. It follows that we have the same meridian irrespective of the θ-angle and that this meridian makes a certain slope with the hydrostatic axis.

These features are shown in Fig. 7.12.

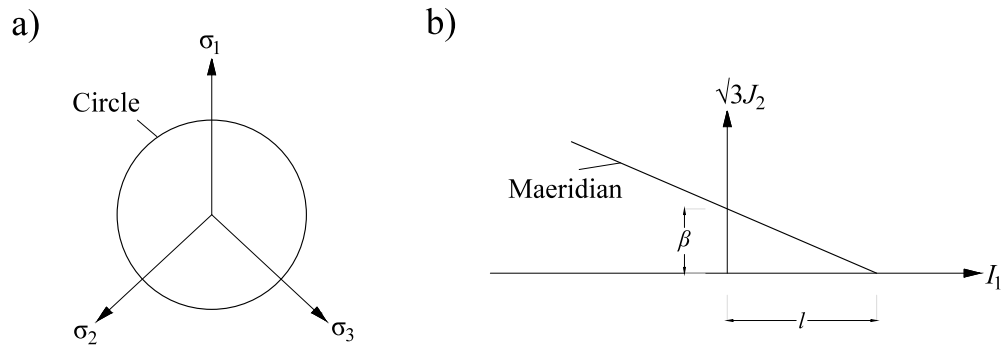

Figure 7.12: Drucker-Prager criterion; a) deviatoric plane; b) meridian plane.

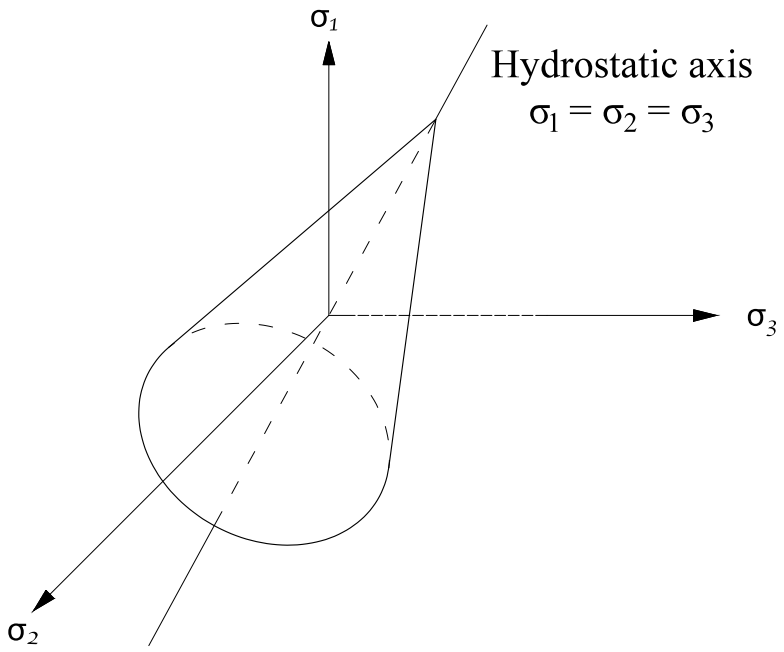

Figure 7.13: Drucker-Prager surface in the principal stress space

Since $\sqrt{3J_2}$ is a non-negative quantity, we conclude from (7.23) with $I_1 = 0$ that β is a positive material parameter. Moreover, as illustrated in Fig. 7.12b) the Drucker-Prager surface intersects the I_1-axis for $I_1 = \beta/\alpha$. Considering failure conditions, it is evident that a material like rock or concrete will break for a sufficiently large hydrostatic tension. Therefore, the dimensionless parameter α must be a non-negative quantity as illustrated in Fig. 7.12b). For plane stress conditions, i.e. $\sigma_3 = 0$, (7.23) reduces to

$$\sqrt{\sigma_1^2 + \sigma_2^2 - \sigma_1\sigma_2} + \alpha(\sigma_1 + \sigma_2) - \beta = 0 \qquad (7.25)$$

which obviously reduces to the von Mises expression for $\alpha = 0$. As shown in Fig. 7.14, (7.25) represents an off-center ellipse in the $\sigma_1\sigma_2$-plane.

The uniaxial tensile strength σ_t, uniaxial compressive strength σ_c, biaxial tensile strength σ_{bt} and biaxial compressive strength σ_{bc} are illustrated in fig 7.14 and from equation (7.25) we derive that

$$\sigma_t = \frac{\beta}{1+\alpha}; \qquad \sigma_c = \frac{\beta}{1-\alpha};$$
$$\sigma_{bt} = \frac{\beta}{1+2\alpha}; \qquad \sigma_{bc} = \frac{\beta}{1-2\alpha}; \tag{7.26}$$

These relations may be used to identify the material parameters α and β.
Due to the elimination of the $cos3\theta$ –term, the Drucker-Prager criterion should be used with caution. In practice, it can only be used with sufficient accuracy when α is small, i.e. when the influence of the hydrostatic stress I_1 is moderate.
Cast iron may be representative of such a material.

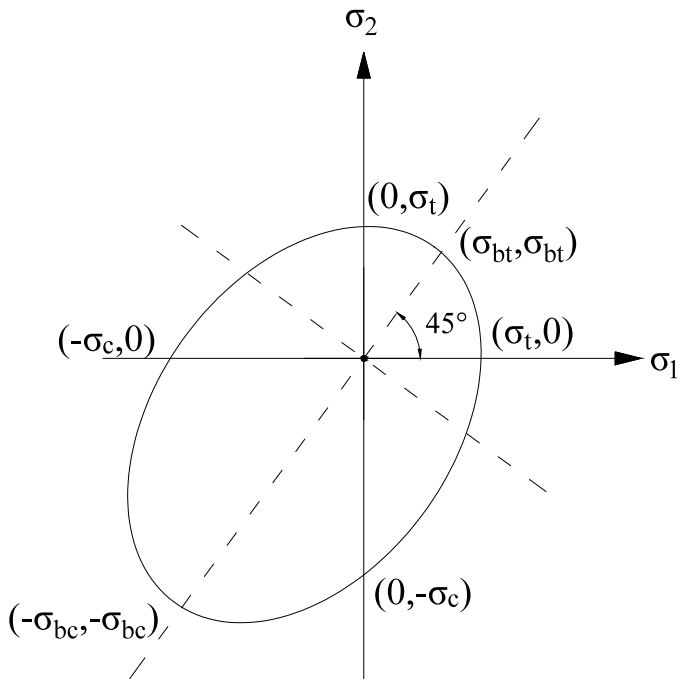

Figure 7.14: Drucker-Prager off-center ellipse in the $\sigma_1\,\sigma_2$ plane

7.4.2 Coulomb criterion

We will again consider failure characteristics for concrete, soil and rocks, but instead of the formulation (4.30), we will adopt the description given by (7.6), i.e.

$$F(\sigma_1,\sigma_2,\sigma_3)=0 \qquad (7.27)$$

with the convention that

$$\sigma_1 \geq \sigma_2 \geq \sigma_3$$

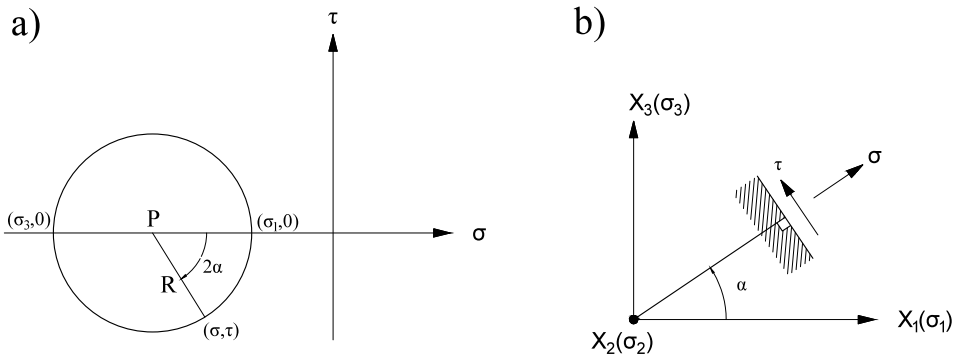

Figure 7.15: a) Mohr's circle of stress; b) corresponding interpretation of σ and τ

In general, (7.27) is quite complicated and in order to simplify the expression, it is tempting to assume that the intermediate principal stress σ_2 is of minor importance, i.e. we assume that

$$F(\sigma_1,\sigma_3)=0$$

The most simple expression of this form is then provided by a linear relation between σ_1 and σ_3, i.e.

$$k\sigma_1 - \sigma_3 - m = 0 \qquad (7.28)$$

where k and m are material parameters. Requiring that this expression should predict the uniaxial compressive strength value σ_c the stress state $(\sigma_1,\sigma_2,\sigma_3) = (0,0,-\sigma_c)$ should fulfill (7.28) and we find

$$k\sigma_1 - \sigma_3 - \sigma_c = 0 \qquad (7.29)$$

This so-called Coulomb criterion was suggested by Coulomb (1776) and is the oldest criterion ever proposed.

Mohr's circle of stress is shown in Fig. 7.15a). In Fig. 7.15b), the x_1, x_2, x_3 coordinate system is collinear with the principal directions of σ_1, σ_2 and σ_3 and the interpretation of the stress point (σ, τ) in Fig. 6.15a) is shown in Fig. 7.15b). That is, the normal stress σ and the shear stress τ act on the section having a normal, which makes the angle α with the σ_1-direction. From Fig. 7.15a), the center position P and the radius R of Mohr's circle are given by

$$P = \frac{1}{2}(\sigma_1 + \sigma_3); \qquad R = \frac{1}{2}(\sigma_1 - \sigma_3) \qquad (7.30)$$

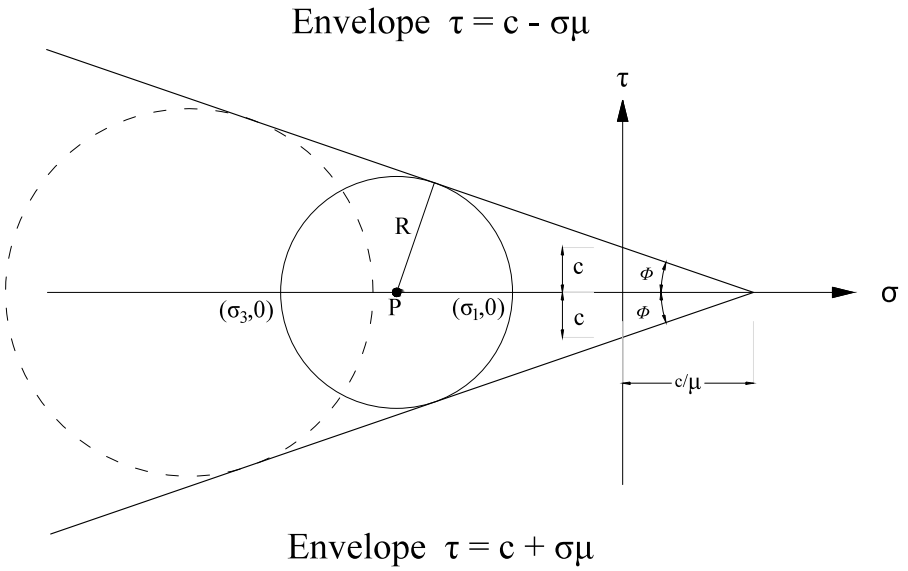

Figure 7.16: Coulomb criterion in Mohr's diagram

It is assumed that the stress state fulfills Coulombs criterion. Therefore, insertion of σ_3 as determined by (7.29) into (7.30) yields

$$P = \frac{1}{2}\left[(k+1)\sigma_1 - \sigma_c\right]; \qquad R = \frac{1}{2}\left[\sigma_c - (k-1)\sigma_1\right]$$

and elimination of σ_1 provides

$$R = \frac{\sigma_c}{k+1} - \frac{k-1}{k+1}P$$

Thus, the radius R varies linearly with the center position P. Consequently, and as shown in Fig. 7.16, all Mohr's circles of stress that fulfill the Coulomb criterion have two symmetrically positioned straight lines as their envelopes.
These straight lines can be written as

$$|\tau| = c - \mu\sigma \qquad (7.31)$$

where c and μ are non-negative material parameters. It appears that (7.31) provides an alternative formulation of the Coulomb criterion.

Referring to Fig. 7.16 and (7.31), we see that $|\tau| = c$ is the shear strength when the normal stress $\sigma = 0$, i.e. c is the cohesion of the material. If σ is negative, i.e. σ corresponds to a pressure, it follows that the shear strength $|\tau|$ is increased and μ is therefore called the friction coefficient of the material.

Consequently, we have obtained a direct physical interpretation of the Coulomb criterion and, most frequently, this criterion is postulated directly in the form given by (7.31).

With this discussion, it is no surprise that the linear expression (7.31) may be generalized to achieve

$$|\tau| = h(\sigma) \tag{7.32}$$

where $h(\sigma)$ denotes an arbitrary function of σ. This so-called Mohr criterion was suggested by Mohr (1900) and it is illustrated in Fig. 7.17. Just like the Coulomb criterion, the Mohr criterion (7.32) serves as the envelope of all Mohr's circles of stress when the material is loaded to failure.

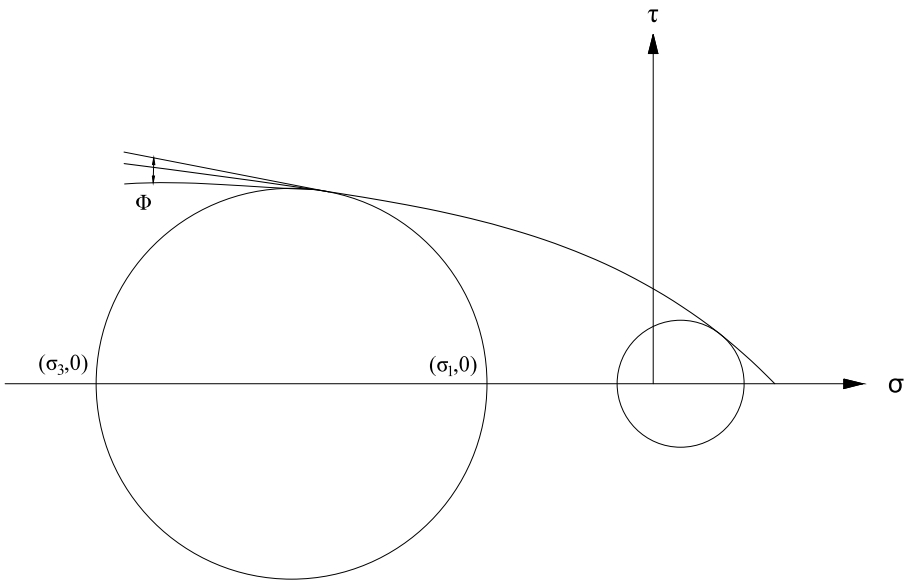

Figure 7.17: Mohr criterion; illustration of current friction angle ϕ

Returning to the Coulomb criterion, it is of interest to compare the material parameters k and σ_c in (7.29) with the material parameters c and μ in (7.31). First, we observe from Fig. 7.16 that

$$\tan\phi = \mu$$

where ϕ is termed the friction angle. Let us next consider a hydrostatic stress state $(\sigma_1,\sigma_2,\sigma_3) = (\sigma,\sigma,\sigma)$. It follows from (7.29) that $\sigma=\sigma_c/(k - 1)$ and from Fig. 7.16, we have $\sigma = c/\mu$. This provides

$$\frac{c}{\mu} = \frac{\sigma_c}{k-1} \qquad (7.33)$$

Observing that P for the situation displayed in Fig.7.16 is a negative quantity, cf. (7.30), we obtain from Fig. 7.16, (7.33) and (7.30) that

$$\sin\phi = \frac{R}{\frac{c}{\mu} - P} = \frac{\frac{1}{2}(\sigma_1 - \sigma_3)}{\frac{\sigma_c}{k-1} - \frac{1}{2}(\sigma_1 + \sigma_3)}$$

i.e.

$$\frac{1+\sin\phi}{1-\sin\phi}\sigma_1 - \sigma_3 - \frac{2\sigma_c}{(k-1)}\frac{\sin\phi}{(1-\sin\phi)} = 0$$

A comparison with (7.29) reveals that

$$k = \frac{1+\sin\phi}{1-\sin\phi} \qquad i.e. \qquad k \geq 1$$

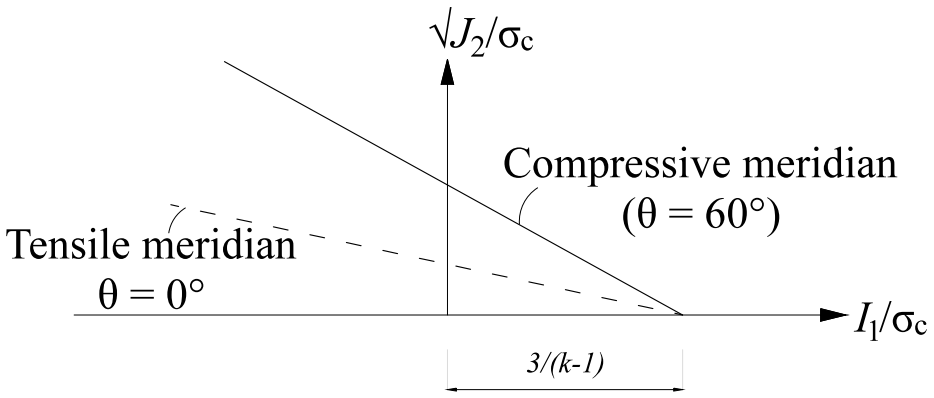

Figure 7.18: Coulomb criterion in meridian plane

i.e.

$$\sin\phi = \frac{k-1}{k+1} \tag{7.34}$$

As $tan\phi = sin\phi\sqrt{1 - sin\phi^2}$ this implies

$$\mu = \tan\phi = \frac{k-1}{2\sqrt{k}} \tag{7.35}$$

Moreover, this expression and (7.33) yield

$$c = \frac{\sigma_c}{2\sqrt{k}} \tag{7.36}$$

With this discussion of the relations between the various material parameters, we return to the Coulomb criterion given in the form of (7.29). Suppose that the stress state ($\sigma_1,\sigma_2,\sigma_3$) fulfills the criterion. Let us on this stress state superpose a hydrostatic stress state given by the quantity p, this results in the stress state ($\sigma_1+p,\sigma_2+p,\sigma_3+p$). It is evident that this new stress state fulfills criterion (7.29) only if $p(k - 1) = 0$, i.e. if $k = 1$. It is concluded that criterion (7.29) depends on the hydrostatic stress state if $k \neq 1$, i.e.

The Culomb criterion depends on the hydrostatic stress if $k \neq 1$ *(7.37)*

Criterion (7.29) defines a plane in the principal stress space, i.e. the meridians take the form of straight lines. Moreover, the trace in the deviatoric plane ($0° \leq \theta \leq 60°$ corresponding to $\sigma_1 \geq \sigma_2 \geq \sigma_3$) is also a straight line. Let us now examine the compressive and tensile meridians.

Along the compressive meridian ($\theta = 60°$ corresponding to $\sigma_1 = \sigma_2 > \sigma_3$) we obtain

$$I_{1c} = 2\sigma_1 + \sigma_3; \qquad \sqrt{J_{2c}} = \frac{1}{\sqrt{3}}(\sigma_1 - \sigma_3) \tag{7.38}$$

where subscript c refers to the compressive meridian. Expressing σ_1 and σ_3 in terms of I_{1c} and $\sqrt{J_{2c}}$ and insertion into (7.29) result in

$$\sqrt{J_{2c}} + \frac{k-1}{\sqrt{3}(k+2)} I_{1c} - \frac{\sqrt{3}\sigma_c}{k+2} = 0 \tag{7.39}$$

As expected $\sqrt{J_{2c}}$ is independent on the hydrostatic stress when $k=1$.
Along the tensile ($\theta = 0°$ corresponding to $\sigma_1 > \sigma_2 = \sigma_3$), we have

$$I_{1t} = \sigma_1 + 2\sigma_3; \qquad \sqrt{J_{2t}} = \frac{1}{\sqrt{3}}(\sigma_1 - \sigma_3) \tag{7.40}$$

where subscript t refers to the tensile meridian. Expressing σ_1 and σ_3 in terms of I_{1t} and $\sqrt{J_{2t}}$ and insertion into (7.29) provide

$$\sqrt{J_{2t}} + \frac{k-1}{\sqrt{3}(2k+1)} I_{1t} - \frac{\sqrt{3}\sigma_c}{2k+1} = 0 \tag{7.41}$$

Expressions (7.39) and (7.41) are illustrated in Fig. 7.18.
To determine the trace in the deviatoric plane, we recall that here $I_1 = I_{1t} = I_{1c}$, i.e. elimination of this quantity from (7.39) and (7.41) yields

$$\frac{\rho_c}{\rho_t} = \frac{\sqrt{2J_c}}{\sqrt{2J_t}} = \frac{2k+1}{k+2} \tag{7.42}$$

where $\rho = \sqrt{2J_2}$. Recalling that the trace of the Coulomb criterion in the deviatoric plane is a straight line when $\sigma_1 \geq \sigma_2 \geq \sigma_3$ corresponding to $0° \leq \theta \leq 60°$, we obtain the result shown in principle in Fig. 7.19.

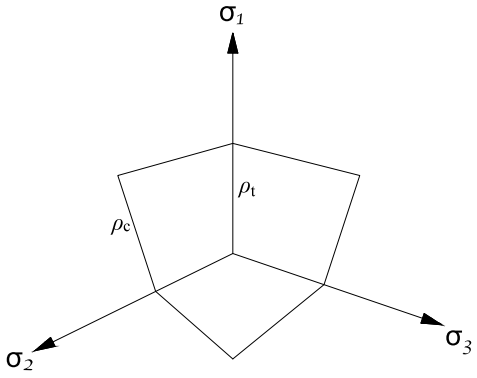

Figure 7.19: Coulomb criterion in the deviatoric plane

In order to further elucidate the properties of the Coulomb criterion, we consider its predictions for plane stress conditions. From (7.29), the results shown in Fig. 7.20 are easily obtained (note that in this figure the usual convention of $\sigma_1 \geq \sigma_2 \geq \sigma_3$ has been abandoned). It appears that the predicted uniaxial tensile strength becomes $\sigma_t = \sigma_c / k$.

Due to its simplicity, the Coulomb criterion is widely used in analytical applications, cf. for instance Chen (1975) for soil applications and Nielsen (1984) for concrete applications. In numerical applications, however, its use is impeded by the corners of the surface, cf. Fig. 7.19. By calibration of the parameter k, the criterion can be used to model a large variety of material, but, as we will see later, the ignorance of the influence of the intermediate principal stress σ_2 implies that the criterion, in general, will underestimate the experimentally determined failure stresses.

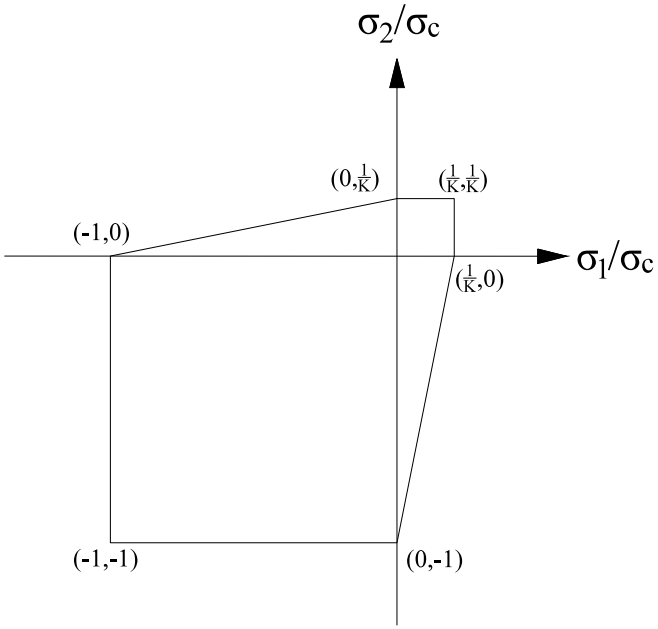

Figure 7.20: Coulomb criterion for plane stress conditions

7.4.3 Mohr's failure mode criterion

This failure mode criterion dates back to Mohr (1900) and it is based on Fig. 7.15b) and the discussion following (7.31). From Figs. 7.15 and 7.16, we may have the situation shown in Fig. 7.21.

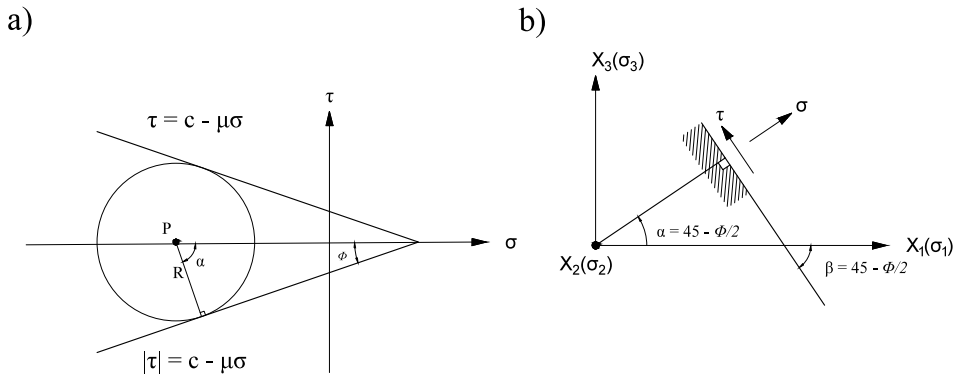

Figure 7.21: a) Coulomb criterion and Mohr's circle; b) interpretation of σ and τ

Consider the stress state *(σ, τ)* that satisfies the Coulomb criterion (7.31) in accordance with Fig. 7.21a). From Mohr's circle of stress, the interpretation of σ and τ is displayed in Fig. 7.21b) where the x_1, x_2, x_3-coordinate system is collinear with the principal directions of σ_1, σ_2 and σ_3. From Fig. 7.21 a) follows that $2\alpha+90°+\phi=180°$, i.e.

$$\alpha = 45° - \frac{\phi}{2}$$

It seems tempting to assume that the plane illustrated in Fig. 7.21b) on which the failure stresses σ and τ act is also a failure plane where failure takes place in the form of sliding. This plane is also called a slip plane since the failure mode is postulated to be a movement along the plane. The angle β, which the failure plane makes with the largest principal stress direction (σ_1) becomes $\beta= 45°+\phi/2$ as shown in Fig. 7.21b).

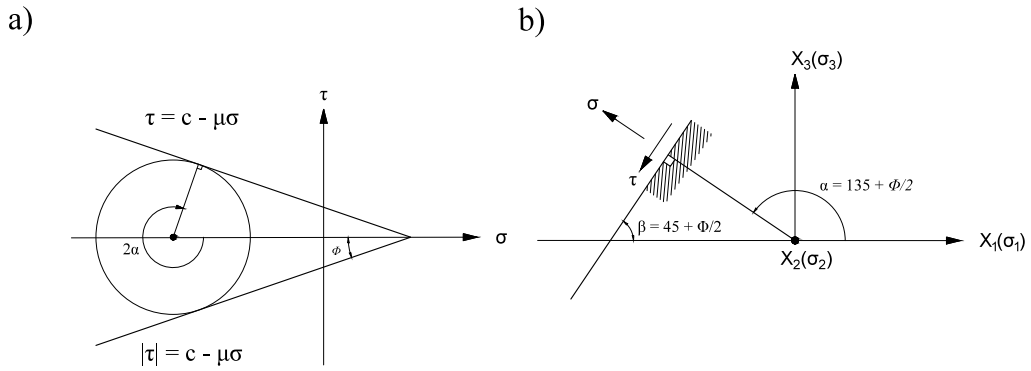

Figure 7.22: a) Coulomb criterion and Mohr's circle; b) interpretation of σ and τ

Consider next the situation where the stress state *(σ, τ)* that satisfies the Coulomb criterion is located as displayed in Fig. 7.22a), the corresponding interpretation of σ and τ is shown in Fig. 7.22b). From Fig. 7.22a) follows that $360°-2\alpha+90°+\phi=180°$, i.e.

$$\alpha = 135° + \frac{\phi}{2}$$

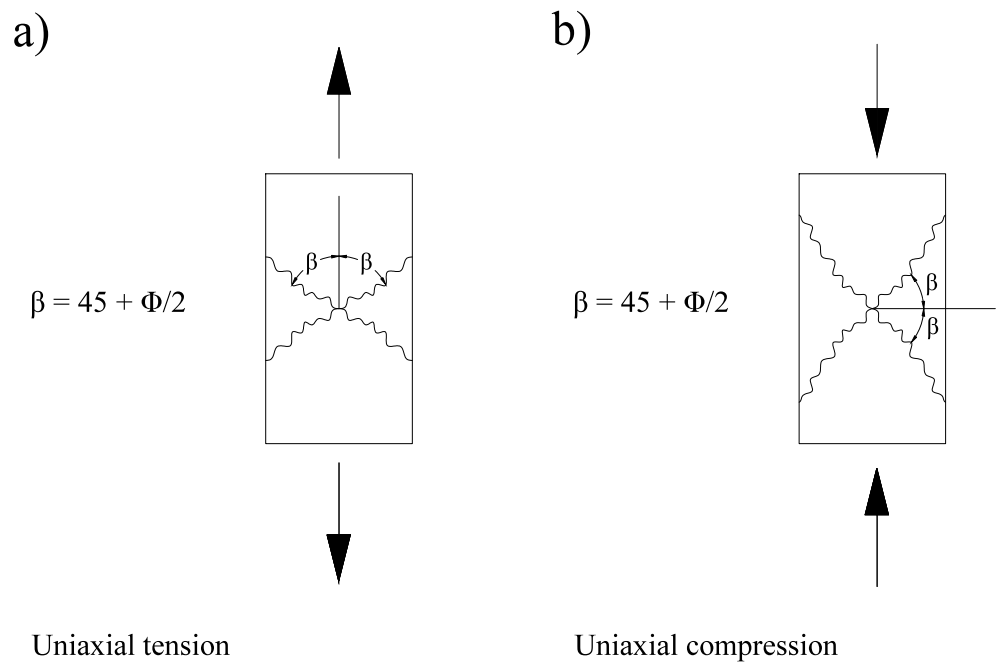

Figure 7.23: illustration of Mohr's failure mode criterion; a) uniaxial tension; b) uniaxial compression

Again it is assumed that the plane in Fig. 7.22b) on which the failure stresses σ and τ act is a failure plane. The angle β which this failure plane makes with the largest principal stress direction (σ_1) becomes β = 45°+ϕ/2 as illustrated in Fig. 7.22b). It is observed that the two failure planes shown in Figs. 7.21b) and 7.22b) both contain the direction of the intermediate principal stress direction (σ_2). From the discussion above we conclude that

Mohr's failure mode criterion postulates that two failure planes exist. These planes contain the direction of the intermediate principal stress direction and they both make the angle $\beta = 45° + \phi/2$ *with the largest principal stress direction* (7.43)

It is emphasized that the angle $\beta = 45°+\phi/2$ is the angle to the largest principal stress direction (σ_1) and that $\sigma_1 \geq \sigma_2 \geq \sigma_3$, where tension is considered as a positive quantity. From the discussion above follows directly that if a Mohr criterion is used and if ϕ denotes the current friction angle, cf. Fig. 7.17, then conclusion (7.43) also holds. Conclusion (7.43) is illustrated in Fig. 7.23.
It turns out that Mohr's failure mode criterion is often in fair agreement with experimental results for a variety of materials.

7.4.4 Rankine criterion and modified Coulomb criterion

The Mohr-Coulomb criterion is a generalization of the Tresca criterion, to which it reduces for $\phi=0$. The other extreme, $\phi=90°$, leads to the Rankine criterion (1858), which provides the simplest basis for plasticity modeling for concrete.

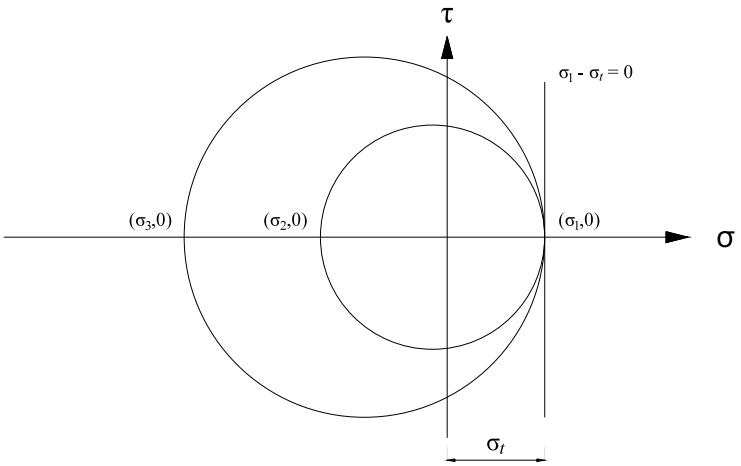

Figure 7.24: Rankine criterion viewed as a Coulomb criterion with the friction angle $\phi=90°$

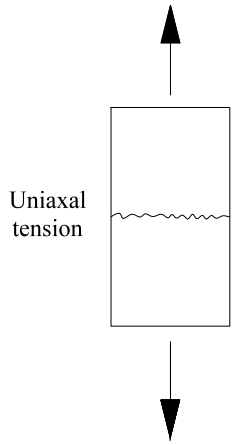

Figure 7.25: Mohr's failure mode criterion for Rankine failure

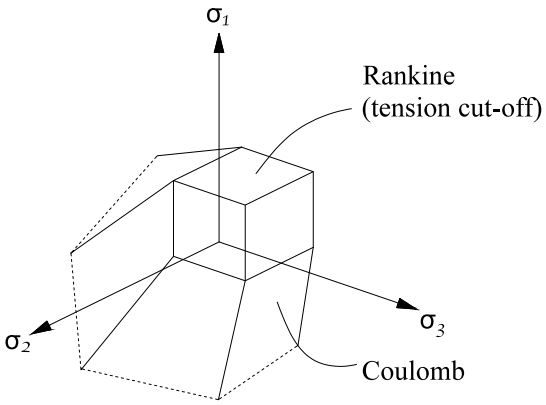

Figure 7.26: modified Coulomb criterion in the principal stress space

This so-called Ranking criterion has the form

$$\sigma_1 - \sigma_t = 0; \qquad \sigma_1 \geq \sigma_2 \geq \sigma_3 \tag{7.44}$$

and for obvious reasons, it is occasionally referred to as the maximum principal stress criterion. In a Mohr diagram, (7.44) takes the form shown in Fig. 7.24 and

it is evident that (7.44) may be viewed as the envelope of all Mohr's stress circles for which the stress state fulfills (7.44).

With $\phi=90°$ and Mohr's failure mode criterion (7.43) we obtain the failure plane for uniaxial tension as shown in Fig. 7.25, only one failure plane exists and it is perpendicular to the maximum principal stress direction. This result is in close agreement with experimental results for concrete and rocks where the failure manifests itself as a crack perpendicular to the maximum principal stress direction.

Let us return to the Coulomb criterion and its prediction given by Fig. 7.20.

To remedy the too high uniaxial tensile strength predicted by the Coulomb criterion, we may use a combined failure criterion, which states that failure is obtained, if

$$k\sigma_1 - \sigma_3 - \sigma_c = 0 \qquad or \qquad \sigma_1 - \sigma_t = 0 \tag{7.45}$$

is fulfilled. This is the modified Coulomb criterion, which due to its simplicity often is used in analytical calculations, cf. Nielsen (1984).

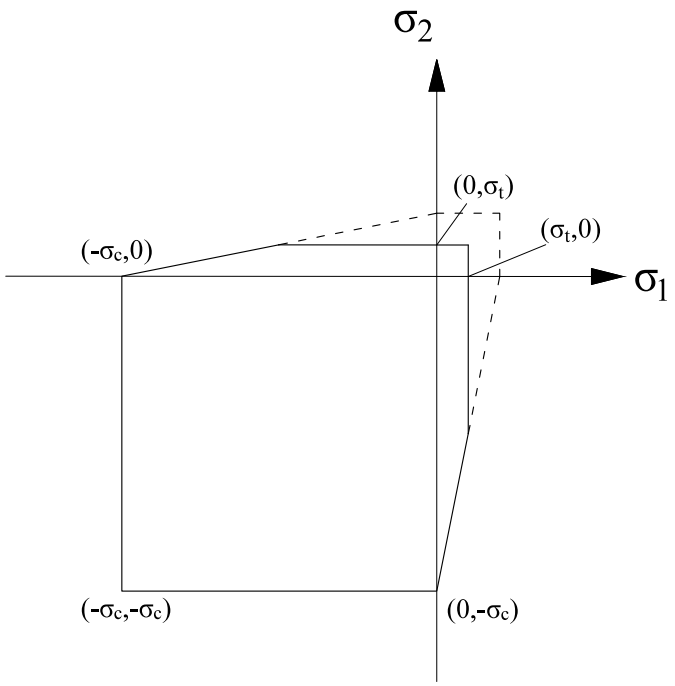

Figure 7.27: modified Coulomb criterion for plane stress conditions

Often the Rankine criterion is called a tension cut-off criterion and the appearance of the modified Coulomb criterion in the principal stress space is shown in Fig. 7.26. For biaxial stress state the modified Coulomb criterion is illustrated in Fig. 7.27.

7.5 Yield criteria independent of Hydrostatic Pressure

The yield criterion defines the elastic limits of a material under combined state of stress. As we know, the elastic limit in a simple tension test is the yield stress σ_0, while in a simple shear test, it is the yield stress τ_0. In general the elastic limit or

yield stress is a function of the state of stress, σ_{ij}. Hence, the yield condition can generally be expressed as

$$f(\sigma_{ij}, k_1, k_2, ...) = 0 \qquad (7.46)$$

where k_1, k_2, … are material constants, which, like σ_0 and τ_0 are to be determined experimentally.

For isotropic materials, the orientation of the principal stresses, is immaterial, and the values of the principal stresses suffice to describe the state of stress uniquely. A yield criterion therefore consists in a relation of the form

$$f(\sigma_1, \sigma_2, \sigma_3, k_1, k_2, ...) = 0 \qquad (7.47)$$

It has been shown that the three principal stresses σ_1, σ_2 and σ_3 can be expressed in terms of the combinations of the three stress invariants I_1, J_2 and J_3, where I_1 is the first invariant of the stress tensor σ_{ij} and J_2 and J_3 are the second and the third invariants of the deviatoric tensor s_{ij}. Thus, one can replace eq. (7.47) by

$$f(I_1, J_2, J_3, k_1, k_2, ...) = 0 \qquad (7.48)$$

Furthermore, these three particular principal invariants are directly related to Haigh-Westergaard coordinates ξ, ρ, θ in stress space. Therefore eq. (7.48) can also be written as

$$f(\xi, \rho, \theta, k_1, k_2, ...) = 0 \qquad (7.49)$$

Yield criteria of materials should be determined experimentally. An important experimental fact for metals, shown by Bridgman and others (1950), is that the influence of a hydrostatic pressure effect means that the yield function can be reduced to the form

$$f(J_2, J_3, k_1, k_2, ...) = 0 \qquad (7.50)$$

A stress-strain curve in simple tension does not, in itself, provide any information on the behavior under combined stress. The combined stress tests, analogous to simple tension, are termed proportional or radial loading tests. In these tests, all stresses are increased proportionately. In a biaxial state of stress, for example, σ_1 and σ_2 are increased so as to keep the ratio σ_1/σ_2 constant. It seems that we would need to perform a number of tests in order to construct a yield locus. However, we will show that one point on the yield locus may give rise to twelve points (fig. 7.28) if the material (1) is isotopic, (2) is hydrostatic pressure independent, and (3) has equal yield stresses in tension and compression. Now suppose that a material yields in a state of stress, $(3\sigma, \sigma, 0)$. Point $A_1\,(3\sigma, \sigma, 0)$ in fig. 7.28 then lies on the yield locus on the $\sigma_1 - \sigma_2$ plane. If the material is isotropic, there is no reason why we should not relabel the axes in alternative way. We thus conclude that point $A_1\,(\sigma, 3\sigma, 0)$ also lies on the yield locus. Further, if the material has the same response to tension and compression, points $A_3\,(-3\sigma, -\sigma, 0)$ and $A_4\,(-\sigma, -3\sigma, 0)$ will also lie on the yield locus. Now considering A_1 and A_2 or A_3 and A_4, we see that they are mirror images about a lane *aa'* bisecting the σ_1 and σ_2 axes. Similarly, A_1 and A_4 or A_3 and A_2 are symmetric about another line *bb'* perpendicular to *aa'*. Hence, there are two symmetric axes for the yield locus. Moreover, if hydrostatic pressure has no effect on yielding we can add a hydrostatic state of stress, (h, h, h), to a yield stress state to generate another yield point. For example, if a hydrostatic pressure $(-3\sigma, -3\sigma, -3\sigma)$ is added to the

yield stress point *(3σ, σ, 0)* then the stress state *(0, -2σ, -3σ)* is another yield point. Now we alter its coordinate such that a yield point B_1 *(-2σ, -3σ, 0)* is obtained on the σ_1 - σ_2 plane. Similarly, one can get a new yield point C_1 *(2σ,σ,0)* on the σ_1 - σ_2 plane by adding *(-σ, -σ, -σ)* to *(3σ, σ, 0)* and altering the coordinates correspondingly. Finally, because of symmetry, points B_1 and C_1 like point A_1, can generate four positions B_1, B_2, B_3, B_4 and C_1, C_2, C_3, C_4 respectively, lying on yield locus.

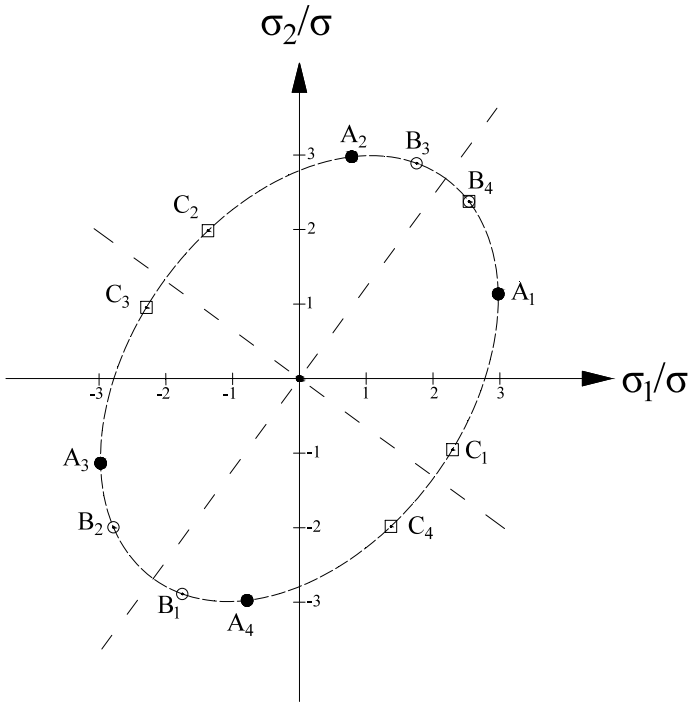

Figure 7.28: yield locus on $\sigma_1\sigma_2$ plane (σ_3=0) generated from one test point A_1

Now, we have generated a total of twelve yield points on the σ_1 - σ_2 plane from one test point. Connecting these points with a smooth curve, we construct a yield locus as shown in fig. 7.28. Noting that this locus is generated from only one radial test point, it can be considered an approximation of the yield function of a biaxial state of stress for a material with isotropy, with the same response in tension and compression, and with no hydrostatic pressure effect on yielding.

We have discussed so far the general form and some characteristics of a yield function. The very useful yield criteria of Tresca and Von Mises for metals will be studied in the following sections.

7.5.1 The Tresca Yield Criterion

Historically the first yield criterion for a combined state of stress for metals was that proposed in 1864 by Tresca, who suggested that yielding would occur when the maximum shearing stress at a point reaches a critical value *c*. Stating this in terms of principal stresses, one half of the greatest absolute value of the difference between the principal stresses taken in pairs must be equal to *c* at yield, namely,

$$Max\left(\frac{1}{2}|\sigma_1-\sigma_2|,\frac{1}{2}|\sigma_3-\sigma_2|,\frac{1}{2}|\sigma_1-\sigma_3|\right)=c \qquad (7.51)$$

where the material constant *c*, which is the cohesion, may be determined from the simple tension test. Then

$$c=\frac{\sigma_0}{2} \qquad (7.52)$$

in which σ_0 is the yield stress in simple tension.

We recall that the hydrostatic stress has no influence on yielding and we may achieve this property by choosing the parameter *k = 1* in Coulomb criterion, cf. (7.37). In this case (7.29) reduces to

$$\sigma_1-\sigma_3-m=0; \qquad \sigma_1\geq\sigma_2\geq\sigma_3 \qquad (7.53)$$

where *m* is a parameter. Requiring that this expression for uniaxial tension should provide the initial yield stress σ_{y0} cf. Fig. 7.1, we obtain

$$\sigma_1 - \sigma_3 - \sigma_{y0} = 0 \qquad (7.54)$$

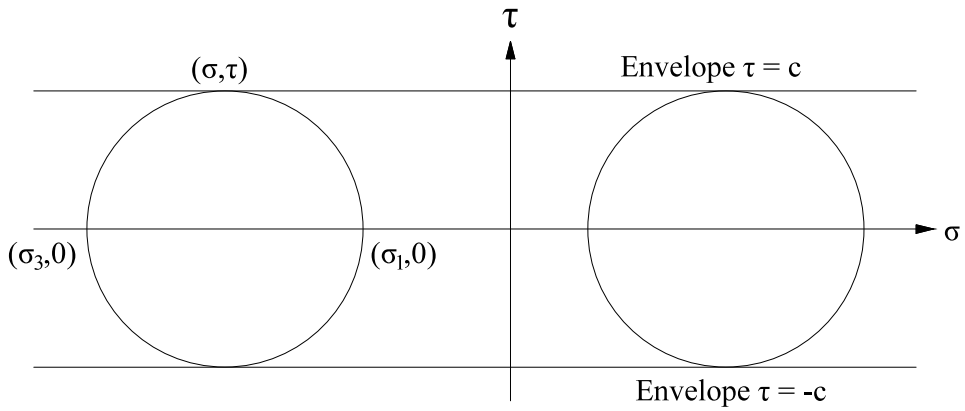

Figure 7.29: Tresca criterion in Mohr diagram

Since *k = 1*, we conclude from (7.34) and (7.36) that the friction angle ϕ and the cohesion *c* are given by

$$\phi = 0; \qquad c = \frac{\sigma_{y0}}{2}$$

i.e. in terms of the formulation (7.31), (7.53) is equivalent with

$$|\tau| = c$$

Therefore, in analogy with Fig. 7.16, we achieve the interpretation of this expression as shown in Fig. 7.29.

There are six different expressions in various regions of the σ_1 - σ_2 plane, depending upon the relative magnitudes and the signs of σ_1 and σ_2 (see fig. 7.30). In the first quadrant, between the σ_1 axis ant the bisector of the two axes, the order of the stress requires that

$$\tau_{\max} = \frac{\sigma_1}{2} \qquad (7.55)$$

Hence, the yield criterion becomes $\sigma_1 = \sigma_0$ and gives the line *AB*. In the same quadrant, between the bisector and the σ_2 axis, we have

$$\tau_{\max} = \frac{\sigma_2}{2} \qquad (7.56)$$

and the yield criterion $\sigma_2 = \sigma_0$ is represented by the lane *BC*. In the second quadrant we have

$$\tau_{\max} = \frac{\sigma_2 - \sigma_1}{2} \qquad (7.57)$$

Thus the yield criterion becomes $\sigma_2 - \sigma_1 = \sigma_0$, and line *CD* is obtained. By proceeding similarly for the third and fourth quadrants, it can be found that the yield locus for plane stress is hexagon *ABCDEF* as shown in fig. 7.30.

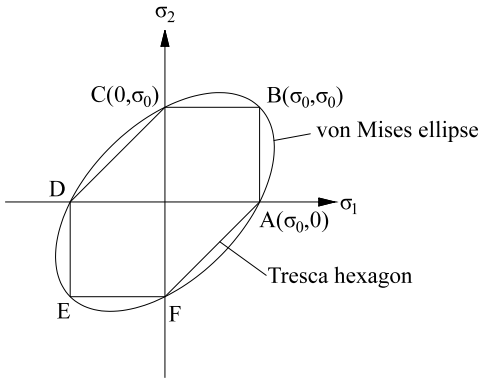

Figure 7.30: yield criteria matched in tension in the coordinate plane $\sigma_3 = 0$

To represent the yield surface in the principal stress space, eq. (4.35) is used here for the principal stresses. Assuming the ordering of stresses to be $\sigma_1 > \sigma_2 > \sigma_3$, we can write eq. (7.51) in the form

$$\frac{1}{2}(\sigma_1 - \sigma_3) = \frac{1}{\sqrt{3}}\sqrt{J_2}\left[\cos\theta - \cos\left(\theta + \frac{2}{3}\pi\right)\right] = k \qquad (0 \le \theta \le 60°) \qquad (7.58)$$

Expanding this equation and noting eq. (7.52), we obtain the Tresca criterion in terms of invariants,

$$f(J_2,\theta) = 2\sqrt{J_2}\sin\left(\theta + \frac{1}{3}\pi\right) - \sigma_0 = 0 \qquad (0 \le q \le 60°) \qquad (7.59)$$

or identically in terms of the variables ξ, ρ, θ

$$f(\rho,\theta) = \sqrt{2}\rho\sin(\theta + \frac{1}{3}\pi) - \sigma_0 = 0 \qquad (7.60)$$

Since the hydrostatic pressure has no effect on the yield surface, eq. (7.59) or eq. (7.60) must be independent of hydrostatic pressure I_1 or ξ, representing a cylindrical surface whose generator is parallel to the hydrostatic axis. On the deviatoric plane, eq. (7.59) or eq. (7.60) is a straight line passing through point *A* (with θ=0 and $\rho=\sqrt{\frac{2}{3}}\sigma_0$) and point *B* (with θ=60° and $\rho=\sqrt{\frac{2}{3}}\sigma_0$), as shown in fig. 7.33. This is one sector of the yield locus on the deviatoric plane. Each of the five other possible orderings of the magnitude of the principal stresses gives similar lines in the appropriate sectors of the yield locus on the deviatoric plane and a regular hexagon *ABCDEF* is thus obtained.

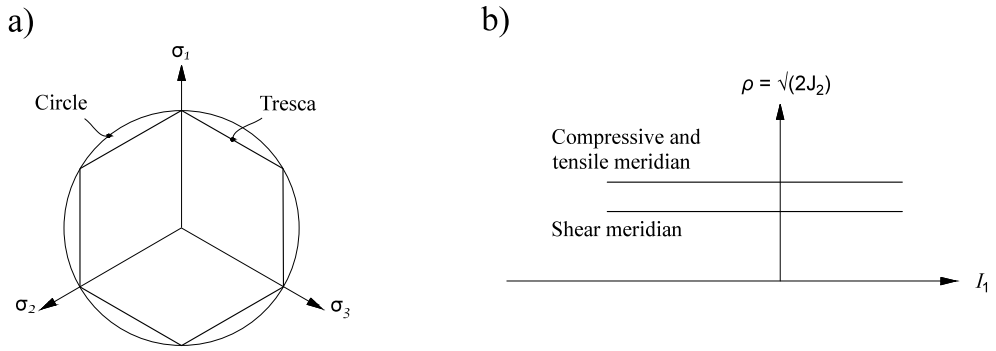

Figure 7.31: Tresca criterion; a) deviatoric plane; b) meridian plane

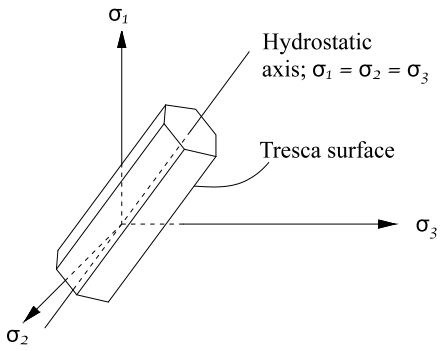

Figure 7.32: Tresca surface in the principal stress space

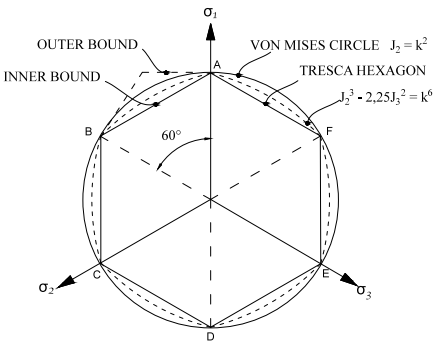

Figure 7.33: yield criteria matched in tension in a deviatoric plane

Now we can see that the yield surface is a regular hexagonal prism in principal stress space, as shown in fig. 7.32. The yield locus for a biaxial state of stress shown in fig. 7.30 is the intersection of the cylinder with the coordinate plane $\sigma_3=0$.

Isotropy means that there is no need to draw the yield surface in a general stress space (σ_{ij}). Nevertheless, some intersections of particular planes with the surface in general stress space are of interest, e.g., the intersection with the $\sigma_x - \tau_{xy}$ plane. The latter intersection is the yield locus for combined normal stress and shear (fig. 7.35),

$$\sigma_x^2 + 4\tau_{xy}^2 = \sigma_0^2 \qquad (7.61)$$

which represents an ellipse in the σ-τ-plane. Expression (7.61) may be compared with the corresponding result using the von Mises criterion.

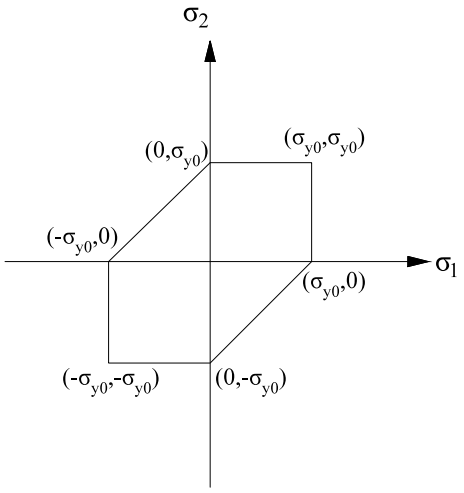

Figure 7.34: Tresca criterion for plane stress conditions

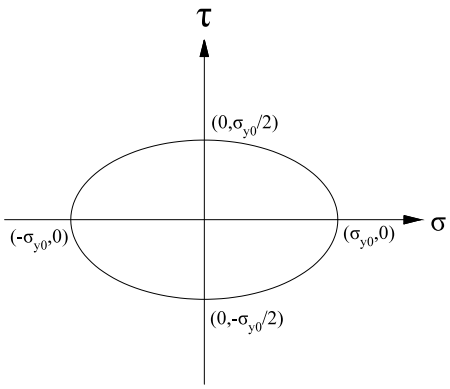

Figure 7.35: Tresca ellipse in the στ plane

From (7.61) with $\sigma = 0$, the initial yield shear stress becomes

$$\tau_{y0} = \frac{\sigma_{y0}}{2} \qquad (7.62)$$

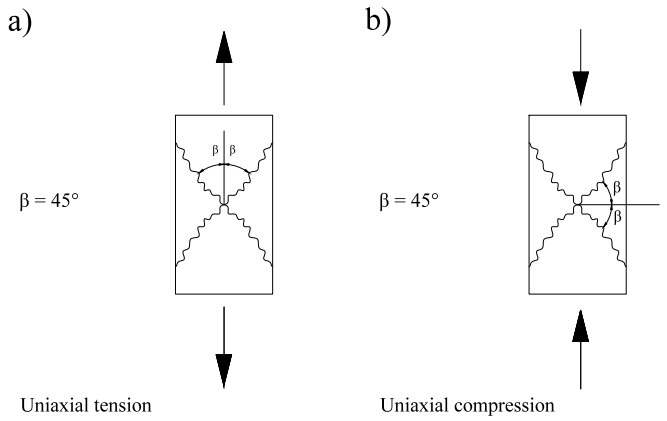

Figure 7.36: Mohr's failure mode criterion for Tresca yielding; a) uniaxial tension; b) uniaxial compression

As this shear stress is located along the shear meridian and as the maximum deviation between the von Mises criterion and the Tresca criterion occurs along this meridian, cf. Fig. 7.31a), a comparison between (7.67) and (7.62) reveals that any Tresca yield stress, at most, is 13.4% lower than the corresponding von Mises yield stress.

Since the friction angle $\phi = 0$ for Tresca's criterion, Mohr's failure mode criterion (7.34) states that any failure plane (slip plane) makes 45° with the maximum principal stress direction. This is illustrated in Fig. 7.36 and this prediction is in close agreement with experimental results for metals and steel.

7.5.2 The Von Mises Yield Criterion

Although the maximum shearing stress criterion is simple, it does not reflect any influence of the intermediate principal stress. The octahedral shearing stress or the strain energy of distorsion is the key variable for causing yielding of materials, which are pressure independent. The invariant J_2 is in fact proportional to the distorsional strain energy, i.e. to the energy due to the changes of shape. Consequently, the von Mises criterion is equivalent to the condition that the

distorsional strain energy at the onset of yielding reaches a critical value. For initial yielding of metals and steel, the general experimental evidence is summarized in (7.13). As the hydrostatic stress I_1 has no influence on the yielding, the general criterion (4.30) reduces to (7.12). The simplest assumption is then to ignore the influence of the complicated term $cos3\theta$, which leads to $F(J_2) = 0$, i.e. it is assumed that J_2 takes a constant value at yielding, i.e. $\sqrt{J_2}-c=0$ where c is a constant. This relation may be written in various manners, but the most convenient expression is obtained by

$$\sqrt{3J_2} - \sigma_{y0} = 0 \qquad (7.63)$$

where, for convenience, the factor 3 in front of J_2 is inserted since $\sqrt{3J_2}$ for uniaxial tension reduces to $\sqrt{3J_2}=\sigma$. According to the criterion, $\sqrt{3J_2}$ takes a constant value for initial yielding and this constant value then becomes σ_{y0} i.e. the initial yield stress in tension. Note that the second deviatoric invariant J_2 is always nonnegative, and so its square root is a real number. The theory based on von Mises yield condition is often referred to as a J_2*-plasticity.*

Criterion (7.63) is independent of the hydrostatic stress I_l, i.e. it represents a cylindrical surface in the principal stress space with the meridians being parallel with the hydrostatic axis. This means that only the deviatoric stresses influence the criterion. Moreover, it is evident that (7.63) in the deviatoric plane represents a circle, i.e. all meridians are located at the same distance to the hydrostatic axis. These properties are illustrated in Fig. 6.37 and it appears that the circle in the deviatoric plane falls between the lower and upper bounds shown in Fig. 7.33. With these properties, the appearance of the yield surface in the principal stress space takes the form shown in Fig. 7.38. The von Mises yield condition means that the material yields when the distance of the corresponding stress point from the hydrostatic axis in the principal stress space reaches a certain limit value,

$\rho_0=\tau_0\sqrt{2}$. In the deviatoric plane, the points satisfying the yield condition fill a circle. Since the hydrostatic component of stress has no effect on the J_2 invariant, the yield surface corresponding to the von Mises criterion is a cylinder, rotationally symmetric with respect to the hydrostatic axis.

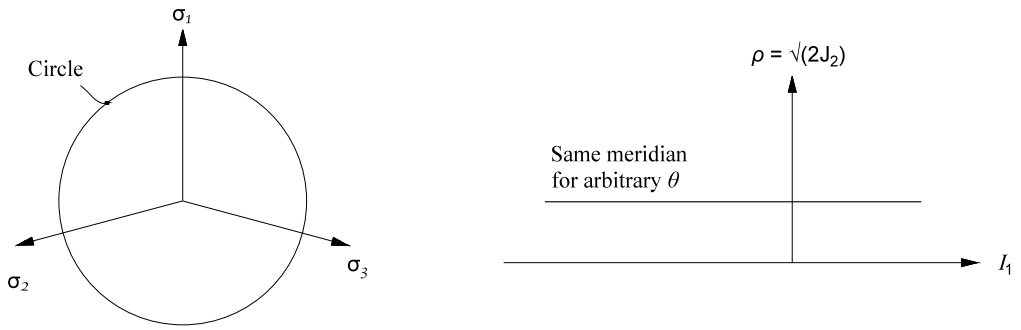

Figure 7.37: von mises criterion (6.63); a) deviatoric plane; b) meridian plane

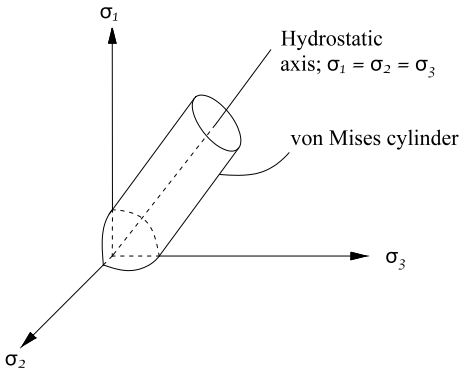

Figure 7.38: von Mises surface in the principal stress space

The criterion (7.63) was suggested by Von Mises (1913) and it is therefore called the von Mises criterion, it was anticipated, to some extent, by the proposal of Huber (1904) and the criterion is thus occasionally called the Huber-von Mises criterion. Hencky (1924) suggested an interesting physical interpretation of the criterion. Inside the initial yield surface given by (7.63), the material behaves linear elastic. The strain energy W of a linear elastic and isotropic material can be written as

$$W = W_d + W_v$$

where

$$W_d = G e_{ij} e_{ij}; \qquad W_v = \frac{1}{2} K \varepsilon_{kk} \varepsilon_{mm}$$

It appears that W_d represents the deviatoric strain energy whereas W_v is the volumetric strain energy. Moreover, as e_{ij} and ε_{kk} are decoupled W_d and W_v are also decoupled. With Hookes law for the deviatoric response, we obtain

$$W_d = \frac{1}{4G} s_{ij} s_{ij} = \frac{1}{2G} J_2$$

i.e. the von Mises yield criterion may be interpreted by saying that initial yield occurs when the deviatoric strain energy achieves a certain value.

The octahedral shear stress τ_0 is given by $\tau_0 = \sqrt{\frac{3}{2} J_2}$.

Another physical interpretation of the von Mises criterion is therefore to claim that the yielding occurs when the octahedral shear stress τ_0, that acts on the octahedral plane exceeds a certain value. Expressed in the principal stresses, criterion (7.63) takes the form

$$\sqrt{\frac{1}{2}\left[(\sigma_1 - \sigma_2)^2 + (\sigma_1 - \sigma_3)^2 + (\sigma_3 - \sigma_2)^2\right]} - \sigma_{y0} = 0 \qquad (7.64)$$

For plane stress conditions for $\sigma_3 = 0$ holds, it follows that

$$\sqrt{\sigma_1^2 + \sigma_2^2 - \sigma_1 \sigma_2} - \sigma_{y0} = 0 \qquad (7.65)$$

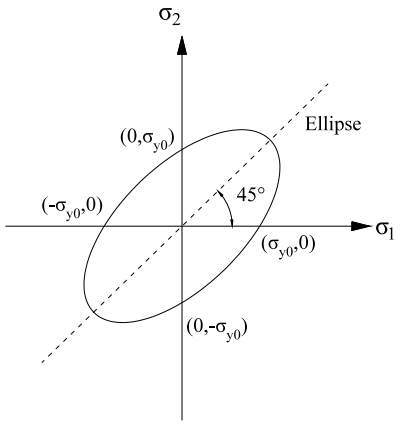

Figure 7.39: von Mises ellipse in the $\sigma_1\sigma_2$ plane

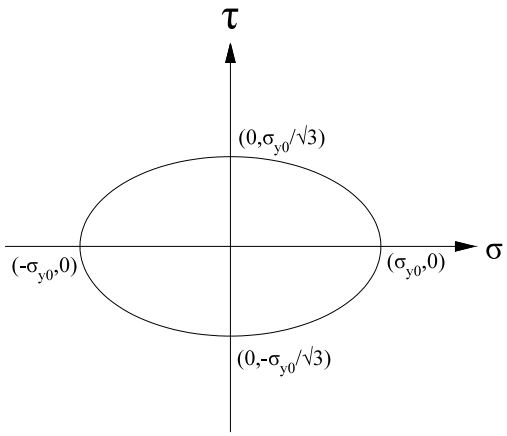

Figure 7.40: von Mises ellipse in the $\sigma\tau$ plane

which represent an ellipse in the $\sigma_1\sigma_2$ plane as shown in fig. 7.39. Another stress state of interest is obtained by simultaneous uniaxial stressing and torsion of, for instance, a thin walled tube. This stress state is given by

$$\sigma_{ij} = \begin{bmatrix} \sigma & \tau & 0 \\ \tau & 0 & 0 \\ 0 & 0 & 0 \end{bmatrix} \qquad i.e. \qquad \mathbf{s}_{ij} = \begin{bmatrix} \frac{2}{3}\sigma & \tau & 0 \\ \tau & -\frac{1}{3}\sigma & 0 \\ 0 & 0 & -\frac{1}{3}\sigma \end{bmatrix}$$

We then obtain from (7.63) that

$$\sqrt{\sigma^2 + 3\tau^2} - \sigma_{yo} = 0 \qquad (7.66)$$

which represent an ellipse in the $\sigma\tau$ plane, cf. Fig. 7.40. It may be of interest to determine the initial yield shear stress τ_{y0} when $\sigma=0$ and from (7.66) we find that

$$\tau_{y0} = \frac{\sigma_{y0}}{\sqrt{3}} \qquad (7.67)$$

7.5.3 Experimental results for metals and steel - von Mises versus Tresca

For initial yielding of metals and steel, we have already summarized the general experimental evidence in (7.13). Moreover, in relation to Figs. 7.33, 7.37 and 7.31 it can then be argued that Tresca's criterion must provide a lower bound whereas the von Mises criterion is located between the lower and upper bound. We also found that any Tresca yield stress, at most, is 13.4% lower than the corresponding von Mises yield stress. Let us now investigate whether these conclusions are in accordance with experimental data.

It was claimed that initial yielding of metals and steel is independent of the hydrostatic stress I_1. According to the extensive test series of Bridgman (1952),

this assumption is closely fulfilled when $|I_l| \leq$ about $4\sigma_{y0}$ i.e. for all cases of practical interest. The next issue mentioned in the summary (7.13) is that if the stress state σ_{ij} results in initial yielding so does the stress state - σ_{ij}. Also this assumption is closely fulfilled and as an example, the initial yield stress is the same for uniaxial tension and uniaxial compression. The last issue mentioned in (7.13) is the convexity of the yield surface and we will see that this assumption is also closely fulfilled.

The classical results of Taylor and Quinney (1931) shown in Fig. 7.41 were obtained by subjecting thin-walled tubes to combined tension and torsion. The figure also shows the ellipses of von Mises and Tresca in accordance with (7.66) and (7.62) and it appears that the von Mises criterion fits the experimental data considerably better than the Tresca criterion.

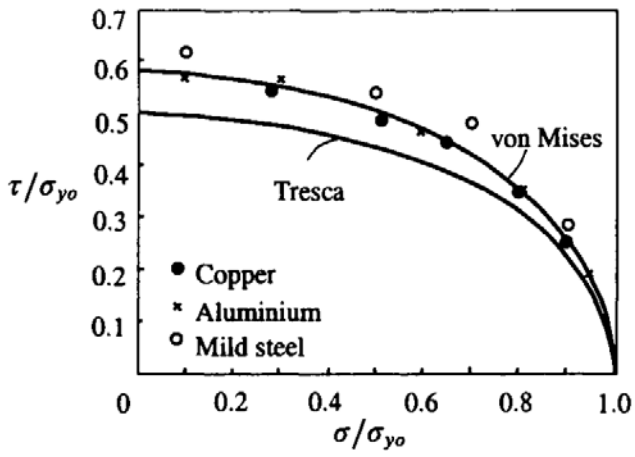

Figure 7.41: experimental results of Taylor and Quinney (1931)

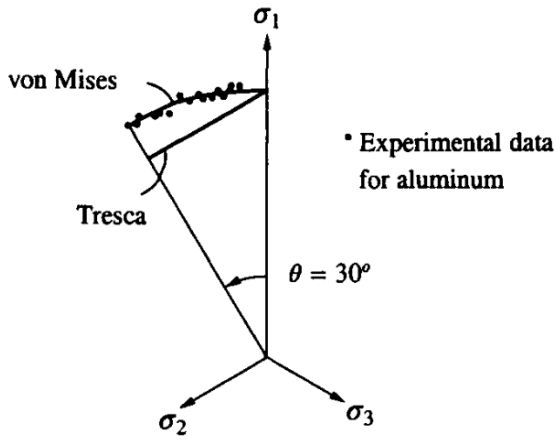

Figure 7.42: deviatoric plane; experimental data of Lianis and Ford (1957)

The same conclusion may be drawn from the experimental results of Lianis and Ford (1957). They tested commercially pure aluminum specially treated so that a well defined yield stress is obtained. They used a specially designed notched specimen whereby arbitrary uniform states of combined stresses can be produced, the results are illustrated in the deviatoric plane in Fig. 7.42 together with the predictions of von Mises and Tresca. This figure also demonstrates the convexity of the yield surface.

It is concluded that the general experimental evidence summarized in (7.13) is well-founded and that the von Mises criterion fits the experimental data very closely and it should therefore, in general, be preferred as compared with the Tresca criterion.

8 Theory of Plasticity

The salient property for which the behavior of a material is called plastic is the irreversibility of deformation upon unloading. In fact in plasticity, strains exist when the material is unloaded and these residual strains are the plastic strains. In the previous chapter, we discussed various initial yield criteria, i.e. conditions for which plastic effects are initiated. When the stress state exceeds the initial yield criterion, plastic strains will.

The basic behavior of an elasto-plastic material is summarized in Fig. 8.1.

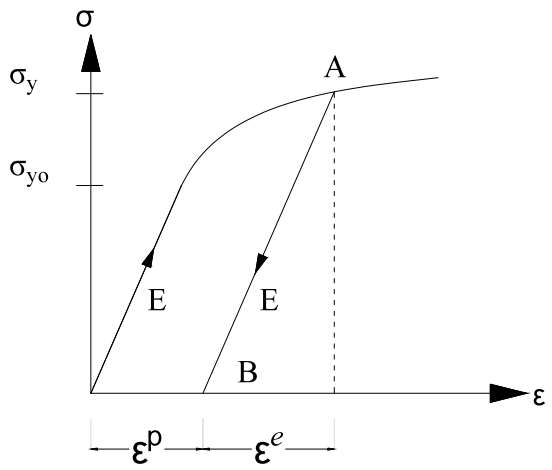

Figure 8.1: basic response of elasto-plastic material

The behavior is linear elastic with stiffness E until the initial yield stress σ_{y0}, is reached, after that plastic strains develop. Unloading from point A, see Fig. 8.1,

occurs elastically with the stiffness E so that at complete unloading to point B, the residual strain amounts to the plastic strain ε_p developed at point A. Therefore, at point A, the total strain ε consists of the sum of the elastic and plastic strains, i.e.

$$\varepsilon = \varepsilon_e + \varepsilon_p \tag{8.1}$$

If we reload again from point B, cf. Fig. 8.1, the material responds elastically until the stress reaches the value σ_y at point A. The value σ_y is therefore the current yield stress, which, in general, differs from the initial yield stress σ_{y0}.
On loading beyond point A the material behaves as if the previous unloading from point A had never occurred.
The behavior sketched in Fig. 8.1 is our model for the real material behavior, but it turns out that this model behavior closely agrees with the real behavior of elasto-plastic materials.

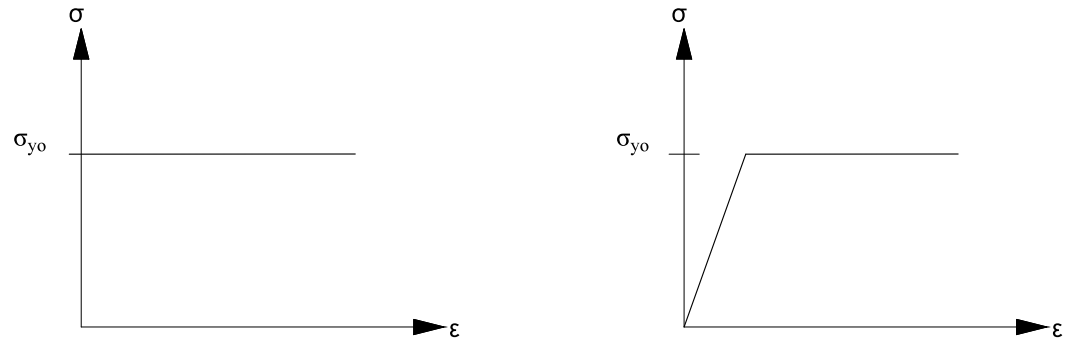

Figure 8.2: a) stiff-ideal plastic behavior; b) elastic-ideal plastic behavior

To characterize plastic behavior, a number of idealized responses have been identified. For the simplest response shown in Fig. 8.2a), the behavior is termed stiff-ideal plastic since no deformation occurs before the yield point has been reached and since the yield stress is unaffected by the amount of plastic strains.

The behavior shown in Fig. 8.2b) is termed elastic-ideal plastic behavior: for many practical applications, a material may be idealized and assumed to have a negligible strain hardening effect, i.e. its uniaxial stress-strain diagram beyond the yield point can be approximated by a horizontal straight line, with a constant stress level σ_{y0}. Thus, plastic deformation is assumed to occur under a constant flow stress.

In Fig. 8.3a) hardening plasticity is displayed. The material hardens in the sense that the stress needed to induce plastic flow increases. The hardening response shown in Fig. 8.3a) means that the current yield stress σ_y increases with increasing plastic strain, cf. Fig. 8.1, and this behavior is characteristic for alloyed steel and aluminum; moreover, aluminum lacks a sharply defined initial yield stress.

In Fig. 8.3b), combined ideal and hardening plasticity is shown and this behavior is characteristic for mild steel.

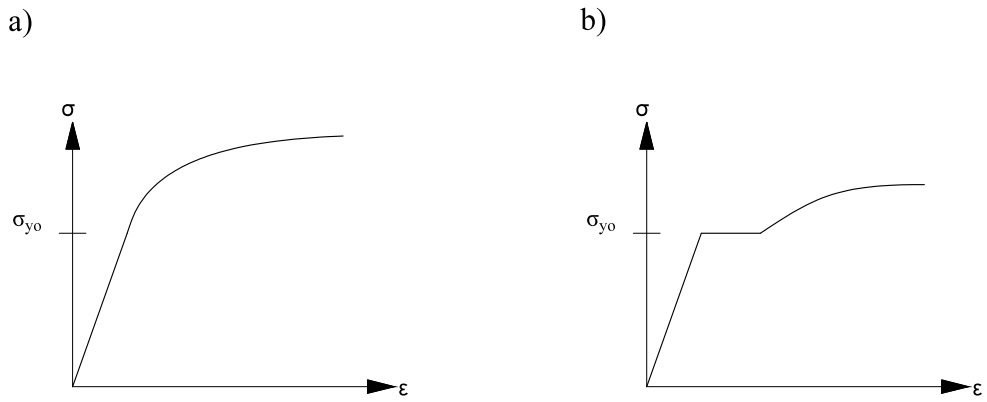

Figure 8.3: a) hardening plasticity characteristic for alloyed steel and aluminum; b) combined ideal and hardening plasticity characteristic for mild steel

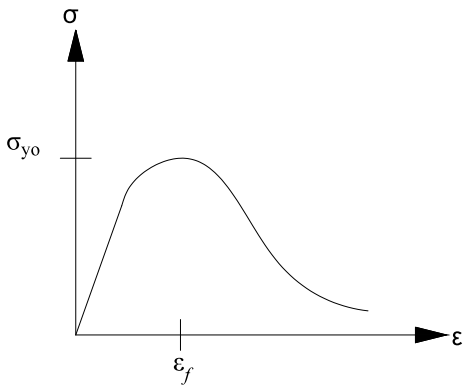

Figure 8.4: hardening plasticity followed by softening plasticity; characteristic for rocks and concrete in compression

Finally, Fig. 8.4 shows the development of hardening plasticity followed by softening plasticity, this response is typical for concrete, soil and rocks loaded in compression.

The stress-strain plastic models in uniaxial case as shown in fig 8.1 are rather simple. However, the general behavior of the material under a complex stress state is not straightforward, because it involves six stress and six strain components. The question arises as to how the simple stress-strain relationship observed from a uniaxial stress test can be generalized to predict the behavior of the material under any general combined stress state. Thus a general framework for plasticity formulations will be established in this chapter.

8.1 Hardening

Let’s recall that a perfectly elastoplasic material subjected to uniaxial loading yields at a constant stress. During plastic flow under general multiaxial loading, the stress state can move along the yield surface, but the surface itself remains the same. However, in reality the microstructure of the material changes as plastic flow continues, and this results in a change of the properties observable in the macroscale. Under uniaxial loading, the stress transmitted by a yielding material can increase or decrease. An increase of the yield stress can be referred

as to hardening, and its decrease is called softening. Typically, many materials initially harden and later soften. We will sometimes use the term hardening in a broader sense, meaning yield stress changes of any sign, negative hardening meaning softening.

During hardening in a broad sense, the elastic domain undergoes an evolution. The elastic domain of a material is bounded by the initial yield surface, also called the elastic limit envelope. Due to microstructural changes in the material introduced by plastic flow, the elastic domain changes in size or position, or both. Its boundary at an intermediate state is usually called a loading surface. Loading surface is the yield surface for an elastoplastically deformed material, which defines the boundary of the current elastic region. If a stress point lies within this region, no additional plastic deformation takes place. If the stress state is on the boundary of the elastic region and tends to move out of the current loading surface, additional plastic deformation will occur, in addition to a change of configuration in the current loading surface. The current loading surface will change its configuration when plastic deformation takes place.

This change of yield surface is called the hardening rule, i.e.

$$\textit{Hardening rule} = \textit{rule for how the yield surface changes with the plastic loading}$$

Since the yield surface is fundamental to the plasticity theory, we will first discuss this issue.

In general, we describe the initial yield surface by

$$F(\sigma_{ij}) = 0; \qquad \textit{initial yield surface}$$

Since the yield surface in general varies with the development of plastic strains, we may express the current yield surface by

$$f(\sigma_{ij}, K_1, K_2, ...) = 0 \tag{8.2}$$

where we have introduced the so-called hardening parameters K_1, K_2,... that characterize the manner in which the current yield surface changes its size, shape and position with plastic loading. Before any plasticity is initiated, we know per definition that $K_\alpha = 0$. As yet, the number of hardening parameters is unknown, and, as indicated, we may have one, two or more hardening parameters. Moreover, at this point we do not know the type of the hardening parameters, which may be scalars or higher-order tensors. Therefore, we may collect all these hardening parameters into the notation K_α and use the following definition

$$\begin{aligned} &K_\alpha = \textit{hardening paramers } (\alpha = 1,\ 2,\ ...) \\ &K_\alpha = 0 \textit{ initially} \end{aligned} \tag{8.3}$$

i.e. eq. (8.2) can be written as

$$f(\sigma_{ij}, K_\alpha) = 0 \qquad \textit{current yield surface} \tag{8.4}$$

Since $K_\alpha = 0$ holds initially, it follows that

$$f(\sigma_{ij}, 0) = F(\sigma_{ij}) \tag{8.5}$$

i.e. when the hardening parameters are zero, the current yield surface coincides with the initial yield surface. Through the hardening parameters, (8.3) describes how the size, shape and position of the current yield surface vary with plastic loading and the explicit manner in which this occurs is given by the hardening rule, i.e.

$$Choice\ of\ hardening\ parameters\ =\ choice\ of\ hardening\ rule$$

The hardening parameters K_α vary with the plastic loading. To model this, we assume that there exist some internal variables that characterize the condition, i.e. the state of the elasto-plastic material. As internal variables we may, for instance, use the plastic strains $\boldsymbol{\varepsilon_p}$ or some combinations of this tensor.

The important point is that the internal variables are used to memorize the plastic loading history. As the internal variables characterize the state of the material, they are often termed state variables.

Starting with the simplest case of ideal plasticity, as illustrated in Fig. 8.2b), the yield surface is unaffected by the plastic deformations, i.e. it remains fixed in the stress space.

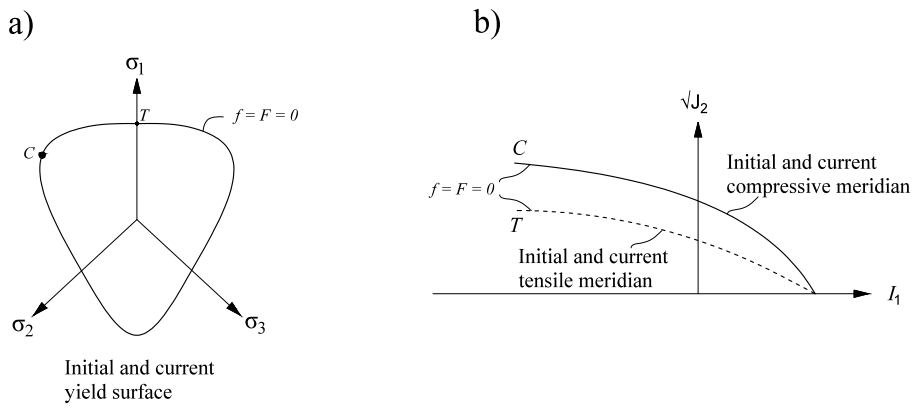

Figure 8.5: ideal plasticity where the yield surface remains fixed; a) deviatoric plane; b) meridian plane

This situation is illustrated in Fig. 8.5, where *C* refers to the compression meridian and *T* to the tensile meridian. In that case, no hardening parameters exist, i.e. (8.4) reduces with (8.5) to

$$f(\sigma_{ij}, K_\alpha) = F(\sigma_{ij}) = 0 \qquad \textit{ideal plasticity} \tag{8.6}$$

i.e. the current yield surface coincides with the initial yield surface. We conclude that

For ideal plasticity, the yield surface remains fixed in the stress space

8.1.1 Isotropic Hardening

Let us next assume that the shape and position of the yield surface remain fixed whereas the size of the yield surface changes. This situation is called isotropic hardening and is usually attributed to Hill (1950). As an example, we may consider the von Mises criterion where the initial yield surface is given by

$$F(\sigma_{ij}) = \sqrt{3J_2} - \sigma_{y0} = 0 \tag{8.7}$$

we may accomplish isotropic hardening by writing

$$f(\sigma_{ij}) = \sqrt{3J_2} - \sigma_{y0} - K = 0 \tag{8.8}$$

Instead of the formulation (8.8), we may write

$$f(\sigma_{ij}, K_\alpha) = F(\sigma_{ij}) - K = 0 \tag{8.9}$$

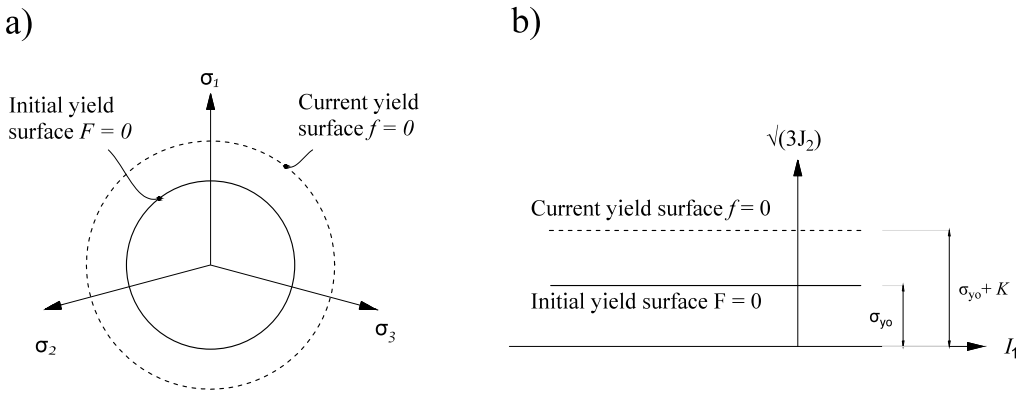

Figure 8.6: isotropic hardening of the von Mises criterion; a) deviatoric plane; b) meridian plane

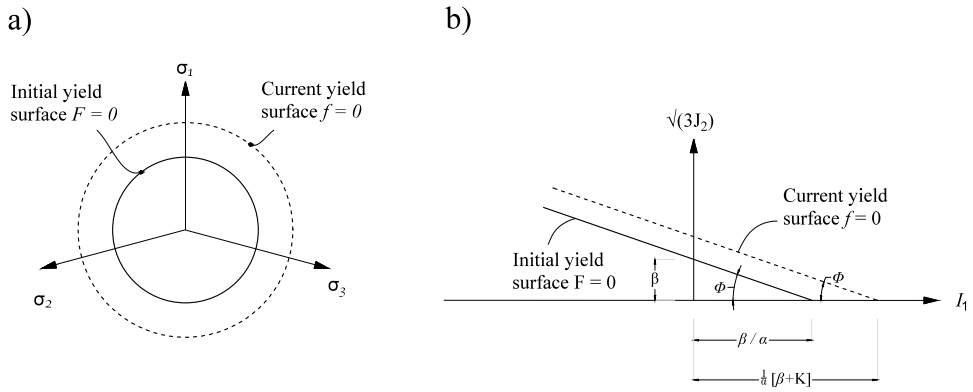

Figure 8.7: isotropic hardening of the Drucker Prager criterion; a) deviatoric plane; b)meridian plane

Isotropic hardening of the von Mises criterion is shown in Fig. 8.6. In this figure, the yield surface expands with increasing plastic deformation and this increase of the current yield stress evidently corresponds to the case of hardening plasticity illustrated in Figs. 8.1 and 8.3a). Mathematically, this is obtained by letting the function K in (8.9) increase with increasing plastic deformation. It is of interest that if, at some stage, we let the function K decrease with increasing plastic

deformation then the von Mises surface shanks in size and this decrease of the current yield stress corresponds to softening plasticity as illustrated in Fig. 8.4.
As the next example of isotropic hardening, consider the Drucker-Prager criterion. Referring to (7.23), the initial yield surface is here given by

$$F(\sigma_{ij}) = \sqrt{3J_2} + \alpha I_1 - \beta = 0$$

where α and β are parameters and α is dimensionless. We observe that if $\alpha=0$ then the Drucker-Prager criterion reduces to the von Mises criterion of (8.7).
The interpretation of the parameters α and β is illustrated in Fig. 8.7b). To obtain an isotropic hardening concept for the Drucker-Prager criterion, we recall that isotropic hardening is characterized by the shape and position of the yield surface being fixed while the size of the yield surface changes. Referring to the interpretation of the parameters α and β in Fig. 8.7b) we therefore obtain isotropic hardening by the formulation

$$f(\sigma_{ij}, K_\alpha) = \sqrt{3J_2} + \alpha I_1 - \beta - K = 0 \qquad (8.10)$$

This isotropic hardening formulation is illustrated in Fig. 8.7 and we observe that it is possible to write (8.10) as

$$f(\sigma_{ij}, K_\alpha) = F(\sigma_{ij}) - K = 0$$

i.e. a format identical to that achieved for isotropic von Mises hardening, cf. (8.9).
With this discussion, we may generally formulate isotropic hardening for an arbitrary yield function as

$$f(\sigma_{ij}, K_\alpha) = F(\sigma_{ij}) - K = 0; \qquad \textit{isotropic hardening} \qquad (8.11)$$

which may be expressed as

> *For isotropic hardening, the position and shape of the yield surface remain fixed, whereas the size of the yield surface changes with plastic deformation*

Returning to isotropic hardening of the von Mises criterion, it is obvious that we may write (8.8) as

$$\sqrt{3J_2} - \sigma_y(\kappa) = 0; \qquad \sigma_y(\kappa) = \sigma_{y0} + K \qquad (8.12)$$

where σ_y is the current yield stress. For uniaxial loading, (8.12) reduces to $|\sigma| = \sigma_y$. As illustrated in Fig. 8.9a), this implies that if we reverse the loading from point *A* where $\sigma = \sigma_y$, the isotropic hardening model will predict elastic unloading until we reach point *B* where $|\sigma| = -\sigma_y$. As a result, even after plastic strains have developed, the isotropic hardening model of von Mises predicts the same yield stress in tension and in compression.

This prediction does not agree well with experimental results for metals and steel. Referring to Fig. 8.9b), experimental results show that point *B*, where plastic effects are again encountered, occurs much earlier than that predicted by the isotropic hardening model. This phenomenon was first observed by Bauschinger (1886) and is therefore called the Bauschinger effect.

8.1.2 Bauschinger Effect

The isotropic hardening model is simple to use, but it applies mainly to monotonic loading without stress reversals. Because the loading surface expands uniformly (or isotropically) and remains self similar with increasing plastic deformation (Fig. 8.8), it cannot account on the Bauschinger effect exhibited by most structural materials.

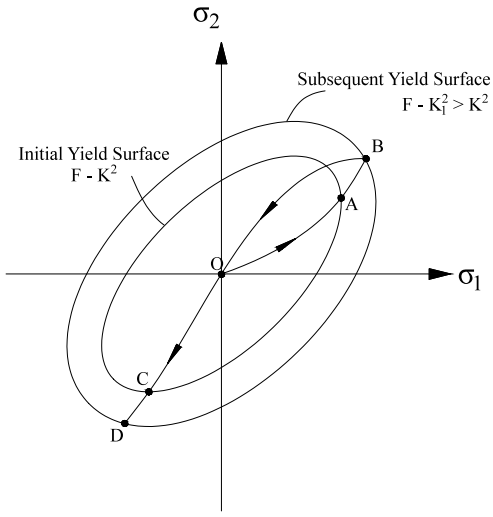

Figure 8.8: subsequent yield surface for isotropic hardening material

The term Bauschinger effect refers to a particular type of directional anisotropy induced by a plastic deformation; namely, an initial plastic deformation of one sign reduces the resistance of the material with respect to a subsequent plastic deformation of the opposite sign. The behavior predicted by the isotropic hardening rule is, in fact, contrary to this observation. The rule implies that because of work hardening, the material will exhibit an increase in the compressive yield stress equal to the increase in the tension yield stress. This is illustrated in fig.8.8, where the yield limit in the first loading direction *(OAB)* and in the reversed loading direction *(OCD)* are equal in magnitude. Since plastic deformation is an anisotropic process, it cannot be expected that the theory of isotropic hardening will lead to a realistic result when complex loading path with stress reversal are considered.

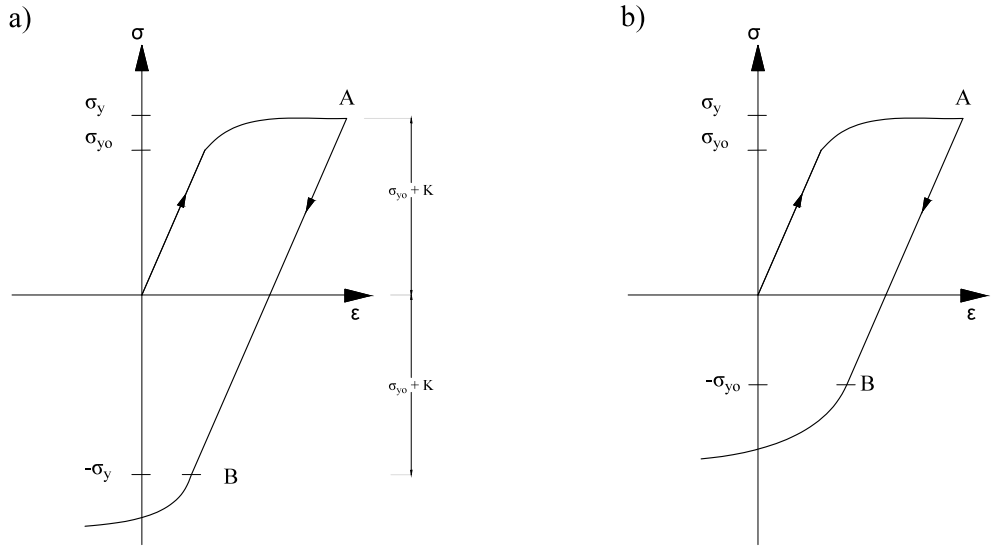

Figure 8.9: a) isotropic hardening; b) Bauschinger effect

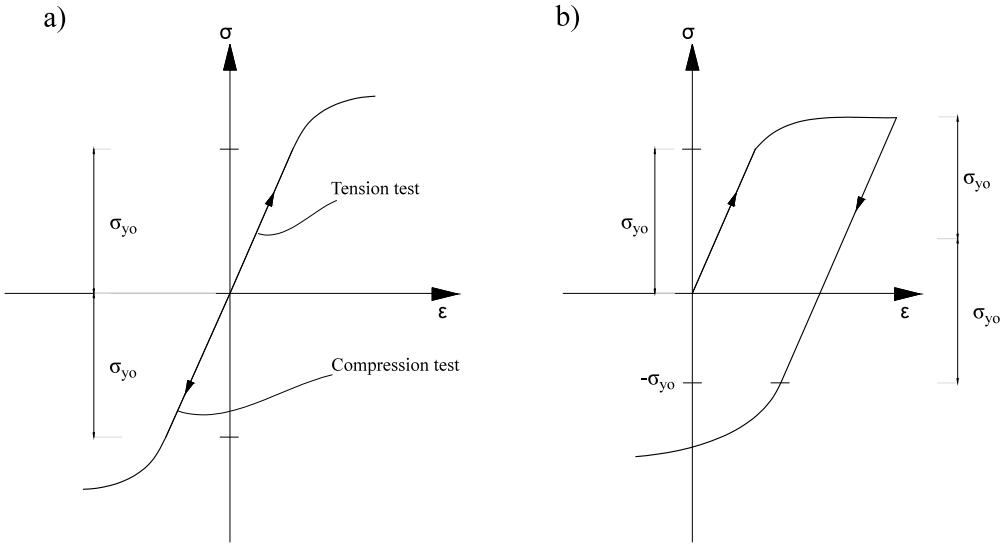

Figure 8.10: metals and steel; a) tension and compression test; b) kinematic hardening model for uniaxial loading

8.1.3 Kinematic hardening

The kinematic hardening rule assumes that during plastic deformation, the loading surface translates as a rigid body in stress space, maintaining the size, shape and orientation of the initial yield surface. This hardening rule, due to

Prager, provides a simple means of accounting for the Bauschinger effect. This rule is illustrated in fig. 8.11. As the stress point moves along its loading path from point *A* to point *B*, the yield surface translates as a rigid body. Thus the subsequent yield surface will wind up in the position indicated in fig. 8.11 when the stress point has reached position *B*. The new position of the yield surface represent the most current yield function, whose center is denoted by α_{ij}. Note that if the stress is unloaded from point *B* along the initial path of loading, i.e., if *B* now traces out path *BAO*, the material behaves elastically from point *B* to point *V* but then begins to flow again before the stresses are completely relieved. In fact the subsequent yield surface may or may not enclose the origin in stress space. As a consequence of assuming a rigid body translation of the loading surface, the kinematic hardening rule predicts an ideal Bauschinger effect for a complete reversal of loading conditions. For kinematic hardening, the equation of the loading surface has the general form

$$f(\sigma_{ij}) = F(\sigma_{ij} - \alpha_{ij}) - K^2 = 0 \qquad (8.13)$$

where K is a constant and α_{ij} are the coordinates of the center of the loading surface (vector OO_1), which changes with the plastic deformation.
Equation (8.13) may be expressed as

For kinematic hardening the size and the shape of the yield surface remain fixed whereas the position of yield surface changes with plastic deformation

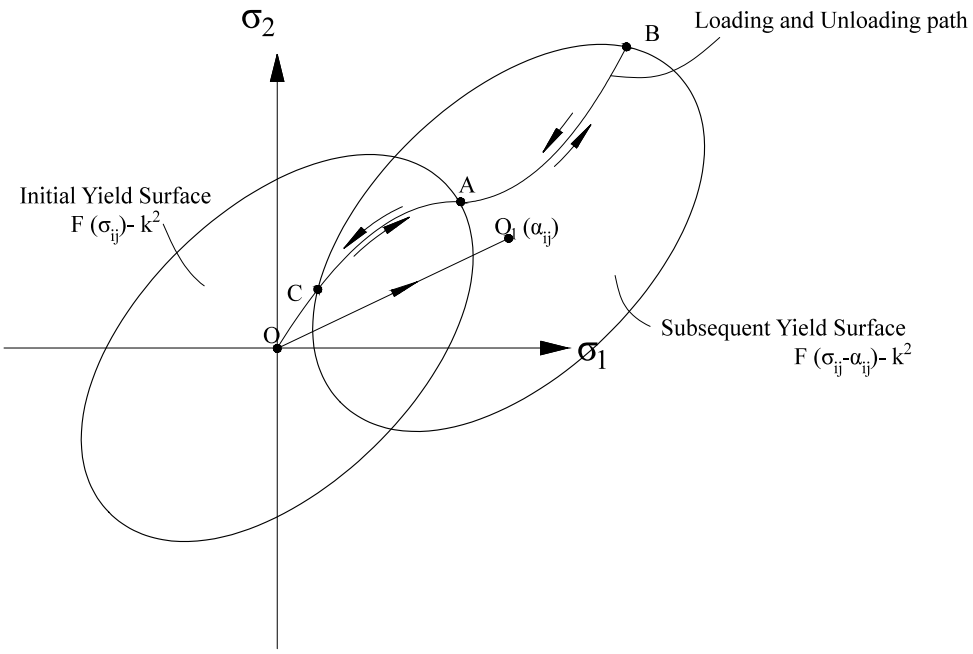

Figure 8.11: subsequent yield surface for kinematic hardening material

8.2 Plastic strains-Remarks

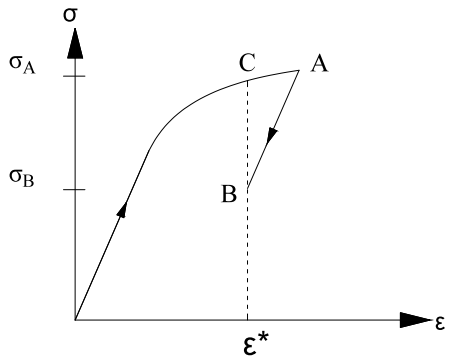

Figure 8.12: for a given strain ε, the corresponding stress is unknown unless we know the load history*

Consider the uniaxial loading in Fig. 8.12 where we unload to point *B* where the strain is ε^*. It is obvious that if only the strain value ε^* is known, we do not know whether the corresponding stress is σ_B or σ_C. We conclude that in plasticity, no

unique relation exists between the stress state σ_{ij} and the strain state ε_{ij}. Therefore, the constitutive relation for elasto-plasticity must be of an incremental nature. This means that for a given strain state the corresponding stress state is obtained by an integration of the incremental constitutive relations and the result of this integration will depend on the integration path, i.e. the load history. This load history dependence is illustrated in Fig. 8.12.

The total strain $\boldsymbol{\varepsilon}$ is assumed to consist of the elastic and plastic strains, i.e.

$$\boldsymbol{\varepsilon} = \boldsymbol{\varepsilon}_e + \boldsymbol{\varepsilon}_p \qquad or \qquad \varepsilon_{ij} = \varepsilon_{ij}^e + \varepsilon_{ij}^p \tag{8.14}$$

The elastic strains are determined by Hooke's law i.e.

$$\sigma_{ij} = D_{ijkl}\varepsilon_{kl}^e \qquad or \qquad \varepsilon_{ij}^e = C_{ijkl}\sigma_{kl} \tag{8.15}$$

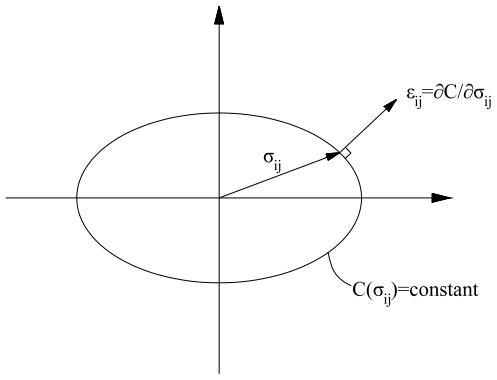

Figure 8.13: linear elasticity. Normality of strain tensor ε_{ij} to the surface in the stress space described by $C(\sigma_{ij})$=constant

In solid mechanics, as well as in other branches of mechanics, many problems may be formulated by means of a potential function. This means that one quantity is obtained by differentiation of a scalar function, the potential function.

In the previous chapters, we also encountered such a potential function, namely the complementary energy $C(\sigma_{ij})$ from which we obtain the strains by a differentiation, i.e.

$$\varepsilon_{ij} = \frac{\partial C}{\partial \sigma_{ij}} \tag{8.16}$$

and this relation is characteristic for hyper-elasticity. For linear elasticity, the complementary energy C is given by

$$C = \frac{1}{2}\sigma_{ij}\varepsilon_{ij} = \frac{1}{2}\sigma_{ij}C_{ijkl}\sigma_{kl} > 0 \tag{8.17}$$

which proves that the flexibility tensor C_{ijkl} is positive definite. From (8.16) and (8.17) we conclude that

$$\sigma_{ij}\varepsilon_{ij} = \sigma_{ij}\frac{\partial C}{\partial \sigma_{ij}} > 0 \tag{8.18}$$

If we consider the expression $C(\sigma_{ij}) = constant$, then this expression describes a surface in the stress space as illustrated in Fig. 8.13. According to (8.16), the strain tensor is orthogonal to this surface and following (8.18) the scalar product $\sigma_{ij}\varepsilon_{ij}$ is positive, i.e. ε_{ij} is directed outwards, as shown in Fig. 8.13.

We have observed that the strain tensor ε_{ij} is normal to the surface $C(\sigma_{ij})=constant$. Let us next prove that C is convex. For a one-dimensional function $g(x)$, convexity requires that $d^2g/dx^2>0$, cf. Fig. 8.14.

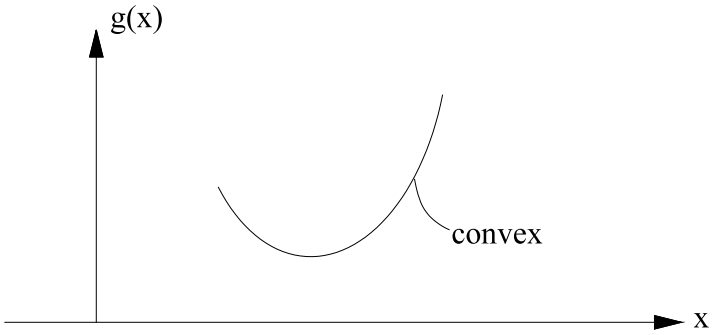

Figure 8.14: convex function in one dimension

For the multidimensional function $C(\sigma_{ij})$, the requirement of convexity is that the quantity $\partial^2 C / \partial\sigma_{ij}\,\partial\sigma_{kl}$ is positive definite. From Hooke's law $\varepsilon_{ij}=C_{ijkl}\sigma_{kl}$ and (8.16) we obtain

$$\frac{\partial \varepsilon_{ij}}{\partial \sigma_{kl}} = C_{ijkl} = \frac{\partial^2 C}{\partial \sigma_{kl}\partial \sigma_{ij}}$$

Since C_{ijkl} is positive definite so is $\partial^2 C / \partial\sigma_{ij}\,\partial\sigma_{kl}$, i.e. C is convex.

8.2.1 Drucker's postulate

We have already said what hardening and softening plasticity mean, and for uniaxial loading these phenomena are illustrated in Figs. 8.3 and 8.4. To obtain definitions applicable to general stress states, we will adopt the Drucker's postulate (1951, 1964) and it will turn out that this postulate leads to the associated flow rule as well as to the convexity of the yield surface and the normality of the plastic flow.

Because of the irreversible character of plastic deformation, work expended on plastic deformation cannot be reclaimed. This means that the work of the stresses on the change of plastic strain is positive whenever a change of plastic strain occurs. In this section we shall investigate what restrictions this irreversibility condition imposes on the plastic stress-strain relationship. Consider a unit

volume of material in which there is a homogeneous state of stress σ^*_{ij} on or inside the yield surface (Fig.8.15a). Suppose an external agency adds stresses along a path *ABC* lying inside the surface until σ_{ij} on the yield surface is just reached. Only elastic work has taken place so far. Now suppose that the external agency keeps the stress state σ_{ij} on the yield surface for a short time. Plastic flow must occur, and only plastic work takes place during the flow. The external agency then releases σ_{ij} and returns the state of stress to σ^*_{ij} along an elastic path *DE*. As all purely elastic changes are completely reversible and independent of the path from σ^*_{ij} to σ_{ij} and back to σ^*_{ij}, all the elastic energy is recovered. The plastic work done by the external agency on this loading and unloading cycle is the scalar product of the stress vector σ_{ij}-σ^*_{ij} and the plastic strain increment vector $d\varepsilon^p_{ij}$. The requirement that this work is positive for plastic deformation leads to

$$(\sigma_{ij} - \sigma_{ij}^*)d\varepsilon_{ij}^p \geq 0 \qquad (8.19)$$

The geometric interpretation of the above expression is given below. If plastic strain coordinates are superimposed upon stress coordinates, as in fig 8.15, the positive scalar product requires an acute angle between the stress vector σ_{ij}-σ^*_{ij} and the strain vector $d\varepsilon^p_{ij}$. Since all possible stress vectors, σ_{ij}-σ^*_{ij}, must satisfy eq (8.19), this leads inevitably to the following consequences:

- Convexity: the yield surface must be convex. If not convex as shown in fig. 4.6b, the possible directions of $d\sigma_{ij}$ cover more than 180°for some planes through $d\varepsilon^p_{ij}$. Thus the angle between σ_{ij}-σ^*_{ij} and $d\varepsilon^p_{ij}$ may be greater than 90°. However eq.(8.19) requires the angle between them less than 90°. Hence the surface must be convex.
- Normality: the plastic strain increment vector $d\varepsilon^p_{ij}$ must be normal to the yield surface at a smooth point and lie between adjacent normal at a corner. As shown in fig. 8.15c, if the surface is convex and smooth at

point *A*, $d\varepsilon^p_{ij}$ must be normal to the surface so that it makes a right angle or less with all possible σ_{ij}-σ^*_{ij}, and condition (8.19) is satisfied. If the surface has a corner at point *B*, there is some freedom in the direction of $d\varepsilon^p_{ij}$ but the vector must lie between the normal at an adjacent point to the corner so that eq (8.19) is satisfied.

The irreversible character of plastic deformation requires the increment of plastic work to be positive

$$dW_p = \sigma_{ij} d\varepsilon^p_{ij} = d\lambda \sigma_{ij} \frac{\partial f}{\partial \sigma_{ij}} \geq 0 \qquad (8.20)$$

Since the scalar product of the radius vector σ_{ij} on the yield surface and the exterior normal of the yield surface $\partial f / \partial \sigma_{ij}$ is non-negative, they must make an acute angle for a convex surface. The multiplier $d\lambda$ in is seen to be related to the magnitude of the increment of plastic work dW_p, and this factor $d\lambda$ must always be positive when plastic flow occurs in order to assure the irreversible nature of plastic deformation. Note that the yield function is *f=F-K=0;* thus, $\partial f / \partial \sigma_{ij} = \partial F / \partial \sigma_{ij}$, and eq (8.20) can be reduced to

$$dW_p = d\lambda \sigma_{ij} \frac{\partial F}{\partial \sigma_{ij}} = d\lambda n F$$

when *F* is a homogeneous function of degree n in the stresses, as it is for most theories of plasticity.

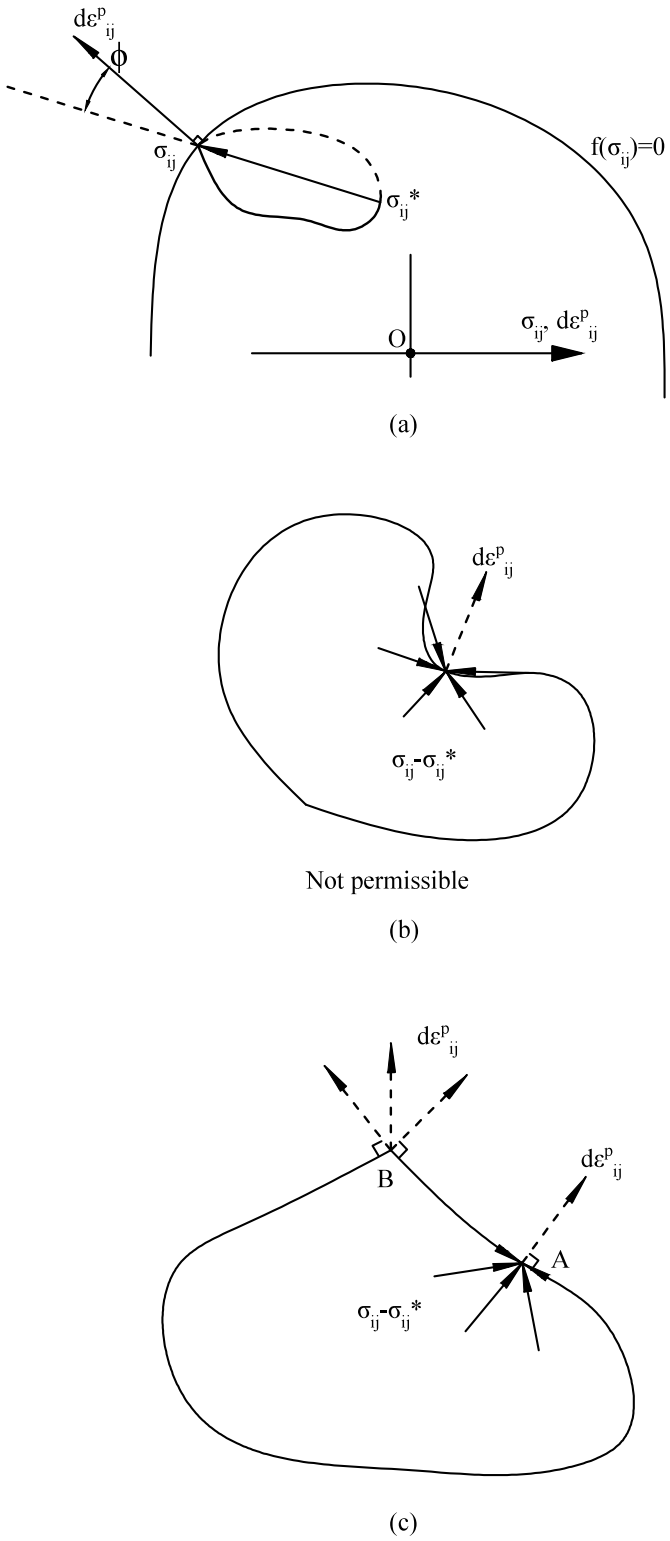

Figure 8.15: convexity of the yield surface and normality of the plastic flow

8.3 Elastic Limit and Yield Function

Generalization of the elastic limit has been discussed in the previous chapter, where the elastic limit of a material under all possible combinations of stress was defined as a yield function in terms of stress σ_{ij} in the form

$$f(\sigma_{ij}) = F(\sigma_{ij}) - k = 0 \qquad (8.21)$$

The significance of this yield function can best be interpreted geometrically as a surface in stress space. For a perfectly plastic material, the yield function is assumed to remain unchanged: the parameter k in eq. (8.21) is constant and the yield surface is therefore fixed in stress space.

8.4 Flow rule

The flow rule or plastic flow, gives the ratio or the relative magnitudes of the components of the plastic strain increment tensor $\dot{\boldsymbol{\varepsilon}}_{\boldsymbol{p}}$. Since the increment $\dot{\boldsymbol{\varepsilon}}_{\boldsymbol{p}}$ may be represented geometrically by a vector with nine components in strain space, the flow rule therefore also defines the direction of the plastic strain increment vector $\dot{\boldsymbol{\varepsilon}}_{\boldsymbol{p}}$ in the strain space. We have seen in the previous chapters that the elastic strain can be derived directly by differentiating the elastic potential function or complementary energy density function with respect to stresses σ_{ij}. In 1928 von Mises proposed the similar concept of the plastic potential function, which is a scalar function of the stresses, $g(\sigma_{ij})$. Then the plastic flow equations can be written in the form

$$\dot{\varepsilon}_{ij}^{p} = \dot{\lambda}\frac{\partial g}{\partial \sigma_{ij}} \qquad (8.22)$$

where $\dot{\lambda}$ is the plastic multiplier, is a positive scalar factor of proportionality, which is nonzero only if plastic deformations occur. The equation $g(\sigma_{ij})=constant$ defines a surface of plastic potential. The direction cosines of the normal vector to this surface at a point σ_{ij} on the surface are proportional to the gradient $\partial g/\partial\,\sigma_{ij}$. The relation above implies that the plastic flow vector $\dot{\boldsymbol{\varepsilon}}_{\boldsymbol{p}}$, if plotted as a free vector in stress space, is directed along the normal to the surface of plastic potential.

Of great importance is the simplest case when the yield function and the plastic potential function coincide, $f=g$. Thus

$$\dot{\varepsilon}_{ij}^{p} = \dot{\lambda}\frac{\partial f}{\partial \sigma_{ij}} \qquad (8.23)$$

and plastic flow develops along the normal to the yield surface with direction $\partial f/\partial\,\sigma_{ij}$ and is directed outwards. We have then established the important property of $\dot{\boldsymbol{\varepsilon}}_{\boldsymbol{p}}$ being normal to the yield surface Fig 8.13. From now on we will recall the direction $\partial f/\partial\,\sigma_{ij}$ with $\boldsymbol{n}$. The above equation is called the associated flow rule because the plastic flow is connected or associated with the yield criterion, while relation (8.23) with $f\neq g$ is called a nonassociated flow rule. Von Mises used the associated flow rule for the development of his plastic stress-strain relations for metals.

8.5 Prager consistency condition

Suppose that we have determined the potential function *g*, which for associated plasticity is taken as the yield function. Then use of the flow rule only determines the direction of the incremental plastic strains. However, the magnitude of $\dot{\boldsymbol{\varepsilon}}_{\boldsymbol{p}}$ is still unknown since the plastic multiplier it is as yet unknown. The next task is therefore to determine this quantity.

It is a fundamental property of plasticity theory that during plastic development, the current stress state is always located on the current yield surface. The current yield surface changes in general during plastic loading but, by definition, the current stress state is always located on the current yield surface during this evolution.

Having chosen the hardening rule, i.e. the hardening parameters, the current yield function is given in its general form by

$$f(\sigma_{ij}, K_{\alpha}) = 0 \tag{8.24}$$

where K_α are the hardening parameters. Since *f=0* during plastic loading, we can express the so-called consistency relation by

$$\dot{f} = 0 \tag{8.25}$$

which leads to

$$\frac{\partial f}{\partial \sigma_{ij}} \dot{\sigma}_{ij} + \frac{\partial f}{\partial K_{\alpha}} \dot{K}_{\alpha} = 0 \tag{8.26}$$

The consistency relation was introduced by Prager (1949) and (8.26) tells us that during plastic loading where the stress state varies, also the hardening parameters K_α vary in such a manner that the stress state always remains on the yield surface. The consistency condition is the key how to establish the magnitude of the plastic multiplier. In fact

$$\dot{\sigma} = \mathbf{E}\dot{\varepsilon}_e \tag{8.27}$$

Since elastic strains can be written as the difference between the total strain and the plastic strain and plastic strains due to the flow rule can be written as

$$\dot{\varepsilon}_{ij}^p = \dot{\lambda}\frac{\partial f}{\partial \sigma_{ij}} \tag{8.28}$$

we obtain the relation which expresses the magnitude of the plastic multiplier

$$\dot{\lambda} = \frac{1}{h_p}\mathbf{n}\mathbf{E}\dot{\varepsilon} \qquad with \qquad h_p = H_p + \mathbf{n}\mathbf{E}\mathbf{m} \qquad where \qquad H_p = \frac{\partial f}{\partial K_\alpha}\frac{\partial K_\alpha}{\partial \lambda} \tag{8.29}$$

If $H_p=0$ we have the elastic perfectly plastic behavior of the material;
If $H_p>0$ we are in the hardening part of the behavior of the material;
If $H_p<0$ we are in the softening part of the behavior of the material.

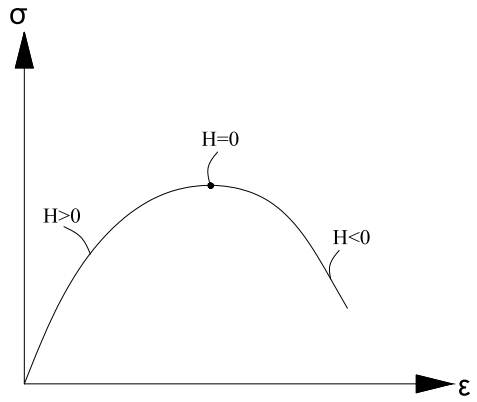

Figure 8.16: interpretation of the plastic modulus H

We have a restriction in the softening behavior, in fact H_p has a limit condition in order to avoid having a *0* value in the denominator of the expression of $\dot{\lambda}$

$$H_p < \mathbf{-nEm} \tag{8.30}$$

8.6 Elastoplastic stiffness relation

Substituting the plastic multiplier into the elastoplastic stress-strain relation yields

$$\dot{\boldsymbol{\sigma}} = \mathbf{E}(\dot{\boldsymbol{\varepsilon}} - \dot{\lambda}\mathbf{m}) = \mathbf{E}\left(\dot{\boldsymbol{\varepsilon}} - \mathbf{m}\frac{\mathbf{nE}\dot{\boldsymbol{\varepsilon}}}{H_p + \mathbf{nEm}}\right) \tag{8.31}$$

Rearranging results in the elasto-plastic tangent operator $\boldsymbol{E_{ep}}$ which relates the stresses and strains rates

$$\dot{\boldsymbol{\sigma}} = \mathbf{E}_{\mathbf{ep}}\dot{\boldsymbol{\varepsilon}} \tag{8.32}$$

where the elastoplastic material operator is

$$\mathbf{E}_{\mathbf{ep}} = \mathbf{E} - \frac{1}{h_p}\mathbf{E}\!:\!\mathbf{m} \otimes \mathbf{n}\!:\!\mathbf{E} = \mathbf{E} - \frac{1}{h_p}\left(\mathbf{E}\!:\!\mathbf{m}\right) \otimes \left(\mathbf{n}\!:\!\mathbf{E}\right) \tag{8.33}$$

8.7 Loading surface and loading criterion

Loading surface is the yielding surface for an elastoplastically deformed material, which defines the boundary of the current elastic region. If a stress point lies within this region, no additional plastic deformation takes place. If the state of stress is on the boundary of the elastic region and tends to move out of the current loading surface, additional plastic deformations will occur with a changed current loading surface, when plastic deformation takes place. Thus, the loading surface may be generally expressed as a function of the current state of stress (or strain) such that

$$f(\sigma_{ij}, \varepsilon_{ij}^{p}, K) = 0 \tag{8.34}$$

in which K is the hardening parameter. The response of the material after initial yielding differs in the various plasticity theories. This post yield response, called the hardening rule, is described by specifying the rule for evolution of the subsequent yield surfaces or loading surfaces. Several hardening rules have been proposed in the past in plastic analysis. Since the configuration change of the

loading surface is related to the plastic loading, it's necessary to discuss the loading criterion for a work hardening material. For uniaxial behavior, the concepts of loading and unloading are evident. However, this is not the case under a mutiaxial stress state, and load/unload must be clearly specified. The loading surface itself is an essential part of defining loading and unloading. Loading or plastic flow occurs only when the stress point is on the loading surface and the additional loading or stress incremental vector $d\sigma_{ij}$ is directed outward from the current elastic region. To express the above statement more precisely, we introduce a unit vector $\boldsymbol{n}$ normal to the loading surface in stress space (fig. 8.17) whose components are given by

$$n_{ij} = \frac{\partial f / \partial \sigma_{ij}}{\left(\dfrac{\partial f}{\partial \sigma_{kl}} \dfrac{\partial f}{\partial \sigma_{kl}} \right)^{1/2}}$$

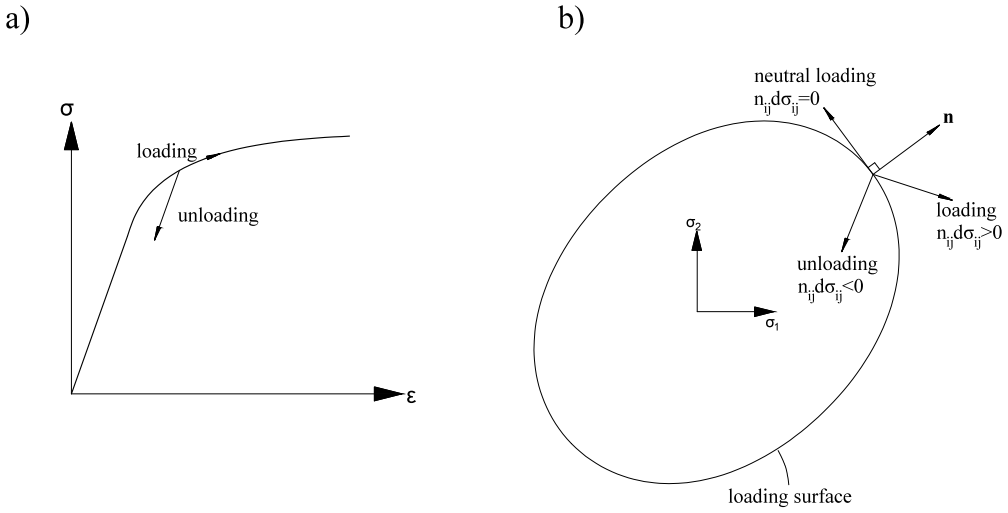

Figure 8.17: loading criterion for a work hardening material; a) uniaxial case; b) multiaxial case

If the angle between the vector $d\sigma_{ij}$ and n_{ij} is acute, additional plastic deformation will occur. Thus, the criterion for loading is

$$if\ f = 0\ and\ n_{ij} d\sigma_{ij} > 0,\ then\ \dot{\varepsilon}_{ij} \neq 0 \tag{8.35}$$

On the other hand, if the two vectors $d\sigma_{ij}$ and n_{ij} form an obtuse angle, unloading will occur. Thus, the criterion for unloading is

$$if\ f = 0\ and\ n_{ij} d\sigma_{ij} < 0,\ then\ \dot{\varepsilon}_{ij} = 0 \tag{8.36}$$

In the neutral loading case, the additional load vector $d\sigma_{ij}$ is perpendicular to the normal vector n_{ij}, and no additional plastic deformation will occur. The criterion for neutral loading is

$$if\ f = 0\ and\ n_{ij} d\sigma_{ij} = 0,\ then\ \dot{\varepsilon}_{ij} = 0 \tag{8.37}$$

Recall the loading criterion for an elastic-perfectly plastic material: in this case, the initial yield surface becomes the limit surface with plastic deformation taking place only when $f=0$ and $d\sigma_{ij}$ is tangent to the yield surface. Thus, for a perfectly plastic material, there is no neutral loading case such as by eq. (8.37).

8.8 Flow rule associated with von Mises Yield function

We shall now take the von Mises yield function

$$f(\sigma_{ij}) = J_2 - k^2 = 0 \tag{8.38}$$

Then the flow rule has the simple form:

$$\dot{\varepsilon}_{ij}^{p} = \dot{\lambda}\frac{\partial f}{\partial \sigma_{ij}} = \dot{\lambda} s_{ij} \qquad (8.39)$$

where s_{ij} is the deviatoric stress tensor and $\dot{\lambda}$ is a factor of proportionality with the value

$$\dot{\lambda} = \begin{cases} = 0 & \text{whenever } J_2 < k^2 \text{ or } J_2 = k^2, \text{ but } dJ_2 < 0 \\ > 0 & \text{whenever } J_2 = k^2 \text{ and } dJ_2 = 0 \end{cases} \qquad (8.40)$$

Equation (8.39) can also be expressed in terms of the components of the strain increment and stresses as

$$\frac{\dot{\varepsilon}_x^p}{s_x} = \frac{\dot{\varepsilon}_y^p}{s_y} = \frac{\dot{\varepsilon}_z^p}{s_z} = \frac{\dot{\gamma}_{yz}^p}{2\tau_{yz}} = \frac{\dot{\gamma}_{zx}^p}{2\tau_{zx}} = \frac{\dot{\gamma}_{xy}^p}{2\tau_{xy}} = \dot{\lambda} \qquad (8.41)$$

The above relation is known as the Prandtl-Reuss equations. The relationship between the plastic strain increment $\dot{\varepsilon}^p{}_{ij}$ and the von Mises yield function $f=J_2$ or the flow rule associated with the von Mises yield condition can be shown graphically in the three dimensional principle stress space. It is best shown by a cross section on the hydrostatic plane and by a cross section on the deviatoric plane of the three-dimensional surface as in fig. 8.18. The normal to the yield surface as viewed along the hydrostatic axis is a radial line that is parallel to the π plane.

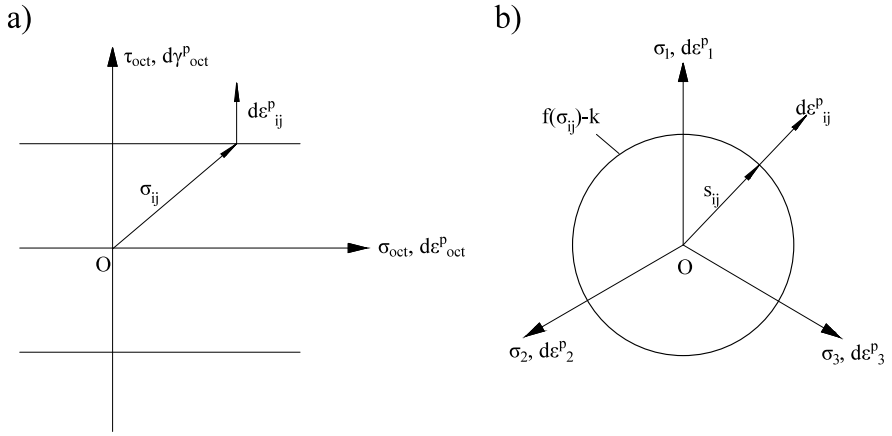

Figure 8.18: flow rule associated with von Mises yield function

Its direction is therefore parallel to the direction of the projection of the appropriate stress vector σ_{ij} onto the π plane, which is precisely its deviatoric stress component vector s_{ij}. Equation (8.39) or (8.41) states that a small increment of plastic strain $\dot{\varepsilon}^p{}_{ij}$ depends only on the current state of deviatoric stress s_{ij}, not on the stress increment $d\sigma_{ij}$, which is required to maintain plastic flow. Also the principal axes of stress σ_{ij} or s_{ij} and the plastic strain increment $\dot{\varepsilon}^p{}_{ij}$ coincide. Note that these equations are only statements about the ratio or the relative magnitudes of the components of the plastic strain increment tensor; they give no direct information about its absolute magnitude. According to eq. (8.39), there is no plastic volumetric deformation; that is,

$$\dot{\varepsilon}^p_{ij} = \dot{\lambda} s_{ij} = 0 \qquad (8.42)$$

This can be seen in fig. 8.18a where the plastic strain increment vector $\dot{\varepsilon}^p{}_{ij}$ is normal to the hydrostatic axis, and the hydrostatic strain component, $\dot{\varepsilon}^p{}_{oct}$ is therefore zero. The total strain increment $\dot{\varepsilon}_{ij}$ is the sum of the elastic and the plastic strain increments. If Hook's law is applied for the elastic component $\dot{\varepsilon}^e{}_{ij}$ and the flow rule for the plastic component $\dot{\varepsilon}^p{}_{ij}$ we have

$$\dot{\varepsilon}_{ij} = \frac{1+\nu}{E}\dot{\sigma}_{ij} - \frac{\nu}{E}\dot{\sigma}_{kk}\delta_{ij} + \dot{\lambda}s_{ij} = \frac{\dot{\sigma}_{kk}}{9K}\delta_{ij} + \frac{\dot{s}_{ij}}{2G} + \dot{\lambda}s_{ij} \qquad (8.43)$$

Equation (8.43) may also be separated into expressions for the volumetric and deviatoric or shear strain increments of the forms

$$\begin{aligned} \dot{\varepsilon}_{ij} &= \frac{1}{3K}\dot{\sigma}_{kk} \\ \dot{e}_{ij} &= \frac{1}{2G}\dot{s}_{ij} + \dot{\lambda}s_{ij} \end{aligned} \qquad (8.44)$$

In practical applications, we expand eq. (8.43) explicitly in terms of stress and strain components, giving rise to three equations for the normal strains of the form

$$\dot{\varepsilon}_x = \frac{1}{E}\left[\dot{\sigma}_x - \nu\left(\dot{\sigma}_y + \dot{\sigma}_z\right)\right] + \frac{2}{3}\dot{\lambda}\left[\sigma_x - \frac{1}{2}\left(\sigma_y + \sigma_z\right)\right], \ \ etc. \qquad (8.45)$$

and three equations for the shear strains of the form

$$\dot{\gamma}_{yz} = \frac{1}{G}\dot{\tau}_{yz} + 2\dot{\lambda}\tau_{yz}, \ \ etc. \qquad (8.46)$$

8.9 Flow rule associated with Tresca Yield function

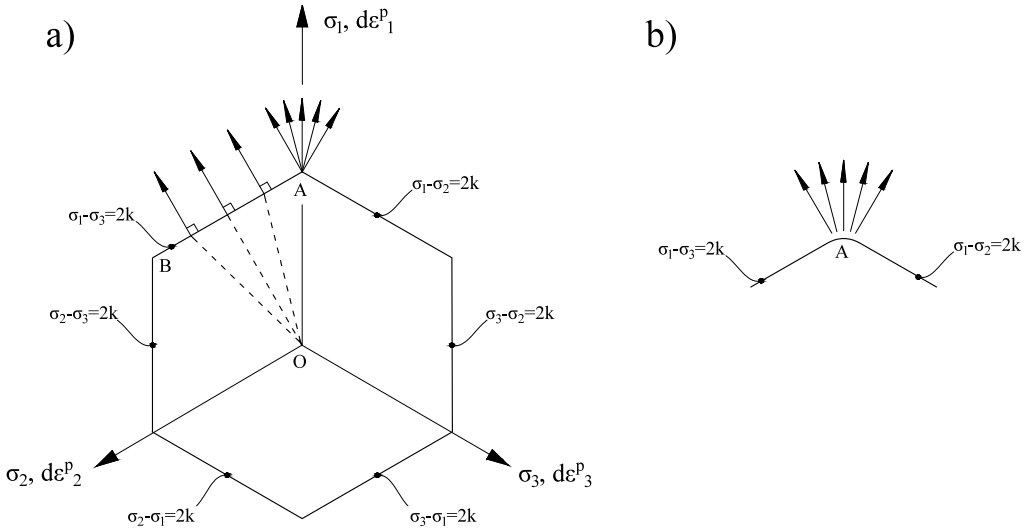

Figure 8.19: flow rule associated with Tresca yield function; a) normality of the plastic strain increment vector; b) vertex A as a limit of smooth surface

We take the Tresca yield function as the plastic potential, which in principal stress space is a hexagonal prism consisting of six planes. The deviatoric section of the prism is shown in fig. 8.19a). Suppose that the principal stresses are $\sigma_1 > \sigma_2 > \sigma_3$; the corresponding yield function is then

$$f = F(\sigma_{ij}) - 2K = \sigma_1 - \sigma_3 - 2K = 0 \tag{8.47}$$

According to the associated flow rule, the principal plastic strain increments satisfy the following relations

$$\begin{aligned} \dot{\varepsilon}_1^p &= \dot{\lambda}\frac{\partial f}{\partial \sigma_1} = \dot{\lambda} \\ \dot{\varepsilon}_2^p &= \dot{\lambda}\frac{\partial f}{\partial \sigma_2} = 0 \\ \dot{\varepsilon}_3^p &= \dot{\lambda}\frac{\partial f}{\partial \sigma_3} = -\dot{\lambda} \end{aligned} \tag{8.48}$$

Similar results can be derived for the other five possible combinations of algebraic orders of magnitude of principal stress / principal strain increment space as shown in fig.8.19a). Anywhere on the plane *AB* where $\sigma_1 > \sigma_2 > \sigma_3$ the directions of the plastic strain increments are parallel to each other and perpendicular to the plane *AB* of the Tresca hexagon. Similar relationships can be developed for other planes of the hexagon. If for example $\sigma_1 > \sigma_2 = \sigma_3$, the situation is more involved, because the maximum shear stress is equal to the yield value *K* not only on the 45° shear planes parallel to the x_2 axis but also on the 45° planes parallel to the x_3 axis. We have therefore the freedom to assume that the shear slip may occur along either of the two possible maximum shear planes

- $$\sigma_{\max} = \sigma_1, \quad \sigma_{\min} = \sigma_3$$
  $$\left(\dot{\varepsilon}_1^p, \dot{\varepsilon}_2^p, \dot{\varepsilon}_3^p\right) = \dot{\lambda}(1,0,-1) \qquad for\ \dot{\lambda} \geq 0$$

- $$\sigma_{\max} = \sigma_1, \quad \sigma_{\min} = \sigma_2$$
  $$\left(\dot{\varepsilon}_1^p, \dot{\varepsilon}_2^p, \dot{\varepsilon}_3^p\right) = \dot{\mu}(1,-1,0) \qquad for\ \dot{\mu} \geq 0$$

In this case we shall assume that the resulting plastic strain increment vector is a linear combination of the two increments given above, i.e.

$$\left(\dot{\varepsilon}_1^p, \dot{\varepsilon}_2^p, \dot{\varepsilon}_3^p\right) = \dot{\lambda}(1,0,-1) + \dot{\mu}(1,-1,0) \qquad for\ \dot{\lambda} \geq 0,\ \dot{\mu} \geq 0 \qquad (8.49)$$

this situation corresponds to the special case where the current state of stress state σ_{ij} lies on a vertex of the hexagon. As a result, the plastic strain increment vector must lie between the directions of the normal to the two adjacent sides of the hexagon (fig.8.19a). This vertex or singular point at a potential surface can

also be viewed as a limiting case of a smooth surface, and the flow rule can still be applied for a smooth surface at this corner point (fig. 8.19b).

In general, at a singular point where several smooth yield surfaces intersect, the strain increments can generally be expressed as a linear combination of those increments given by the normal of the respective surfaces intersecting at the point. As a result, at the vertex, the direction of the strain increment vector cannot be determined uniquely. Further, if the yield surface contains a flat part (fig.8.19a), there also exist no unique relationship between the stress and the strain increment. In general, the correspondence between the plastic strain increment vector $\dot{\varepsilon}^p{}_{ij}$ and the stress vector σ_{ij} is not always one to one. However, it will be shown in the following example that the incremental plastic work dW_p done or the rate of dissipation of energy is always uniquely determined by the magnitude of the plastic strain rate given by

$$dW_p = \sigma_1 \dot{\varepsilon}_1^p + \sigma_2 \dot{\varepsilon}_2^p + \sigma_3 \dot{\varepsilon}_3^p = 2K \max\left|\dot{\varepsilon}^p\right| \qquad (8.50)$$

where $\max|\dot{\varepsilon}^p|$ denotes the absolute value of the numerically largest principal component of the plastic strain increment vector.

8.10 Flow rule associated with Mohr-Coulomb Yield Function

The Mohr-Coulomb yield surface is an irregular hexagonal pyramid. Its deviatoric sections are irregular hexagons as shown in Fig. 8.20. The yield function takes the following form

$$\sigma_1 \frac{1+\sin\phi}{2c\cos\phi} - \sigma_3 \frac{1-\sin\phi}{2c\cos\phi} = 1 \qquad (8.51)$$

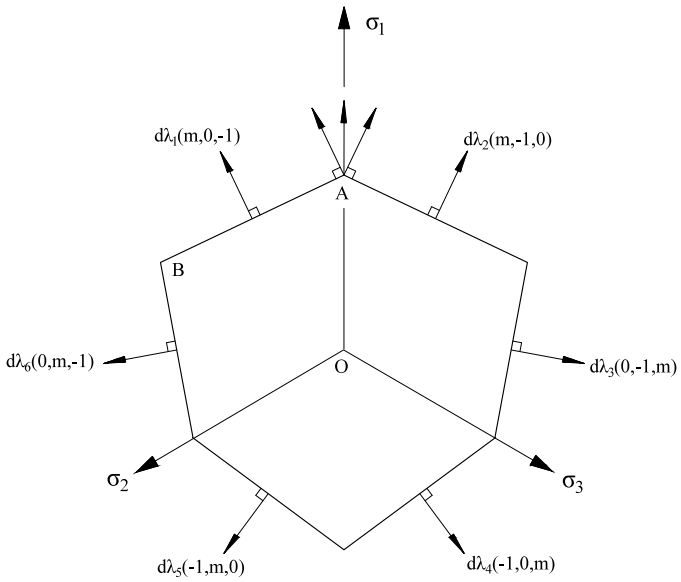

Figure 8.20: flow rule associated with Mohr-Coulomb yield surface

where φ is the angle of internal friction and c is the cohesion. The above equation can also be written in a more compact form

$$m\sigma_1 - \sigma_3 = f'_c \qquad for\ \sigma_1 \geq \sigma_2 \geq \sigma_3 \tag{8.52}$$

where f'_c is the uniaxial compressive strength and m is the strength ratio between f'_c and f'_t, the uniaxial tensile strength. To obtain the expression for the plastic strain increment, the following three cases must be considered separately.

Case1. The yield stress point lies on the surface plane of the pyramid, for example on face AB (see fig. 8.20) where $\sigma_1 > \sigma_2 > \sigma_3$ and eq. (8.52) holds. According to the associated flow rule, we have the following plastic strain increments

$$\varepsilon_1^p = m\dot{\lambda}, \qquad \varepsilon_2^p = 0, \qquad \varepsilon_2^p = -\dot{\lambda} \qquad for\ \dot{\lambda} \geq 0 \tag{8.53}$$

or, in compact form

$$\left(\dot{\varepsilon}_1^p, \dot{\varepsilon}_2^p, \dot{\varepsilon}_3^p\right) = \dot{\lambda}(m, 0, -1) \qquad for\ \dot{\lambda} \geq 0 \tag{8.54}$$

Similar results can be obtained for the other five possible algebraic orderings of the principal stresses σ_1, σ_2 and σ_3. These results are summarized and shown graphically in fig. 8.20.

Notice that the plastic volumetric strain increment is

$$\dot{\varepsilon}_v^p = \dot{\varepsilon}_1^p + \dot{\varepsilon}_2^p + \dot{\varepsilon}_3^p = \dot{\lambda}(m-1) \tag{8.55}$$

since $m = f'_c / f'_t \geq 1$, it follows that the Mohr-Coulomb material model with the associated flow rule aleays predicts volume dilatation except in the special case $m=1$, which reduces to the case of Tresca material model. From eq. (8.55) we can separate the sum of the principal plastic strain increments into two parts: the compressive part

$$\sum \left|\dot{\varepsilon}_c^p\right| = \dot{\lambda} \tag{8.56}$$

and the tensile part

$$\sum \left|\dot{\varepsilon}_t^p\right| = m\dot{\lambda} \tag{8.57}$$

Such a separation can be done as well for the other five plans of the pyramid. Then we have

$$\frac{\sum \dot{\varepsilon}_t^p}{\sum \left|\dot{\varepsilon}_c^p\right|} = m \tag{8.58}$$

and

$$\dot{\varepsilon}_v^p = \sum \dot{\varepsilon}_t^p - \sum \left|\dot{\varepsilon}_c^p\right| \tag{8.59}$$

Now consider further the plastic work increment dW_p. By definition, we have

$$dW_p = \sigma_1 \dot{\varepsilon}_1^p + \sigma_2 \dot{\varepsilon}_2^p + \sigma_3 \dot{\varepsilon}_3^p = \left(\sigma_1 m - \sigma_3\right)\dot{\lambda} \tag{8.60}$$

Using eq. (8.52) and (8.56) eq. (8.60) becomes

$$\begin{aligned} & dW_p = f'_c \sum \left|\dot{\varepsilon}_c^p\right| \\ & or \\ & dW_p = \frac{f'_c}{m} \sum \dot{\varepsilon}_t^p \end{aligned} \tag{8.61}$$

Case2. The yield stress point lies on the edges of the pyramid, for example, along the edge *A* (fig.8.20), where $\sigma_1 > \sigma_2 = \sigma_3$ and the two surfaces

$$m\sigma_1 - \sigma_3 = f'_c$$

and

$$m\sigma_1 - \sigma_2 = f'_c$$

intersect. In this case, the following equation can be applied

$$\dot{\varepsilon}_{ij}^{p} = \sum_{k=1}^{n} \dot{\lambda}_k \frac{\partial f_k}{\partial \sigma_{ij}} \tag{8.62}$$

Thus, the corresponding plastic strain increments are expressed as

$$\left(\dot{\varepsilon}_1^p, \dot{\varepsilon}_2^p, \dot{\varepsilon}_3^p\right) = \dot{\lambda}_1 (m, 0, -1) + \dot{\lambda}_2 (m, -1, 0) = \left[\left(\dot{\lambda}_1 + \dot{\lambda}_2\right) m, -\dot{\lambda}_2, -\dot{\lambda}_1\right] \tag{8.63}$$

This strain vector lies between the directions of the normal to the two adjacent surfaces. Similar relations can be obtained for the other five edges.
The plastic volume change is obtained from eq. (8.63) as

$$\dot{\varepsilon}_v^p = m\left(\dot{\lambda}_1 + \dot{\lambda}_2\right) - \left(\dot{\lambda}_1 + \dot{\lambda}_2\right)$$

which is the sum of two parts: the compressive part

$$\sum \left|\dot{\varepsilon}_c^p\right| = \dot{\lambda}_1 + \dot{\lambda}_2$$

and the tensile part

$$\sum \left|\dot{\varepsilon}_t^p\right| = m(\dot{\lambda}_1 + \dot{\lambda}_2)$$

and we can see that

$$\dot{\varepsilon}_v^p = \sum \dot{\varepsilon}_t^p - \sum \left|\dot{\varepsilon}_c^p\right| \tag{8.64}$$

It can be seen that $\dot{\epsilon}_v^p > 0$ for $m>1$, and that eq. (8.58) and (8.59) are still valid. By a similar deviation to that of eq. (8.60), we can obtain the plastic work increment expression dW_p in the following form

$$dW_p = (\sigma_1 m - \sigma_3)\dot{\lambda}_1 + (\sigma_1 m - \sigma_2)\dot{\lambda}_2 = f'_c\left(\dot{\lambda}_1 + \dot{\lambda}_2\right) = f'_c \sum \left|\dot{\varepsilon}_c^p\right| \qquad (8.65)$$

Case 3. The yield stress point coincides with the apex of the pyramid, where six surfaces intersect. Following the same procedure, a similar expression to eq. (8.63) for the plastic strain $\dot{\epsilon}^p{}_t$, can be obtained. We can also show that equations (8.59) and (8.61) are still valid.

9 Specimens Geometry and Experimental Scenarios

In order to propose a new asymmetric yield function for metallic materials on the first invariant of the stress tensor and the second and third invariant of stress deviator some experiments on aluminum specimens were done, which results are reported in this thesis, and also some experiments on steal material will be performed in the next months. The aluminum specimens are tested under different load scenarios, which generate different stress tensor invariants and are transformed into Haigh–Westergaard coordinates and the corresponding Lode angle for each scenario has been obtained.

In the different loading scenarios, the Lode angle parameter is changing from 0 degrees, which corresponds to uniaxial tension condition and goes up to 30 degrees, which is pure shear condition. The results can show how the third invariant of stress deviator affects the behavior of aluminum material.

To look at the compressive behavior, and capture the possible difference between compressive and tensile behavior, further experiments has been done to go beyond 30 degrees up to 60 degrees which represents the uniaxial compression case. Since the difference between compression and tension cannot be captured by only considering second and third invariants, there is a need to introduce stress triaxiality measure or the first invariant of stress tensor to capture the difference in behavior of aluminum under tension and compression.

Digital Image Correlation (DIC) was used as a full-field measurement method for displacement field and calculation of the strain distribution of the Aluminum specimen under abovementioned loading scenarios. Using this method, plastic flow rule can be obtained by integration of the plastic strain rate through the physical domain of the specimen and it can be expressed in terms of first invariant of stress tensor and the second and third invariant of stress deviator. The results can be used to investigate the crack growth based on the local and global strain distribution.

The pressure- sensitivity of Aluminum has been investigated based on the observed localization angle using the captured images by DIC. In case the observed angle of failure for both tension and compression tests is equal to $\pi/2$, one can say that the behavior of Aluminum follows the Tresca yield criterion and it should be considered to behave like a pressure-insensitive material. In case the angle of friction Φ for Aluminum is not equal to zero, according to the Mohr–Coulomb yield criterion, the observed failure angle will be $\pi/2+\Phi/2$, which shows that Aluminum is behaving like a pressure-sensitive material.

Analytical and numerical localization analysis has been done using an associated flow rule in 3D to calculate the orientation of failure surface considering von Mises, Tresca, developed two invariant formulations and the three invariant formulations. The localization analysis results were compared with experimental results and the difference between them has been discussed in this paper.

9.1 Specimen’s geometry

The experimental program is designed such that it provides insight in the dependence of the yielding and plastic behavior of aluminum on the Lode angle parameter and on the first invariant of the stress tensor over a wide range of stress states. It includes experiments on specimens which are machined from round bars of two inches diameter, such that they have the two ends with a wider

diameter, gradually linked to the central part, which has a smaller diameter of 1 and 1/6 inches. The ends have a wider diameter in order to fasten the specimens in the grips of the axial torsion machine. The central part has a smaller diameter in order to localize the yielding, plastification and eventually failure of the aluminum in a confined zone. The geometry of the specimens was designed depending on the capabilities of the Axial-Torsion Machine, which was used to perform the tests. The maximum torque the Axial-Torsion Machine is capable to apply to the specimen is T = 11.3 kNm (=100 kip-in), the maximum axial force in tension and compression is F =1201.02 kN (=270 kips) and the maximum angle of twist is α=120°. The nominal geometry of the specimens is shown in the figure below.

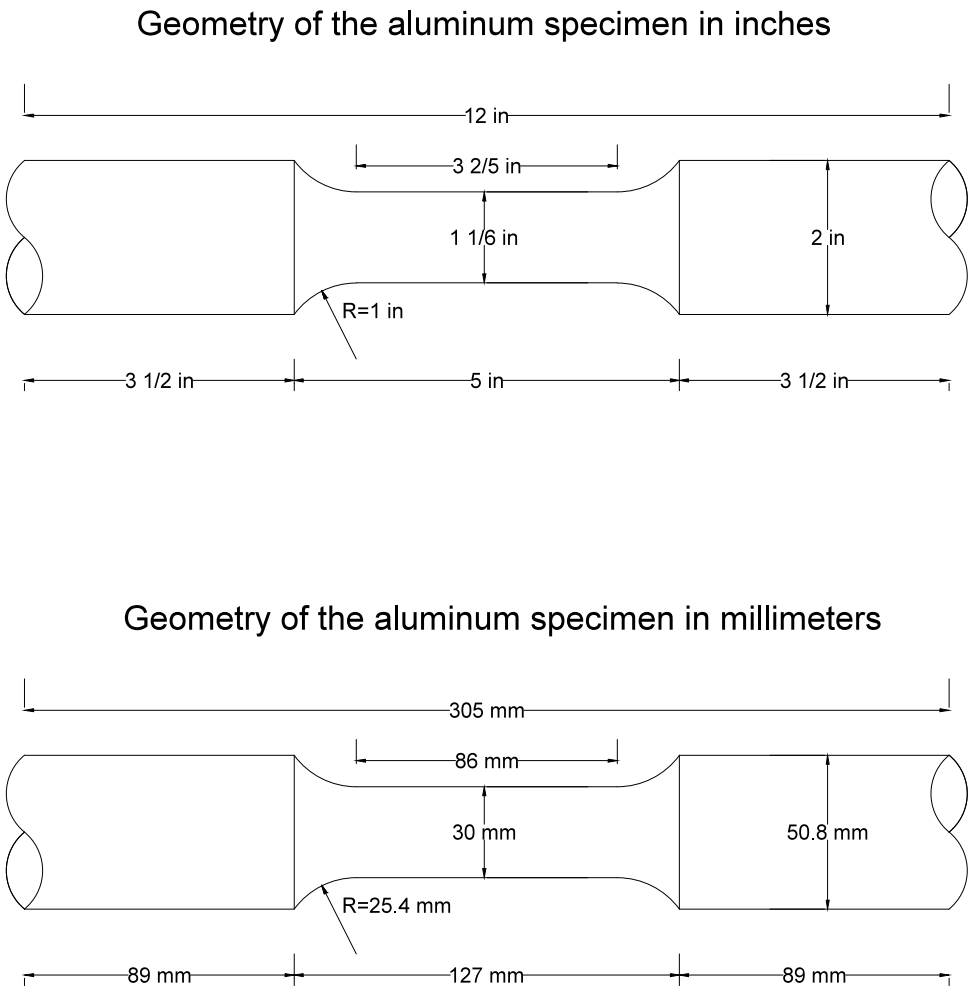

Figure 9.1:nominal geometry of the aluminum specimen

The calculations that were made to make sure the specimens with the proposed geometry could have reached at least yielding with the capabilities of the Axial-Torsion Machine are straightforward and are reported in the table below.

Diameter D	30	[mm]
Length B	127	[mm]
E	68900	[Mpa]
G	26000	[Mpa]
J	39760.8	[mm^4]
σy	260	[Mpa]
σp	310	[Mpa]
τy	150.11	[Mpa]

Fy	**Fp**	**Ty**	**Tp**	**Ncr**	**ϕy**	
[kN]	[kN]	[kNm]	[kNm]	[kN]	[rad]	[°]
183.783	219.126	0.796	1.061	1676.357	0.048882	2.80
<F=1201 kN OK	<F=1201 kN OK	<T=11.3 kNm OK	<T=11.3 kNm OK	>Fy=183.783kN OK	<α=2.09rad OK	<α=120° OK

The actual geometry of the specimens, which were machined with the lathe, is a little different from the nominal geometry due to the shaping of the specimens. The diameter of the central part of the specimens was measured in five different sections in order to capture the possible imperfections due to the degree of precision of the lathe machine.

The actual dimensions of each specimen are reported below.

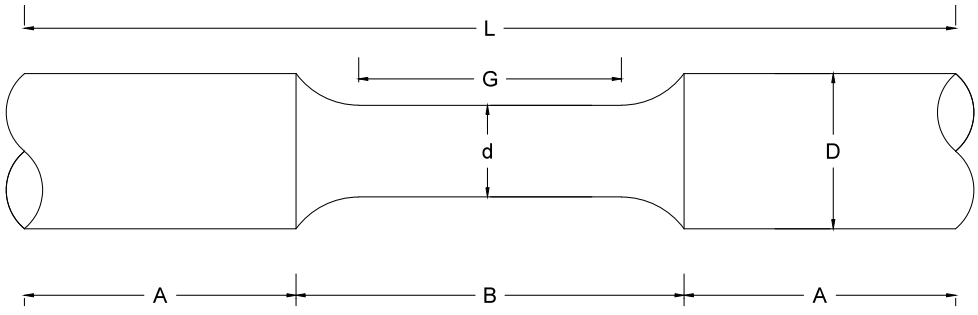

Specimen 1A- Tension Test Lode angle θ=0°	L = 310 mm G = 81.1 mm D = 25.4 mm B = 110 mm A = 100 mm

	d_1 = 29.87 mm d_2 = 29.89 mm d_3 = 29.92 mm d_4 =29.89 mm d_5 = 29.85 mm

Specimen 6A- Tension-Torsion Test Lode angle θ=10°	L = 305 mm G = 81 mm D = 25.4 mm B = 110 mm A = 97.5 mm d_1 = 29.95 mm d_2 = 29.92 mm d_3 = 29.92 mm d_4 =29.92 mm d_5 = 29.92 mm

Specimen 7A- Tension-Torsion Test Lode angle θ=20°	L = 310 mm G = 88.1 mm D = 25.4 mm B = 120 mm A = 95 mm d_1 = 29.69 mm d_2 = 29.67 mm d_3 = 29.64 mm

	d_4 =29.67 mm d_5 = 29.67 mm
Specimen 4A- Torsion Test Lode angle θ=30°	L = 305 mm G = 94 mm D = 25.4 mm B = 125 mm A = 90 mm d_1 = 29.92 mm d_2 = 29.95 mm d_3 = 29.92 mm d_4 =29.95 mm d_5 = 29.92 mm
Specimen 10A- Compression-Torsion Test Lode angle θ=40°	L = 308 mm G = 91 mm D = 25.4 mm B = 125 mm A = 91.5 mm

	d_1 = 29.72 mm d_2 = 29.69 mm d_3 = 29.69 mm d_4 =29.67 mm d_5 = 29.72 mm

Specimen 9A- Tension-Torsion Test Lode angle θ=50°	L = 308 mm G = 88.3 mm D = 25.4 mm B = 125 mm A = 91.5 mm d_1 = 29.87 mm d_2 = 29.85 mm d_3 = 29.82 mm d_4 =29.87 mm d_5 = 29.92 mm

Specimen 8A- Tension-Torsion Test Lode angle θ=50°	L = 307 mm G = 89.6mm D = 25.4 mm B = 124 mm A = 91.5 mm d_1 = 29.77 mm d_2 = 29.77 mm

	d_3 = 29.77 mm d_4 =29.77 mm d_5 = 29.79 mm

9.2 Material

The aluminum used in the specimens is the alloy 6061-T6 Aluminum. The specimens are obtained from turning cold rolled round bars. The mechanical properties and the alloy composition are reported in the tables below.

Alloy composition	Aluminum (Al)	95.9 to 98.6 %
	Magnesium (Mg)	0.8 to 1.2 %
	Silicon (Si)	0.4 to 0.8 %
	Iron (Fe)	0 to 0.7 %
	Copper (Cu)	0.15 to 0.4 %
	Chromium (Cr)	0.04 to 0.35 %
	Zinc (Zn)	0 to 0.25%
	Manganese (Mn)	0 to 0.15 %
	Titanium (Ti)	0 to 0.15 %
	Residuals	0 to 0.15 %

Material properties	Density	2.7 g/cm^3
	Elastic modulus	69 GPa
	Elongation at break	17 %
	Poisson's ratio	0.33
	Shear strength	270 MPa
	Ultimate tensile strength	310 MPa
	Yield tensile strength	260 MPa
	Thermal expansion	23.5 μm/m-K

9.3 Experimental scenarios

To look at the different behavior aluminum exhibits depending on the Lode parameter and on the first invariant of the stress tensor, different testing scenarios were designed in order to vary the Lode angle θ, where θ in the Haigh-Westergaard coordinate system represents the angle in the deviatoric π-plane between the projection of the σ_1 axis and the line, which connects the hydrostatic axis and the stress point (cfr. 4.6).
The different loading scenarios are the following:

θ=0°	Pure Tension Test
θ=10°	Tension-Torsion Test
θ=20°	Tension-Torsion Test
θ=30°	Pure Torsion Test
θ=40°	Compression-Torsion Test
θ=50°	Compression-Torsion Test
θ=60°	Pure Compression Test

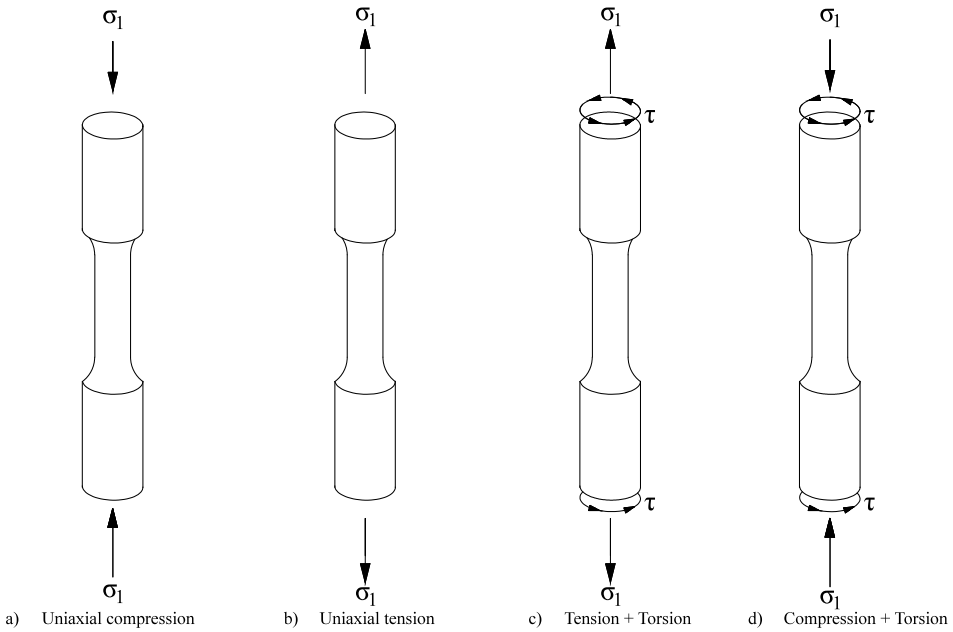

Figure 9.2: a) uniaxial compression, θ=60°; b) uniaxial tension, θ=0°; c) tension-torsion test, θ=10°, θ=20°; d) compression-torsion test, θ=40°, θ=50°.

For each of the seven scenarios, three specimens were tested in order to have a consistent experimental data point for each scenario. With a MatLab code, for each scenario the first invariant of the stress tensor and the second and third invariant of the stress deviator have been calculated in addition to the ratio between the torque and the axial force (tension or compression) as it regards the combined tension-torsion and compression torsion tests.

9.4 Characterization of the stress state for each scenario

For each scenario the stress state was found out with a MatLab code. In order to perform the tension-torsion and the compression-torsion tests, the ratio between the axial force and the torque was also calculated depending on the actual geometry of the specimens for each scenario.

$$\theta = 0^\circ \ (uniaxial\ tension) \ \rightarrow \ \sigma = \begin{bmatrix} 1 & 0 & 0 \\ 0 & 0 & 0 \\ 0 & 0 & 0 \end{bmatrix}$$

$$\theta = 10^\circ \ (tension + torsion) \ \rightarrow \ \sigma = 0.42 \begin{bmatrix} 1.62 & 1 & 0 \\ 1 & 0 & 0 \\ 0 & 0 & 0 \end{bmatrix}$$

$$\theta = 20^\circ \ (tension + torsion) \ \rightarrow \ \sigma = 0.55 \begin{bmatrix} 0.64 & 1 & 0 \\ 1 & 0 & 0 \\ 0 & 0 & 0 \end{bmatrix}$$

$$\theta = 30^\circ \ (puretorsion) \ \rightarrow \ \sigma = \begin{bmatrix} 0 & 1 & 0 \\ 1 & 0 & 0 \\ 0 & 0 & 0 \end{bmatrix}$$

$$\theta = 40^\circ \ (compression + torsion) \ \rightarrow \ \sigma = 0.55 \begin{bmatrix} -0.64 & 1 & 0 \\ 1 & 0 & 0 \\ 0 & 0 & 0 \end{bmatrix}$$

$$\theta = 50^\circ \ (compression + torsion) \ \rightarrow \ \sigma = 0.42 \begin{bmatrix} -1.62 & 1 & 0 \\ 1 & 0 & 0 \\ 0 & 0 & 0 \end{bmatrix}$$

$$\theta = 60^\circ \ (uniaxial\ compression) \ \rightarrow \ \sigma = \begin{bmatrix} -1 & 0 & 0 \\ 0 & 0 & 0 \\ 0 & 0 & 0 \end{bmatrix}$$

Figure 9.3:stress state for each scenario.

$$\theta = 10^\circ \ (tension + torsion) \ \rightarrow \ Specimen \ 6A$$

$$\sigma = 0.42 \begin{bmatrix} 1.62 & 1 & 0 \\ 1 & 0 & 0 \\ 0 & 0 & 0 \end{bmatrix}$$

$$A_{6A} = \frac{\pi \cdot 1.178^2}{4} = 1.089 in^2$$

$$F = \sigma_{11} \cdot A = 1.7656 lb$$

$$T = \frac{\sigma_{12} \cdot \pi \cdot r^3}{2} = 0.3209 lb \cdot in$$

$$\frac{F}{T} = 5.5$$

Figure 9.4: ratio between the torque and the axial force for θ=10°

$$\theta = 20^\circ \ (tension + torsion) \ \rightarrow \ Specimen \ 7A$$

$$\sigma = 0.55 \begin{bmatrix} 0.64 & 1 & 0 \\ 1 & 0 & 0 \\ 0 & 0 & 0 \end{bmatrix}$$

$$A_{7A} = \frac{\pi \cdot 1.177^2}{4} = 1.088 in^2$$

$$F = \sigma_{11} \cdot A = 0.6963 lb$$

$$T = \frac{\sigma_{12} \cdot \pi \cdot r^3}{2} = 0.3201 lb \cdot in$$

$$\frac{F}{T} = 2.175$$

Figure 9.5: ratio between the torque and the axial force for θ=20°

$$\theta = 40° \ (compression + torsion) \ \rightarrow \ Specimen \ \mathbf{10}A$$

$$\sigma = 0.55 \begin{bmatrix} -0.64 & 1 & 0 \\ 1 & 0 & 0 \\ 0 & 0 & 0 \end{bmatrix}$$

$$A_{10A} = \frac{\pi \cdot 1.168^2}{4} = 1.071 in^2$$

$$F = \sigma_{11} \cdot A = -0.6857 lb$$

$$T = \frac{\sigma_{12} \cdot \pi \cdot r^3}{2} = 0.3128 lb \cdot in$$

$$\frac{F}{T} = -2.192$$

Figure 9.6: ratio between the torque and the axial force for θ410°

$$\theta = 50° \ (compression + torsion) \ \rightarrow \ Specimen \ 8A$$

$$\sigma = 0.42 \begin{bmatrix} -1.62 & 1 & 0 \\ 1 & 0 & 0 \\ 0 & 0 & 0 \end{bmatrix}$$

$$A_{8A} = \frac{\pi \cdot 1.172^2}{4} = 1.083 in^2$$

$$F = \sigma_{11} \cdot A = -1.7536 lb$$

$$T = \frac{\sigma_{12} \cdot \pi \cdot r^3}{2} = 0.3177 lb \cdot in$$

$$\frac{F}{T} = -5.5$$

Figure 9.7: ratio between the torque and the axial force for θ=50°

10 Experimental Setting

In order to investigate the influence of the Lode angle parameter, of the second invariant of the stress deviator and of the first invariant of the stress tensor on the behavior of metals, experiments on aluminum specimens were performed using an Axial Torsion Machine, which has the capability to apply torque, axial forces in tension and in compression and combinations of the two abovementioned actions. The Axial Torsion Machine is connected and controlled by a software in which the user can set all the testing features. The same software collects the experimental data as forces and displacements during the whole test. To collect the strain distribution data during the test a Digital Image Correlation System was used.

10.1 Shore Western Axial Torsion Machine

The Axial Torsion Machine used to perform the tests is a load frame structure designed to provide a high rigidity for high force axial-torsion applications. It features a 4-column symmetrical construction with a fixed platen and moveable crosshead on hydraulic lifts. It’s equipped with linear and rotatory actuators, servo valves, service manifold, biaxial load cells, LVDT (linear variable

differential transformer: is a type of electrical transformer used for measuring linear displacement) and RVDT (rotary variable differential transformer); it is supplied with hydraulic crosshead locks, load cells, grips and extensometers. The Axial Torsion Machine utilizes four smooth chrome plated precision ground columns to provide long life and low friction crosshead position changes with high alignment accuracy. The crosshead is vertically adjustable using hydraulic lifts via a simple control panel.

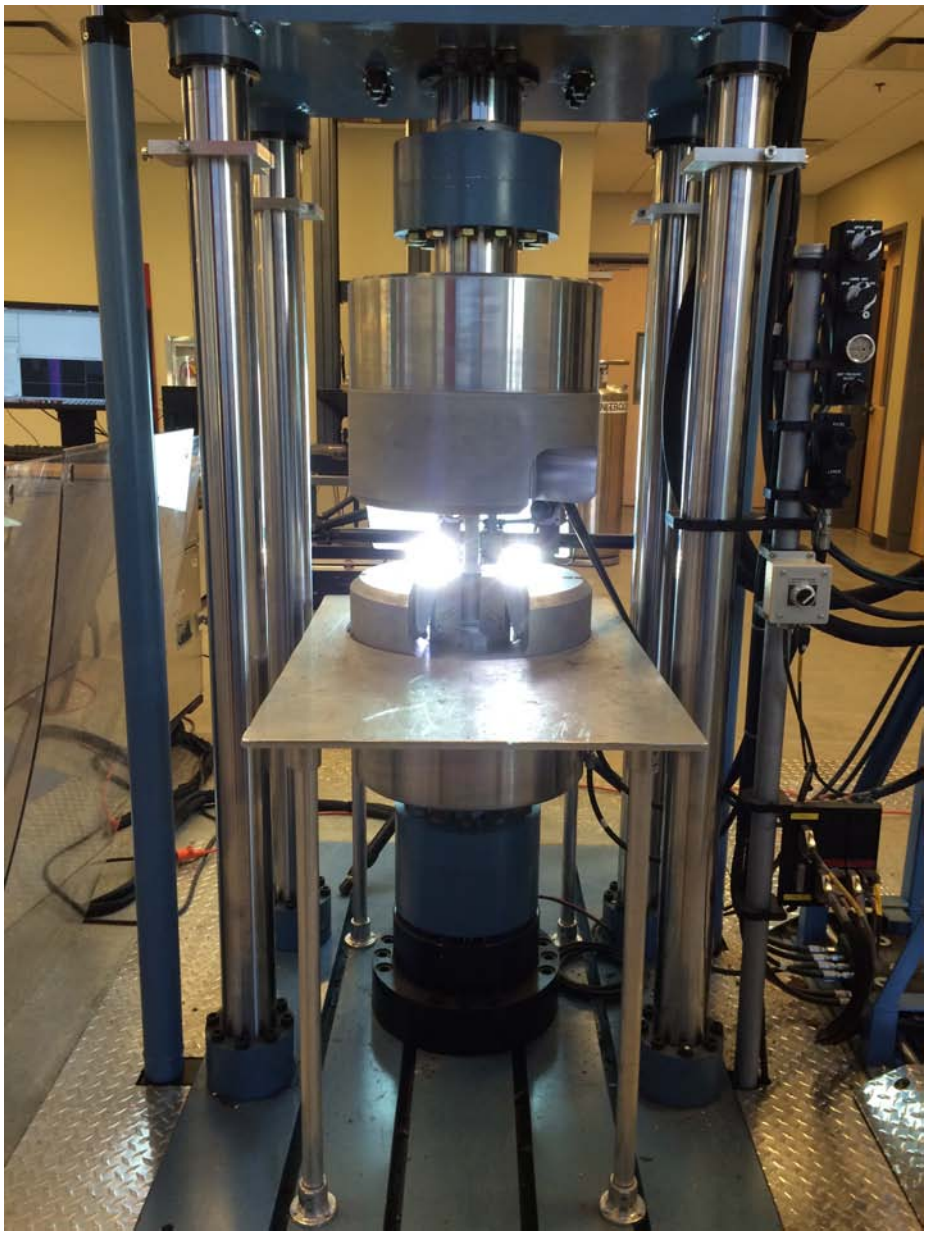

Figure 10.1: Shore Western Axial Torsion Machine

10.2 Shore Western Software

The Shore Western Control System (SWCS) is a program that is graphically built using a series of steps, defined in a flow-based diagram, that can perform simple or very complex multi-threaded tasks. The user interface can be built by Shore Western engineers, or you may choose to build them or modify them yourself. In our case we built it ourselves. Once the user-interface has been built, we simply selected from a menu of pre-defined screens that provided us with all the parameters we need to run our test. A very powerful feature of the SWCS is its Block Programming capability. A feature rich menu of blocks are available to string together to perform highly complex process control tasks. Blocks are added from a pallet into the program, and wired together on the output tab of one, and on the input tab of another. Blocks can easily be rewired or deleted too. With a right click, they can be copied and pasted within the program, or across to another one. The blocks can be moved on a grid, and named to create a visual view of the block program that is very easy to understand at a glance. The block programmer provides automatic branching when the system encounters a Warning, Soft Stop, Hard Stop, Station Stop or E-Stop event, so that users can define actions that are responses to those conditions. The programmer supports multiple threads, with inter-thread communication via virtual switches or flags, so that multiple actions can be performed in parallel. For example, you may want to ramp up in displacement control, while monitoring load. When a certain load is reached, you may want to ramp to a different level. In this case, you can define the ramps in the main program, and create a second thread that monitors loads. When the load is reached, the second thread notifies the main thread via a virtual switch, and the main thread moves on to the next step.

Blocks are available in the following categories:

Algorithm

- Mode Switch. For example, from displacement control to load control.
- Auto balance. This block is typically used in a program that turns on low pressure to the actuator. Before applying pressure, you need to be sure the servo loop output is zero, to close the servo valve and prevent actuator motion.

Data Acquisition

- Start/Stop Data Acquisition and Logging
- Taring. To remove transducer and command offsets. For example, if you load a specimen in displacement control, and the actuator is not at midstroke, you may want to call the new position “zero” so that your test data is easier to read.
- Level Switches. These blocks are used to monitor response channels, and switch when they reach a certain levels. The levels can be absolute, or there is a block that can watch for a level drop, or level increase. This is useful for monotonic tests, where you want to detect specimen failure, or perhaps you need to wait for a pressure to rise before continuing.

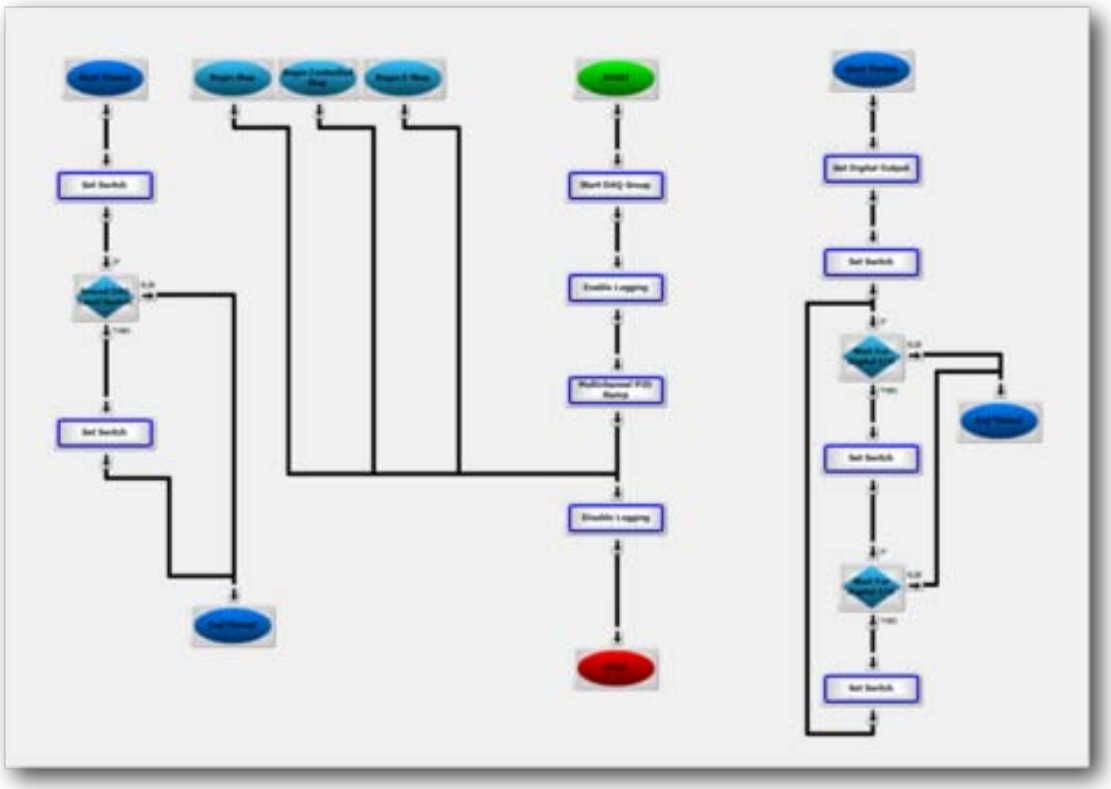

Figure 10.2: Shore Western Block Programming

One of the reasons Block Programming is so powerful is that it can be linked in to a custom user interface. The user environment is set up in hierarchical layers: Controls and Panels.

Custom Controls

Controls are individual groupings of buttons, lights, meters and sliders that can be invoked as floating windows, or embedded into Panels. Controls can be nested within each other, so that a given layout can be used in many places throughout the user environment. For example, you may have a control for turning-on the hydraulics. One button runs a Block Program that checks the status of the system, asks the user a question or two, auto balances the servo loops, and turns the hydraulics to low pressure. Another button may turn from low pressure to high pressure. The panel may also include buttons to reset interlocks, indicate E-

Stop status, and so on. The control can be created, and embedded anywhere in the software. All the elements in a custom control can be copied and pasted within the control, and also across controls. Controls can be saved to disk or imported from another source.

Custom Panels

The user interface is divided into four quadrants. The quadrants can be split and resized, to create custom views. Any one quadrant can fill the window. The quadrants themselves contain panels. These may be predefined, such as the Multi-Axis Function Generator, or the Calibration screen, or they can be custom built. Custom buttons, lights, meters, sliders, and pop-up controls can be embedded into the Panels, as can Controls (above). This means that you can create a panel to perform PID tuning, for example, that takes an instance of the Multi-Axis Function Generator, adds hydraulic controls, and pop-ups for the PID tuning sliders. The panel includes a scope, and the function generator parameters, the settings of which can all be saved in the Application (see below). All the end-user needs to do, is select the tuning window from the Applications list, and everything is at their fingertips.

Panels can be saved to disk or imported from another source. Note that Card Diagrams, the Block Program Editor, and Event Log are not panels that can be customized.

Figure 10.3: Custom Panel

Displays

Three different data displays are available in the software, a time history oscilloscope, a frequency domain analyzer, and an X-Y plotter. The displays feature the following capabilities:

- Multiple Axes for plotting different variables (scope only)
- Auto Scaling
- Manual Scaling
- Zoom Scaling
- Filtering and decimation of displayed signals (scope and X-Y)
- Setting colors and line widths
- Saving, exporting, and importing

Data Acquisition

Two types of data acquisition can be defined for a test: continuous logging, or cycle-based logging. It is possible to trigger continuous data collection manually, by using the start button on the Multi-Axis Function Generator, or via a block in the Block Programmer. You can define cyclic logging where, for example, you can collect 10 cycles of data every 1000 cycles of testing. At the same time, we collect data into a circular buffer, typically 200 cycles long. If something happens in the test, you can step back through the buffer, and examine each cycle in turn, to see where the change occurred.

Figure 10.4: Shore Western Software

10.3 Digital Image Correlation System (DIC)

In addition to the data acquisition from the Axial Torsion Machine trough the Shore Western software, also a Digital Image Correlation System was used in order to capture the displacements and the strains which occurred during the tests. Digital image correlation is an optical method that employs tracking and image registration techniques for accurate 2D and 3D measurements of changes in images. This is often used to measure deformation (engineering), displacement and strain. DIC tracks the position of the same physical points shown in a reference image and a deformed image. To achieve this, a square subset of pixels are identified on the speckle pattern around point of interest on a reference image and their corresponding location determined on the deformed image. The digital images are recorded and processed using an image correlation algorithm.

Many parameters are included while obtaining accurate DIC results. Some of the parameters include speckle size, speckle density, type of algorithm, subset size, subset overlap, gray level interpolation, etc. Highly optimized input parameters provide very accurate results.

Before starting with the measuring procedure with the DIC system it was necessary to prepare the specimens. The specimens were painted with a white varnish and subsequently, black random dots were drawn on the smooth surface of the specimens to generate a speckle pattern, which needed to have a good contrast to allocate the pixels in the images and it had to be non glossy.

Figure 10.5: specimens painted with a white varnish and black random dots

After being painted, the specimen was fixed in the grips of the Axial Torsion Machine. Before starting the testing, two 12 megapixel Gigabit cameras with 50 mm fixed local lenses were placed in front of the sample as shown in the figure below and calibration procedures were done in order to determine the correct working distance of the device and the position and the position of the cameras with respect to each other.

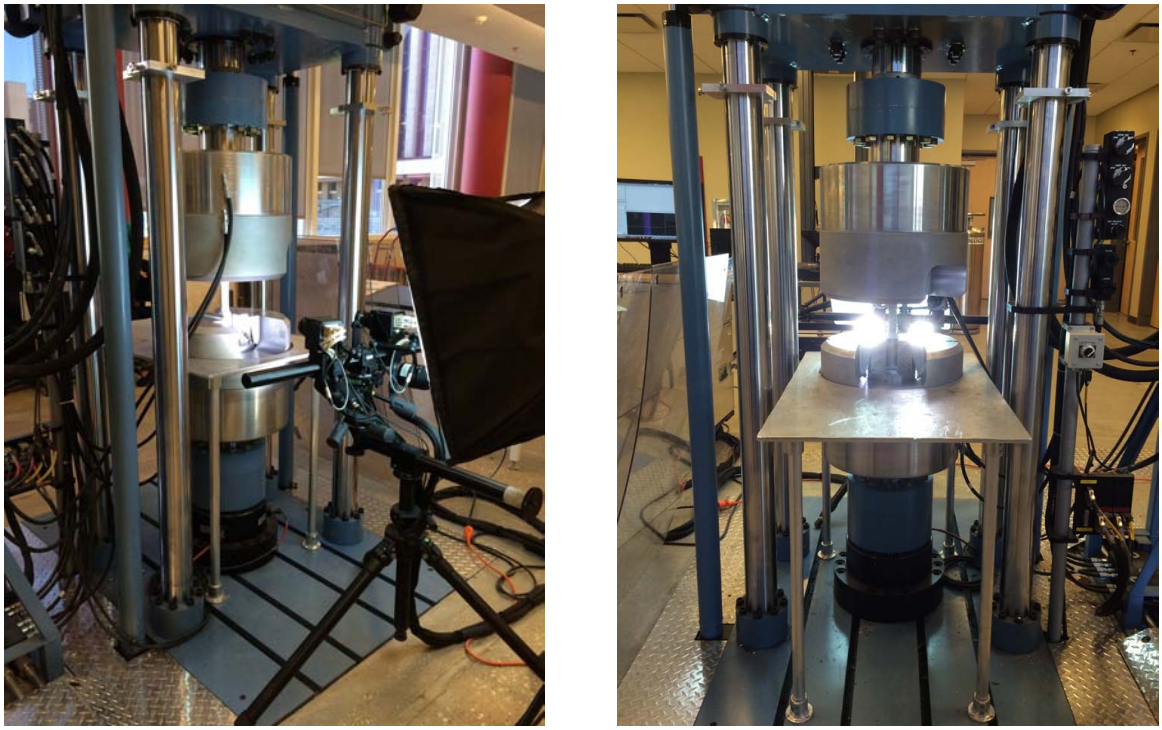

Figure 10.5: test setup and position of the DIC system

In order to eliminate interruptions from surrounding light, a powerful light source was employed to illuminate the sample and a corresponding filter was utilized to let only the reflected light go through the cameras lenses.

Figure 10.6: light source with a filter

Calibrating the DIC system is a key process to ensure that the measured results are accurate. Both cameras can be calibrated at the same time. DIC calibration gives the metric information to relate the ideal model of camera to the actual physical device and to determine the position and orientation of the camera with respect to a world reference system. This metric information includes two kinds of parameters, intrinsic parameters and extrinsic parameters. The intrinsic parameters indicate the internal geometric and optical characteristics of the camera, such as focal length of the lenses, distortions of the lenses, and the positions between the lenses and CCD image device. The extrinsic parameters indicate the external geometric relation between the camera and the specimen, such as rotation matrix and translation vector. With the calibration data, DIC system can translate the image coordinate to geometric coordinate. The calibration plate should be placed in the same plane as that of the CCD chip of the cameras and at a same distance as that of the specimen or in front of the specimen.

The calibration can be initiated when the software shows the color pattern of dots as shown in the live image as shown below, this indicates that the plate is in the same plane or it is parallel to the CCD Chip plane. An image of the calibration plate is also shown below.

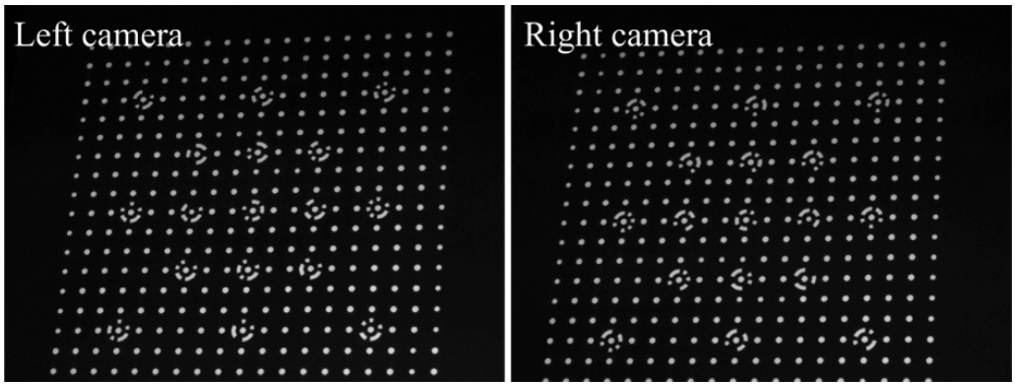

Figure 10.7: Calibration Plate

The two cameras took pictures at presetted time intervals during the test and measure the movement of target points on the surface of the specimen. The first image corresponds to the undeformed or reference state. The cameras were connected to a computer in which the images are recorded and the data are acquired and evaluated using the ARAMIS software from GOM.

The processing of the data is done by using the ARAMIS software in order to obtain displacements and strains. ARAMIS in fact computes the motion of each point comparing the images at different stages. The software indicates on the first image several square boxes known as facets or subsets on the surface of the specimen, where each of these facets contains *n x n* pixels. The spatial position of the center point of these subsets is calculated by averaging the position of the corners. The facets are monitored in each successive image. The basic principle of this technique is the matching of the same subsets between the images recorded before and after deformation. A facet is chosen rather than an individual pixel, is that it includes a wider variation of grays and in this way it is more distinguishable from other facets and therefore more uniquely identifiable in the target of deformed state. In order to evaluate the similarity degree between the reference and the deformed facets, a correlation criterion is needed.

The basic principle of the processing work is done by the software ARAMIS we used; it calculates the average gray scale intensity over the subset in the reference image and deformed image and compares them. Equation *(10.1)* shows the basic form of the cross-correlation term using the two consecutive images.

$$c(u,v) = \sum_i \sum_j L_1(r_i, s_j) L_2(r_i + u_L, s_j + v_L) \qquad (10.1)$$

$$u_L = u + \frac{\partial u}{\partial r} \cdot (r_L - r_C) + \frac{\partial u}{\partial s} \cdot (s_L - s_C) \qquad (10.2)$$

$$v_L = v + \frac{\partial v}{\partial r} \cdot (r_L - r_C) + \frac{\partial v}{\partial s} \cdot (s_L - s_C) \qquad (10.3)$$

where, u and v are the displacements of the center point of a subset located at (r_C,s_C) and u_L and v_L are the displacement of an arbitrary point (r_L,s_L) in the subset. L_1 represents the intensity of pixel in the deformed image. Solving for the variables u and v gives the in-plane deformation in the x direction and y direction, respectively. The size of the subset is 2n x 2n. The complete term from Equation *(10.1)* gets different values at different positions in the deformed image. The maximum value of the term shows the matched position of the most similar pattern in the deformed image compared to the reference image. A more accurate approach is the normalized correlation equation. Equation *(10.4)* shows the normalized correlation equation.

$$C(u,v) = \frac{\sum_i \sum_j L_1(r_i, s_j) L_2(r_i + u_L, s_j + v_L)}{\sqrt{\sum_i \sum_j L_1^2(r_i, s_j) \sum_i \sum_j L_2^2(r_i + u_L, s_j + v_L) L_2(r_i + u_L, s_j + v_L)}} \qquad (10.4)$$

In the Equation *(10.4)* the normalized correlation coefficient $C(u, v)$ reaches its maximum at one. The in- plane displacements can be determined by identifying a subset around a point at one position in the reference image and comparing it to the subset around a point in the deformed image having the same intensity distribution.

Figure 10.8:Digital Image Correlation System setup: lightning source, two cameras and ARAMIS software

11 Results

For each experiment the acquisition of the data was done both with the Shore Western software and the Digital Image correlation System. The Shore Western software was directly connected with Axial Torsion Machine and gave information regarding the force and/or the torque applied at each step to the

specimen and the axial displacement and/or the angle of twist the specimen was undergoing in each phase of the test.
The DIC system on the other hand allowed us to collect the data regarding the actual displacement and the strains (cfr.10.3) of the aluminum specimen, which were taking place during the whole testing.
In this section are presented the data collected not for all the tests which were performed (three for each scenario) but only the data of one test for each scenario.

11.1 Tension Test – Lode angle θ=0°

The uniaxial tension test was performed on specimen number 1A, whose actual geometry is reported in section 9.1. The nominal values of the yield stress, yield strain and yield force were calculated from the mechanical properties of the material and from the actual geometry of the specimen:

Specimen 1A-nominal values				
Diameter D	29.85	[mm]	1.175	[in]
Length B	110	[mm]	4.33	[in]
σy	260	[Mpa]	37709.88	[lb/in^2]
E	68900	[Mpa]	9993118.2	[lb/in^2]
A	699.81	[mm^2]	1.08	[in^2]
Fy	181.95	[kN]	40.89	[kips]
εy	0.42	[mm]	0.016	[in]

The experiment was performed in displacement control and two displacement rate stages were defined:

- I rate: 0.005inches/60sec (0.127mm/60sec) for the elastic region;
- II rate: 0.025inches/60sec (0.635mm/60sec) for the plastic region.

Some graphs representing the data collected from the Shore Western software and from the DIC system are reported and commented below.

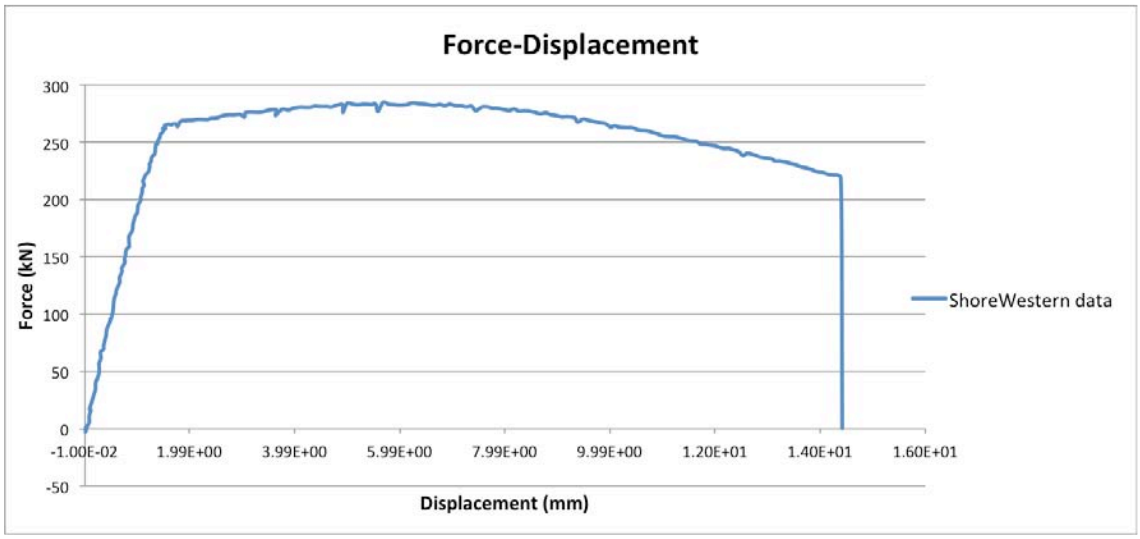

Figure 11.1: force-displacement diagram of the Shore Western data recorded each 10 seconds

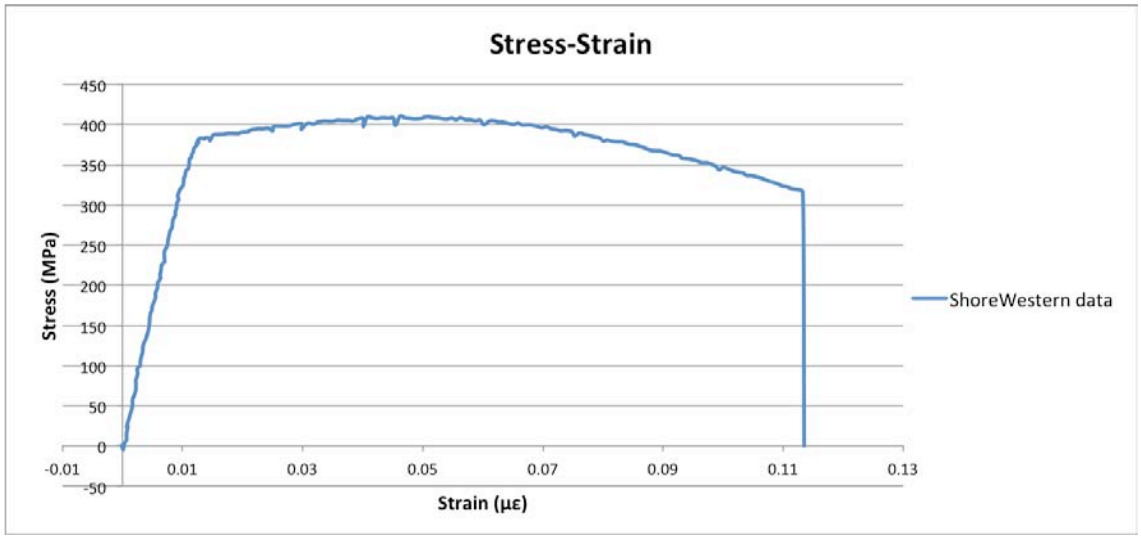

Figure 11.2: stress-strain diagram of the Shore Western data recorded each 10 seconds.

From figure 11.2 it is possible to observe the behavior of the specimen under uniaxial tension. The strain is reported in με and is calculated as the true strain:

$$\varepsilon_{true} = \int_{l_0}^{l_1} \frac{dl}{l} = \ln\left(\frac{l_1}{l_0}\right) = \ln\left(\frac{l_0 + \Delta l}{l_0}\right) = \ln\left(1 + \frac{\Delta l}{l_0}\right)$$

where l_0 is the length of the undeformed specimen and Δl is the amount of elongation due to the tensile force applied.

The aluminum specimens shows a linear behavior in the first part of the diagram and at a certain stress between 350 and 400 MPa yielding occurs. After yielding we have an hardening behavior till the peak is reached at around 410 MPa. The post peak behavior shows some softening till failure is reached at a stress of about 320 MPa.

In order to evaluate the Young modulus E of the material, the elastic part of the previous diagram is considered and a trend line is drawn.

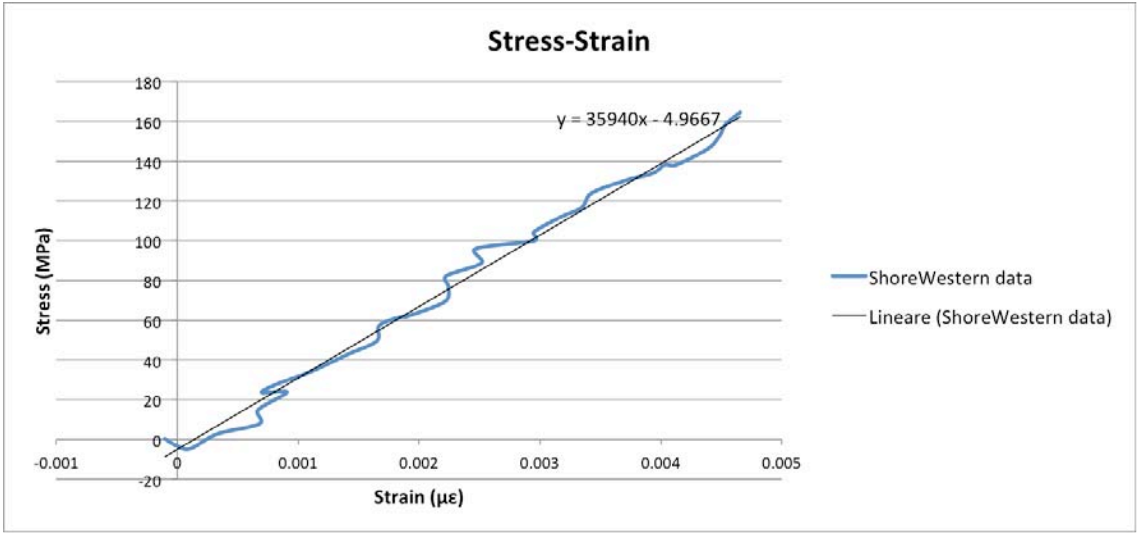

Figure 11.3: first part of the stress-strain diagram before yielding of the Shore Western data recorded each 10 seconds interpolated with a trend line

The slope of the trend line represent the Young modulus which from the Shore Western data turns out to be equal to 35490 MPa. The nominal value of E for the aluminum 6061-T6 is 69000 MPa, almost two times the one obtained from the Shore Western data. For this reason it was necessary to check the accuracy of this value, looking at the data obtained with the DIC system.

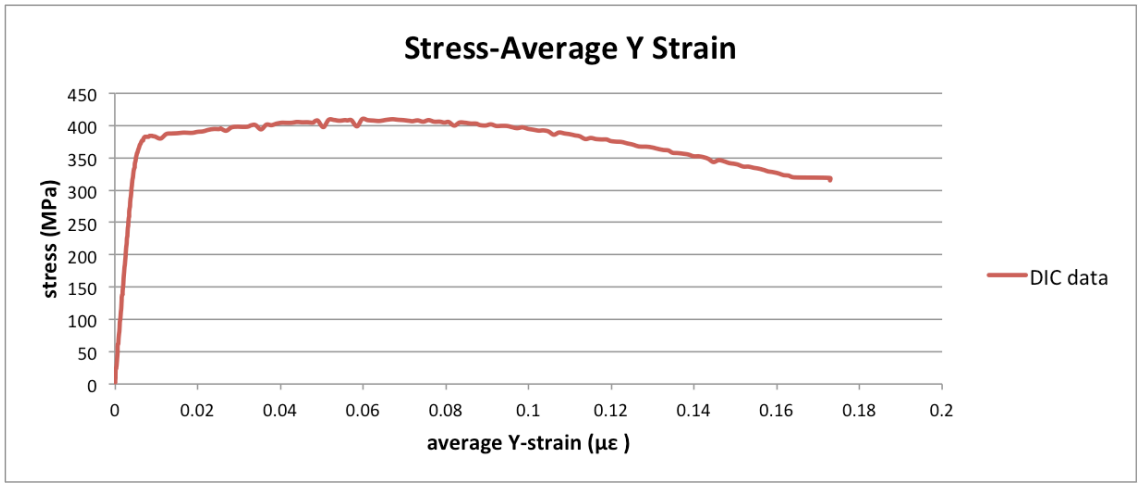

Figure 11.4: stress-strain of the DIC data recorded each 10 seconds

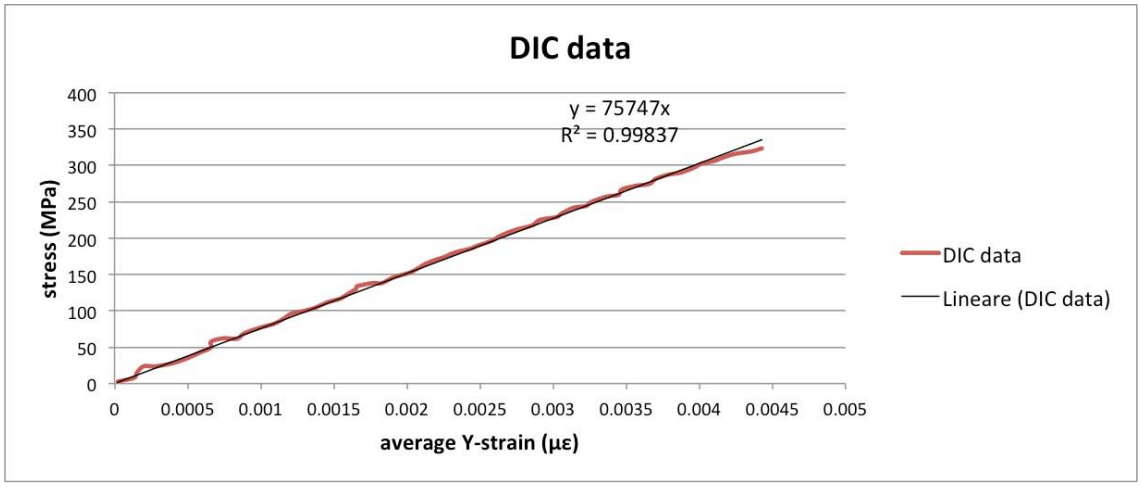

Figure 11.5: first part of the stress-strain diagram before yielding of the DIC data recorded each 10 seconds interpolated with a trend line

As it regards the DIC data, we obtain from the ARAMIS software the strains in five vertical sections of the specimen and for this reason an average strain of this five was then calculated. The slope of the trend line, which interpolates the DIC data represents the Young modulus, which turns out to be equal to 75747 MPa. This value of E is closer to the nominal one, which is for the aluminum 6061-T6 is 69000 MPa. For this reason, comparing the Young Modulus obtained from the Shore Western data and the one provided by the DIC data, we concluded that we had some errors during the record of the Shore Western data, probably due to a slip of the specimen in the grips in the first moments of the testing, which

caused an increased value of strain and a lower slope of the trend line, which interpolates the Shore Western data.

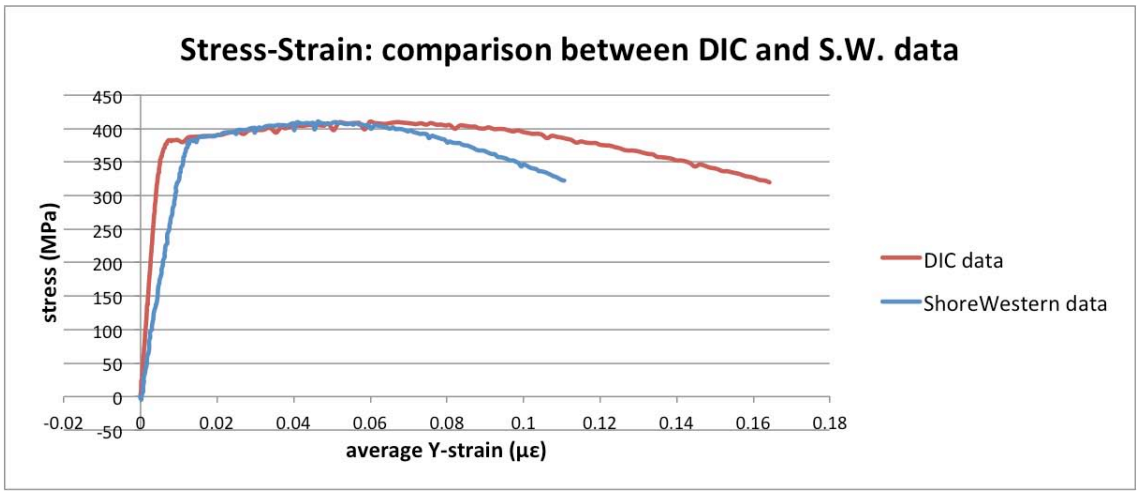

Figure 11.6: comparison between the stress-strain DIC curve and the stress-strain Shore Western curve. The different slopes in the elastic region are probably due to a slip of the specimen in the grips.

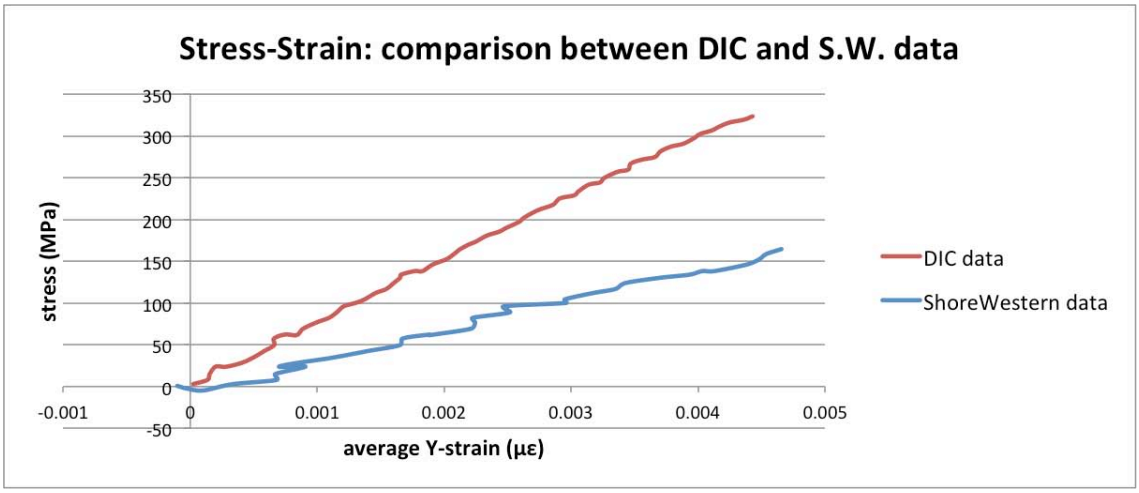

Figure 11.7: different slopes in the elastic region are probably due to a slip of the specimen in the grips.

To detect the precise point of yielding, since this point was not completely clear from the test data, it is evaluate as the so-called $\sigma_{0.2\%}$-stress, i.e. the stress at which the remaining plastic strain after unloading is equal to 0.2%.

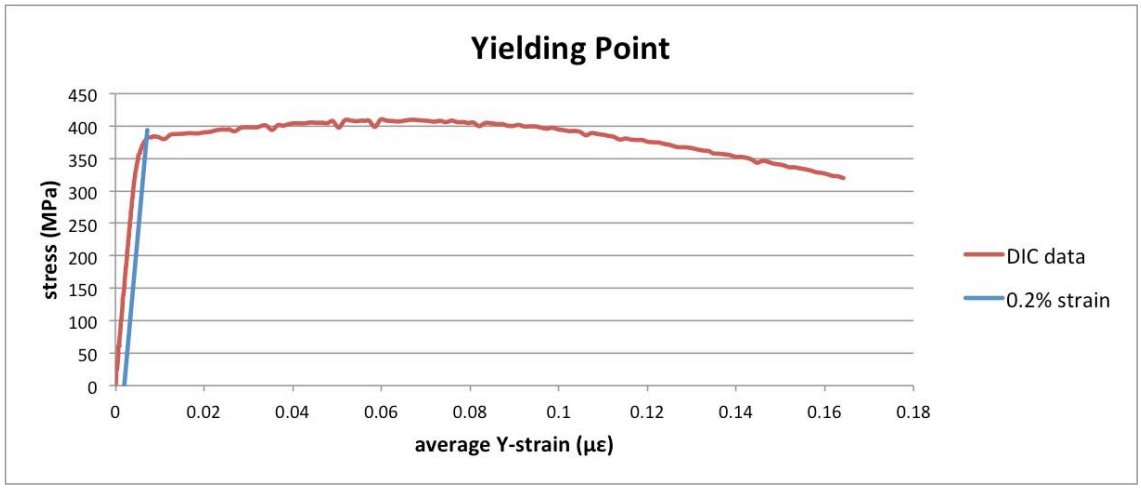

Figure 11.8: yielding point evaluate as the $\sigma_{0.2\%}$-stress

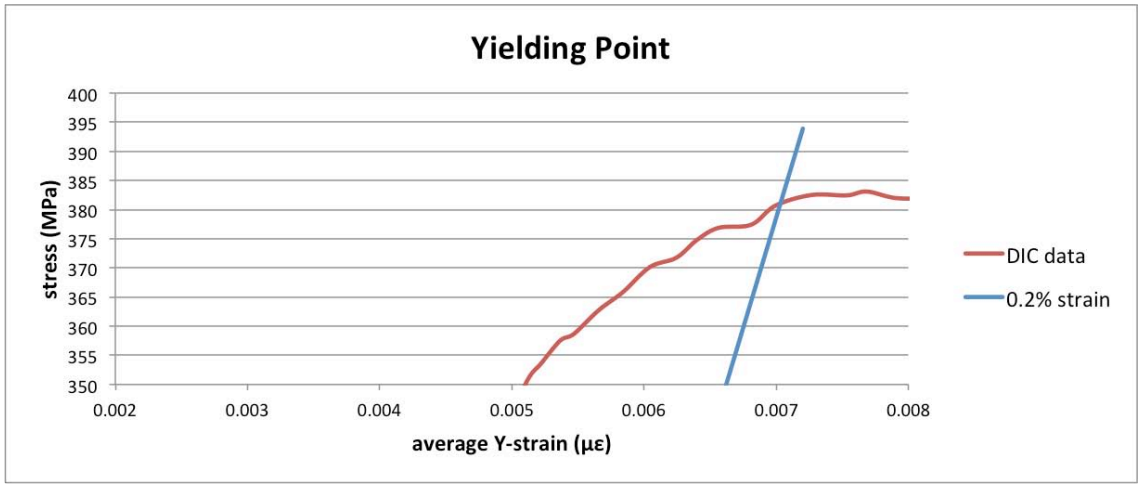

Figure 11.9: detail of the yielding point

The intersection between the DIC data curve and the 0.2% strain straight line locate the yielding point, which in this case occurs at a stress equal to 382MPa.

Below is reported a table, which summarizes the most important values of this test.

Name of the specimen	1A
Lode Angle	0°
Length (mm)	110
Diameter (mm)	29.85
Tensile Yield point: stress (MPa)	382
Tensile Yield point: strain (με)	0.0072
Peak point: stress (MPa)	410.22
Peak point: strain (με)	0.059
Failure point: stress (MPa)	315.10
Failure point: strain (με)	0.173
Yield load (kN)	267
E (GPa)	75.7

Some pictures of the specimen and its failure are now reported.

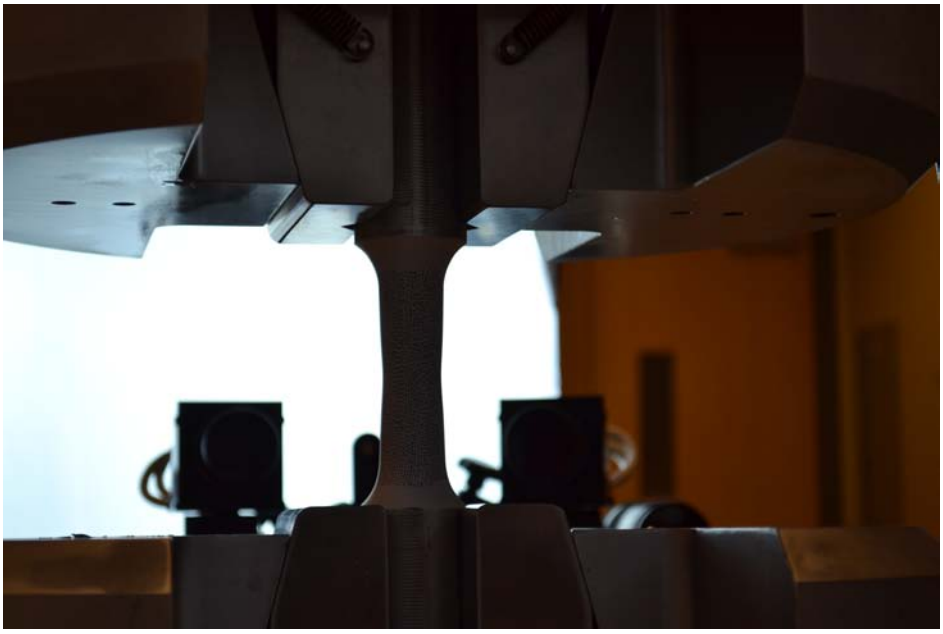

Figure 11.10: tension test, starting of the necking

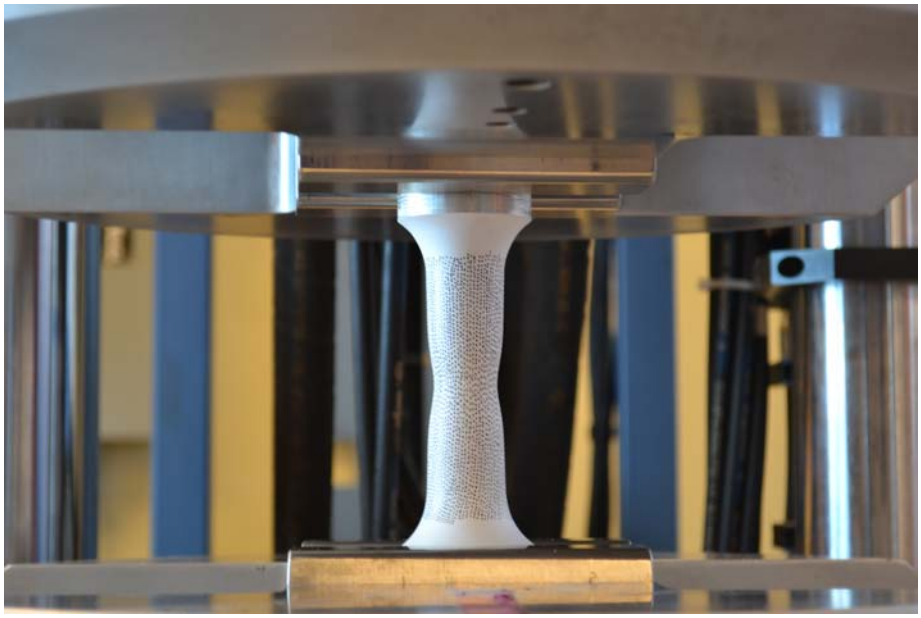

Figure 11.11: tension test, evident necking taking place

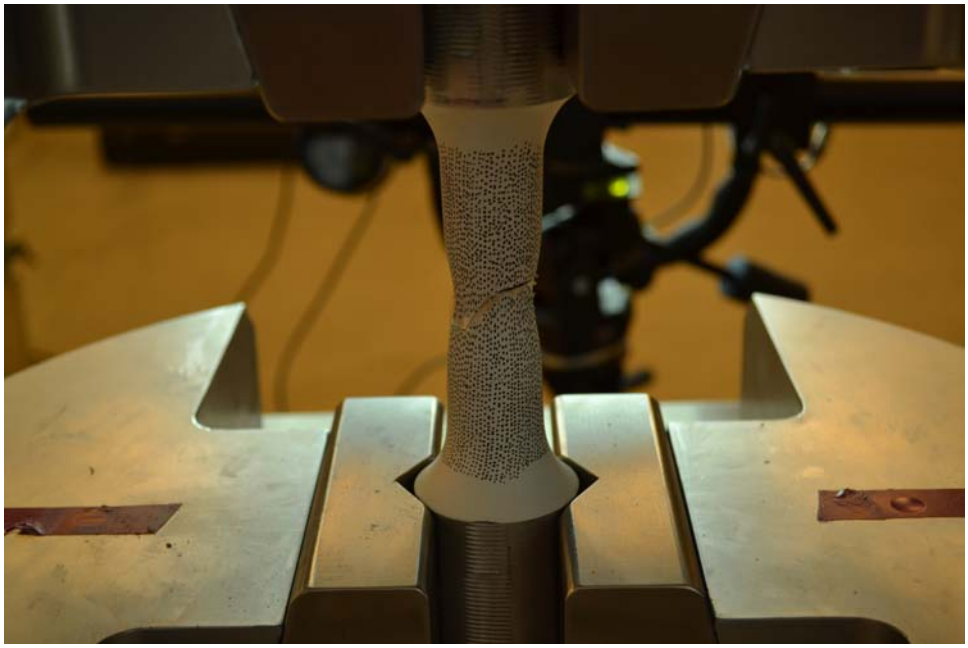

Figure 11.12: failure mode

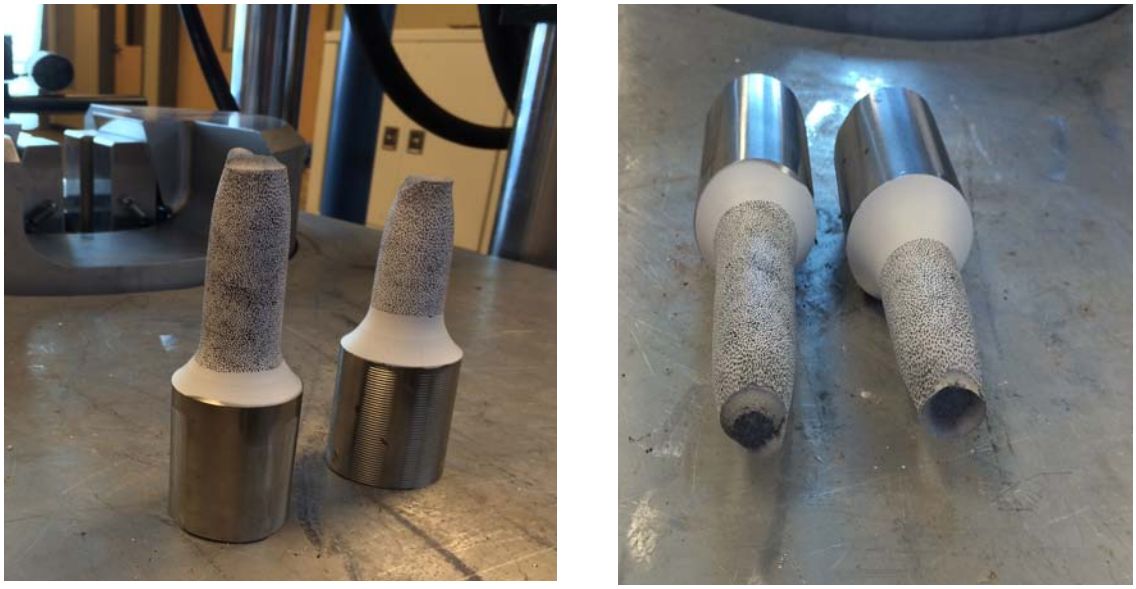

Figure 11.13: failure of the traction specimen

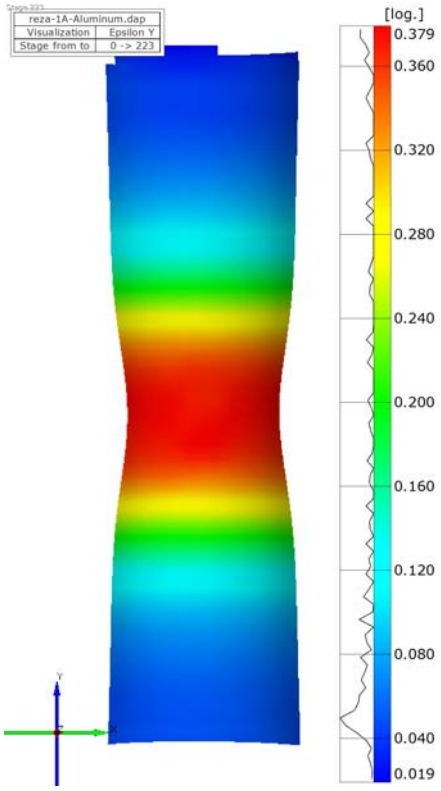

Figure 11.13: contour of the strain in the vertical direction: image obtained by post processing of the DIC data recorded

11.2 Tension - Torsion Test – Lode angle θ=10°

The tension torsion test was performed on specimen number 6A, whose actual geometry is reported in section 9.1. The nominal values of the yield stress, yield strain and yield force were calculated from the mechanical properties of the material and from the actual geometry of the specimen:

Specimen 6A-nominal values				
Diameter D	29.92	[mm]	1.178	[in]
Length B	110	[mm]	4.33	[in]
σy	260	[Mpa]	37709.88	[lb/in^2]
E	68900	[Mpa]	9993118.2	[lb/in^2]
A	703.09	[mm^2]	1.09	[in^2]
Fy	181.58	[kN]	40.82	[kips]
Ty	0.84	[kNm]	7.420	[kip-in]

The experiment was performed in torque and consequently in traction control since the ratio between tension and torsion in the imperial units must be kept 5.5 (cfr. section 9.4).

Some graphs representing the data collected from the Shore Western software and from the DIC system are reported and commented below.

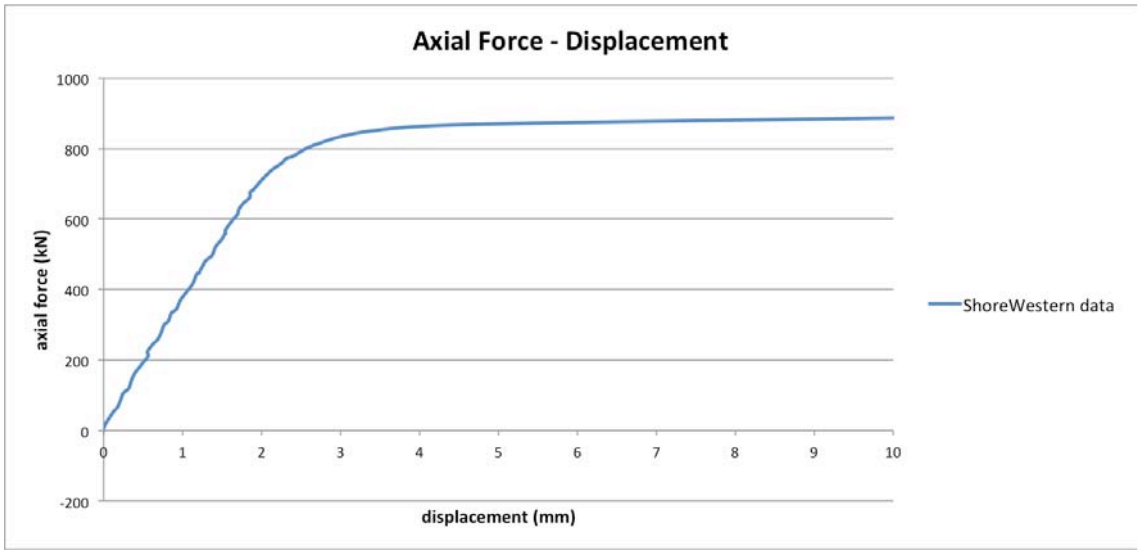

Figure 11.14: axial force-displacement diagram of the Shore Western data recorded each 10 seconds

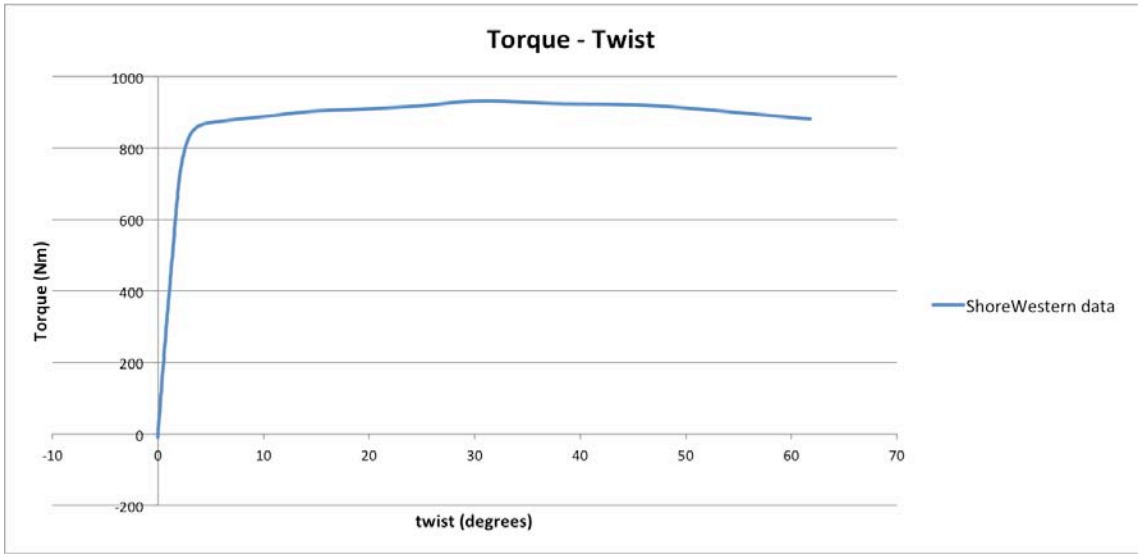

Figure 11.15: torque-twist diagram of the Shore Western data recorded each 10 seconds

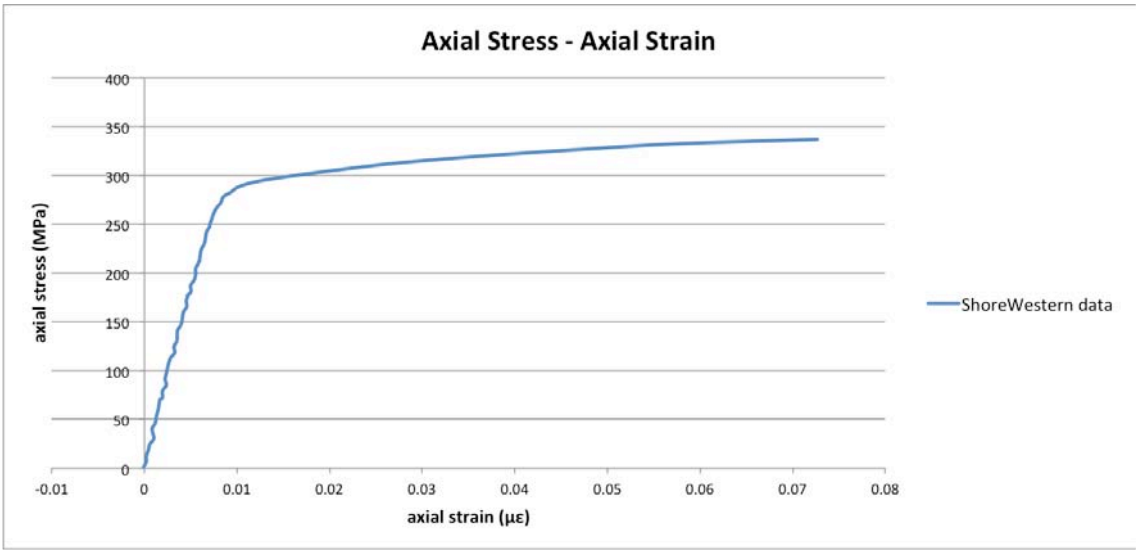

Figure 11.16:axial stress-axial strain diagram of the Shore Western data recorded each 10 seconds.

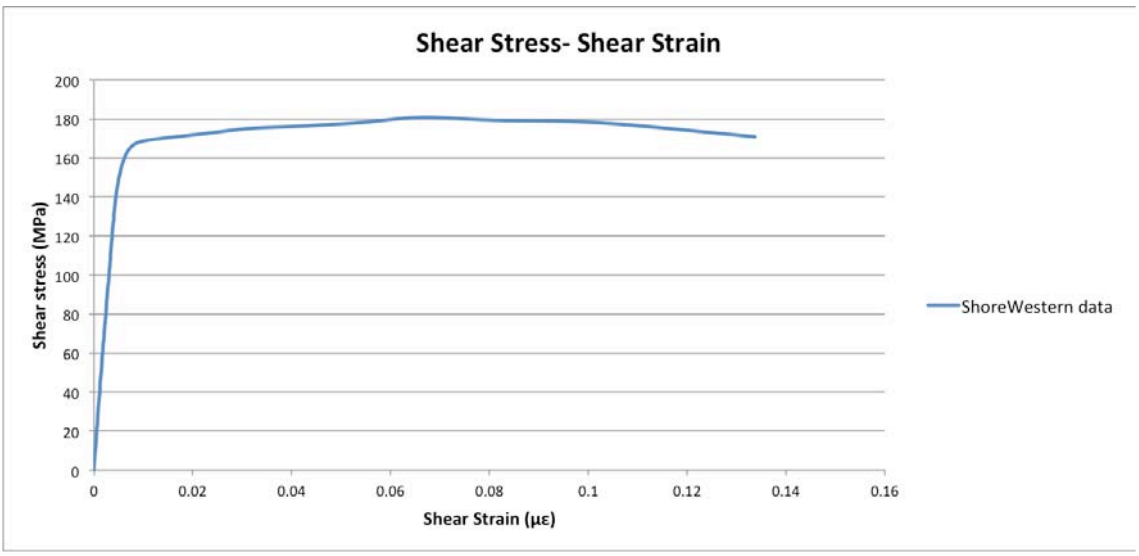

Figure 11.17: shear stress-shear strain diagram of the Shore Western data recorded each 10 seconds.

From figures 11.16 and 11.17 it is possible to observe the behavior of the specimen under tension-torsion. The strain is reported in με and is calculated as the true strain.

The aluminum specimens shows a linear behavior in the first part of the axial stress-axial strain diagram and at a certain stress between 250 and 300 MPa yielding occurs. After yielding we have an hardening behavior till the peak is reached at around 340 MPa. As it regards the behavior of the specimen under torque we notice a linear behavior in the first part of the shear stress-shear strain diagram and at a certain stress between 160 and 180 MPa yielding occurs. After

yielding we have an hardening behavior till the peak is reached at around 180 MPa. The post peak behavior shows some softening till failure is reached at a stress of about 170 MPa.

In order to evaluate the shear modulus G of the material, the elastic part of the shear stress-shear strain diagram is considered and a trend line is drawn.

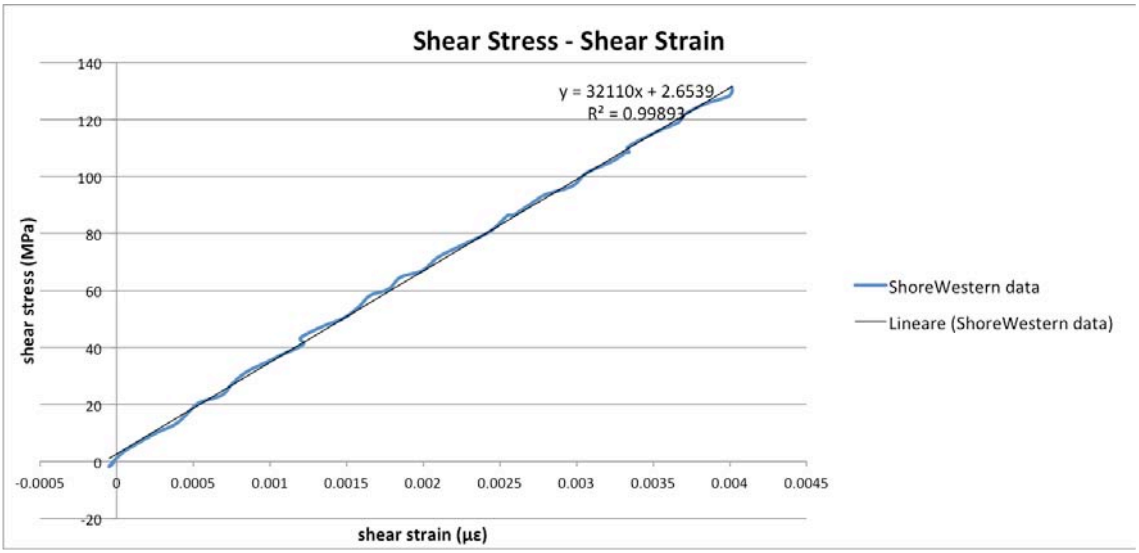

Figure 11.18: first part of the shear stress-shear strain diagram before yielding of the Shore Western data recorded each10 seconds, interpolated with a trend line

The slope of the trend line represent the shear modulus G which, from the Shore Western data turns out to be equal to 32110 MPa. The nominal value of G for the aluminum 6061-T6 is 26000 MPa, very similar to the value obtained from the Shore Western data.

In order to evaluate the Young modulus E of the material, the elastic part of the axial stress-axial strain diagram is considered and a trend line is drawn.

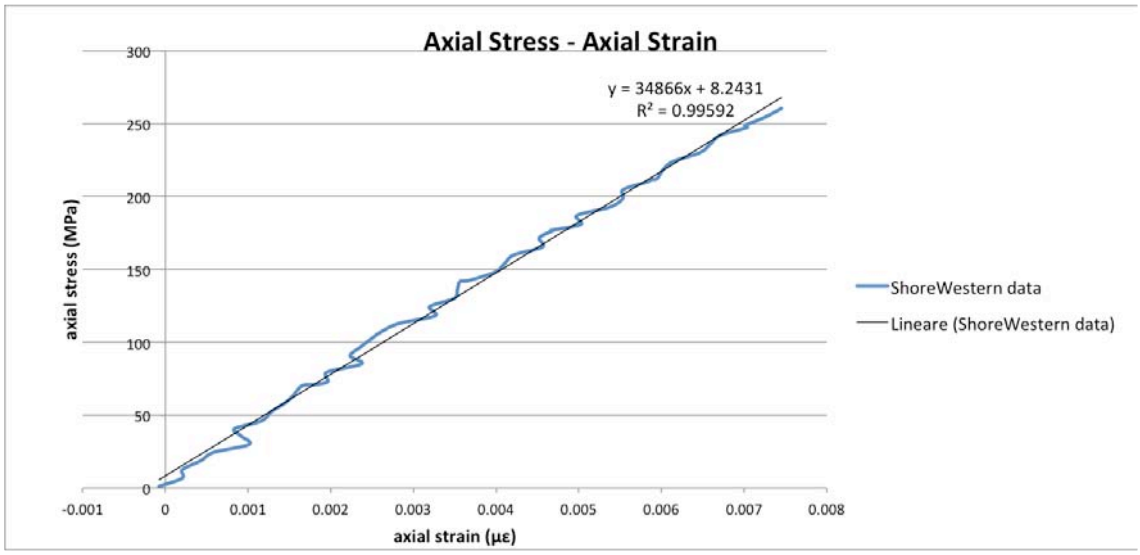

Figure 11.19: first part of the axial stress-axial strain diagram before yielding of the Shore Western data recorded each 10 seconds interpolated with a trend line

The slope of the trend line represent the Young modulus which from the Shore Western data turns out to be equal to 34866 MPa. The nominal value of E for the aluminum 6061-T6 is 69000 MPa, almost two times the one obtained from the Shore Western data. For this reason it was necessary to check the accuracy of this value, looking at the data obtained with the DIC system.

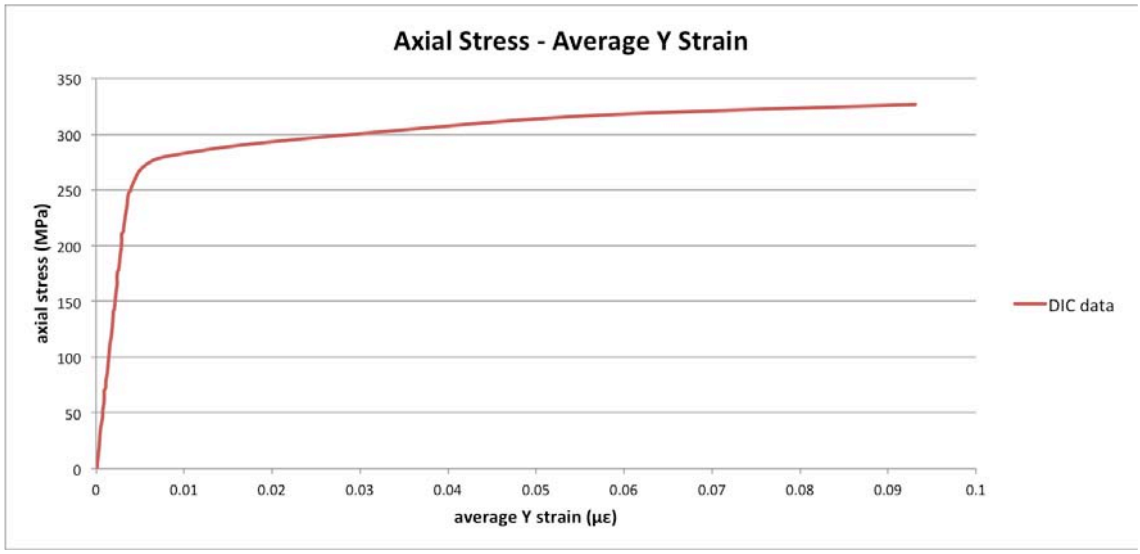

Figure 11.20: axial stress-average Y strain of the DIC data recorded each 10 seconds

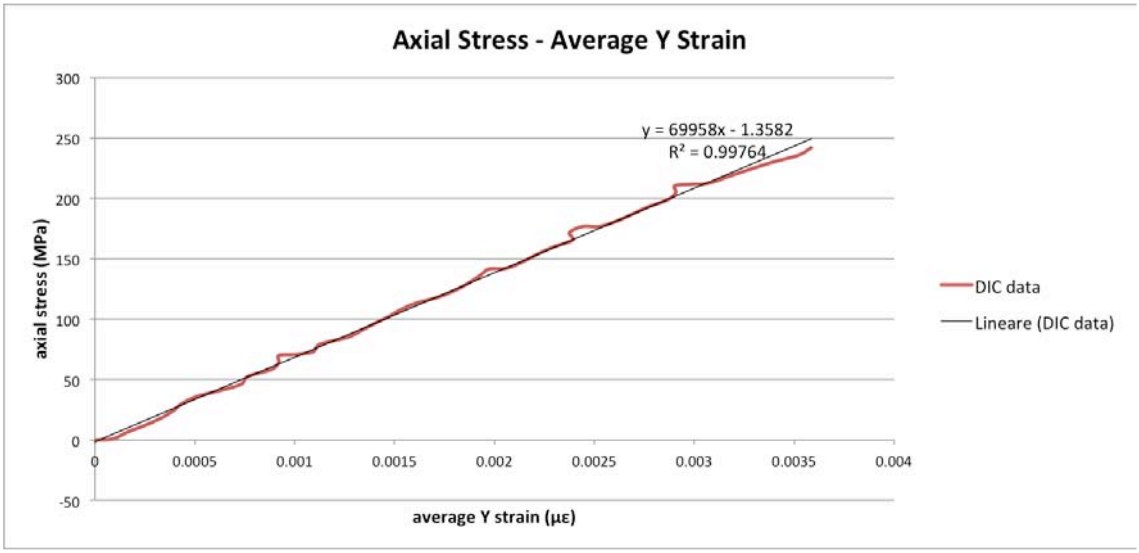

Figure 11.21: first part of the axial stress- average Y strain diagram before yielding of the DIC data recorded each 10 seconds interpolated with a trend line

As it regards the DIC data, we obtain, from the ARAMIS software, the strains in five vertical sections of the specimen and for this reason an average strain of this five was then calculated. The slope of the trend line, which interpolates the DIC data represents the Young modulus, which turns out to be equal to 69958 MPa. This value of E is much closer to the nominal one, which is for the aluminum 6061-T6 is 69000 MPa. For this reason, comparing the Young Modulus obtained from the Shore Western data and the one provided by the DIC data, we concluded that we had some errors during the record of the Shore Western data, which caused an increased value of strain and a lower slope of the trend line, which interpolates the Shore Western data.

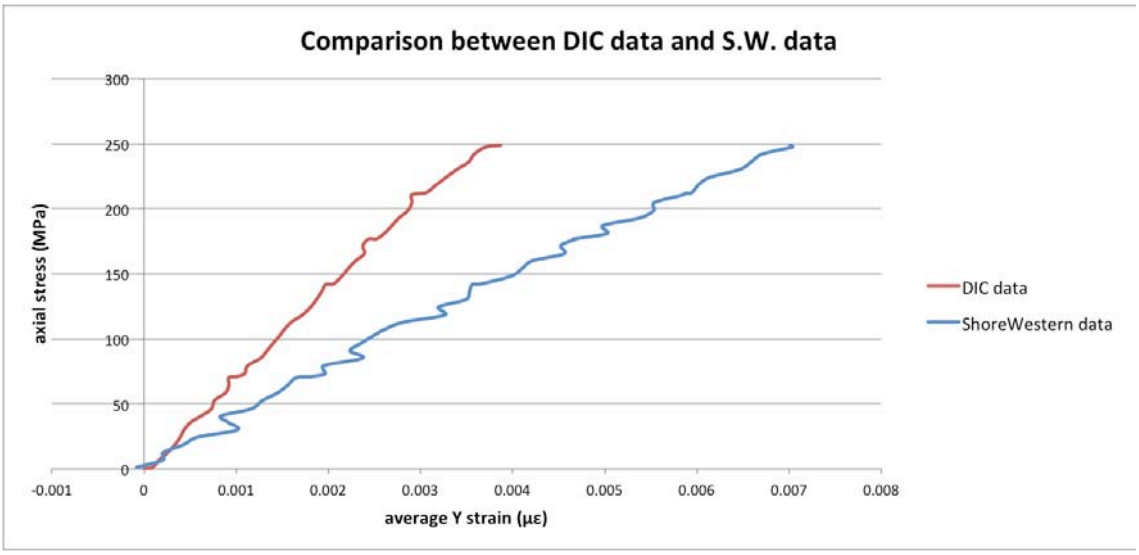

Figure 11.22: comparison between the axial stress-average Y strain DIC curve and the axial stress-average Y strain Shore Western curve: different slopes in the elastic region.

To detect the precise point of yielding as it regards the axial force, it is evaluate as the so-called $\sigma_{0.2\%}$-stress, i.e. the stress at which the remaining plastic strain after unloading is equal to 0.2%.

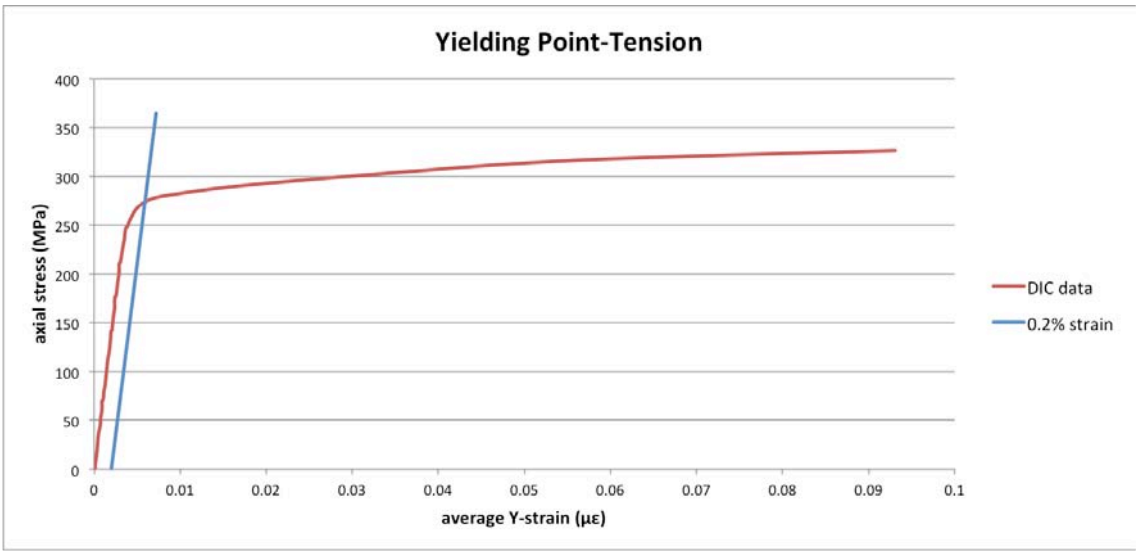

Figure 11.23: yielding point for the axial force evaluate as the $\sigma_{0.2\%}$-stress

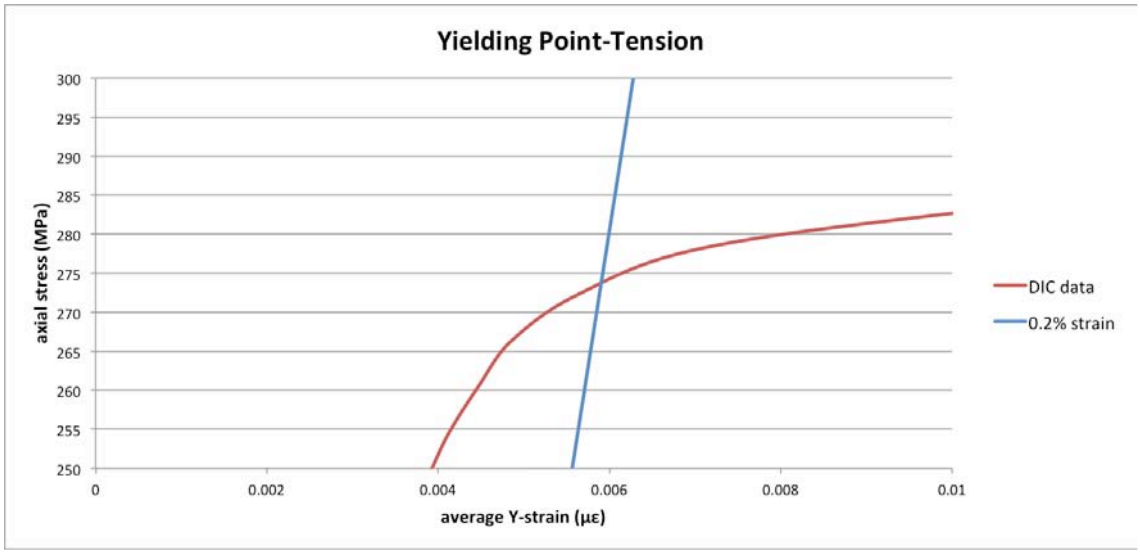

Figure 11.24: detail of the tensile yielding point

The intersection between the DIC data curve and the 0.2% strain straight line locate the yielding point, which in this case occurs at a stress equal to 274MPa.

The same procedure is used to detect the precise point of yielding as it regards the torque.

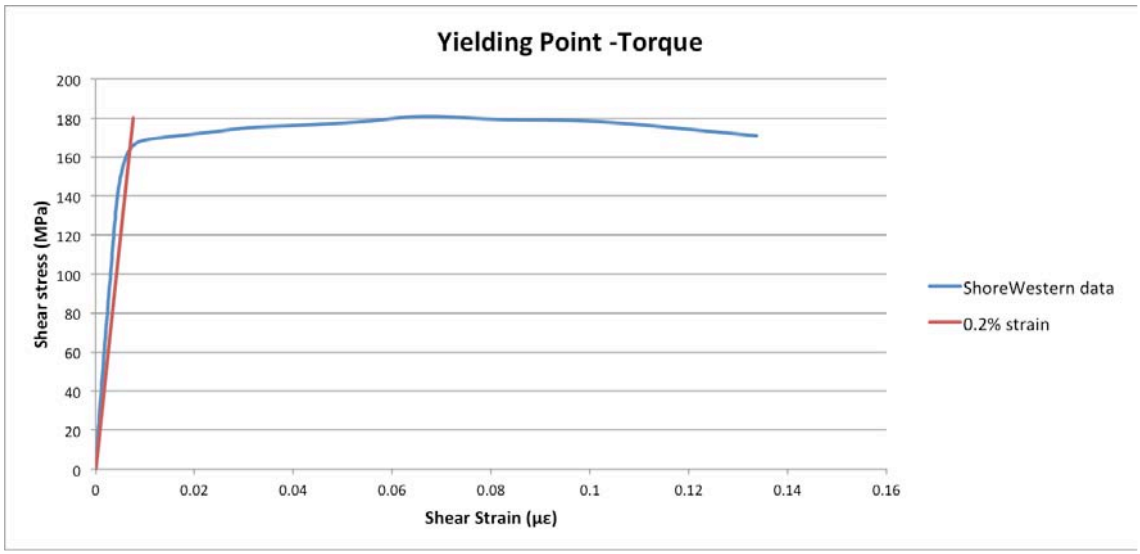

Figure 11.25: yielding point for the torque evaluate as the $\sigma_{0.2\%}$-stress

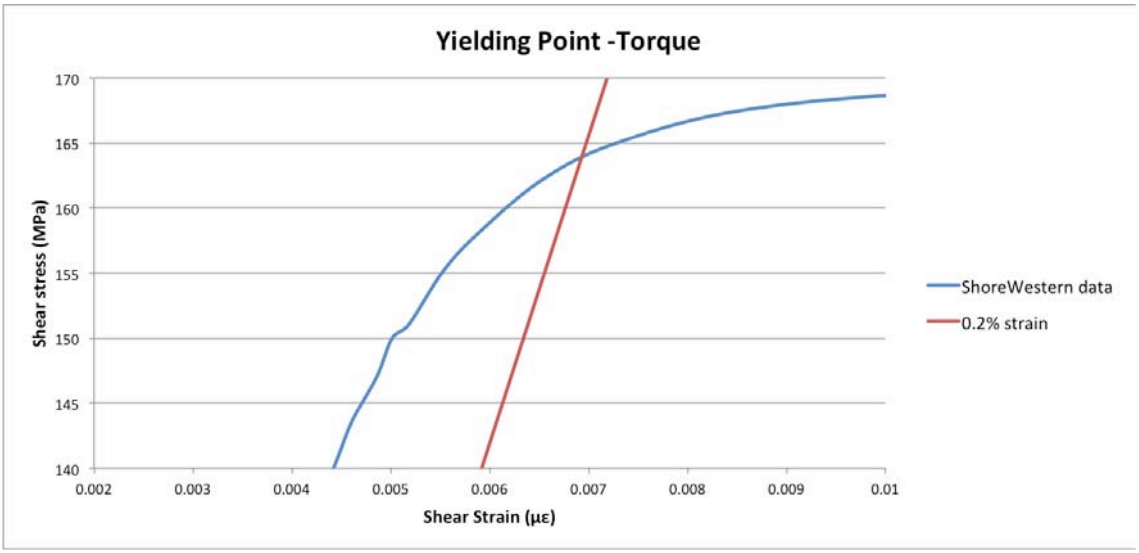

Figure 11.26: detail of the torque yielding point

The intersection between the DIC data curve and the 0.2% strain straight line locate the torque yielding point, which in this case occurs at a stress equal to 164MPa.

Below is reported a table, which summarizes the most important values of this test.

Name of the specimen	6A
Lode Angle	10°
Length (mm)	110
Diameter (mm)	29.92
Tensile Yield point: stress (MPa)	272
Tensile Yield point: strain (με)	0.0056
Torque Yield point: stress (MPa)	164.96
Torque Yield point: strain (με)	0.0073
Tensile peak point: stress (MPa)	326.51
Tensile peak point: strain (με)	0.093
Torque peak point: stress (MPa)	180.77
Torque peak point: strain (με)	0.066
Tensile failure point: stress (MPa)	326.51
Tensile failure point: strain (με)	0.093
Torque failure point: stress (MPa)	170.93
Torque failure point: strain (με)	0.134
Tensile yield load (kN)	191
Torque yield load (Nm)	867.8
Torque yield twist (°)	2.16
Tensile failure load (kN)	229.2

Torque failure load (Nm)	898.79
Torque failure twist (°)	61.78
E (GPa)	69958
G (GPa)	32110

Some pictures of the specimen and its failure are now reported.

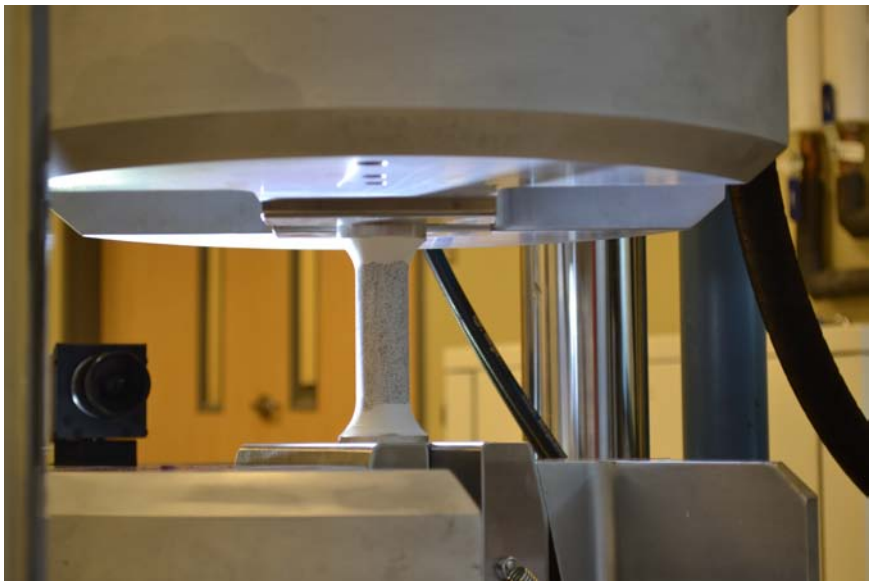

Figure 11.27: specimen 6A placed in the grips

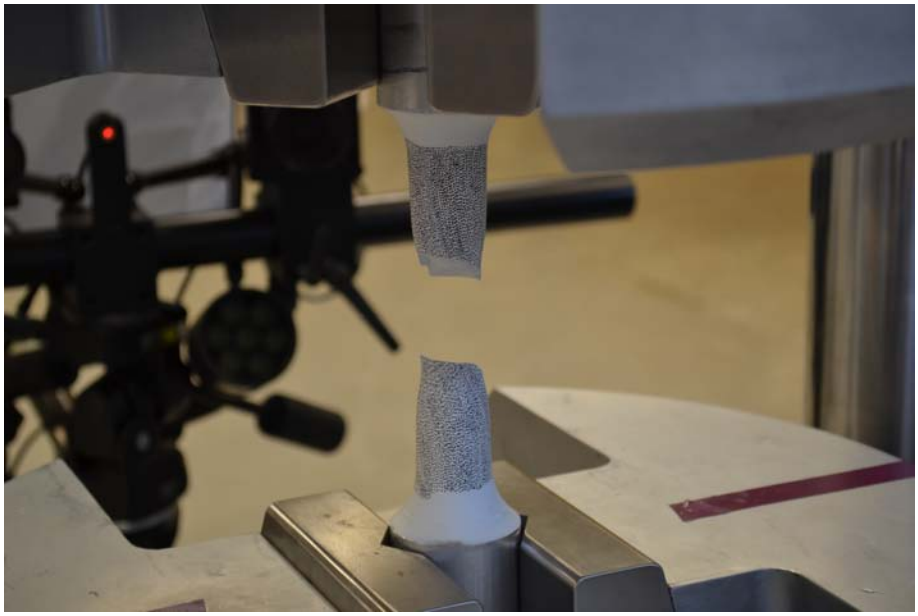

Figure 11.28: collapse of the specimen

Figure 11.29: failure of the specimen

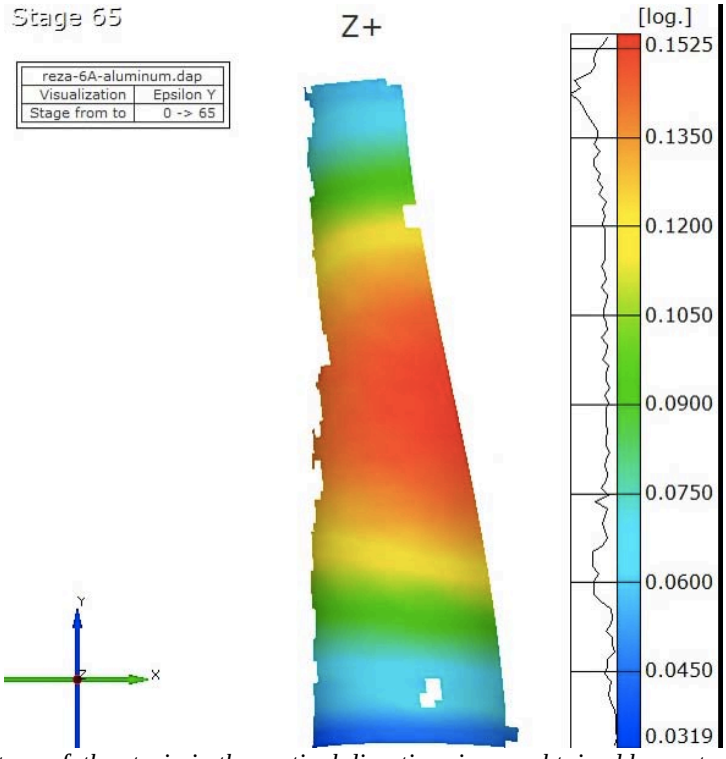

Figure 11.30: contour of the strain in the vertical direction: image obtained by post processing the DIC data recorded

11.3 Tension - Torsion Test – Lode angle θ=20°

The tension torsion test was performed on specimen number 7A, whose actual geometry is reported in section 9.1. The nominal values of the yield stress, yield strain and yield force were calculated from the mechanical properties of the material and from the actual geometry of the specimen:

Specimen 7A-nominal values				
Diameter D	29.64	[mm]	1.167	[in]
Length B	120	[mm]	4.72	[in]
σy	260	[Mpa]	37709.88	[lb/in^2]
E	68900	[Mpa]	9993118.2	[lb/in^2]
A	690.00	[mm^2]	1.07	[in^2]
Fy	93.95	[kN]	21.12	[kips]
Ty	1.10	[kNm]	9.710	[kip-in]

The experiment was performed in torque and consequently in traction control since the ratio between tension and torsion in the imperial units must be kept 2.175 (cfr. section 9.4).
Two torque rate stages were defined:

- I rate: 1 kip-in/60sec (0.113 kNm/60sec) for the elastic region;
- II rate: 1 kip-in/300sec (0.113 kNm/300sec) for the plastic region.

Some graphs representing the data collected from the Shore Western software and from the DIC system are reported and commented below.

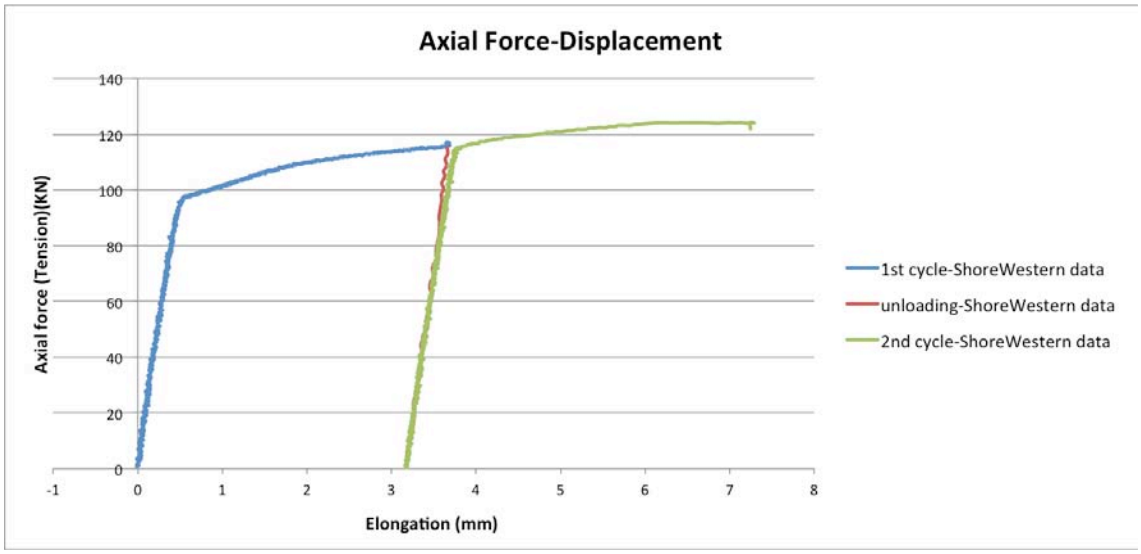

Figure 11.31: axial force-displacement diagram of the Shore Western data

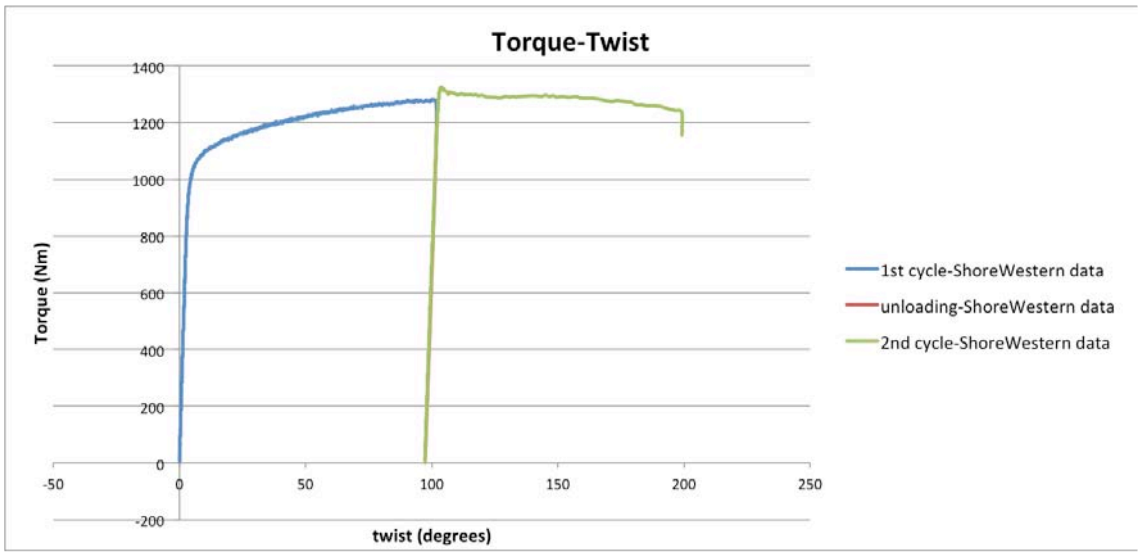

Figure 11.32: torque-twist diagram of the Shore Western data

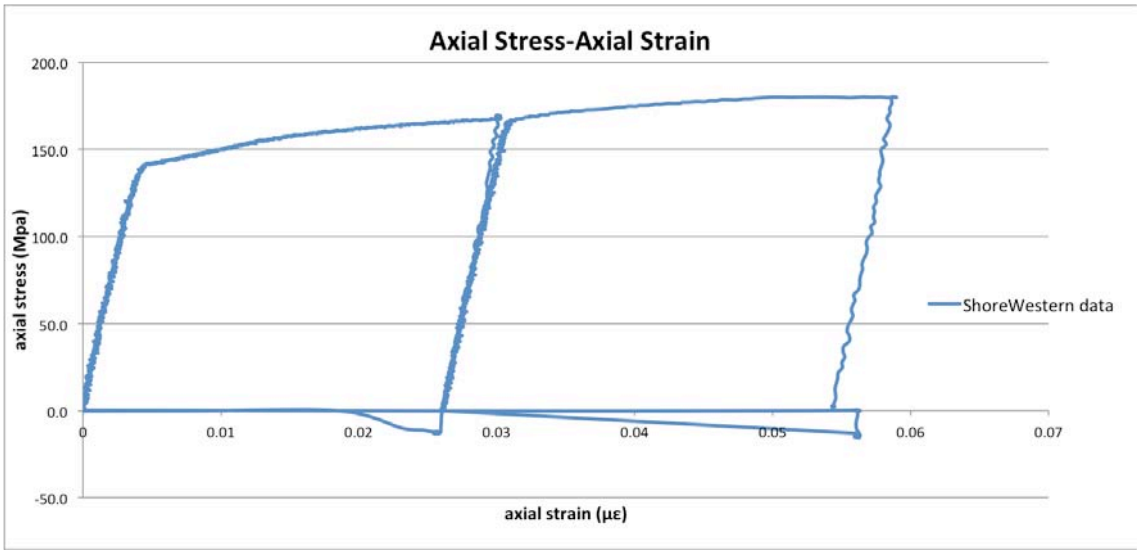

Figure 11.33:axial stress-axial strain diagram of the Shore Western data.

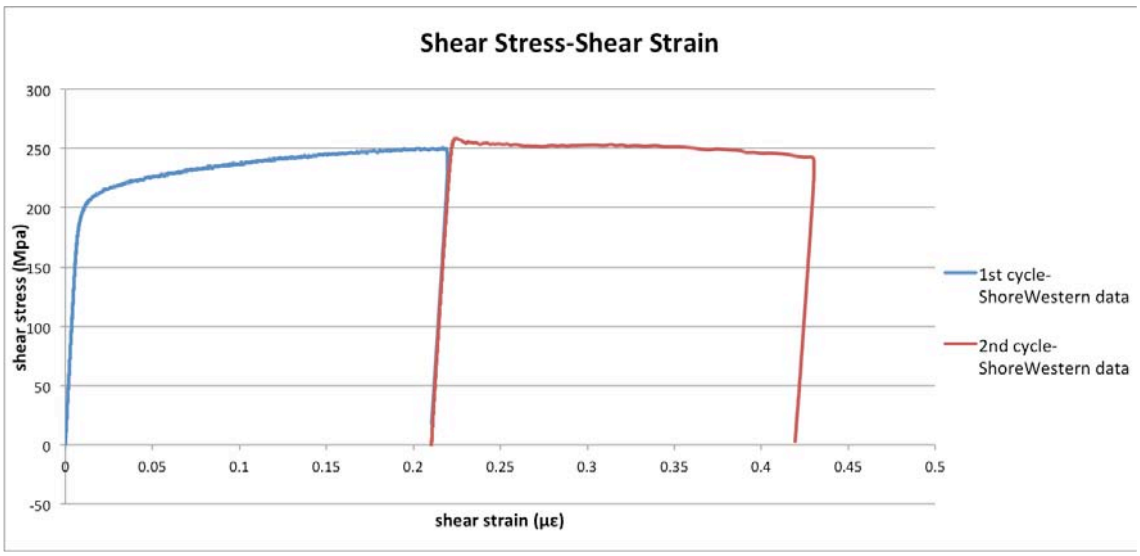

Figure 11.34: shear stress-shear strain diagram of the Shore Western.

From figures 11.33 and 11.34 it is possible to observe the behavior of the specimen under tension-torsion. The strain is reported in με and is calculated as the true strain.

The aluminum specimens shows a linear behavior in the first part of the axial stress-axial strain diagram and at a certain stress between 130 and 150 MPa yielding occurs. After yielding we have an hardening behavior till unloading is applied. The second cycle shows a wider linear behavior in fact in the second cycle, plastification occurs at an axial stress between 160 and 170 MPa. The peak is reached at around 179-180 MPa. As it regards the behavior of the specimen

under torque we notice a linear behavior in the first part of the shear stress-shear strain diagram and at a certain stress between 190 and 200 MPa yielding occurs. After yielding we have an hardening behavior till unloading is applied. The second cycle shows a wider linear behavior in fact in the second cycle, plastification occurs at an axial stress between 230 and 250 MPa. The peak is reached at around 250 MPa. The post peak behavior shows some softening till failure is reached at a stress of about 240 MPa.

In order to evaluate the shear modulus G of the material, the elastic part of the shear stress-shear strain diagram is considered and a trend line is drawn.

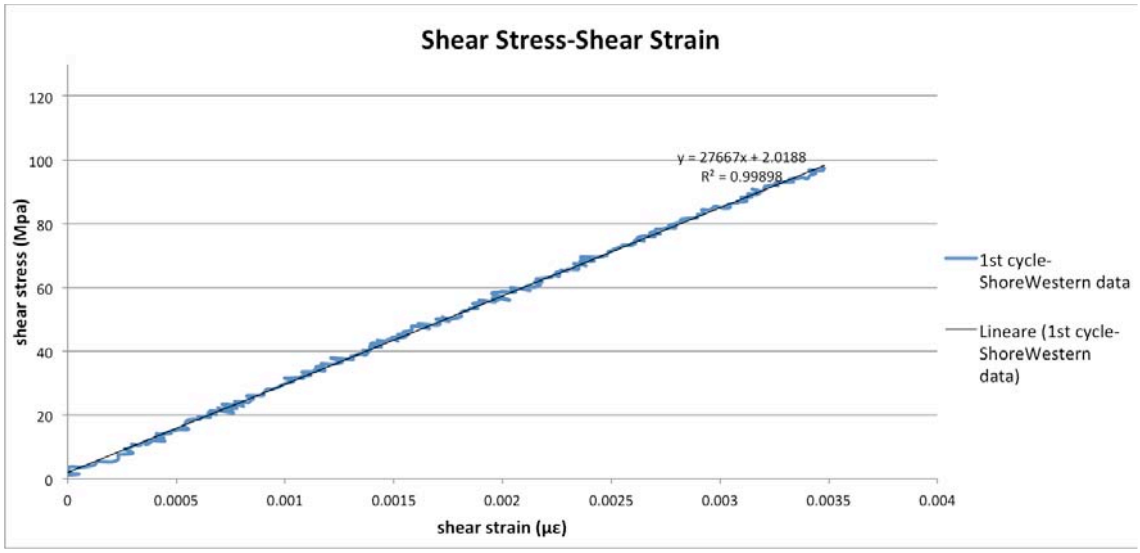

Figure 11.35: first part of the shear stress-shear strain diagram before yielding of the Shore Western data, interpolated with a trend line

The slope of the trend line represents the shear modulus G, which, from the Shore Western data turns out to be equal to 27667 MPa. The nominal value of G for the aluminum 6061-T6 is 26000 MPa, very similar to the value obtained from the Shore Western data.

In order to evaluate the Young modulus E of the material, the elastic part of the axial stress-axial strain diagram is considered and a trend line is drawn.

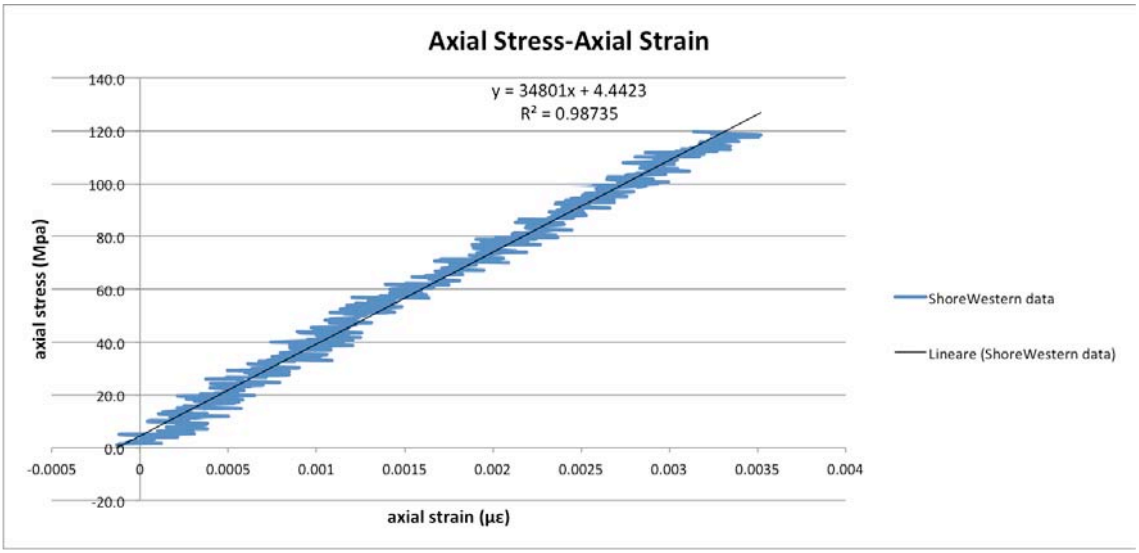

Figure 11.36: first part of the axial stress-axial strain diagram before yielding of the Shore Western data interpolated with a trend line

The slope of the trend line represents the Young modulus, which from the Shore Western data turns out to be equal to 34801 MPa. The nominal value of E for the aluminum 6061-T6 is 69000 MPa, almost two times the one obtained from the Shore Western data. For this reason it was necessary to check the accuracy of this value, looking at the data obtained with the DIC system.

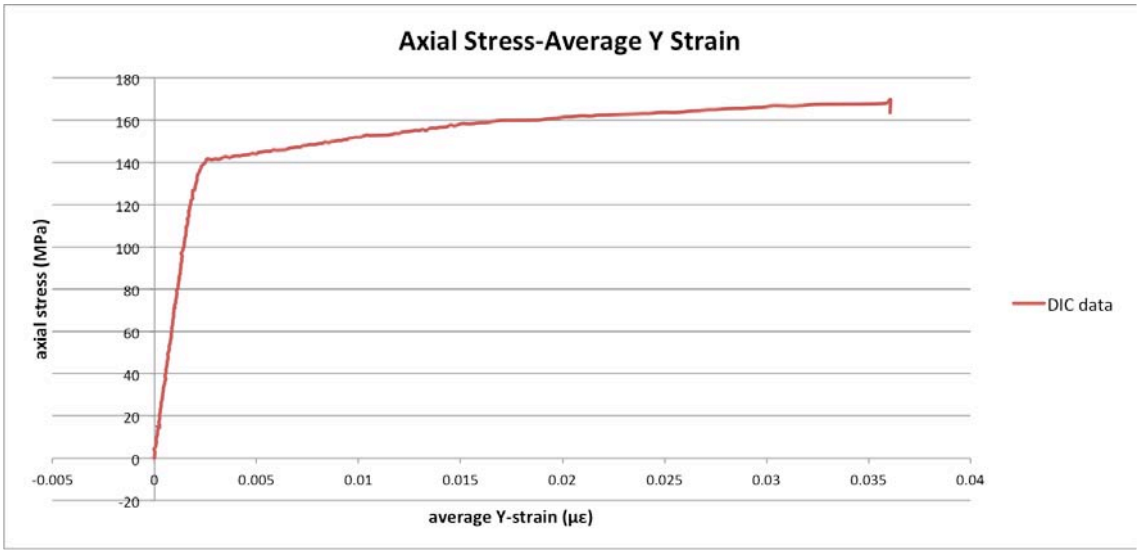

Figure 11.37: axial stress-average Y strain of the DIC data recorded each 10 seconds

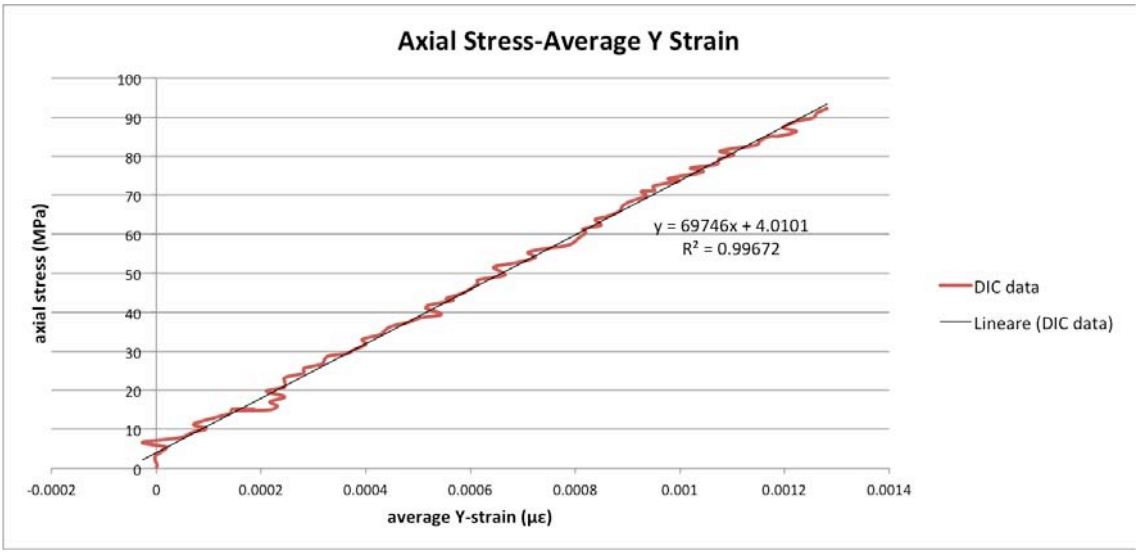

Figure 11.38: first part of the axial stress- average Y strain diagram before yielding of the DIC data recorded each 10 seconds interpolated with a trend line

As it regards the DIC data, we obtain, from the ARAMIS software, the strains in five vertical sections of the specimen and for this reason an average strain of this five was then calculated. The slope of the trend line, which interpolates the DIC data represents the Young modulus, which turns out to be equal to 69746 MPa. This value of E is much closer to the nominal one, which is for the aluminum 6061-T6 is 69000 MPa. For this reason, comparing the Young Modulus obtained from the Shore Western data and the one provided by the DIC data, we concluded that we had some errors during the record of the Shore Western data, which caused an increased value of strain and a lower slope of the trend line, which interpolates the Shore Western data.

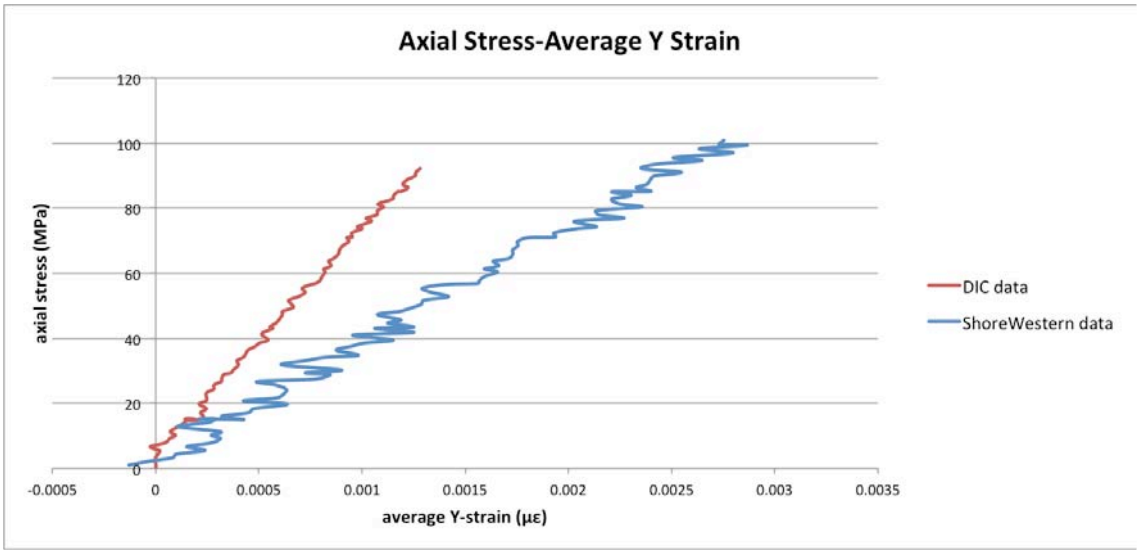

Figure 11.39: comparison between the axial stress-average Y strain DIC curve and the axial stress-average Y strain Shore Western curve: different slopes in the elastic region.

To detect the precise point of yielding as it regards the axial force, it is evaluate as the so-called $\sigma_{0.2\%}$-stress, i.e. the stress at which the remaining plastic strain after unloading is equal to 0.2%.

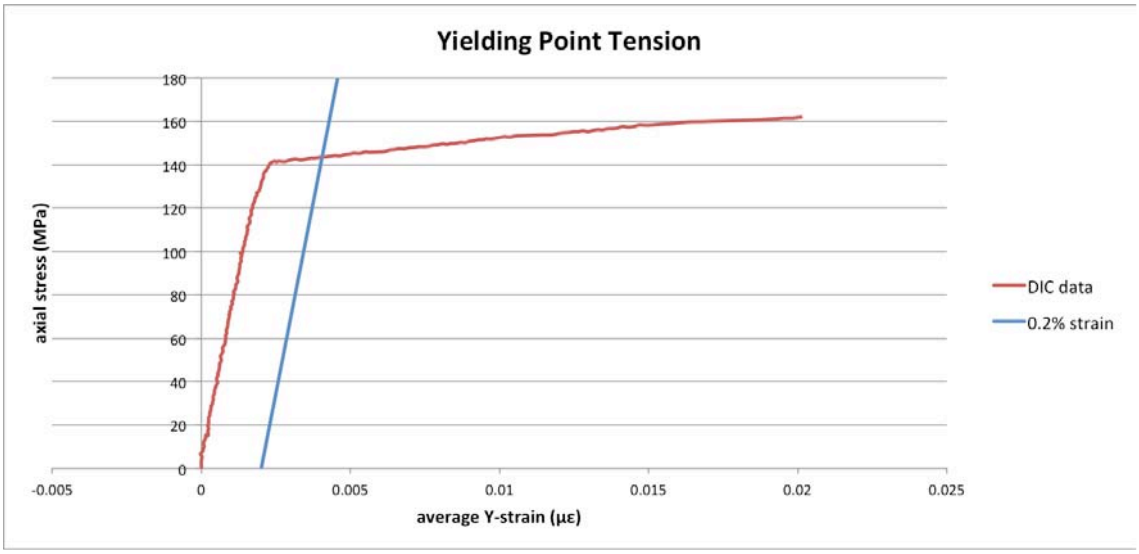

Figure 11.40: yielding point for the axial force evaluate as the $\sigma_{0.2\%}$-stress

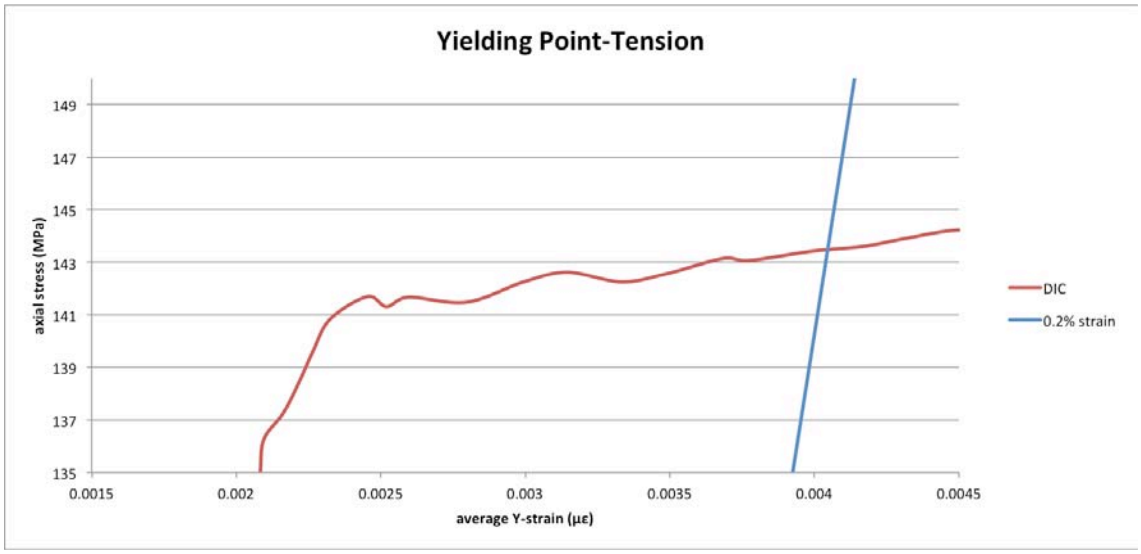

Figure 11.41: detail of the tensile yielding point

The intersection between the DIC data curve and the 0.2% strain straight line locate the yielding point, which in this case occurs at a stress equal to 143MPa.

The same procedure is used to detect the precise point of yielding as it regards the torque.

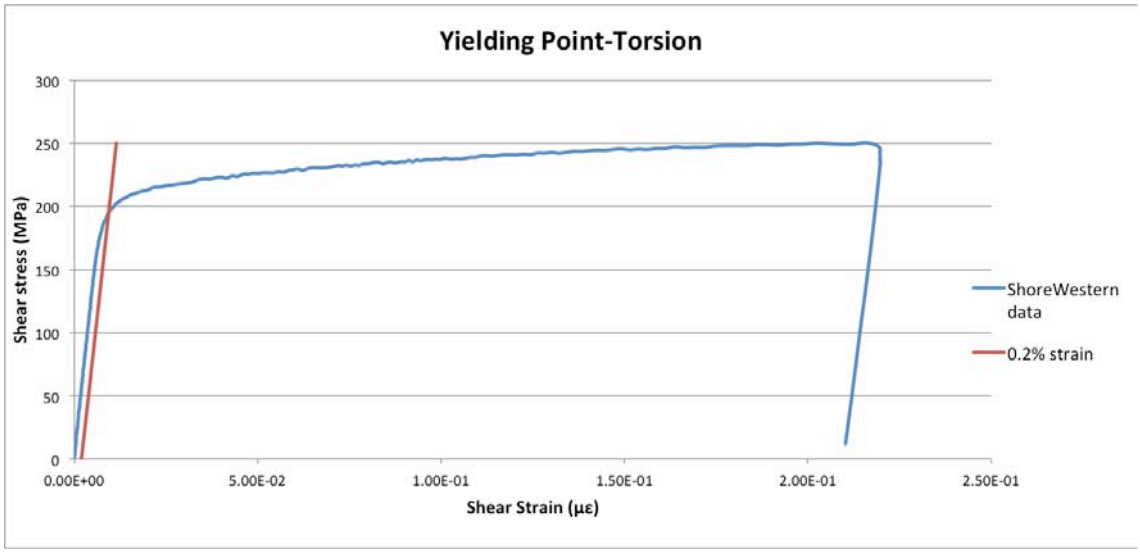

Figure 11.42: yielding point for the torque evaluate as the $\sigma_{0.2\%}$-stress

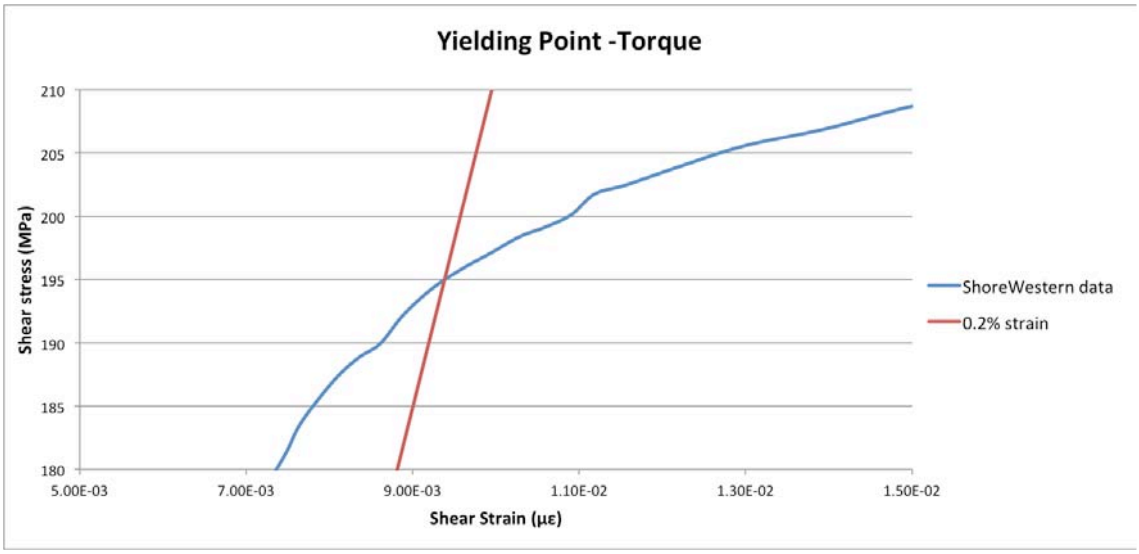

Figure 11.43: detail of the torque yielding point

The intersection between the DIC data curve and the 0.2% strain straight line locate the torque yielding point, which in this case occurs at a stress equal to 195MPa.

Below is reported a table, which summarizes the most important values of this test.

Name of the specimen	7A
Lode Angle	20°
Length (mm)	120
Diameter (mm)	29.64
Tensile Yield point: stress (MPa)	143
Tensile Yield point: strain (με)	0.0043
Torque Yield point: stress (MPa)	195
Torque Yield point: strain (με)	0.0096
Tensile peak point: stress (MPa)	163.59
Tensile peak point: strain (με)	0.036
Torque peak point: stress (MPa)	250.36
Torque peak point: strain (με)	0.216
Tensile failure point: stress (MPa)	180
Tensile failure point: strain (με)	0.059
Torque failure point: stress (MPa)	242.25
Torque failure point: strain (με)	0.429
Tensile yield load (kN)	98.67
Torque yield load (Nm)	997.01
Torque yield twist (°)	3.27
Tensile failure load (kN)	124.2
Torque failure load (Nm)	1238.6

Torque failure twist (°)	199.22
E (GPa)	69746
G (GPa)	27667

Some pictures of the specimen and its failure are now reported.

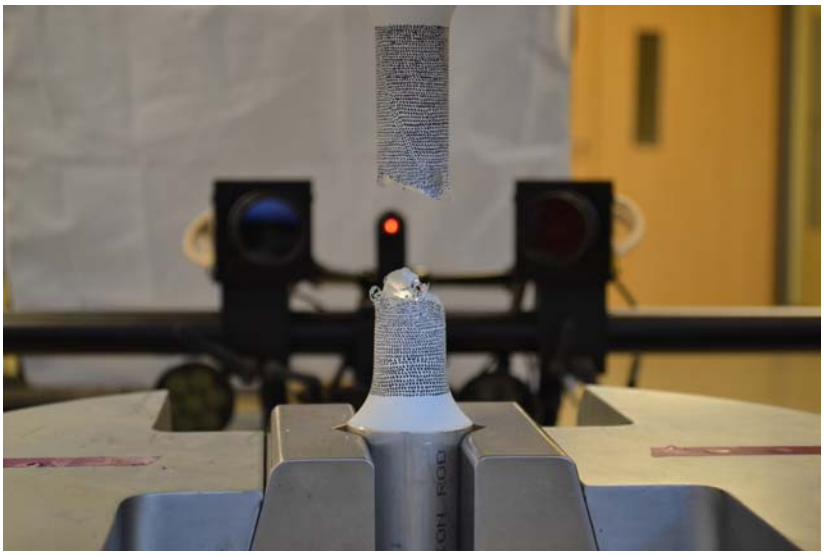

Figure 11.44: specimen 7A failed

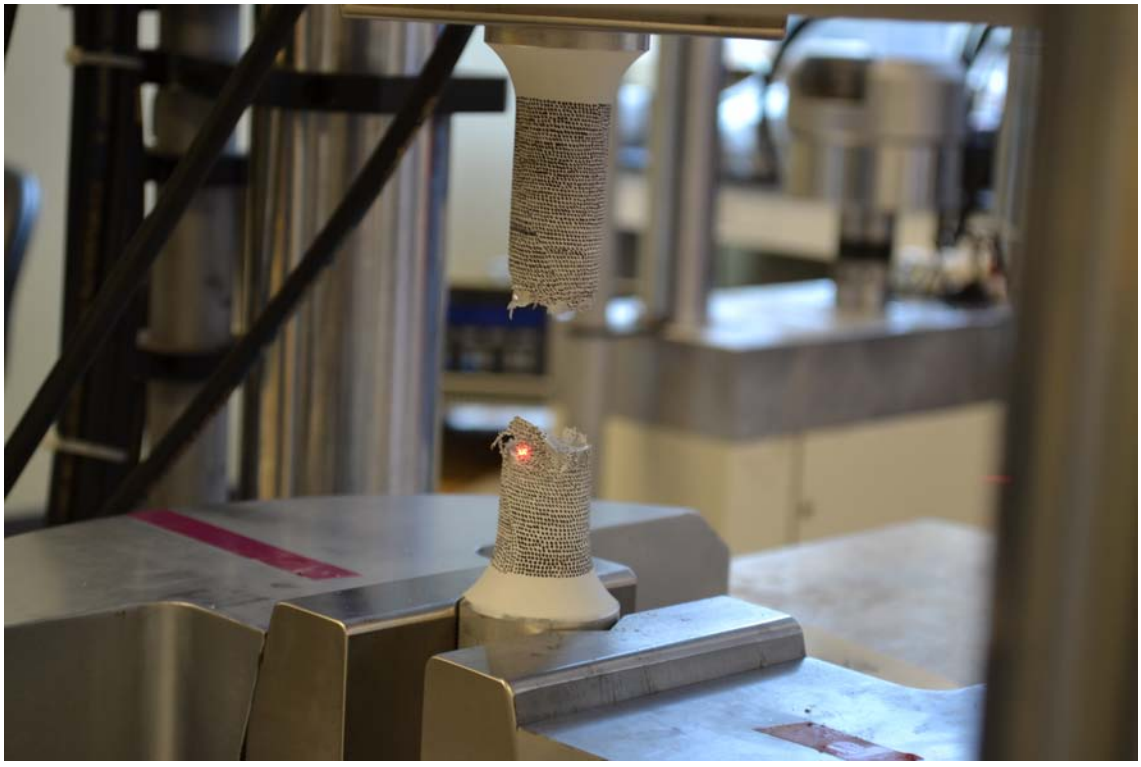

Figure 11.45: collapse of the specimen

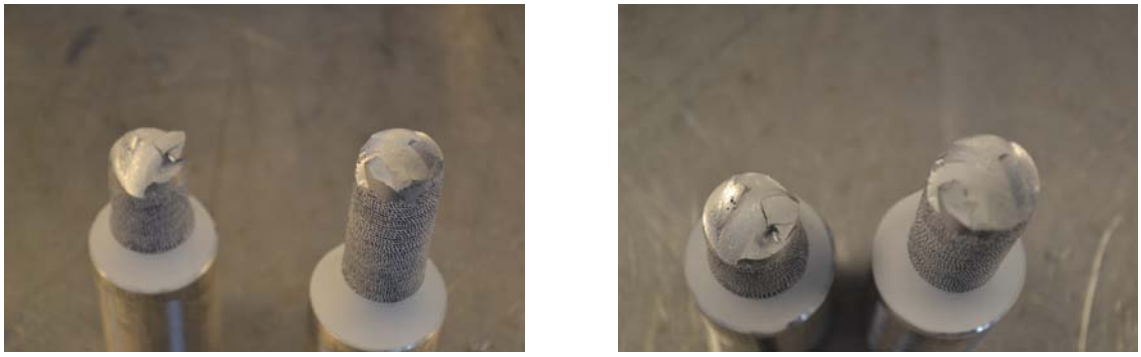

Figure 11.46: failure of the specimen

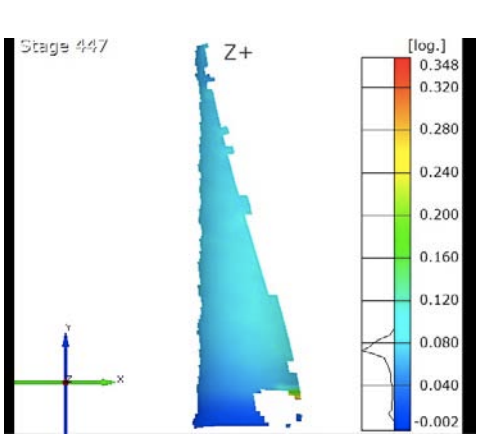

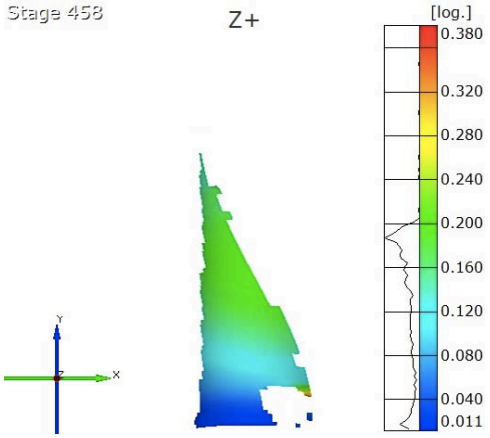

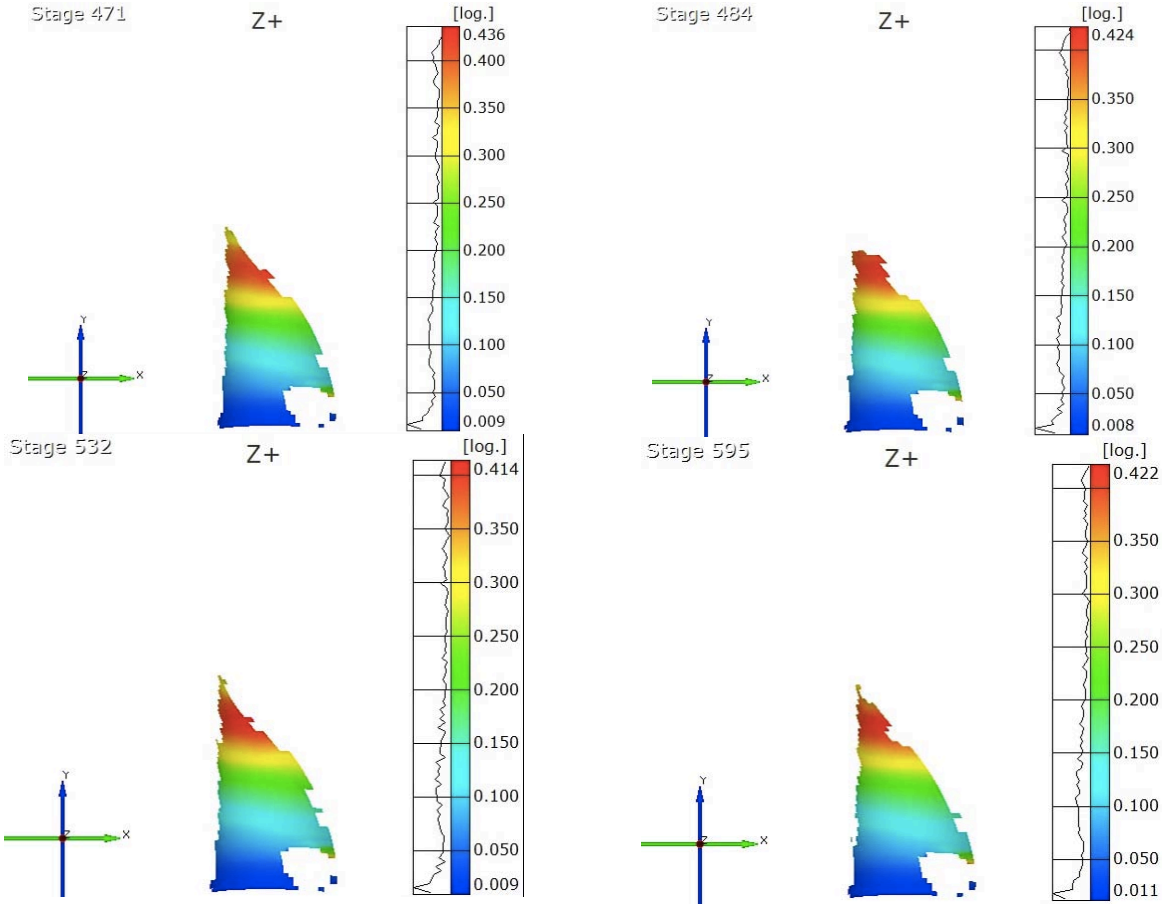

Figure 11.47: contour of the strain in the vertical direction: images obtained by post processing the DIC data recorded

11.4 Torsion Test – Lode angle θ=30°

The torsion test was performed on specimen number 4A, whose actual geometry is reported in section 9.1. The nominal values of the yield stress, yield strain and yield force were calculated from the mechanical properties of the material and from the actual geometry of the specimen:

Specimen 4A-nominal values				
Diameter D	29.92	[mm]	1.178	[in]
Length B	125	[mm]	4.92	[in]
σy	260	[Mpa]	37709.88	[lb/in^2]
E	68900	[Mpa]	9993118.2	[lb/in^2]
A	703.09	[mm^2]	1.09	[in^2]
Ty	0.79	[kNm]	6.99	[kip-in]
αy	0.05	[rad]	2.764	[°]

The experiment was performed in torque control.

Some graphs representing the data collected from the Shore Western software and from the DIC system are reported and commented below.

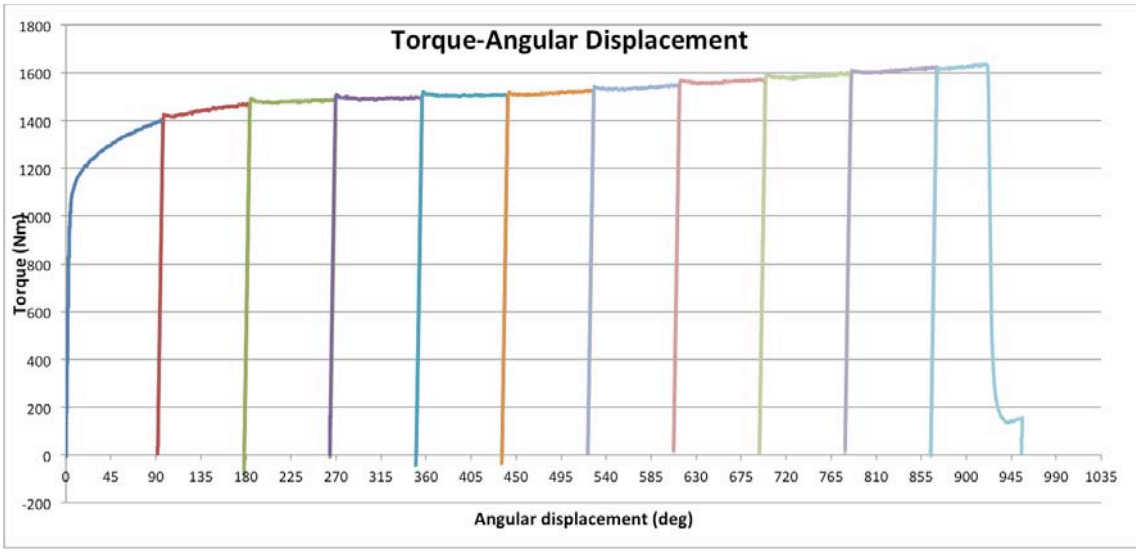

Figure 11.48: torque-twist diagram of the Shore Western data

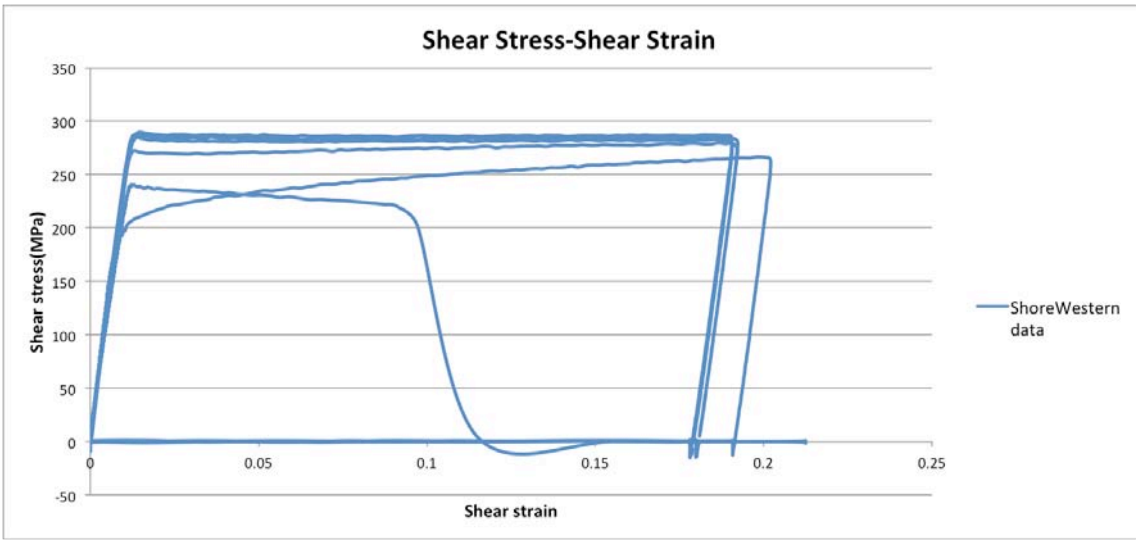

Figure 11.49: shear stress-shear strain diagram of the Shore Western.

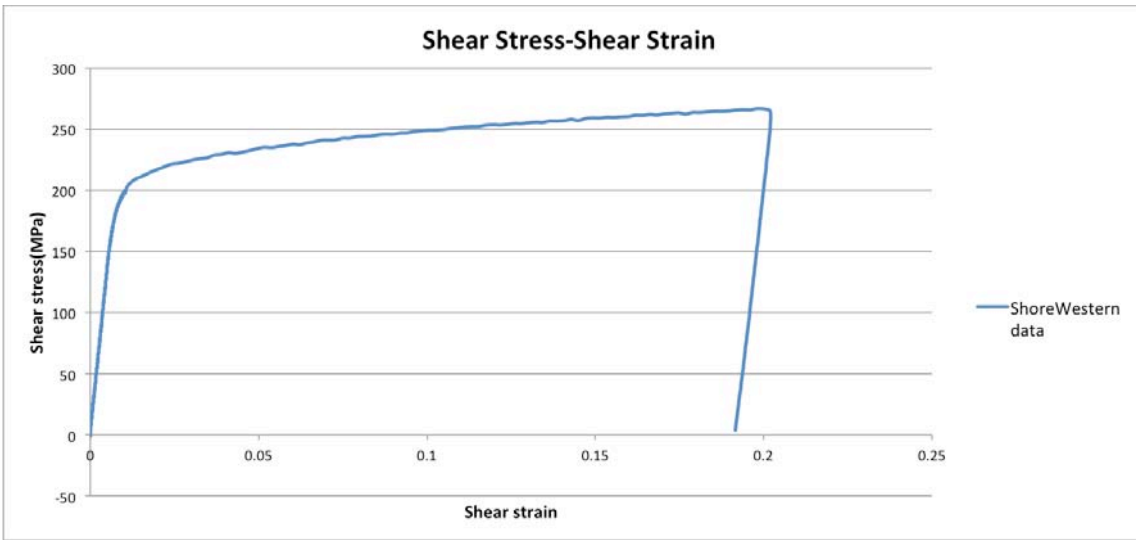

Figure 11.50: shear stress-shear strain diagram of the first cycle; Shore Western data

From figures 11.49 and 11.50 it is possible to observe the behavior of the specimen under torsion. The strain is reported in με and is calculated as the true strain.

The aluminum specimen under torque shows a linear behavior in the first part of the shear stress-shear strain diagram and at a certain stress between 190 and 200 MPa yielding occurs. After yielding we have an hardening behavior till unloading is applied. The second cycle shows a wider linear behavior in fact in

the second cycle, plastification occurs at an axial stress between 260 and 270 MPa. The peak is reached at around 280 MPa.
In order to evaluate the shear modulus G of the material, the elastic part of the shear stress-shear strain diagram is considered and a trend line is drawn.

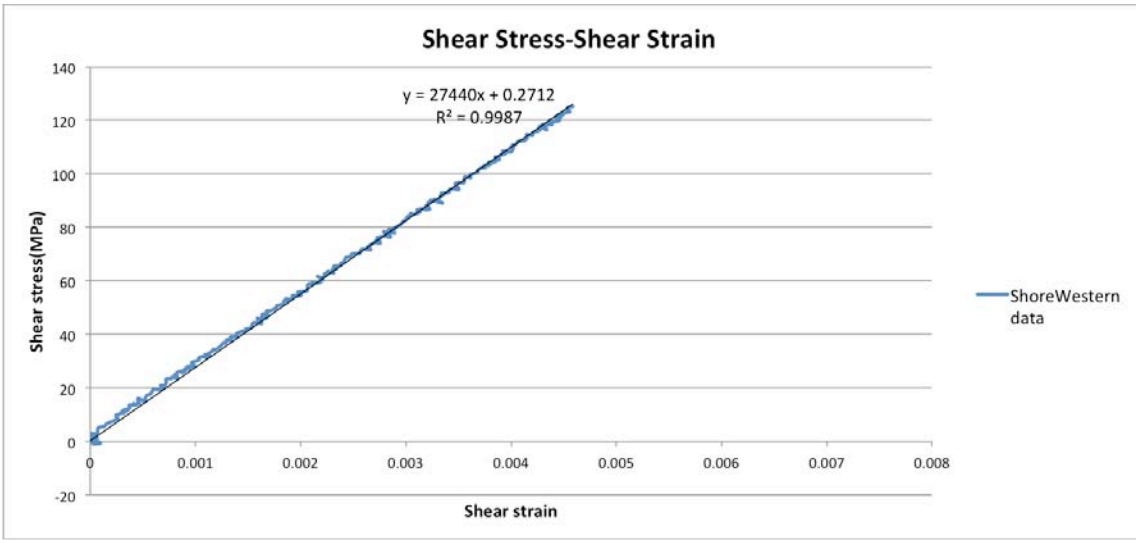

Figure 11.51: first part of the shear stress-shear strain diagram before yielding of the Shore Western data, interpolated with a trend line

The slope of the trend line represents the shear modulus G, which, from the Shore Western data turns out to be equal to 27440 MPa. The nominal value of G for the aluminum 6061-T6 is 26000 MPa, very similar to the value obtained from the Shore Western data.

To detect the precise point of yielding as it regards torque, it is evaluate as the so-called $\sigma_{0.2\%}$-stress, i.e. the stress at which the remaining plastic strain after unloading is equal to 0.2%.

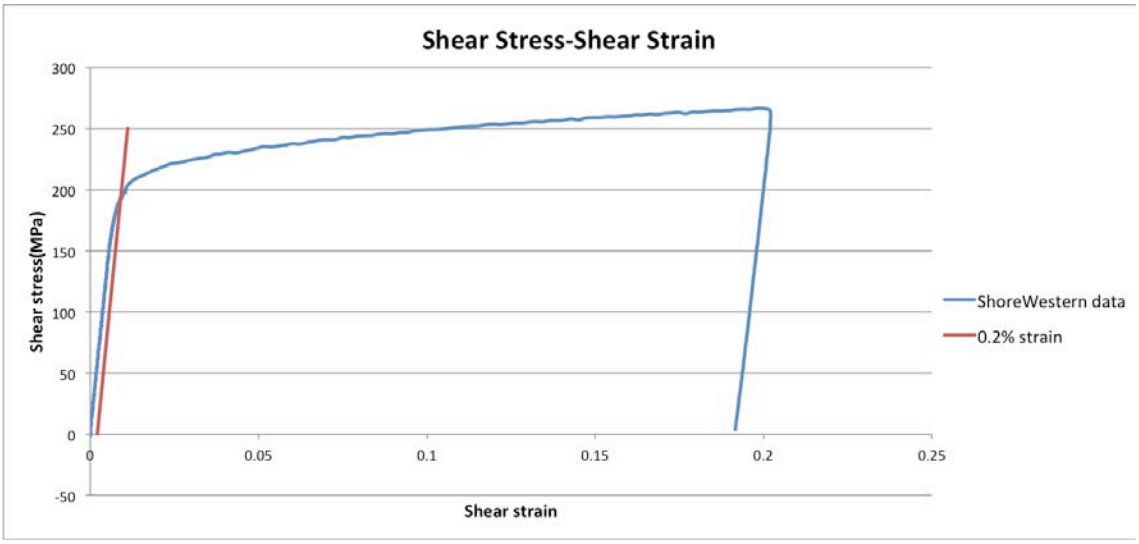

Figure 11.52: yielding point evaluate as the $\sigma_{0.2\%}$-stress

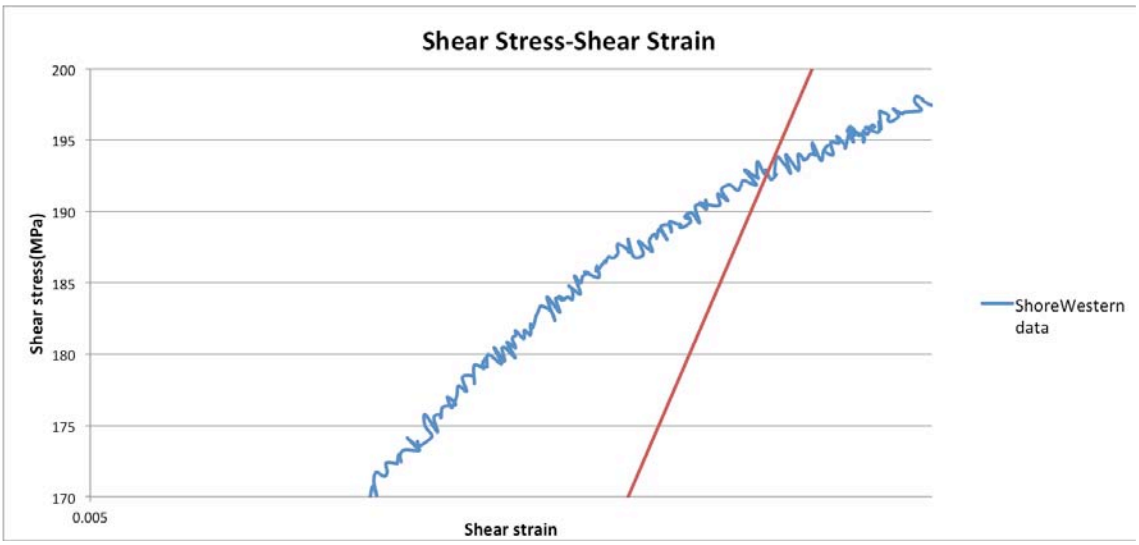

Figure 11.53: detail of the torque yielding point

The intersection between the DIC data curve and the 0.2% strain straight line locate the yielding point, which in this case occurs at a stress equal to 193MPa.

Below is reported a table, which summarizes the most important values of this test.

Name of the specimen	4A
Lode Angle	30°
Length (mm)	125
Diameter (mm)	29.92

Torque Yield point: stress (MPa)	193
Torque Yield point: strain (με)	0.0094
Torque failure point: stress (MPa)	310
Torque yield twist (°)	3.36
Torque failure twist (°)	945
Torque failure load (Nm)	1015.01
G (GPa)	27440

Some pictures of the specimen and its failure are now reported.

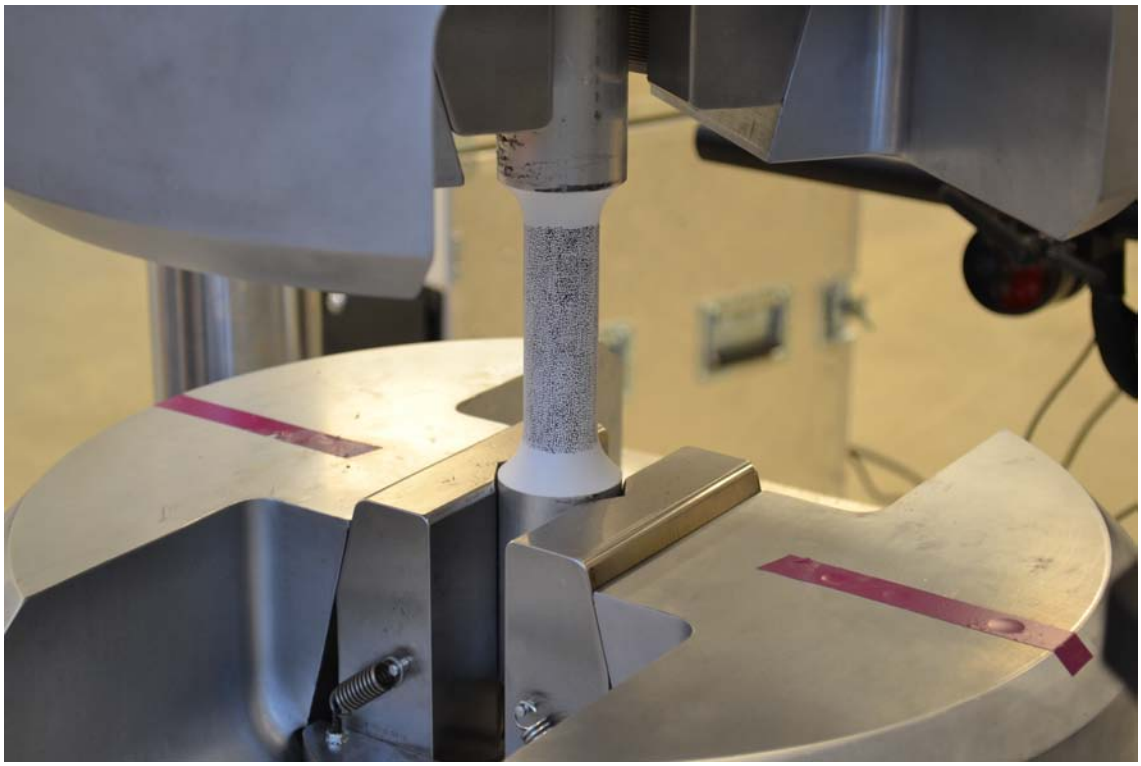

Figure 11.54: specimen 4A in the grips

Figure 11.55: specimen 4A failed

Figure 11.56: collapse of the specimen

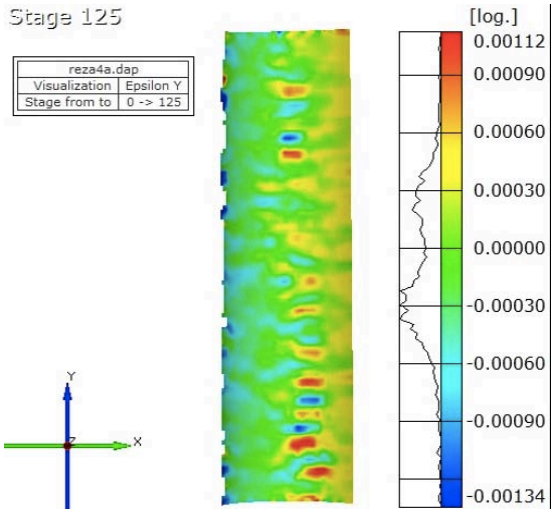
Stage 125
reza4a.dap
Visualization | Epsilon Y
Stage from to | 0 -> 125
[log.]
0.00112
0.00090
0.00060
0.00030
0.00000
-0.00030
-0.00060
-0.00090
-0.00134
Y
X
Z

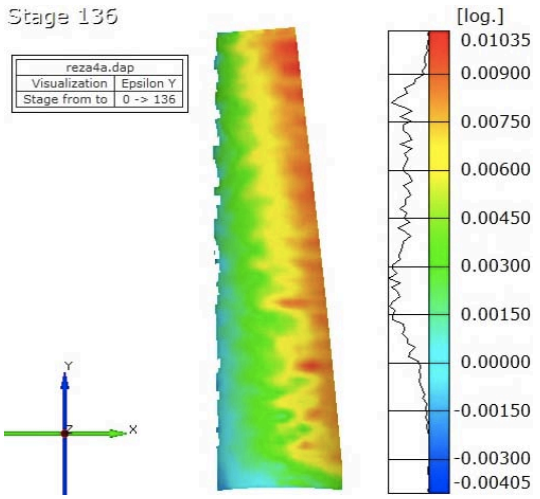
Stage 136
reza4a.dap
Visualization | Epsilon Y
Stage from to | 0 -> 136
[log.]
0.01035
0.00900
0.00750
0.00600
0.00450
0.00300
0.00150
0.00000
-0.00150
-0.00300
-0.00405
Y
X
Z

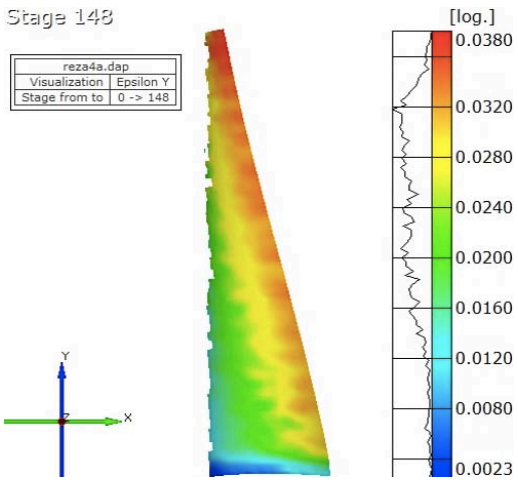
Stage 148
reza4a.dap
Visualization | Epsilon Y
Stage from to | 0 -> 148
[log.]
0.0380
0.0320
0.0280
0.0240
0.0200
0.0160
0.0120
0.0080
0.0023
Y
X
Z

Figure 11.57: contour of the strain in the vertical direction: images obtained by post processing the DIC data recorded

11.5 Tension - Torsion Test – Lode angle θ=40°

The compression torsion test was performed on specimen number 10A, whose actual geometry is reported in section 9.1. The nominal values of the yield stress, yield strain and yield force were calculated from the mechanical properties of the material and from the actual geometry of the specimen:

Specimen 10A-nominal values				
Diameter D	29.67	[mm]	1.68	[in]
Length B	125	[mm]	4.92	[in]
σy	260	[Mpa]	37709.88	[lb/in^2]
E	68900	[Mpa]	9993118.2	[lb/in^2]
A	691.39	[mm^2]	2.22	[in^2]
Fy	-93.95	[kN]	-21.12	[kips]
Ty	1.10	[kNm]	9.710	[kip-in]

The experiment was performed in torque control and consequently in traction control since the ratio between tension and torsion in the imperial units must be kept 2.175 (cfr. section 9.4).
Two torque rate stages were defined:

- I rate: 1 kip-in/60sec (0. 113 kNm/60sec) for the elastic region;
- II rate: 1 kip-in/150sec (0.113 kNm/120sec) for the plastic region.

Some graphs representing the data collected from the Shore Western software and from the DIC system are reported and commented below.

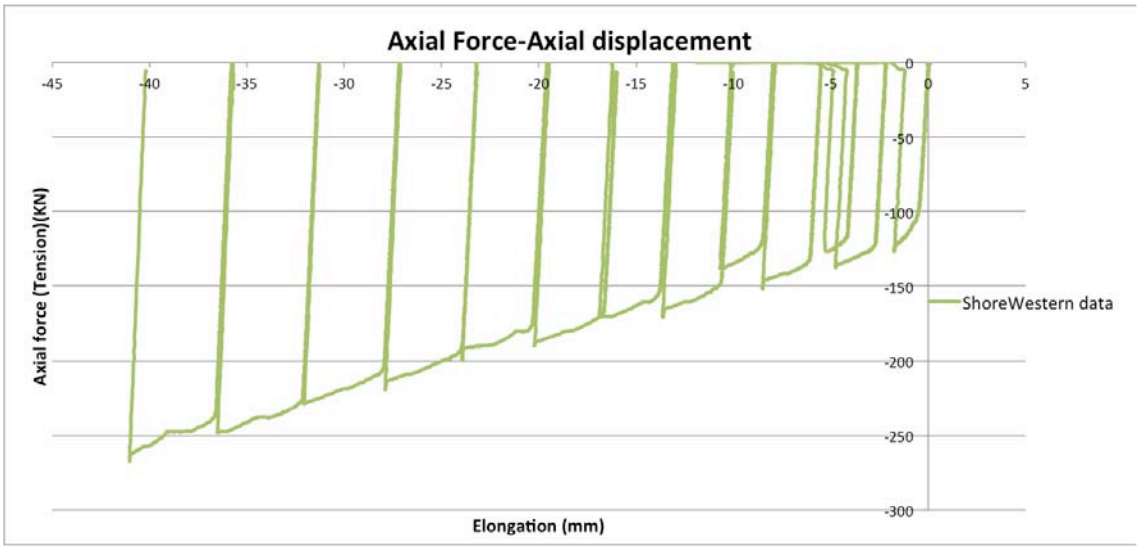

Figure 11.58: axial force-displacement diagram of the Shore Western data

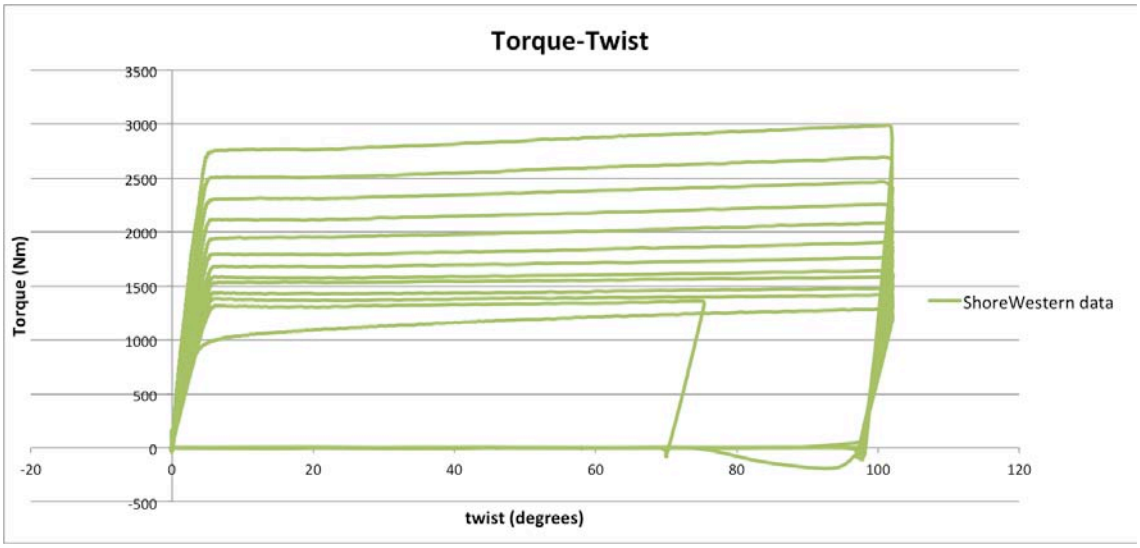

Figure 11.59: torque-twist diagram of the Shore Western data

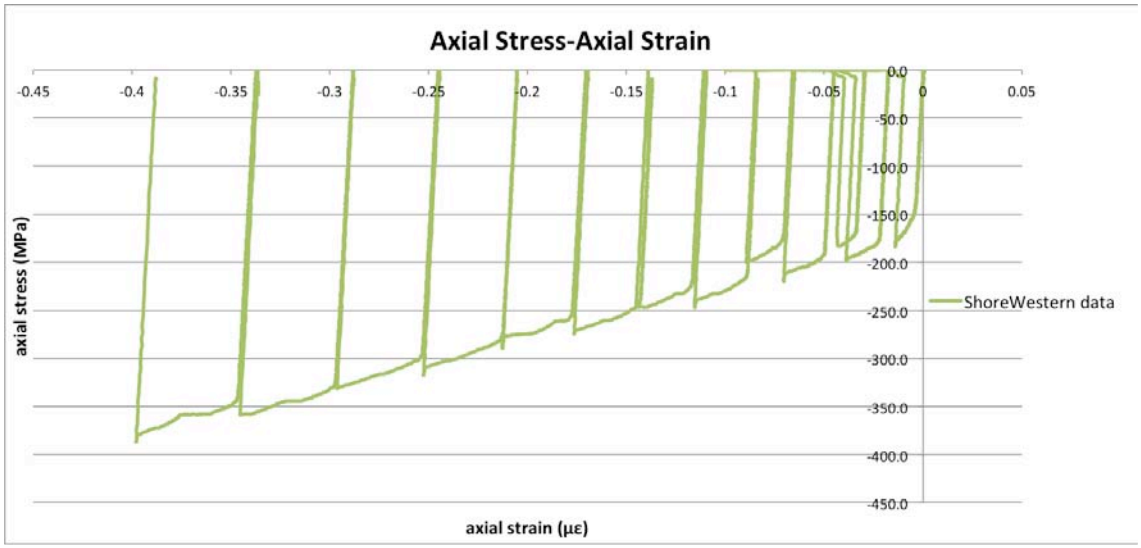

Figure 11.60:axial stress-axial strain diagram of the Shore Western data.

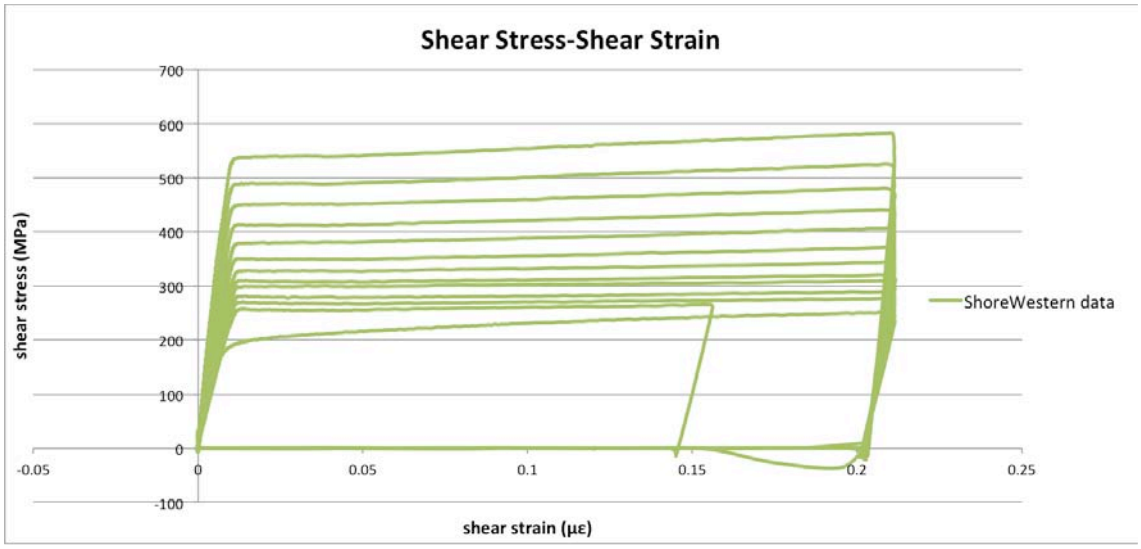

Figure 11.61: shear stress-shear strain diagram of the Shore Western.

From figures 11.61 and 11.62 it is possible to observe the behavior of the specimen under compression-torsion. The strain is reported in με and is calculated as the true strain.

The aluminum specimen shows a linear behavior in the first part of the axial stress-axial strain diagram and at a certain stress around -120 MPa yielding occurs. After yielding we have an hardening behavior till unloading is applied. The peak is reached at around -180 MPa in the first cycle. As it regards the behavior of the specimen under torque we notice a linear behavior in the first part of the shear stress-shear strain diagram and at a certain stress between 180 and

190 MPa yielding occurs. After yielding we have an hardening behavior till unloading is applied.

In order to evaluate the shear modulus G of the material, the elastic part of the shear stress-shear strain diagram is considered and a trend line is drawn.

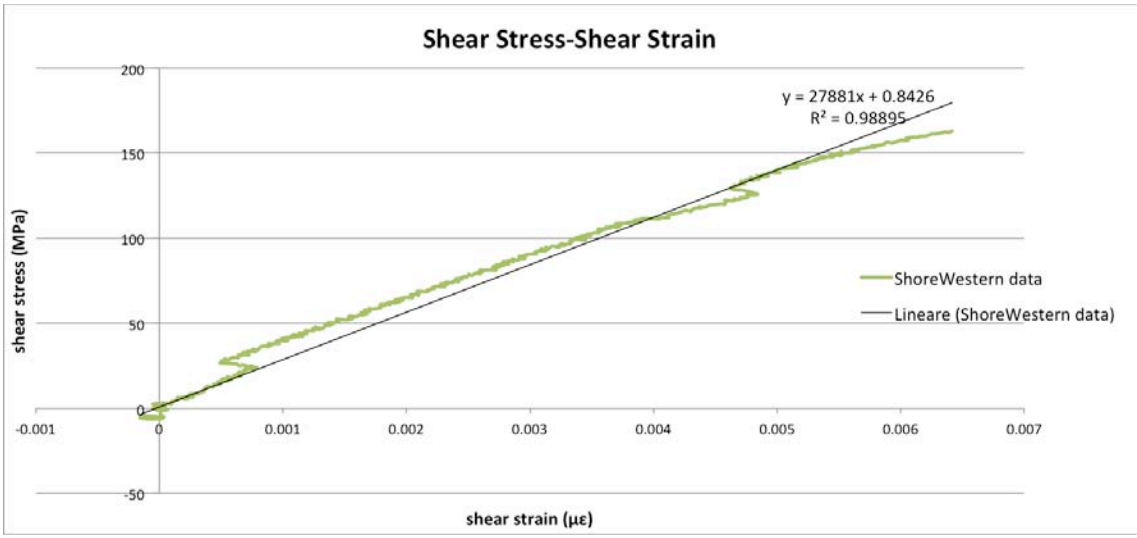

Figure 11.62: first part of the shear stress-shear strain diagram before yielding of the Shore Western data, interpolated with a trend line

The slope of the trend line represents the shear modulus G, which, from the Shore Western data turns out to be equal to 27881 MPa. The nominal value of G for the aluminum 6061-T6 is 26000 MPa, very similar to the value obtained from the Shore Western data.

In order to evaluate the Young modulus E of the material, the elastic part of the axial stress-axial strain diagram is considered and a trend line is drawn.

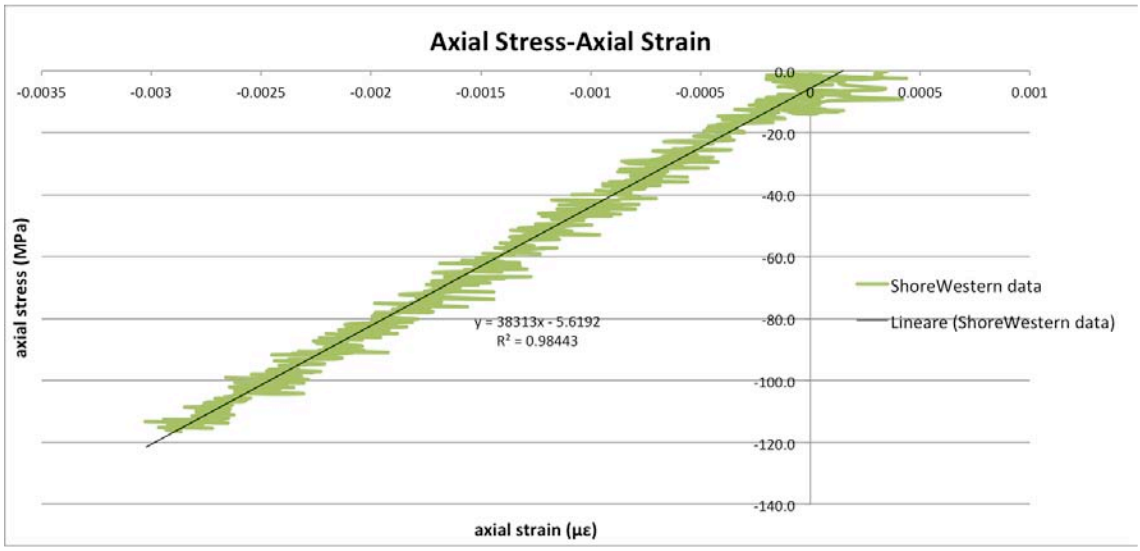

Figure 11.63: first part of the axial stress-axial strain diagram before yielding of the Shore Western data interpolated with a trend line

The slope of the trend line represents the Young modulus, which from the Shore Western data turns out to be equal to 38313 MPa. Checking this value with the DIC data it can be noticed that the true value is 69875 MPa. The nominal value of E for the aluminum 6061-T6 is 69000 MPa.

To detect the precise point of yielding as it regards the axial force, it is evaluate as the so-called $\sigma_{0.2\%}$-stress, i.e. the stress at which the remaining plastic strain after unloading is equal to 0.2%.

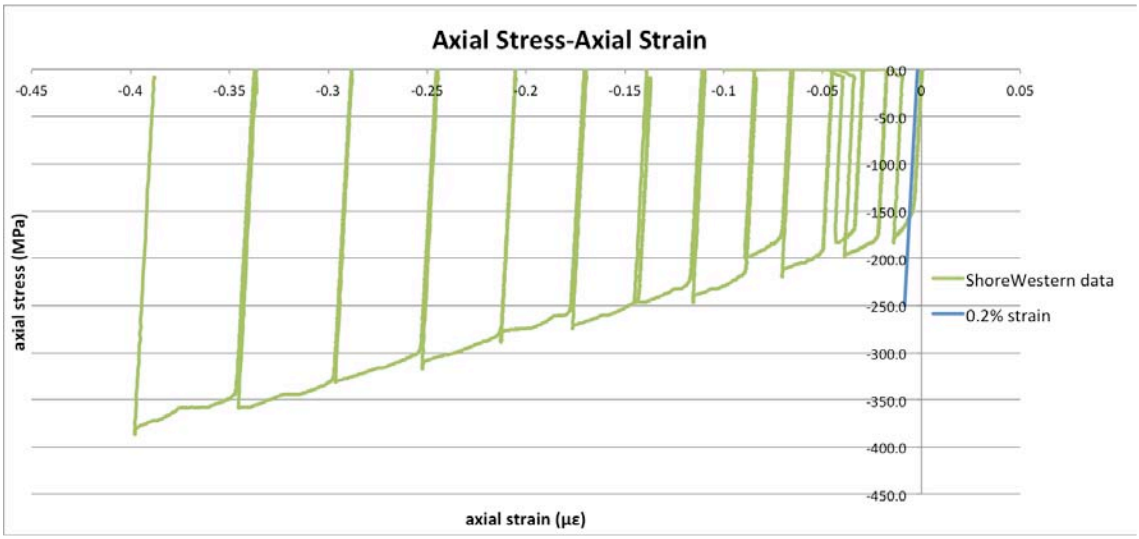

Figure 11.64: yielding point for the axial force evaluate as the $\sigma_{0.2\%}$-stress

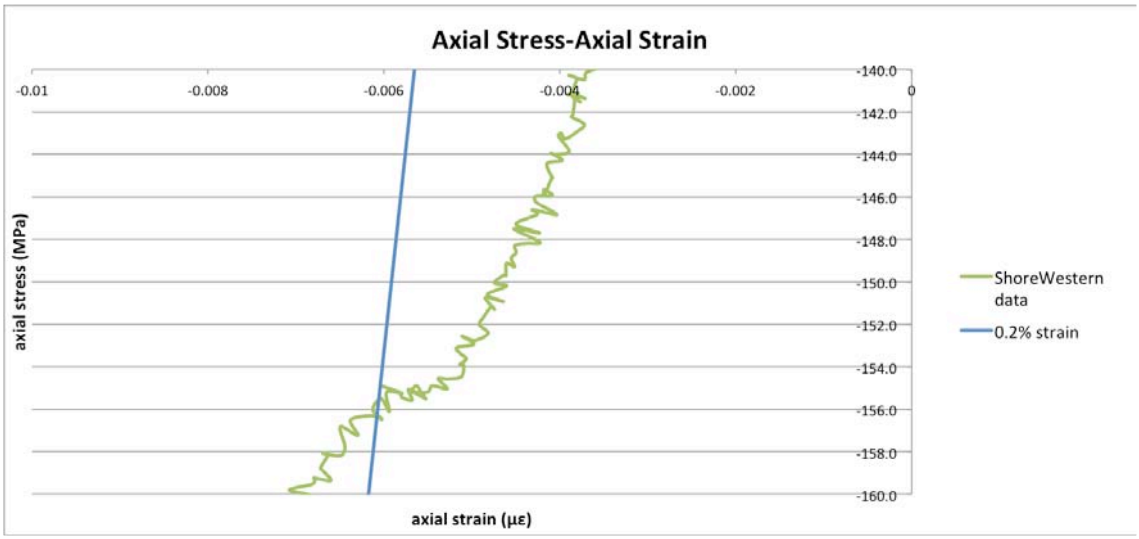

Figure 11.65: detail of the tensile yielding point

The intersection between the Shore Western data curve and the 0.2% strain straight line locate the yielding point, which in this case occurs at a stress equal to -156 MPa.

The same procedure is used to detect the precise point of yielding as it regards the torque.

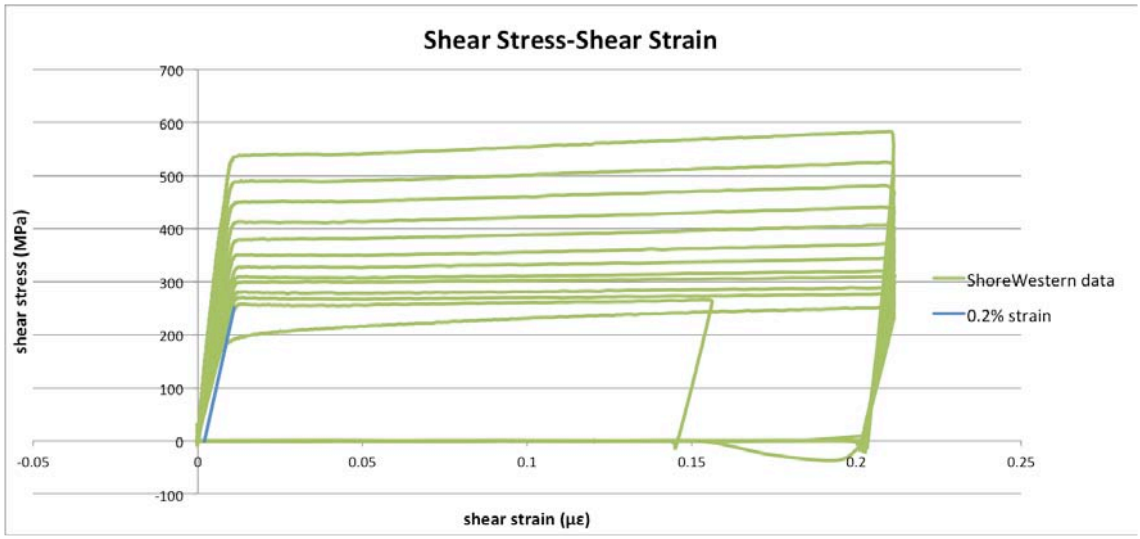

Figure 11.66: yielding point for the torque evaluate as the $\sigma_{0.2\%}$-stress

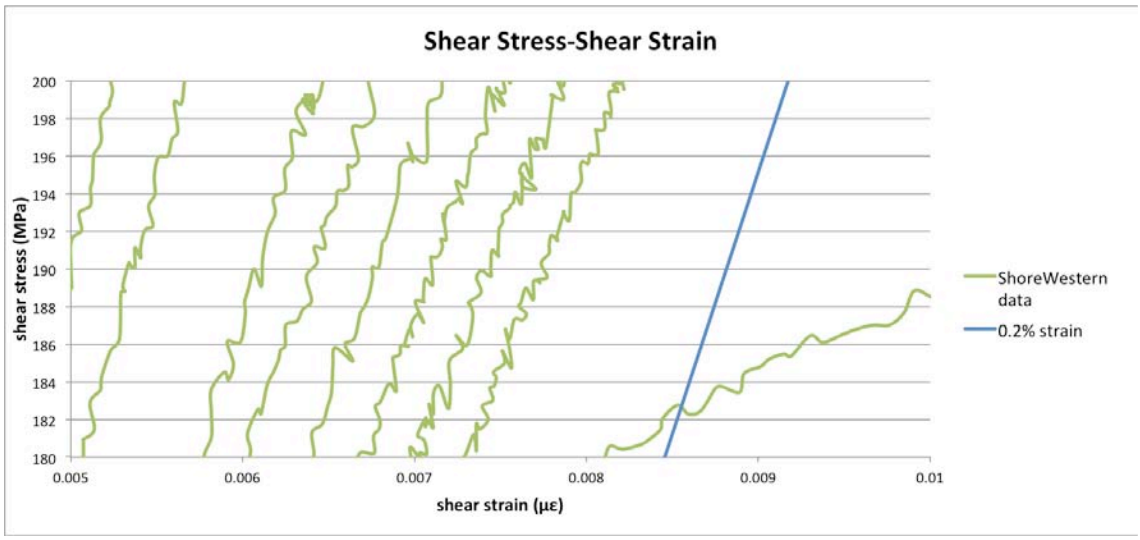

Figure 11.67: detail of the torque yielding point

The intersection between the DIC data curve and the 0.2% strain straight line locate the torque yielding point, which in this case occurs at a stress equal to 182MPa.

Below is reported a table, which summarizes the most important values of this test.

Name of the specimen	10A
Lode Angle	40°
Length (mm)	125
Diameter (mm)	29.67

Tensile Yield point: stress (MPa)	-156
Torque Yield point: stress (MPa)	182
Tensile yield load (kN)	-107.86
Torque yield load (Nm)	933.37
Torque yield twist (°)	3.15
Number of cycles performed	14
E (GPa)	69875
G (GPa)	27881

Some pictures of the specimen and its failure are now reported.

Figure 11.68: specimen 10A in the grips after 3 cycles

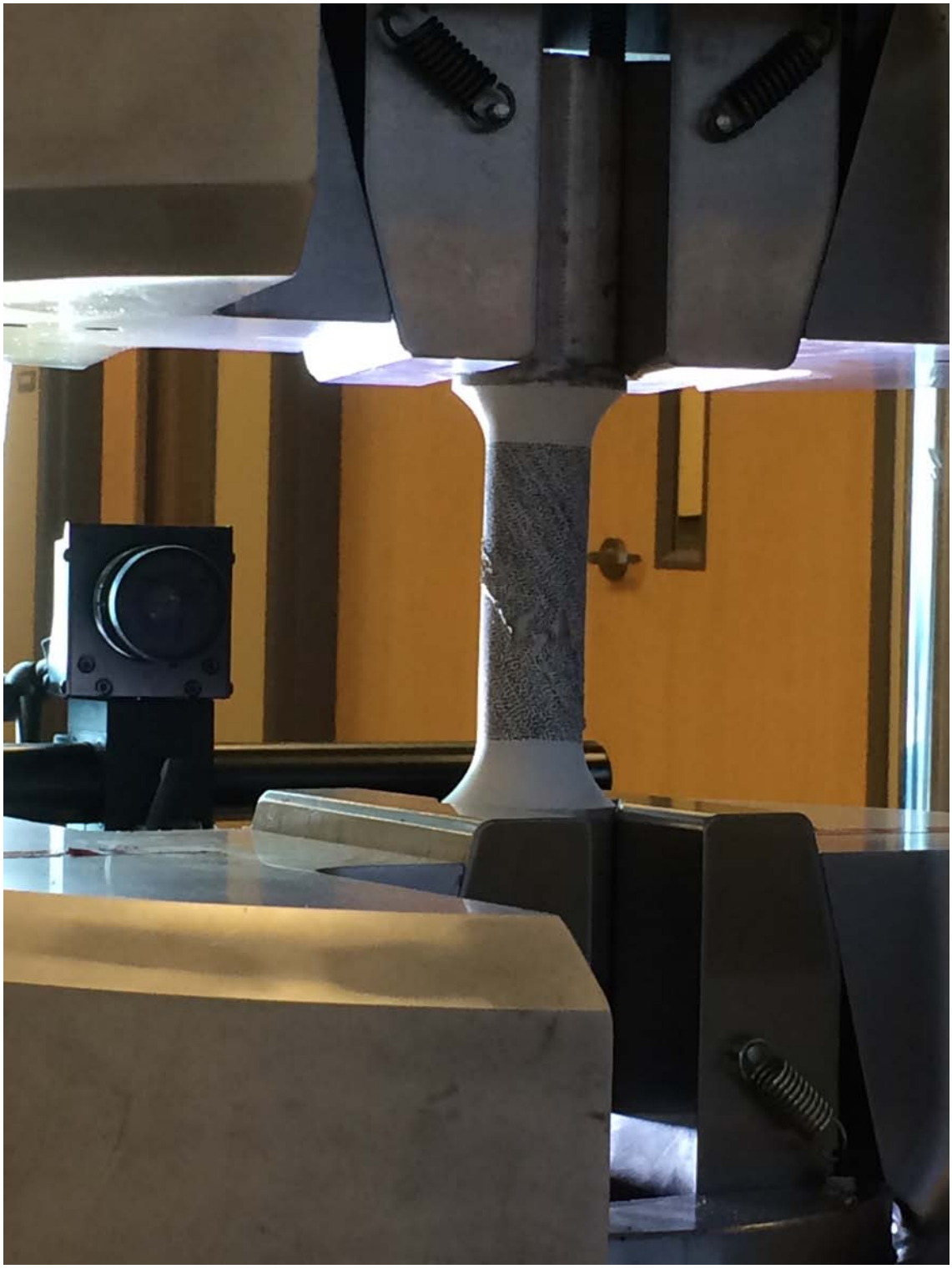

Figure 11.69: specimen 8A under compression-torsion

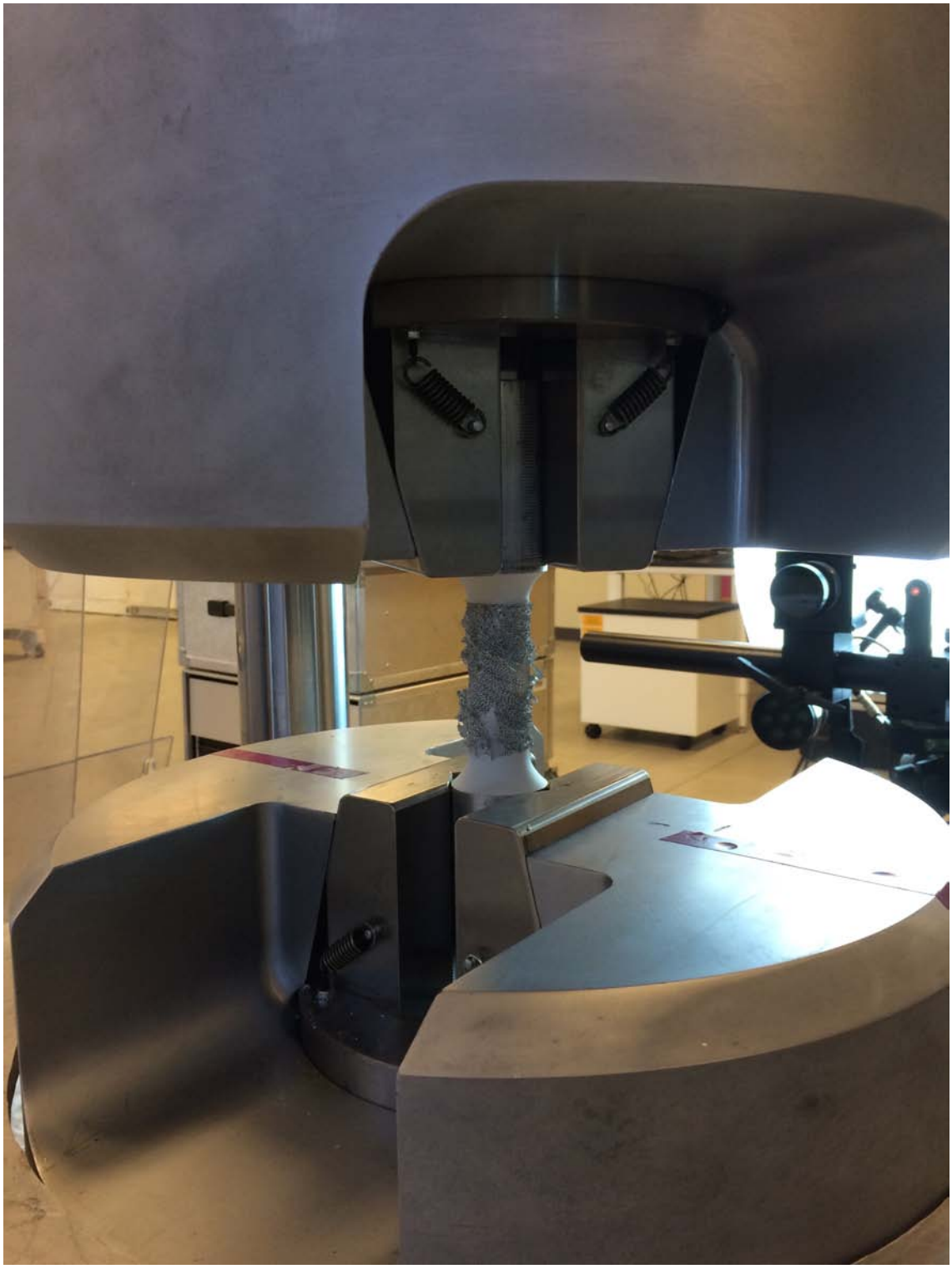

Figure 11.70: specimen 10A after 7 cycles

Figure 11.71: specimen after 14 cycles; a shortening of 3.8 cm is noticed.

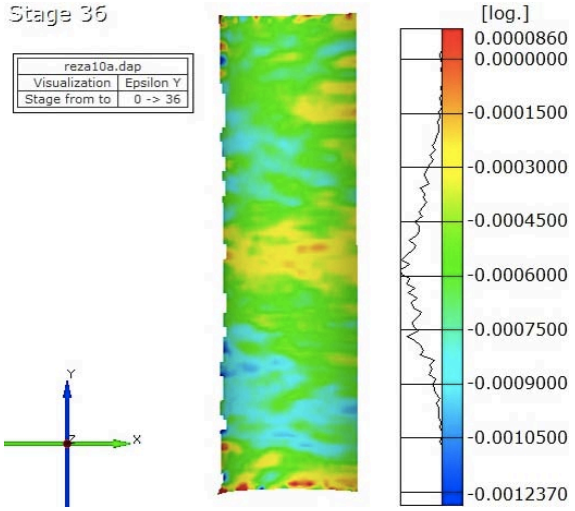
Stage 36
reza10a.dap
Visualization | Epsilon Y
Stage from to | 0 -> 36
[log.]
0.0000860
0.0000000
-0.0001500
-0.0003000
-0.0004500
-0.0006000
-0.0007500
-0.0009000
-0.0010500
-0.0012370
Y
Z
X

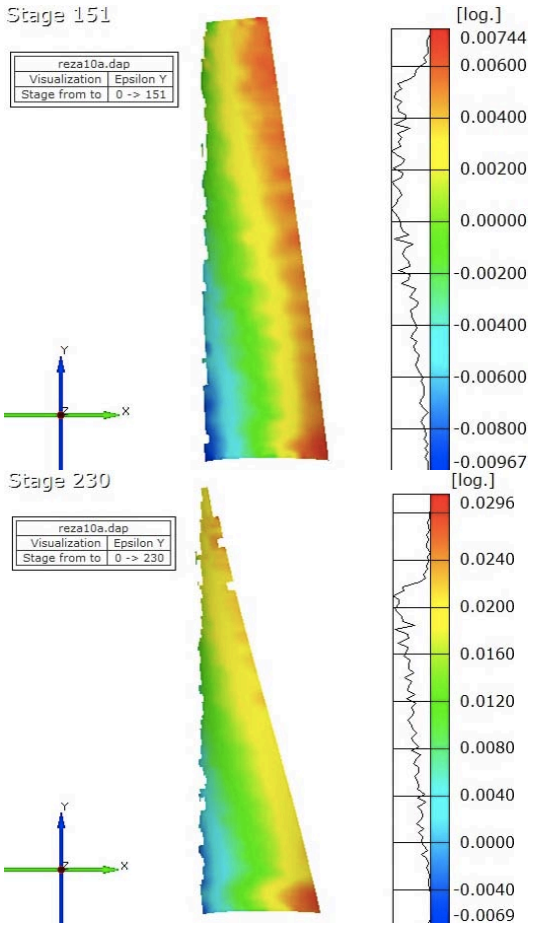
Stage 151
reza10a.dap
Visualization | Epsilon Y
Stage from to | 0 -> 151
[log.]
0.00744
0.00600
0.00400
0.00200
0.00000
-0.00200
-0.00400
-0.00600
-0.00800
-0.00967
Y
Z
X
Stage 230
reza10a.dap
Visualization | Epsilon Y
Stage from to | 0 -> 230
[log.]
0.0296
0.0240
0.0200
0.0160
0.0120
0.0080
0.0040
0.0000
-0.0040
-0.0069
Y
Z
X

Figure 11.72: contour of the strain in the vertical direction: images obtained by post processing the DIC data recorded

11.6 Tension - Torsion Test – Lode angle θ=50°

The compression torsion test was performed on specimen number 8A, whose actual geometry is reported in section 9.1. The nominal values of the yield stress, yield strain and yield force were calculated from the mechanical properties of the material and from the actual geometry of the specimen:

Specimen 8A-nominal values				
Diameter D	29.77	[mm]	1.172	[in]
Length B	124	[mm]	4.88	[in]
σy	260	[Mpa]	37709.88	[lb/in^2]
E	68900	[Mpa]	9993118.2	[lb/in^2]
A	696.06	[mm^2]	1.08	[in^2]
Fy	-181.58	[kN]	-40.82	[kips]
Ty	0.84	[kNm]	7.420	[kip-in]

The experiment was performed in torque control and consequently in traction control since the ratio between tension and torsion in the imperial units must be kept 5.5 (cfr. section 9.4).
Two torque rate stages were defined:

- I rate: 4 kip-in/120sec (0.452 kNm/120sec) for the elastic region;
- II rate: 1 kip-in/120sec (0.113 kNm/120sec) for the plastic region.

Some graphs representing the data collected from the Shore Western software and from the DIC system are reported and commented below.

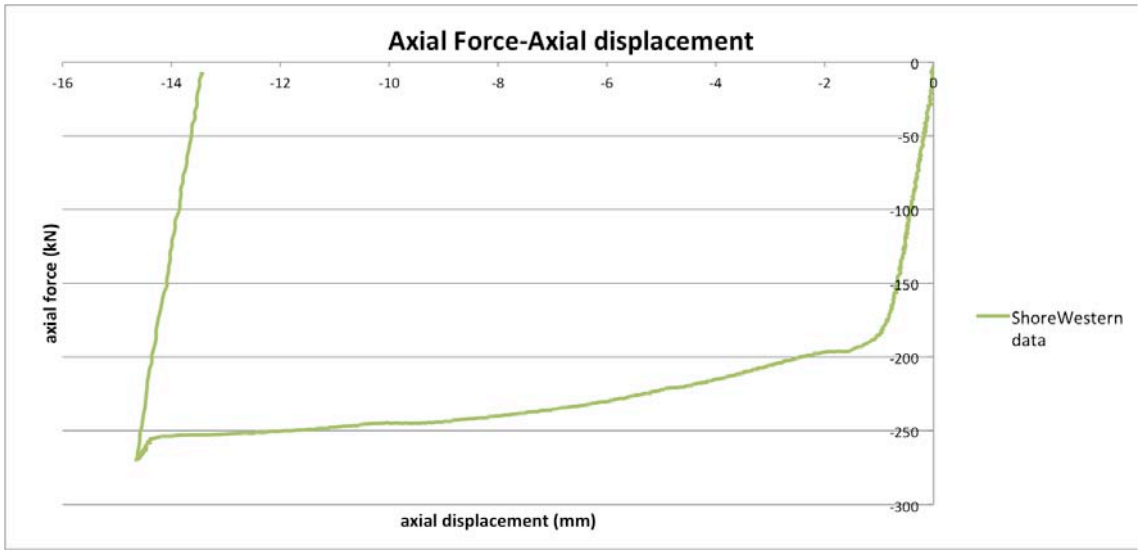

Figure 11.73: axial force-displacement diagram of the Shore Western data

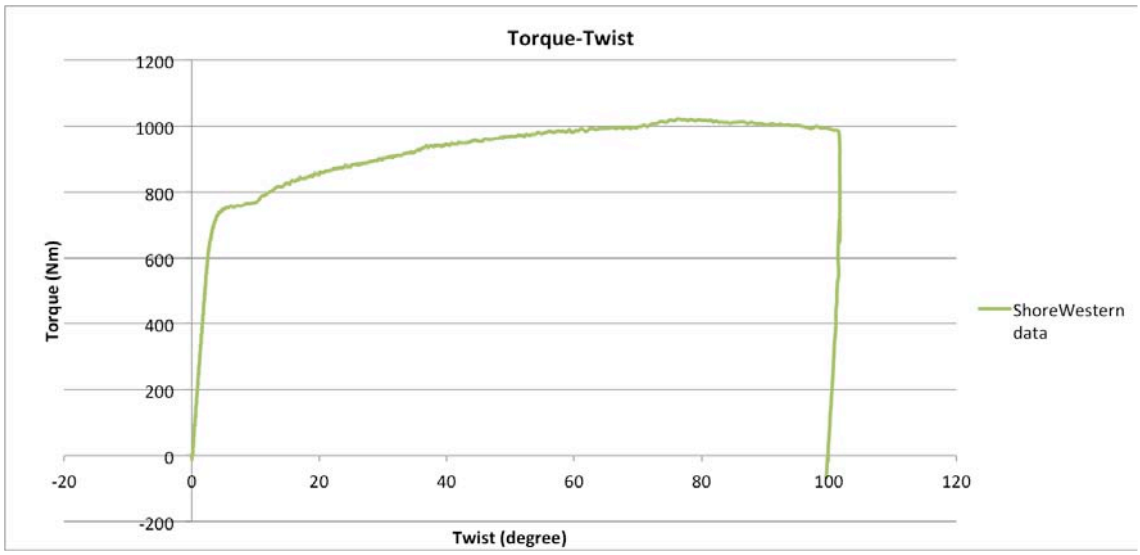

Figure 11.74: torque-twist diagram of the Shore Western data

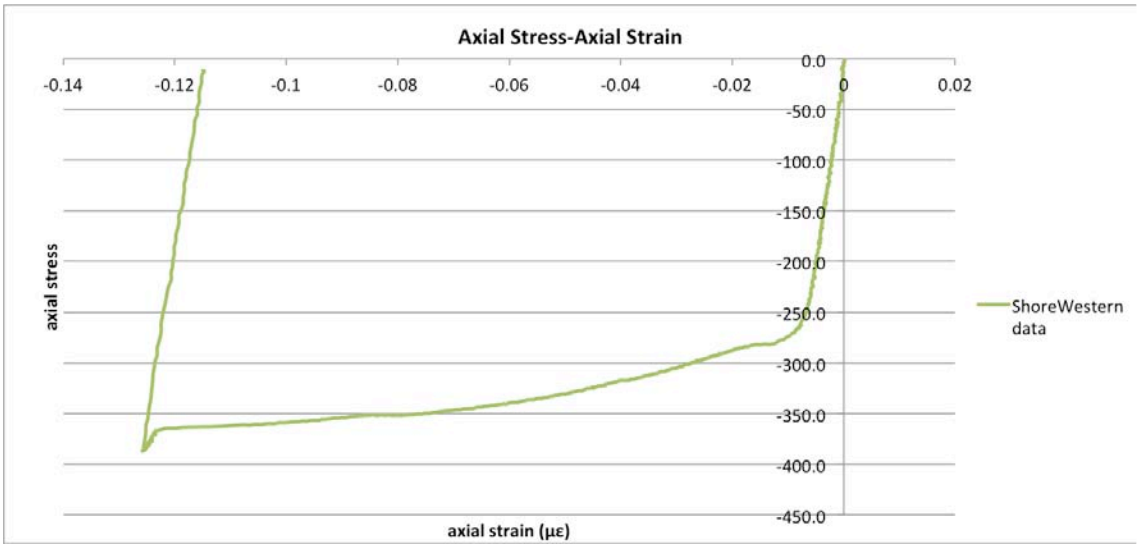

Figure 11.75:axial stress-axial strain diagram of the Shore Western data.

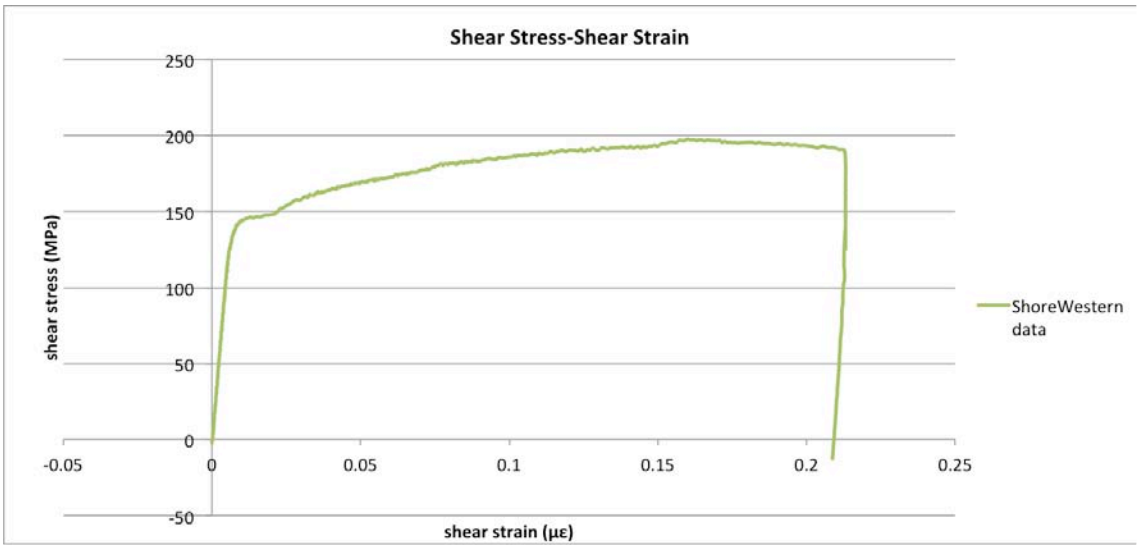

Figure 11.76: shear stress-shear strain diagram of the Shore Western.

From figures 11.76 and 11.77 it is possible to observe the behavior of the specimen under compression-torsion. The strain is reported in με and is calculated as the true strain.

The aluminum specimen shows a linear behavior in the first part of the axial stress-axial strain diagram and at a certain stress around -250 MPa yielding occurs. After yielding we have an hardening behavior till unloading is applied. The peak is reached at around 350 MPa. As it regards the behavior of the specimen under torque we notice a linear behavior in the first part of the shear stress-shear strain diagram and at a certain stress between 140 and 150 MPa

yielding occurs. After yielding we have an hardening behavior till unloading is applied. The peak is reached at around 200 MPa. The post peak behavior shows some softening.

In order to evaluate the shear modulus G of the material, the elastic part of the shear stress-shear strain diagram is considered and a trend line is drawn.

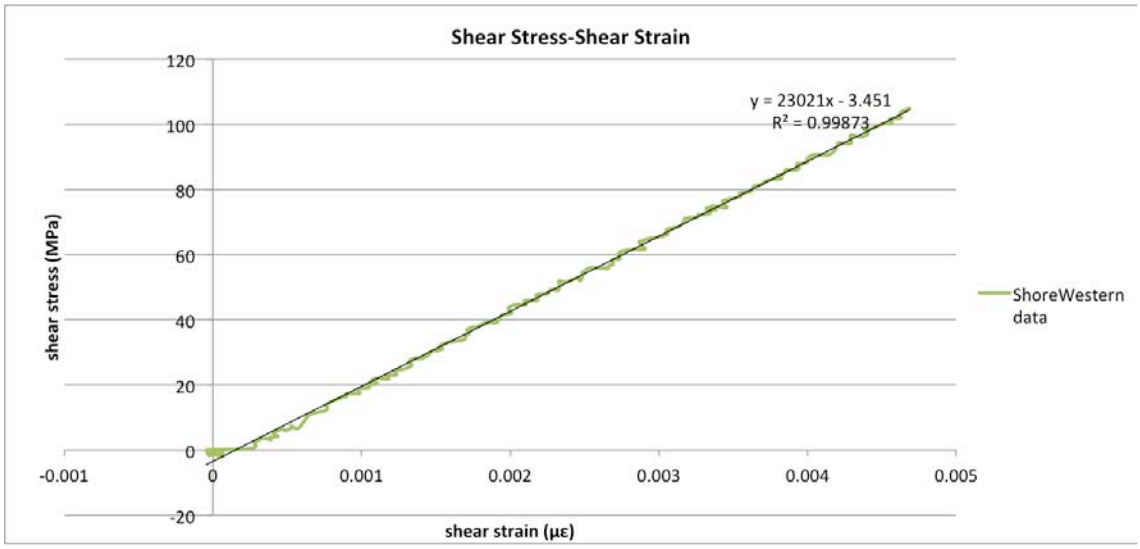

Figure 11.77: first part of the shear stress-shear strain diagram before yielding of the Shore Western data, interpolated with a trend line

The slope of the trend line represents the shear modulus G, which, from the Shore Western data turns out to be equal to 23021 MPa. The nominal value of G for the aluminum 6061-T6 is 26000 MPa, very similar to the value obtained from the Shore Western data.

In order to evaluate the Young modulus E of the material, the elastic part of the axial stress-axial strain diagram is considered and a trend line is drawn.

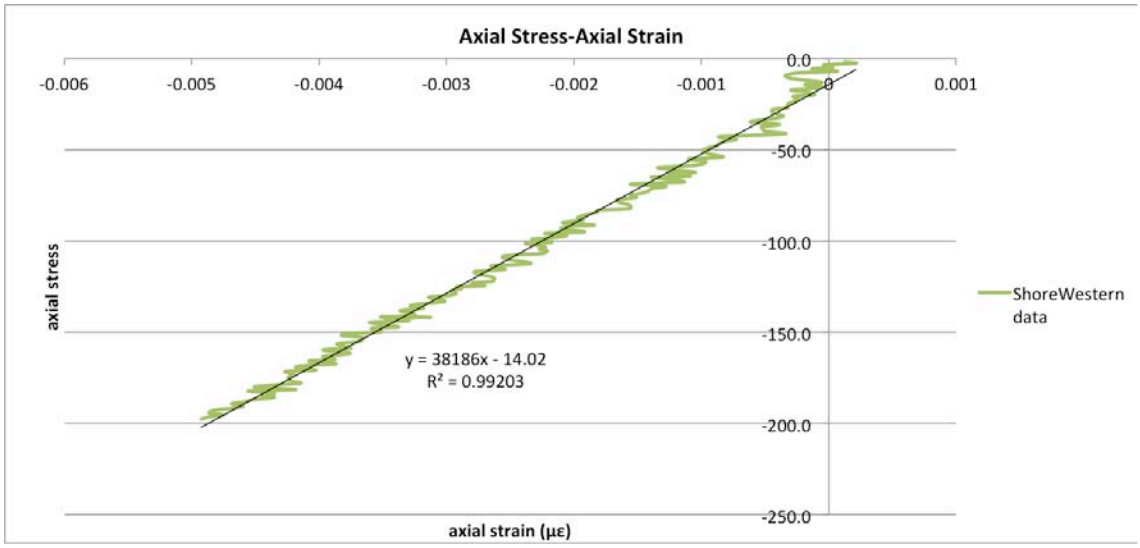

Figure 11.78: first part of the axial stress-axial strain diagram before yielding of the Shore Western data interpolated with a trend line

The slope of the trend line represents the Young modulus, which from the Shore Western data turns out to be equal to 38186 MPa. The nominal value of E for the aluminum 6061-T6 is 69000 MPa, almost two times the one obtained from the Shore Western data. For this reason it was necessary to check the accuracy of this value, looking at the data obtained with the DIC system.

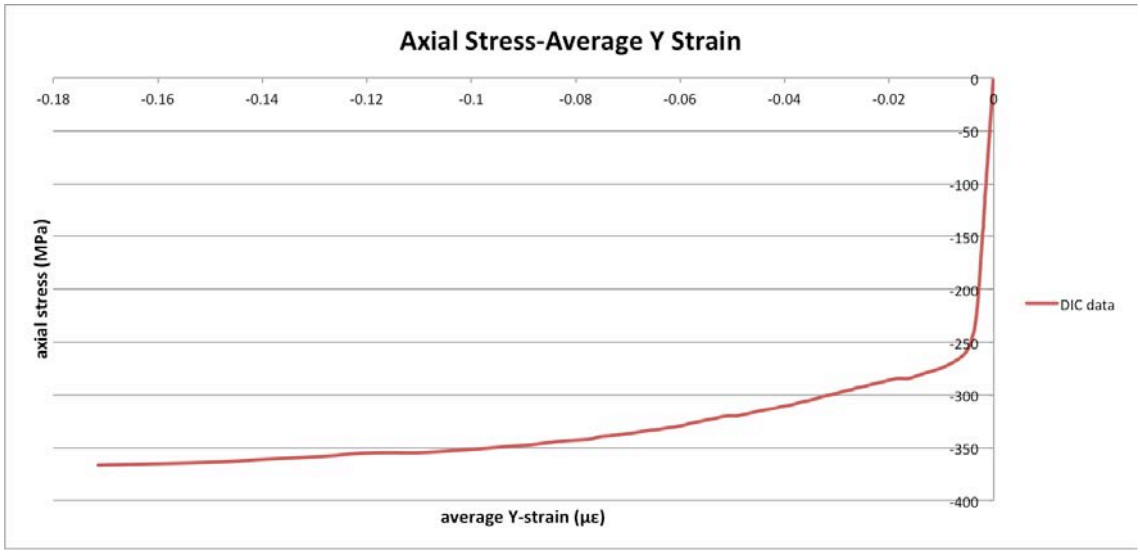

Figure 11.79: axial stress-average Y strain of the DIC data recorded each 10 seconds

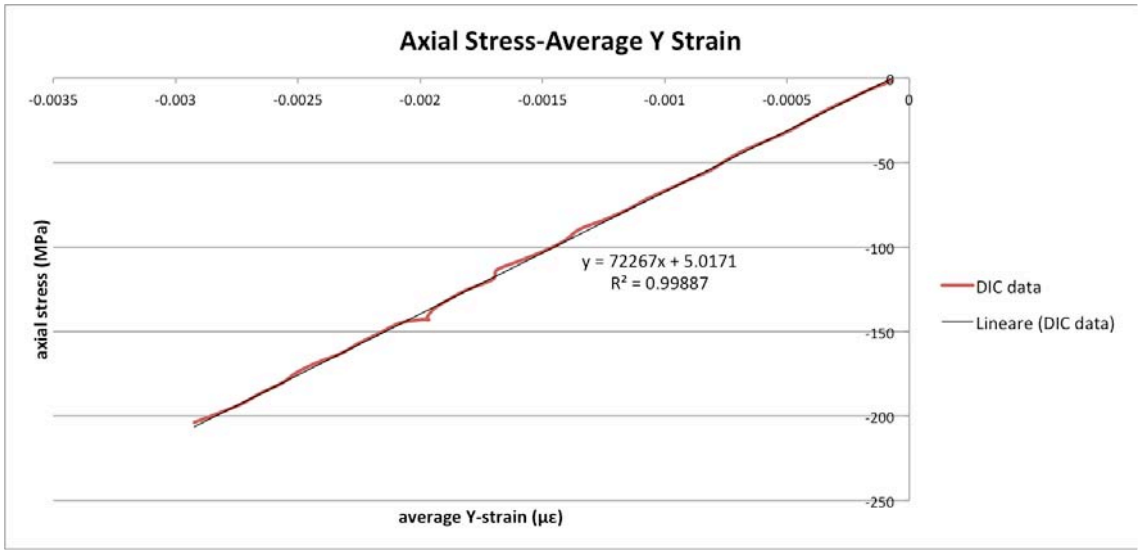

Figure 11.80: first part of the axial stress- average Y strain diagram before yielding of the DIC data recorded each 10 seconds interpolated with a trend line

As it regards the DIC data, we obtain, from the ARAMIS software, the strains in five vertical sections of the specimen and for this reason an average strain of this five was then calculated. The slope of the trend line, which interpolates the DIC data represents the Young modulus, which turns out to be equal to 72267 MPa. This value of E is much closer to the nominal one, which is for the aluminum 6061-T6 is 69000 MPa. For this reason, comparing the Young Modulus obtained from the Shore Western data and the one provided by the DIC data, we concluded that we had some errors during the record of the Shore Western data, which caused an increased value of strain and a lower slope of the trend line, which interpolates the Shore Western data.

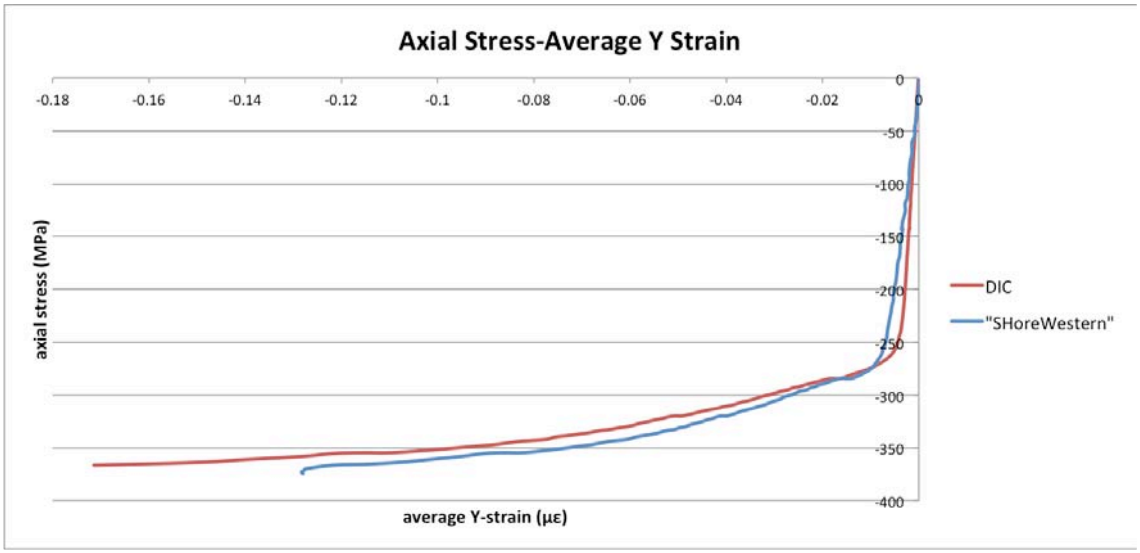

Figure 11.81: comparison between the axial stress-average Y strain DIC curve and the axial stress-average Y strain Shore Western curve: different slopes in the elastic region.

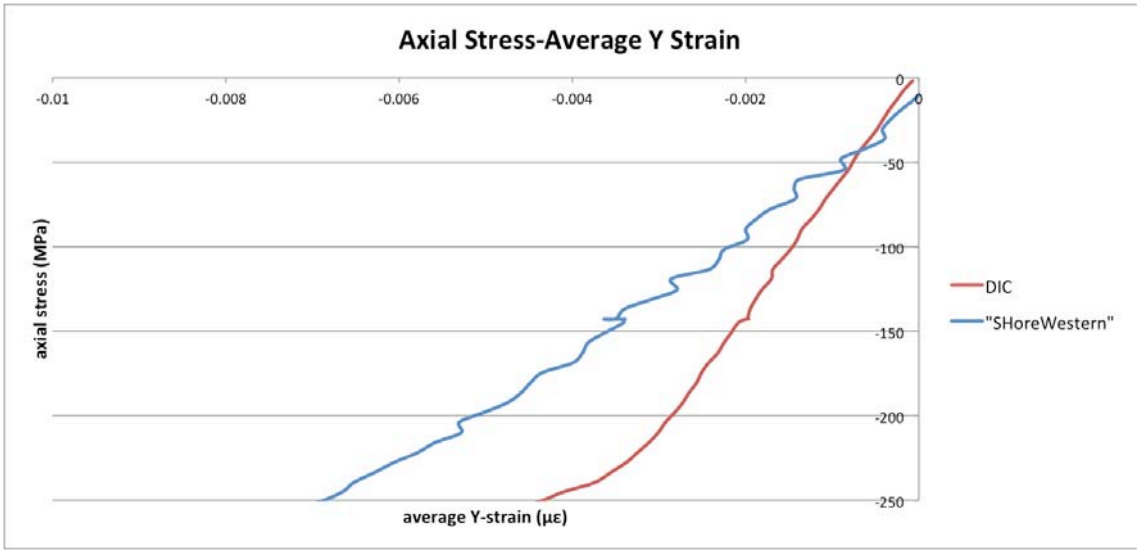

Figure 11.82: comparison between the axial stress-average Y strain DIC curve and the axial stress-average Y strain Shore Western curve: different slopes in the elastic region.

To detect the precise point of yielding as it regards the axial force, it is evaluate as the so-called $\sigma_{0.2\%}$-stress, i.e. the stress at which the remaining plastic strain after unloading is equal to 0.2%.

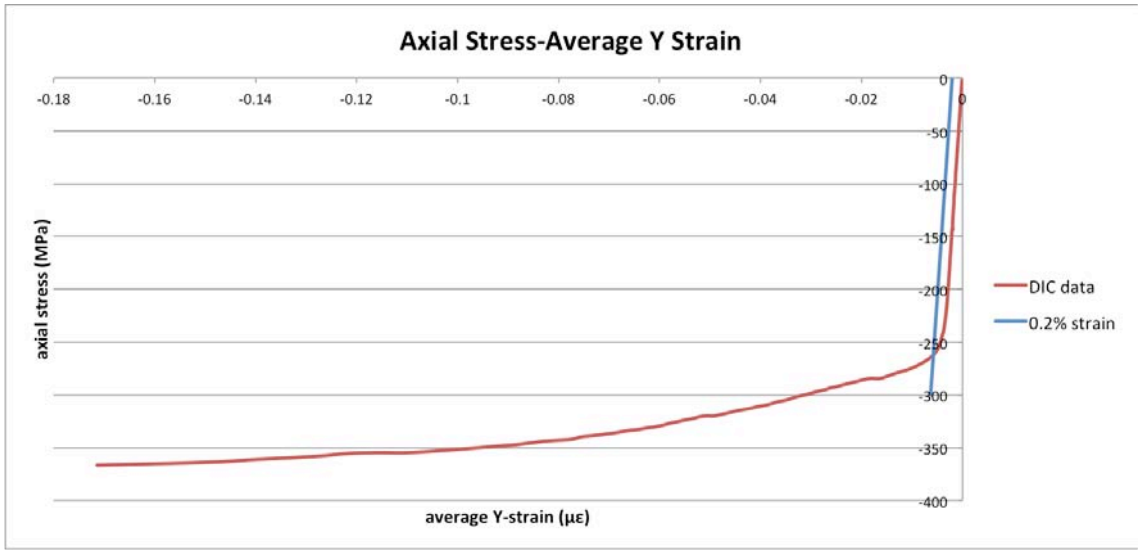

Figure 11.83: yielding point for the axial force evaluate as the $\sigma_{0.2\%}$-stress

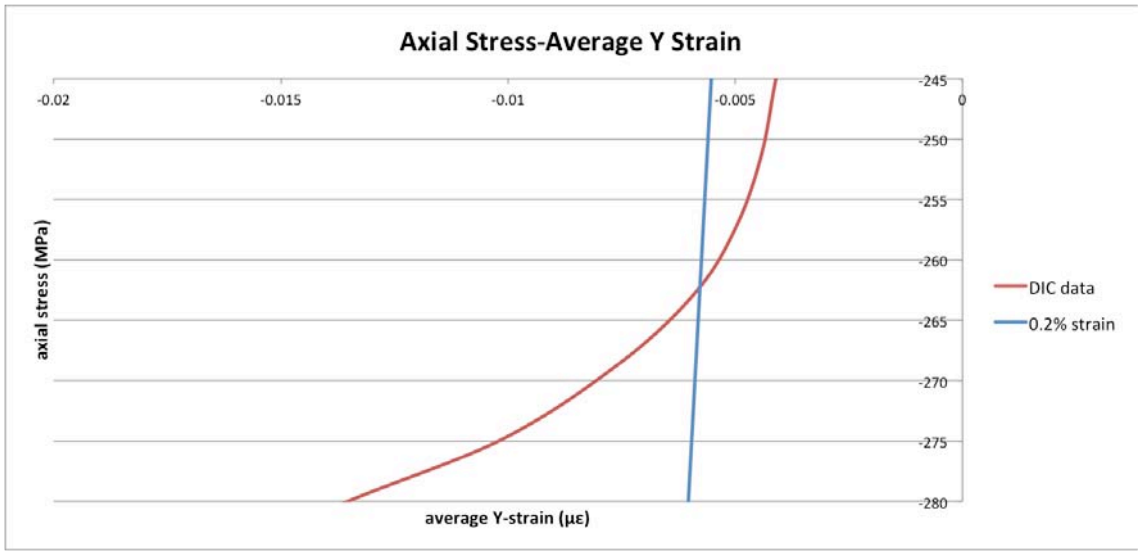

Figure 11.84: detail of the tensile yielding point

The intersection between the DIC data curve and the 0.2% strain straight line locate the yielding point, which in this case occurs at a stress equal to 262 MPa.

The same procedure is used to detect the precise point of yielding as it regards the torque.

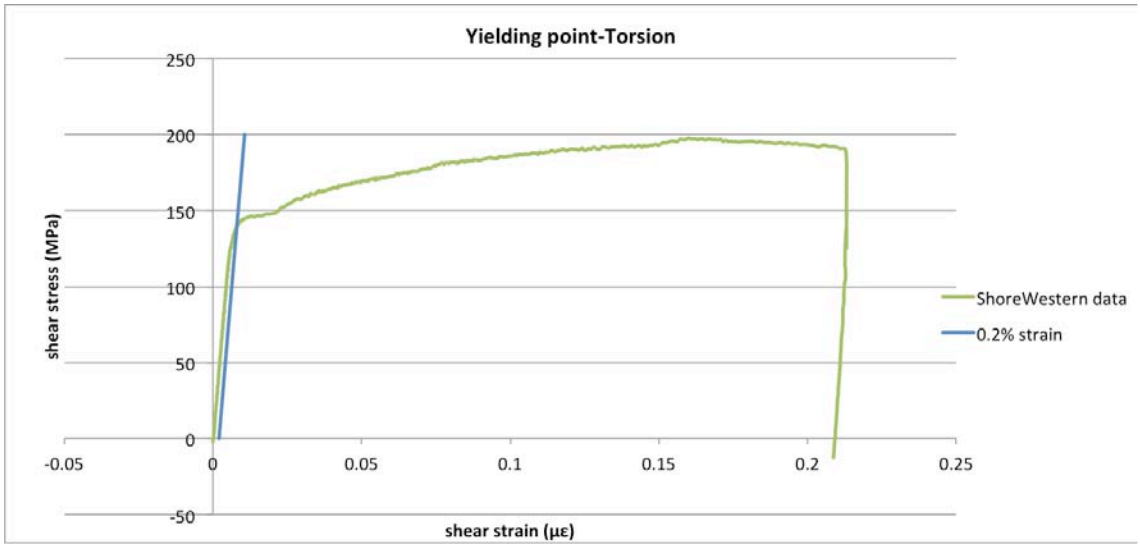

Figure 11.85: yielding point for the torque evaluate as the $\sigma_{0.2\%}$-stress

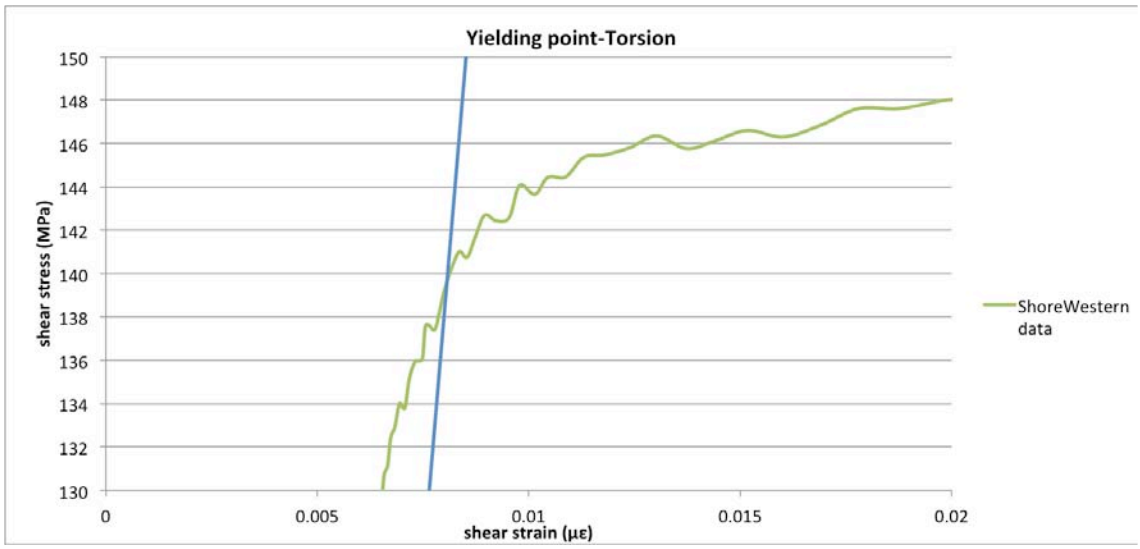

Figure 11.86: detail of the torque yielding point

The intersection between the DIC data curve and the 0.2% strain straight line locate the torque yielding point, which in this case occurs at a stress equal to 140MPa.

Below is reported a table, which summarizes the most important values of this test.

Name of the specimen	8A
Lode Angle	50°
Length (mm)	124
Diameter (mm)	29.77

Tensile Yield point: stress (MPa)	-262
Tensile Yield point: strain (με)	-0.0078
Torque Yield point: stress (MPa)	140
Torque Yield point: strain (με)	0.0082
Tensile peak point: stress (MPa)	-387
Tensile peak point: strain (με)	-0.126
Torque peak point: stress (MPa)	196.7
Torque peak point: strain (με)	0.171
Tensile yield load (kN)	-182.37
Torque yield load (Nm)	725.26
Torque yield twist (°)	2.90
E (GPa)	72267
G (GPa)	23021

Some pictures of the specimen and its failure are now reported.

Figure 11.87: specimen 8A in the grips

Figure 11.88: specimen 8A under compression-torsion

11. Results

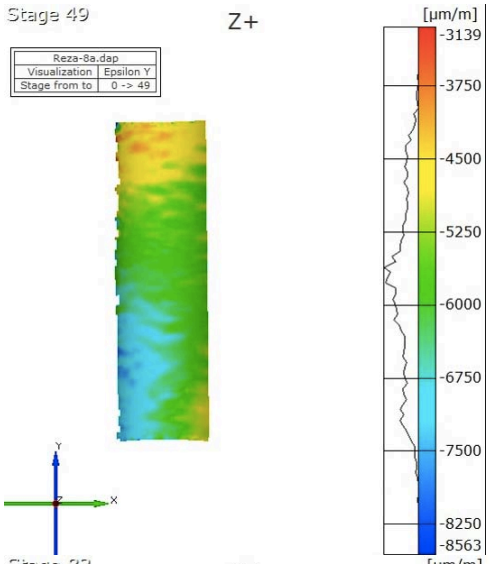
Stage 49
Z+
Reza-8a.dap
Visualization | Epsilon Y
Stage from to | 0 -> 49
[µm/m]
-3139
-3750
-4500
-5250
-6000
-6750
-7500
-8250
-8563

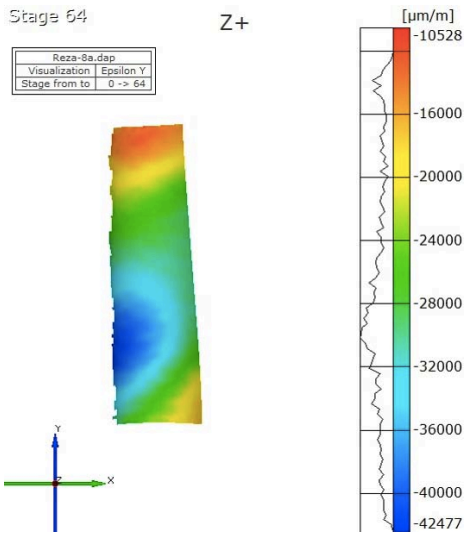
Stage 64
Z+
Reza-8a.dap
Visualization | Epsilon Y
Stage from to | 0 -> 64
[µm/m]
-10528
-16000
-20000
-24000
-28000
-32000
-36000
-40000
-42477

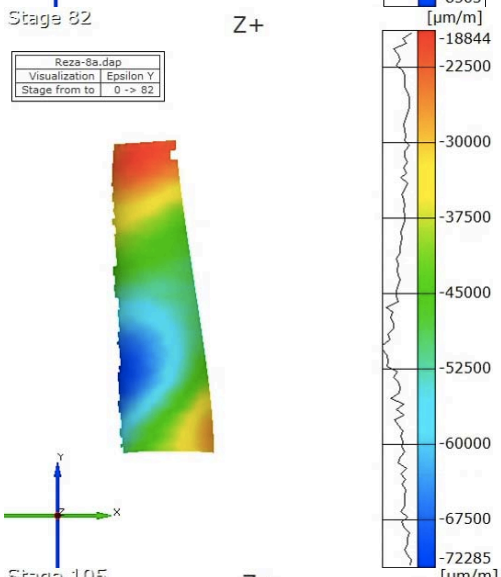
Stage 82
Z+
Reza-8a.dap
Visualization | Epsilon Y
Stage from to | 0 -> 82
[µm/m]
-18844
-22500
-30000
-37500
-45000
-52500
-60000
-67500
-72285

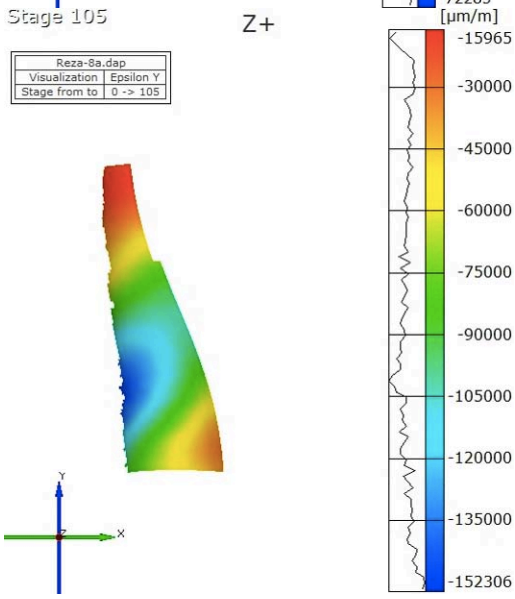
Stage 105
Z+
Reza-8a.dap
Visualization | Epsilon Y
Stage from to | 0 -> 105
[µm/m]
-15965
-30000
-45000
-60000
-75000
-90000
-105000
-120000
-135000
-152306

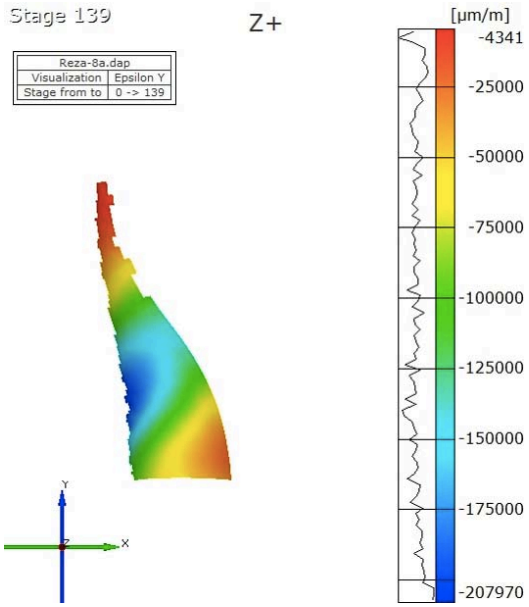

Figure 11.89: contour of the strain in the vertical direction: images obtained by post processing the DIC data recorded

12 Conclusions

The classical J_2 theory of metal plasticity assumes that the hydrostatic pressure on plastic flow is negligible, and further assumes that the flow stress is independent of the third stress invariant of the stress deviator. The experimental data obtained, show some difference between the behavior of aluminum and the behavior described by J_2 metal plasticity.

In order to detect the influence of the Lode angle parameter on the behavior of aluminum 6061-T6 as it regards yielding, it seemed to be useful to compare the von Mises and Tresca yield conditions with the experimental results. In the polar coordinate system, the equivalent stress becomes the radial coordinate, which allows to draw the von Mises yield curve, while the circumferential coordinate is the Lode angle θ. In the deviatoric stress plane, the von Mises yielding condition is represented by a circle. The Tresca yielding is a hexagon inscribed on the von Mises circle. A MatLab code was written for plotting the data points obtained in the experiments in the π-plane.

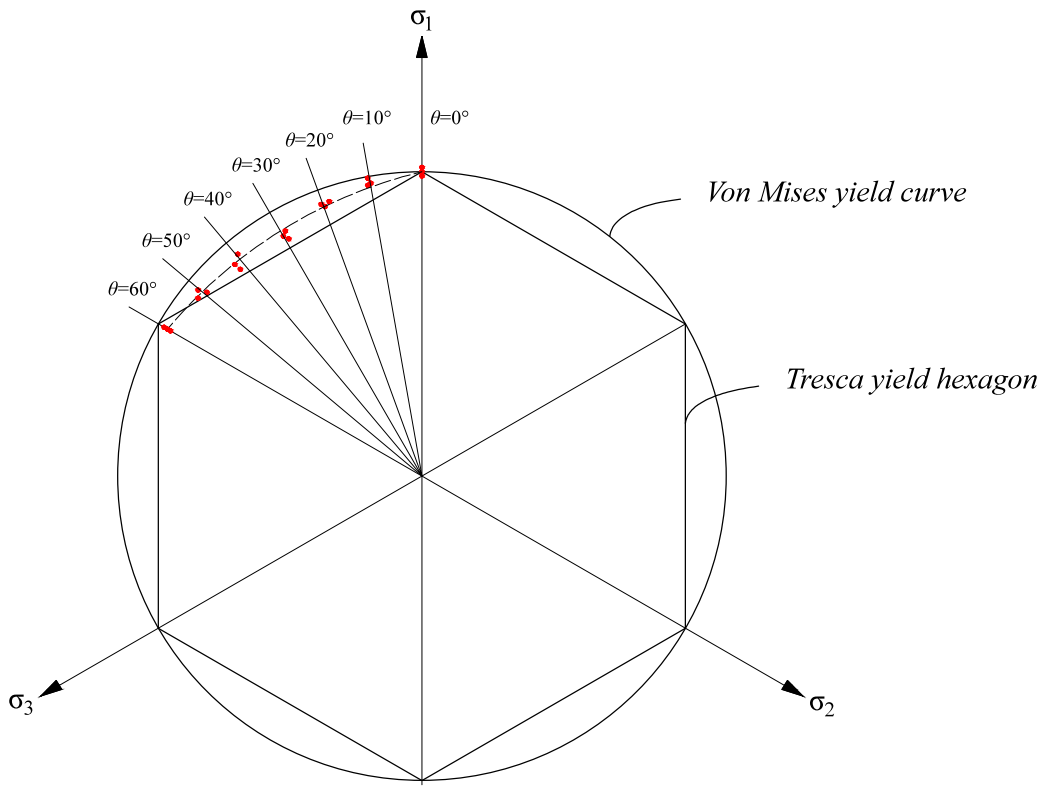

Figure 12.1: representation of the data poinst on the π-plane

Looking at the representation of the data points in the π-plane it is possible to observe that there is a deviation between them ant the Von Mises yield surface, which represent J_2 plasticity. It is therefore possible to assert that an influence of the Lode angle parameter on the yield behavior of aluminum is identified. A possible curve, which interpolates the data points, is reported in figure 12.1, but it is necessary to perform the same testing scenarios also on steel specimens before defining the equation of a new yield curve.

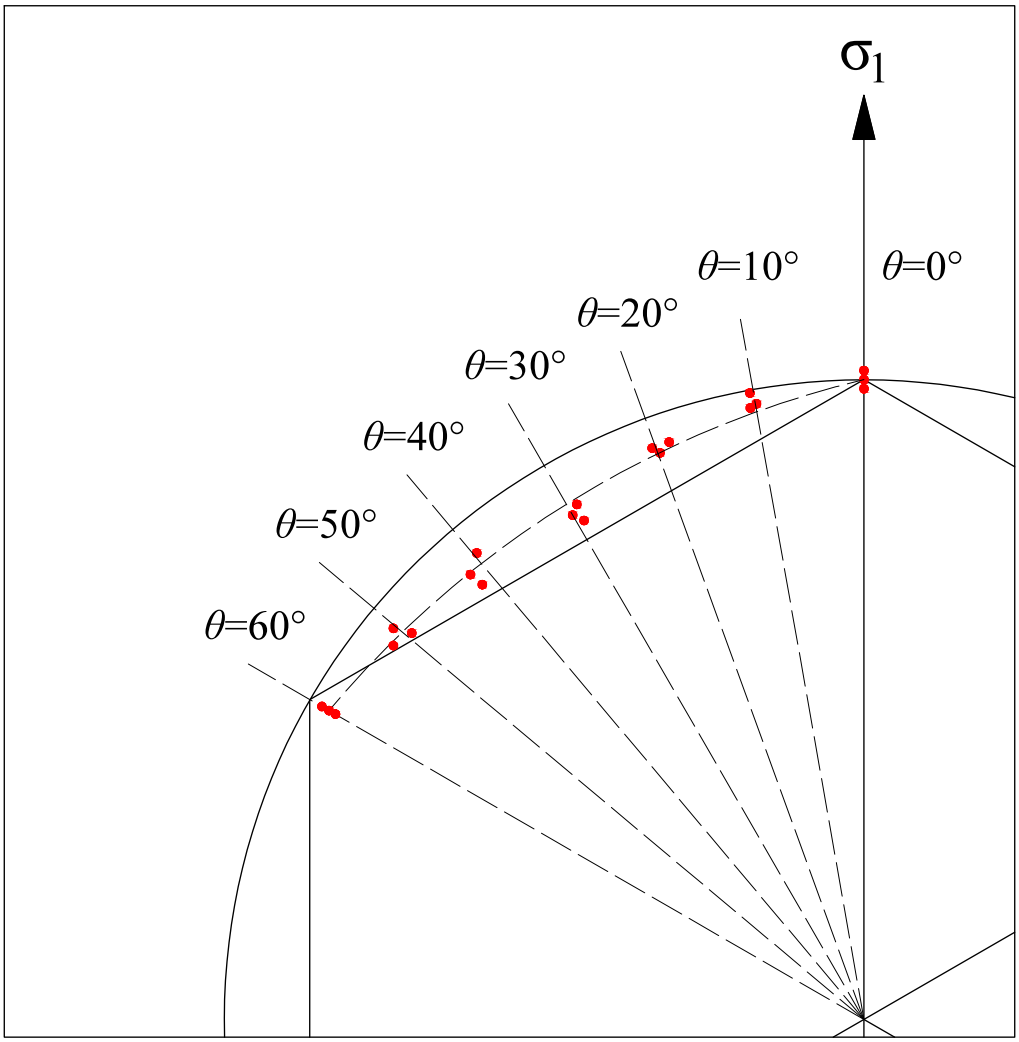

Figure 12.2: detail of the experimental data points

It is in addition possible to notice from figure 12.2 that yielding in tension is clearly different from yielding in compression. The data values derived from the tension test are in fact used to calibrate the von Mises circle. For J_2 metal plasticity we should have the same values of yielding both in tension and in compression, but from the experimental observation we can deny this assumption and assert that, not only a dependence on the Lode angle parameter of the aluminum behavior in yielding is highlighted, but also a dependence on the first invariant of the stress tensor.

As it regards the post yielding behavior, a great difference between the experimental scenarios is observed, both if the Lode parameter is considered or the first invariant of the stress tensor.

To clarify this statement, let us compare the behavior after yielding of the aluminum specimen subjected to the 10° Lode angle scenario with the one subjected to the 50° Lode angle scenario and also the aluminum specimen subjected to the 20° Lode angle scenario with the one subjected to the 40° Lode angle scenario.

The experimental scenario related to the 10° Lode angle parameter and the 50° Lode angle parameter have in fact the same proportion between axial force and torque (P/T=5.5), the only difference is that the axial force for the 10° Lode angle scenario is a tension force; instead the axial force for the 50° Lode angle scenario is a compression force. The same thing can be said for 20° and 40° Lode angle scenarios: the experimental scenario related to the 20° Lode angle parameter and the 40° Lode angle parameter have the same proportion between axial force and torque (P/T=2.175), the only difference is that the axial force for the 20° Lode angle scenario is a tension force, the axial force for the 40° Lode angle scenario is a compression force. For this reason if we neglect the influence of the first invariant of the stress tensor, the behaviors of the abovementioned couples of aluminum specimens should be the same. The experimental results however show a relevant difference in their post-yielding behavior:

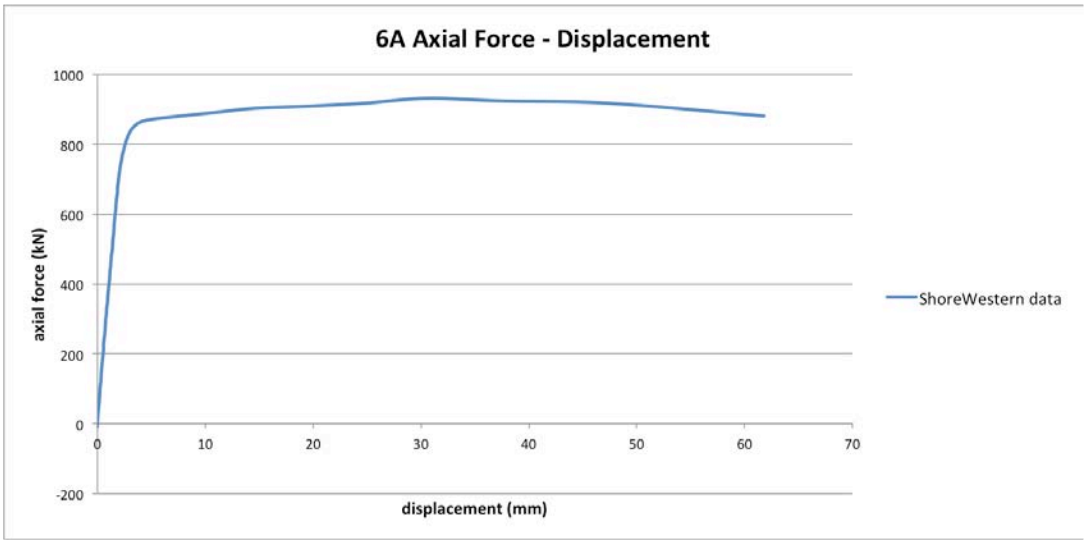

Figure 12.3: specimen 6A, Lode angle θ=10°, axial force-axial displacement

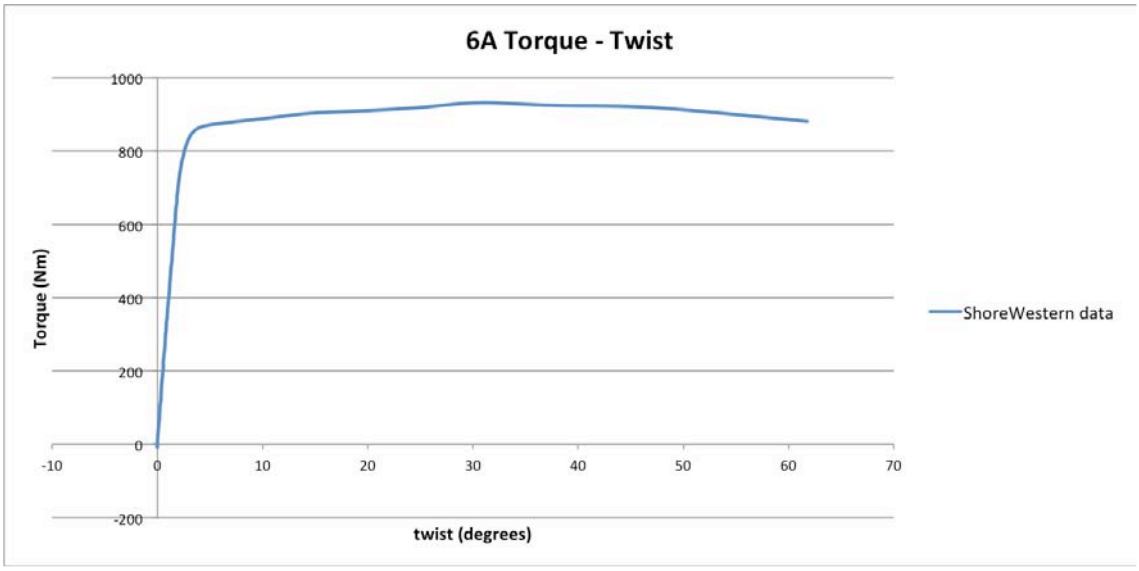

Figure 12.4: specimen 6A, Lode angle θ=10°, torque-twist

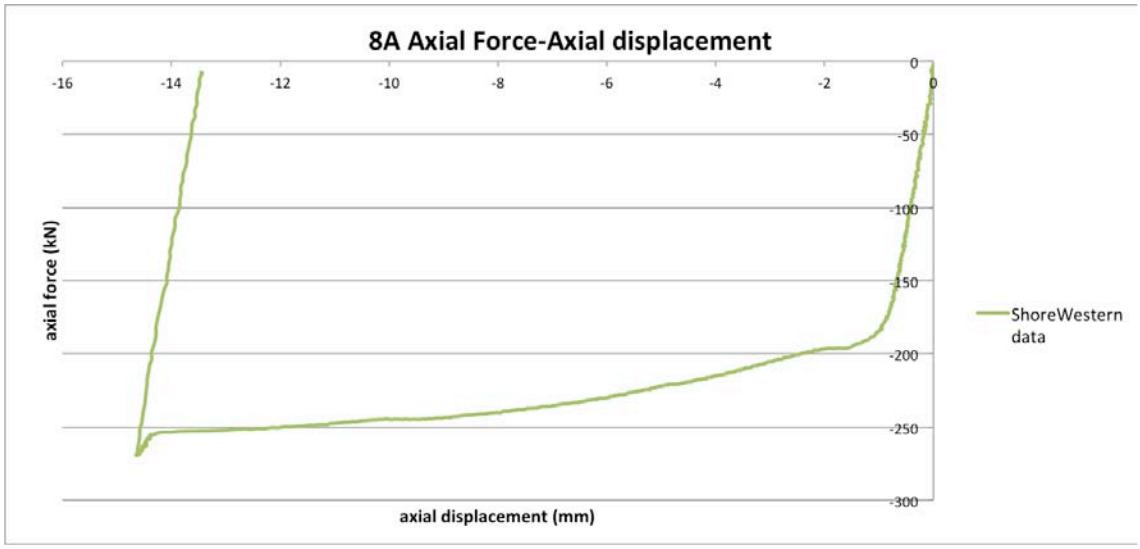

Figure 12.5: specimen 8A, Lode angle θ=50°, axial force-axial displacement

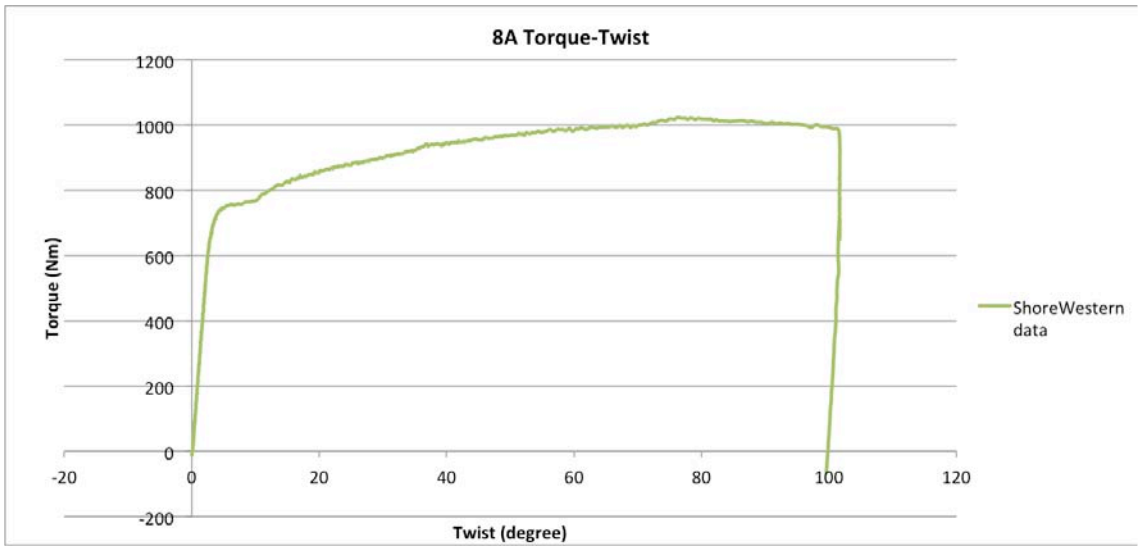

Figure 12.6: specimen 8A, Lode angle θ=20°, torque-twist

Comparing images 12.3 with 12.5 and 12.4 with 12.6 it is possible to observe that, as it regards the loading scenario corresponding to θ=10° where we have torsion and tension, failure occurs after the first cycle of loading; as it regards the loading scenario corresponding to θ=50° where we have compression and tension, failure doesn't occurs after the first cycle of loading. Unfortunately, due to some problems with the axial torsion machine we haven't been able to continue the testing after the first cycle, but the specimen didn't show any signal

of failure. Most probably we would not have been able to reach failure after several cycles.

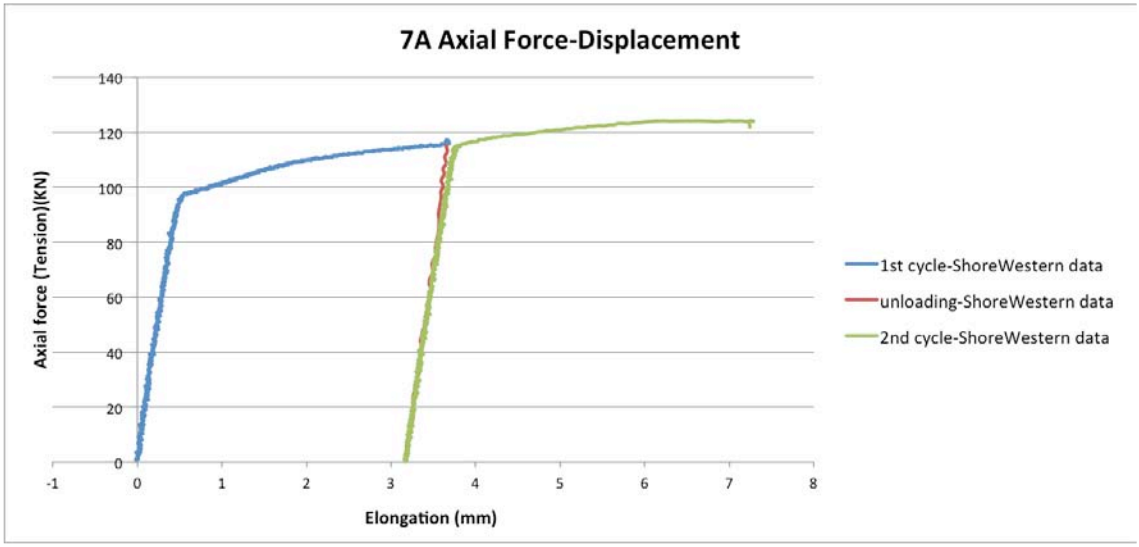

Figure 12.7: Figure 12.8: specimen 7A, Lode angle θ=20°, axial force-axial displacement

Figure 12.9: specimen 7A, Lode angle θ=20°, torque-twist

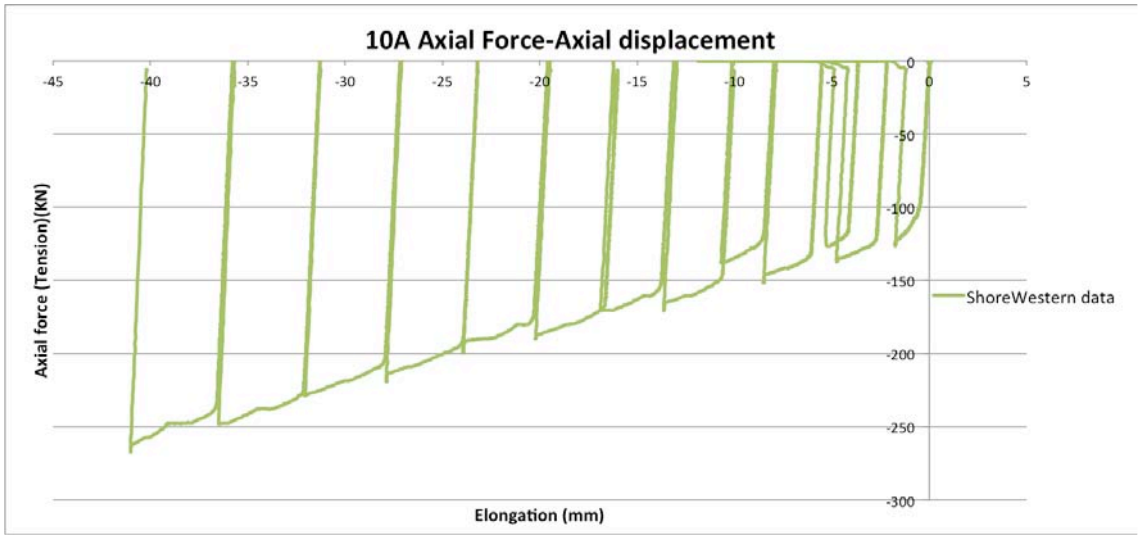

Figure 12.10: specimen 10A, Lode angle θ=40°, axial force-axial displacement

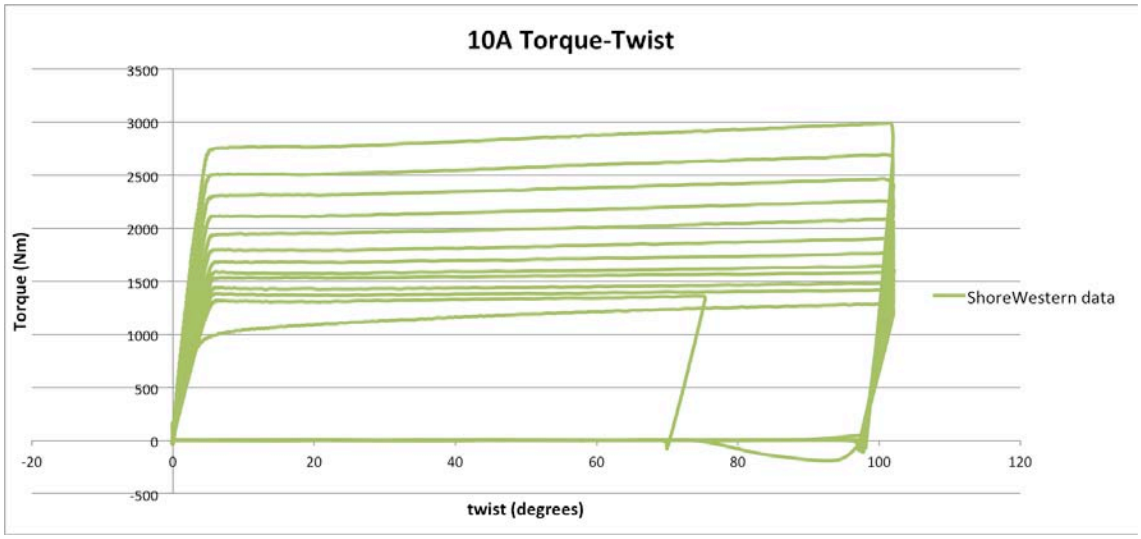

Figure 12.11: specimen 10A, Lode angle θ=40°, torque-twist

The same thing said for specimen 6A and specimen 8A is valid also for specimens 7A and 10A.

Comparing images 12.8 with 12.10 and 12.9 with 12.11 it is possible to observe that, as it regards the loading scenario corresponding to θ=20° where we have torsion and tension, failure occurs after the second cycle of loading; as it regards the loading scenario corresponding to θ=40° where we have compression and tension, failure doesn't occurs after the first cycle of loading. As a matter of fact

we haven’t been able to reach failure not even after several cycles of loading and we were forced to stop the test in order to avoid problems to the Axial Torsion Machine. It is in fact possible to notice that for the compression torsion test, the strength increases after each cycle.

These observations reveals how the difference of the behavior of aluminum specimen subjected to different first invariants of the stress tensor values is evident and not only the Lode angle parameter but also this parameter must been taken in regard.

13 References

[1] Bridgman PW. Studies in large plastic flow and fracture with special emphasis on the effects of hydrostatic pressure. 1st ed.. . New York: McGraw-Hill; 1952.

[2] Mc Clintock FA. A criterion for ductile fracture by the growth of holes. J Appl Mech 1968;35:363–71.

[3] Rice JR, Tracey DM. On the ductile enlargement of voids in triaxial stress fields. J Mech Phys Solids 1969;17:201–17.

[4] Gurson AL. Continuum theory of ductile rupture by void nucleation and growth: part I – yield criteria and flow rules for porous ductile media. J Eng Mater Technol 1977;99:2–15.

[5] Tvergaard V, Needleman A. Analysis of the cup–cone fracture in a round tensile bar. Acta Metall 1984;32:157–69.

[6] Lemaitre J. A continuous damage mechanics model for ductile fracture. J Eng Mater Technol 1985;107:83–9.

[7] Chow CL, Wang J. An anisotropic theory of continuum damage mechanics for ductile fracture. Eng Fract Mech 1987;27:547–58.

[8] Chow CL, Wang J. Ductile fracture characterization with an anisotropic continuum damage theory. Eng Fract Mech 1988;30:547–63.

[9] Atkins AG. Possible explanation for unexpected departures in hydrostatic tension-fracture strain relations. Met Sci 1981;15:81–3.

[10] Johnson GR, Cook WH. Fracture characteristics of three metals subjected to various strains, strain rates, temperatures and pressures. Eng Fract Mech 1985;21:31–48.

[11] Bao Y. Prediction of ductile crack formation in uncracked bodies [Ph.D. thesis]. MIT; 2003.

[12] Wilkins ML, Streit RD, Reaugh JE. Cumulative-strain-damage model of ductile fracture: simulation and prediction of engineering fracture tests, ucrl-53058. Technical report, Lawrence

Livermore Laboratory, Livermore, CA; 1980.

[13] Wierzbicki T, Bao Y, Lee YW, Bai Y. Calibration and evaluation of seven fracture models. Int J Mech Sci 2005;47:719–43.

[14] Xue L, Wierzbicki T. Ductile fracture initiation and propagation modeling using damage plasticity theory. Eng Fract Mech 2008;75:3276–93.

[15] Bai Y, Wierzbicki T. A new model of metal plasticity and fracture with pressure and Lode dependence. Int J Plast 2008;24:1071–96.

[16] Gao X, Zhang T, Hayden M, Roe C. Effects of the stress state on plasticity and ductile failure of an aluminum 5083 alloy. Int J Plast 2009;25:2366–82.

[17] Coppola T, Cortese L, Folgarait P. The effect of stress invariants on ductile fracture limit in steels. Eng Fract Mech 2009;76:1288–302.

[18] Li H, Fu MW, Lu J, Yang H. Ductile fracture: experiments and computations. Int J Plast 2011;27:147–80.

[19] Mirone G, Corallo D. A local viewpoint for evaluating the influence of stress triaxiality and Lode angle on ductile failure and hardening. Int J Plast 2010;26:348–71.

[20] G. Mirone, A. Keshavarz, R. Ghajar. - A new experimental failure model based on triaxiality factor and Lode angle for X-100 pipeline steel (2014)

[21] J. P. Bardet. Lode Dependences for Isotropic Pressure-Sensitive Elastoplastic Materials (1990)

[22] Marcilio Alves, Norman Jones. Influence of hydrostatic stress on failure of axisymmetric notched specimens. (1999)

[23] Z. Zachariah, Sankara Sarma V. Tatiparti, S.K. Mishra, N. Ramakrishnan, U. Ramamurty. Tension–compression asymmetry in an extruded Mg alloy AM30: Temperature and strain rate effects (2013)

[24] Peter Pivonka, Kaspar Willam. The effect of the third invariant in computational plasticity (2003)

[25] Xiaosheng Gao, Tingting Zhang, Matthew Hayden, Charles Roe. Effects of the stress state on plasticity and ductile failure of an aluminum 5083 alloy. (2009)

[26] J.P. Bardet. Lode dependences for isotropic pressure-sensitive elastoplastic materials. (1990)

[27] Matthieu Dunand, Dirk Mohr. On the predictive capabilities of the shear modified Gurson and the modified Mohr–Coulomb fracture models over a wide range of stress triaxialities and Lode angles. (2011)

[28] Meng Luo, Matthieu Dunand, Dirk Mohr. Experiments and modeling of anisotropic aluminum extrusions under multi-axial loading – Part II: Ductile fracture. (2012)

[29] G. Mirone, D. Corallo. A local viewpoint for evaluating the influence of stress triaxiality and Lode angle on ductile failure and hardening. (2010)

[30] Yuanli Bai, Tomasz Wierzbicki. Application of extended Mohr–Coulomb criterion to ductile fracture. (2010)

[31] Laurence E. Malvern. Introduction to the Mechanics of a Continuos Medium. (1969)

[32] Zengtao Chen, Cliff Butcher. Micromecanics Modeling of Ductile Fracture. Springer. (2013)

[33] Niels s. Ottosen, Matti Ristinmaa. The Mechanics of Constitutive Modeling. (2005)

[34] Vlado A. Lubarda. Elastoplasticity Theory. CRC press (2001)

[35] S. Timoshenko. Theory of Elasticity. McGraw-Hill (1951)

[36] P. Menetrey, K. Willam. Triaxial failure criterion for concrete and its generalization. ACI Structural Journal 92, 311–318. (1995)

[37] W.-F. Chen and D.J. Han, “Plasticity for Structural Engineers”, Springer-Verlag, New York, 1988.

[38] J. Lubiner, “Plasticity Theory”, Macmillan Publ. Co., New York, 1990.

[40] J. Lemaitre and J.-L. Chaboche, “Mechanics of Solid Materials”, Cambridge University Press 1990.

[41] G.A. Maugin, “The Thermomechanics of Plasticity and Fracture”, Cambridge University Press, 1992.

[42] J.C. Simo and T.J.R. Hughes, “Computational Inelasticity”, Springer-Verlag New York, Inc., 1998.

[43] K.William, “Constitutive Models for Materials”, Encyclopedia of Physical Science & Technology, 3rd Edition, Academic Press, 2000. http://civil.colorado.edu/william/matl01.pdf

[44] Z.P. Bazant and M.Jirasek, “Inelastic Analysis of Structures”, J. Wiley & Sons Ltd, 2002.

[45] G.Z. Voyiadjiis and P.I. Kattan, “Damage Mechanics”, Taylor& Francis, CRO Press, 2005.

[46] Handouts of the “Elastic Damage and Plasticity” course held by Professor Kaspar Willam, spring 2015, University of Houston.

13. References